Third Benchmark Workshop

on

NUMERICAL ANALYSIS OF DAMS

Paris, France
September 29–30, 1994

Organized by
the **ICOLD**
"ad-hoc" Committee on Computational Aspects
of Dam Analysis and Design

Under the auspices of the
French Committee on Large Dams
in cooperation with

and

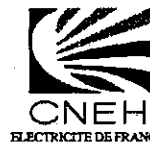

Volume III

Third Benchmark Workshop on
NUMERICAL ANALYSIS OF DAMS
Gennevilliers, France, September 29-30, 1994

THEME B1

Evaluation of pore pressure and settlements of an embankment dam under static loadings

PRESENTATION

&

REFERENCE INFORMATION AND DATA

1. INTRODUCTION

The two previous Benchmark Workshops on Numerical Analysis of Dams have demonstrated the difficulty to define sufficiently precise instructions and to perform numerical analyses of embankment dams.

For the next Benchmark Workshop, a simpler simulation is proposed :

- the load cases are only static loadings,
- the constitutive model of the materials is supposed to be the Mohr Coulomb model and the properties are explicitly provided,
- the requested results are pore pressure and/or settlements and/or effective stresses in the dam.

Any method that gives an evaluation of the requested results may be used :

- seepage analysis (evaluation of pore pressure),
- stability analysis (evaluation of settlements),
- uncoupled analysis (evaluation of pore pressure and settlements **without** taking into account coupling effects between them),
- coupled analysis (evaluation of pore pressure and settlements **with** taking into account coupling effects between them).

The comparison of results obtained by different methods could provide some conclusions on the importance of the coupled effects between mechanical and hydraulic responses of the structure.

The selected dam is the same as that chosen for the first two benchmark workshops and for theme B2 : El Infiernillo dam (Mexico). It is a 145 m high rockfill dam with a central clay core. It was built in 1962-63 and its impounding began in June 1964.

A two-dimensional analysis will be carried out. The retained section of the dam is an upstream-downstream section of maximum height.

It is not compulsory to carry out the whole set of analyses proposed.

The paper should not exceed 14 pages including the requested Figures and Tables. The text should report :

- the methodology of the analysis,
- the selected computation method,
- the main assumptions of the numerical model adopted,
- the software used,
- the computation times for each load case and the hardware used.

2. MATERIAL PROPERTIES

The materials of the various zones are described in Fig. 1. They can be divided into 4 main groups : core, filter, transition material and rockfill. The constitutive model of the materials is supposed to be the Mohr Coulomb model. The parameter sets and the vertical and horizontal permeabilities for each material are given in Table 1. Densities are given in Table 2.

The foundation is composed of sound rock consisting of silicified conglomerate with basaltic dykes. It is presumed to be rigid and impermeable.

Table 1
3rd Benchmark Workshop - Theme B1
Parameter sets to be used with Mohr Coulomb Model

Parameter	Core	Filter	Transition	Compacted rockfill Dumped rockfill
E (MPa)	40	40	40	
ν	0.3	0.3	0.3	
ϕ (°)	25	35	42	
c (MPa)	0	0	0	
ψ (°) (1)	5	5	5	
k_v (m/s)	2.10^{-10}	8.10^{-5}	7.10^{-4}	- (2)
k_h (m/s)	8.10^{-10}	8.10^{-5}	7.10^{-4}	- (2)

(1) dilatancy angle ψ is necessary only for a formulation of the Mohr Coulomb model with a non associated flow rule ; in a standard formulation $\psi = \phi$

(2) rockfills are supposed to be fully drained.

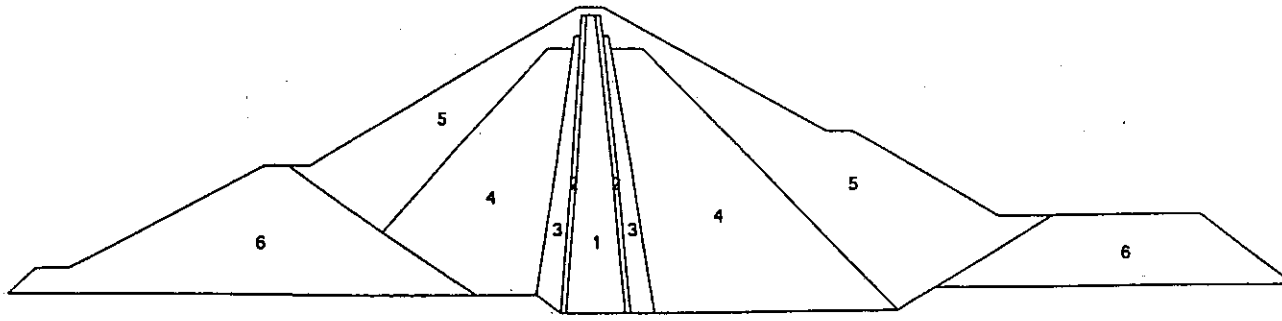

1. Impervious clay core
2. Filters (sand)
3. Transition Zone
4. Inner Shoulder compacted rockfill
5. Outer Shoulder dumped rockfill
6. Cofferdams (integrated) dumped rockfill

Fig. 1 : 3rd Benchmark Workshop - Theme B1
Material property zones

Table 2
3rd Benchmark Workshop - Theme B1
General characteristics of the material

Properties	Core	Filters	Transitions	Rockfill	
Grain density	2.75	2.76	2.75	2.71	
				Dumped	Compacted
Dry density	1.59	1.87	2.02	1.76	1.85
Initial degree of saturation S_o	0.96	-	-	-	-

3. FINITE ELEMENT MESH

A basic mesh is proposed. It is more refined in the core of the dam than the one already used for the two previous Benchmark Workshops. It is illustrated in Fig. 2. It has been optimised with an algorithm for profile and wavefront reduction of sparse matrices. There are two different types of elements : the isoparametric 8-node quadrilateral and 6-node triangle. The node numbering conventions for both elements are also shown in Fig. 2.

No rock foundation was modelized, since it is considered as rigid and impermeable.

The finite element mesh is defined in the diskette by the two files :

ELEMENTS.DAT and NODES.DAT

These files contain lists for elements and nodes respectively. A description of the data format is given at the top of each file.

The basic mesh is made of 1156 nodes and 389 elements. The participants are free to use **another mesh**, for example in order to reduce the number of nodes and elements.

However it is recommended to have at least four elements in the thickness of the core to compute pore pressure and settlement with good precision, because the hydraulic gradient is very high, according to its low permeability and its thickness.

Important : In any case, the points selected for the output must be kept in the modified mesh, so as to enable the comparison of results at the same locations.

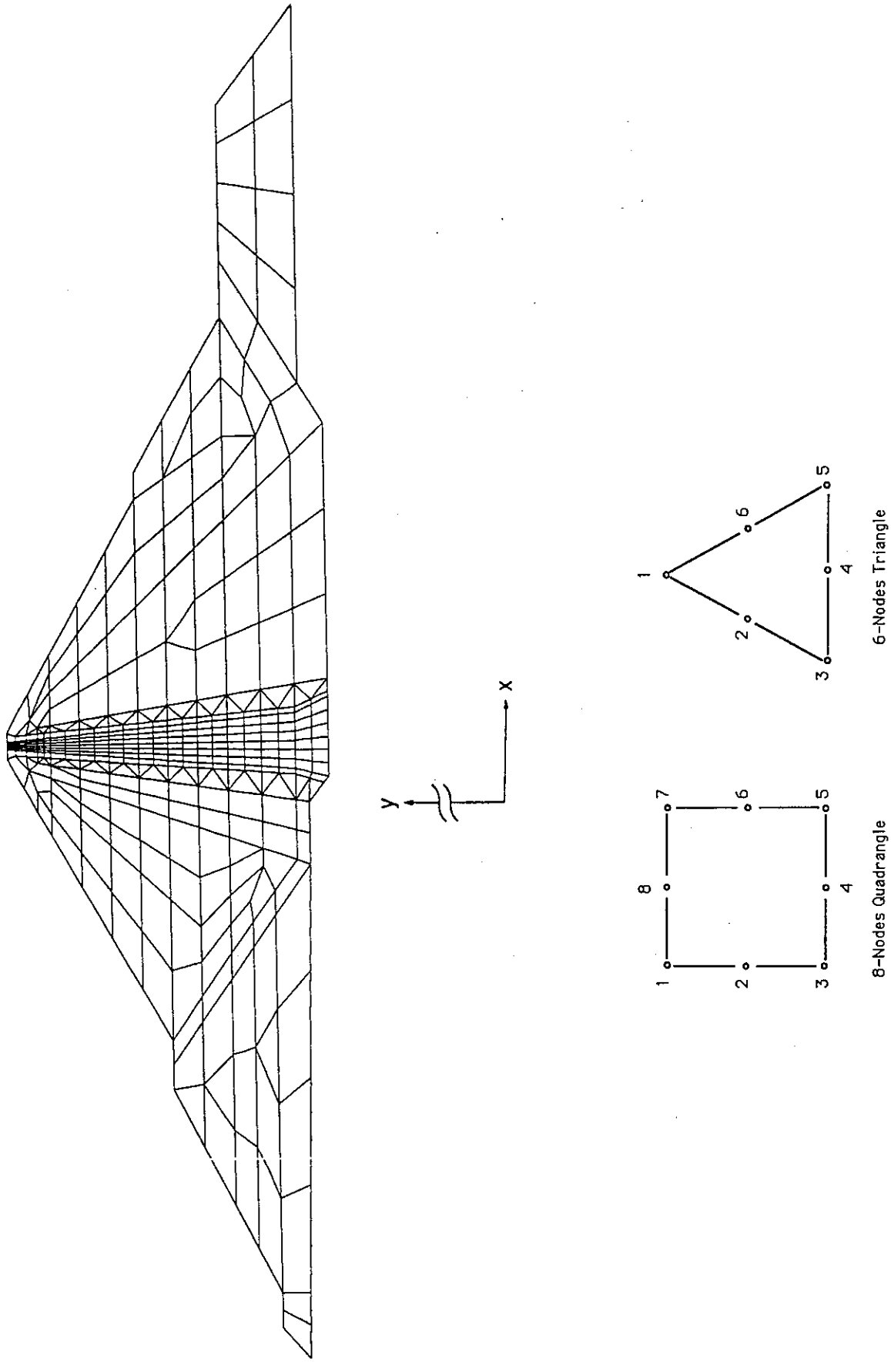

Fig. 2 : 3rd Benchmark Workshop - Theme B1
Finite element mesh

4. DEFINITION OF LOAD CASES

4.1. Introduction

Three load cases, corresponding to the actual history of the dam, are requested : construction period, reservoir impounding, consolidation phase. It is not compulsory to modelize the three load cases : only one or two of them may be performed, depending on the used analysis method. The various phases are detailed in the following sections.

The boundary conditions will take into account the following aspects :

- the rock foundation is assumed to be rigid and impermeable,
- the dam's upstream face boundary conditions (mechanical and hydraulic) are directly related to the reservoir level.

The initial conditions in the materials (unit weight, porosity, degree of saturation, etc.) for the construction phase will be taken from Table 2.

4.2. Construction Phase

The total duration of the dam construction is approximately 15 months, with a very regular rate of elevation versus time : 10 m per month.

Then a consolidation period of 5 months occurs before reservoir impounding, the reservoir level being at El. 60. The analysis corresponding to this first consolidation period remains optional.

4.3. Reservoir Impounding

Fig. 3 gives the observed curve of the reservoir level increase versus time, which can be simplified as follows :

- before point A : Reservoir at El. 60
- between A (El. 60) and B (El. 130) : 0.5 months
- between B (El. 130) and C (El. 160) : 1.5 months
- between C (El. 160) and D (El. 169) : 4 months.

After point D, the reservoir level is assumed to stay at El. 169.

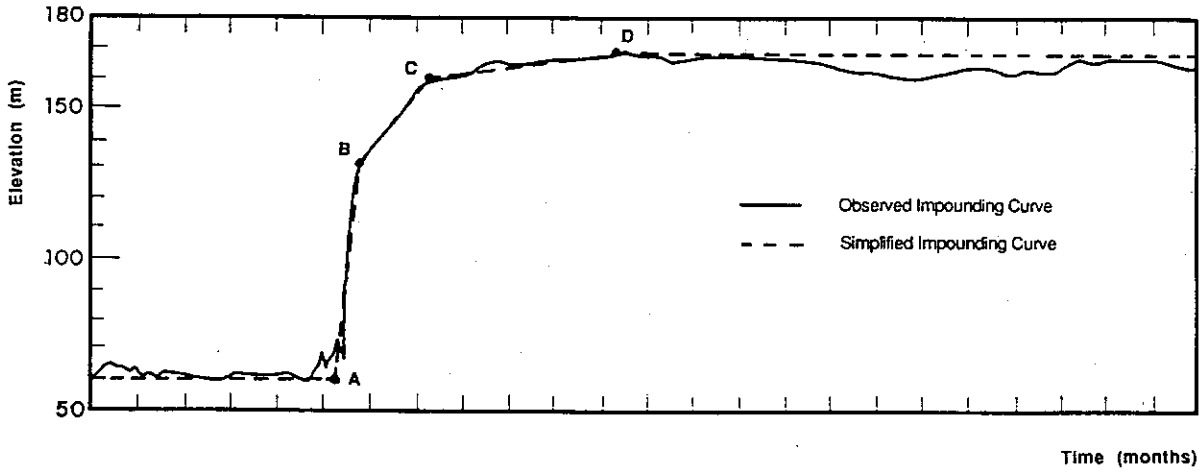

Fig. 3 : 3rd Benchmark Workshop - Theme B1
Reservoir impounding : reservoir level (m) vs. time (months)

4.4. Consolidation

A phase of consolidation will occur after reservoir impounding, so as to obtain stabilization in pore pressures and effective stresses.

5. PRESENTATION OF RESULTS

The participants are free to present all figures and results which they consider interesting for the study. However, in order to facilitate the comparisons and discussions during the meeting, some key results are required as a minimum and are detailed hereafter. Templates are given in the following figures.

Moreover, participants are asked to record the results of Figures 6 to 9 and Table 3, on a floppy disk as indicated in the file RESULT.DAT.

5.1. Effective Stresses

Fig. 4 gives a template for the presentation of the contour lines of horizontal (named Fig. 4a) and vertical (named Fig. 4b) effective stresses as well as shear stresses (named Fig. 4c) in the dam at the end of construction, impounding and consolidation. The results are required for all or some of these phases.

- Geometrical scale : 1/3500
- Contour lines every 0.2 MPa (= 0.2 x 10^6 Nm^{-2}) - Units in MPa.

5.2. Pore Pressures

The contour lines of pore pressure (named Fig. 4d and Fig. 5) are required for the same 3 phases as mentioned above. Fig. 4 also gives the template for the presentation, and Fig. 5 is a zoom on the core material.

- Geometrical scale : 1/3500 (Fig. 4d) and 1/1000 (Fig. 5)
- Contour lines every 0.1 MPa

5.3. Displacements

For each point of the dam, the origin of displacements is taken at the date of placement of the corresponding layer.

Horizontal and vertical displacements are required at the end of the last performed phase, (if 3 phases are performed, at the end of consolidation phase), and will be given along 3 main lines of the dam :

- Vertical line in the core (AA) : See templates in Fig. 6 and 8,
- Horizontal lines at El. 120 (BB) and 80 (CC) : See templates in Fig. 7 and 9.

Scales :

Geometry: 1/1000 for line AA
1/3500 for lines BB and CC

Displacements:

- line AA
  - 1/20 for settlements (Fig. 6)
  - 1/10 for horizontal displacements (Fig. 8)
- lines BB and CC
  - 1/40 for settlements (Fig. 7)
  - 1/20 for horizontal displacements (Fig. 9)

The settlements will be given in Fig. 6 and 7, and Fig. 8 and 9 will be used for the horizontal displacements.

5.4. General Summary

A summary table will also be given for the 5 following nodes :

- Middle axis of the dam (core) at El. 180 (crest), El. 120 and El. 80 (the nodes will be called CC, CM, and CL respectively).
- Upstream and downstream face of the dam at El. 120 (the nodes will be called UM and DM respectively).

The table will summarize the displacements and pore pressure of the 3 main phases : construction, impounding and consolidation (see template in Table 3).

	Points of the Dam Section				
	CC	CM	CL	UM	DM
End of Construction					
End of Impounding					
End of Consolidation					

Horizontal Displacements (10^{-2} m)

	Points of the Dam Section				
	CC	CM	CL	UM	DM
End of Construction					
End of Impounding					
End of Consolidation					

Vertical Displacements (10^{-2} m)

	Points of the Dam Section				
	CC	CM	CL	UM	DM
End of Construction					
End of Impounding					
End of Consolidation					

Pore Pressure (MPa)

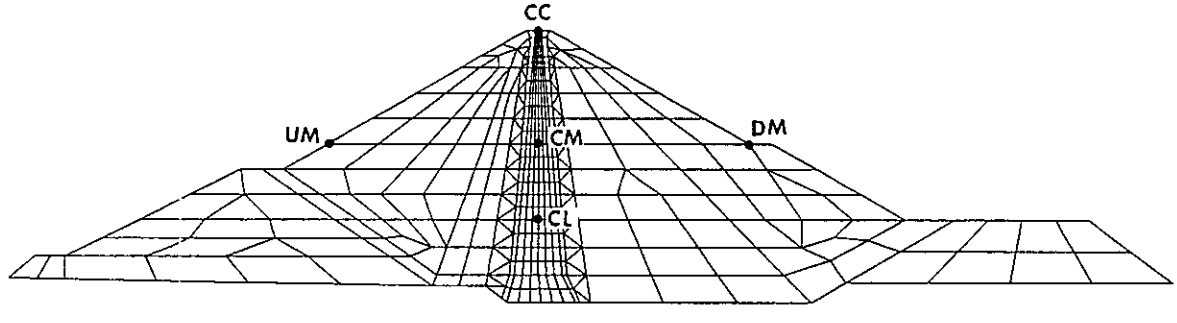

Table 3 : 3rd Benchmark Workshop - Theme B1
GENERAL SUMMARY : Results of displacements and pore pressure after each phase

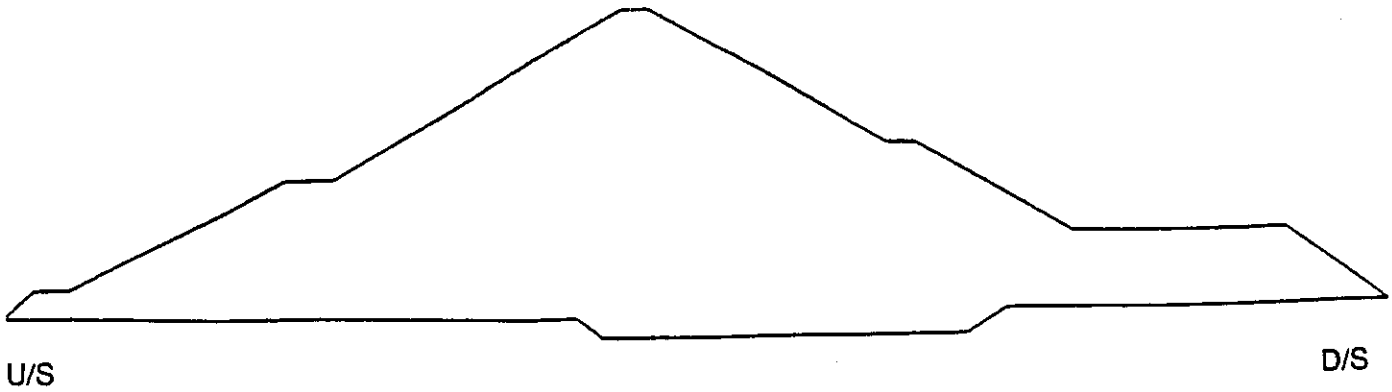

End of Construction

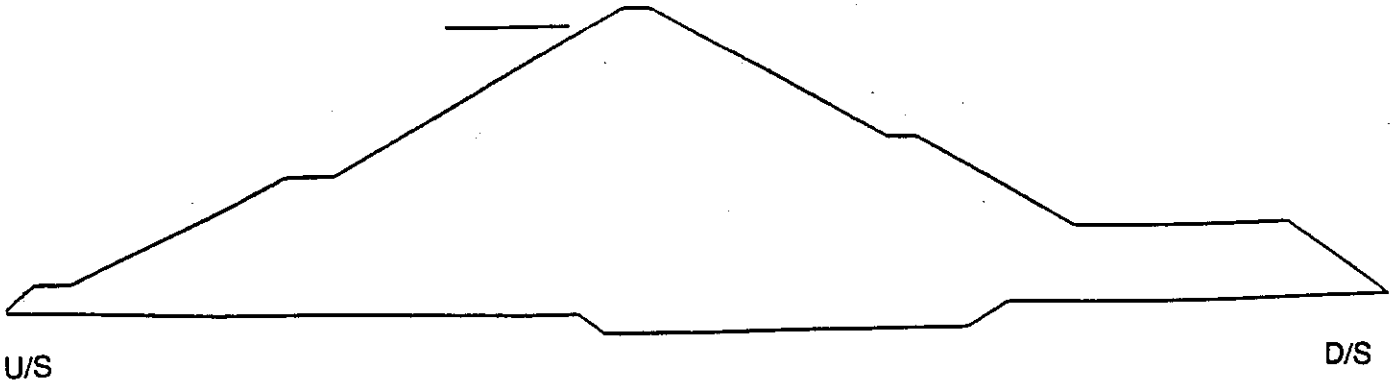

End of Impounding

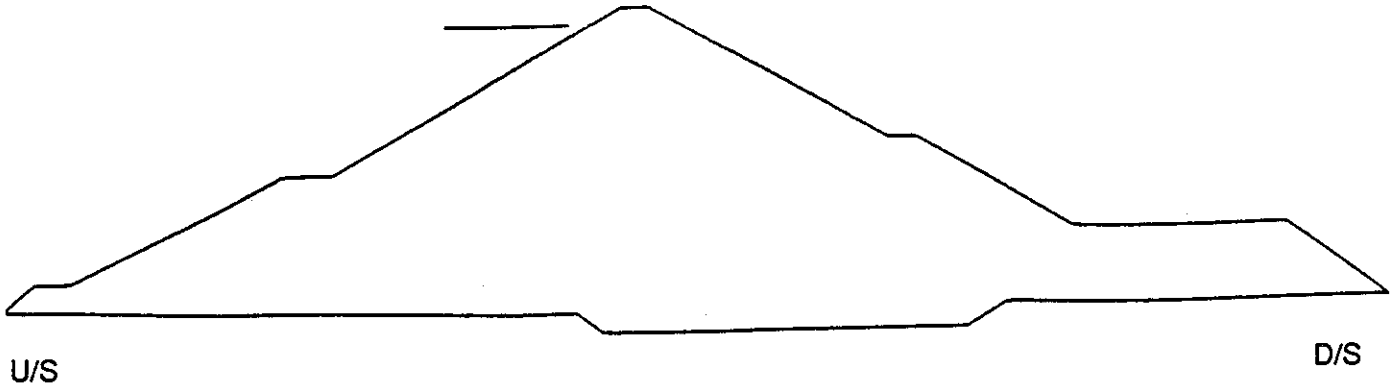

End of Consolidation

Fig. 4 : 3rd Benchmark Workshop - Theme B1
Template for stress and pore pressure distribution

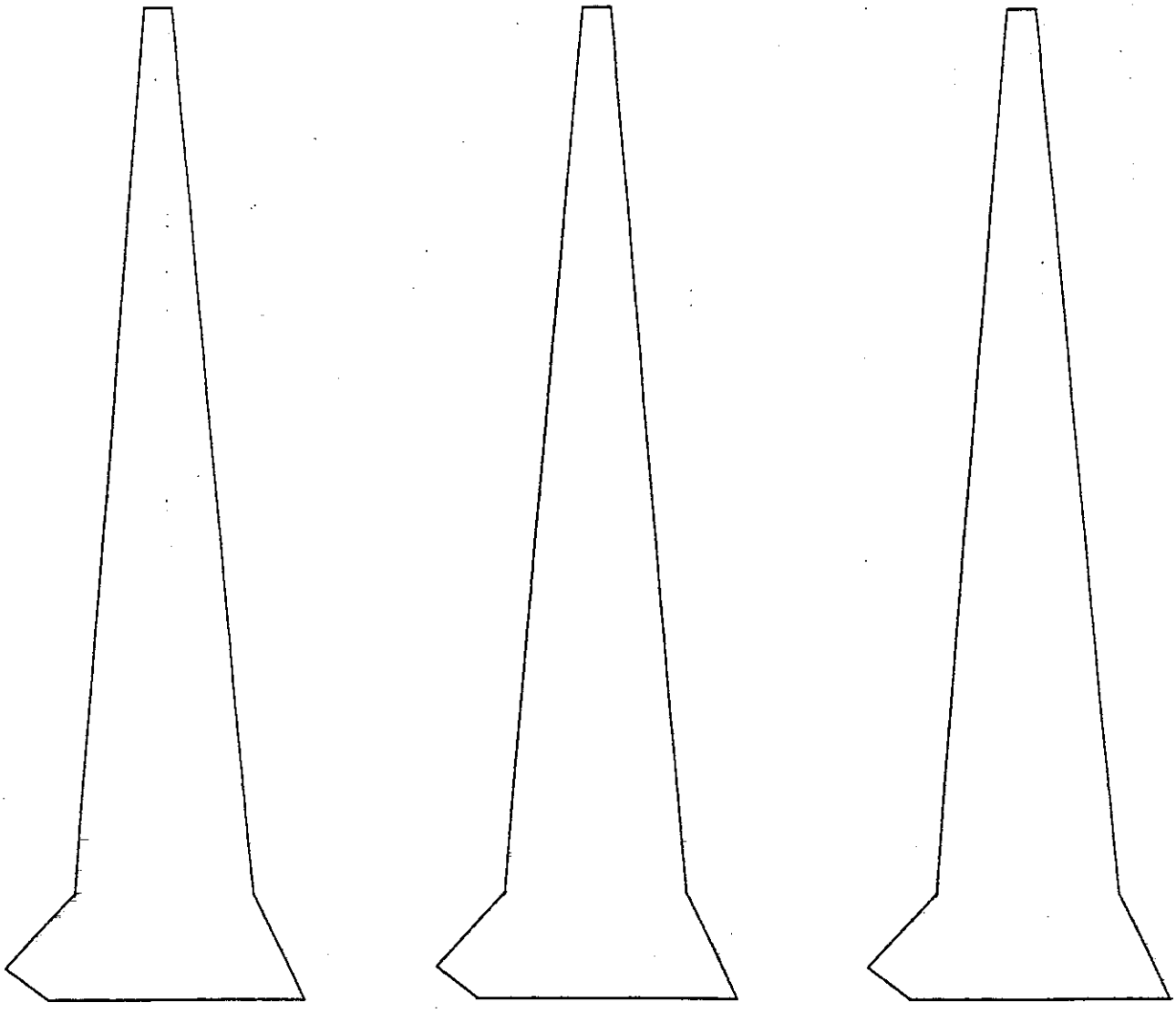

Fig. 5 : 3rd Benchmark Workshop - Theme B1
Template for pore pressure distribution
Zoom on the Core Region

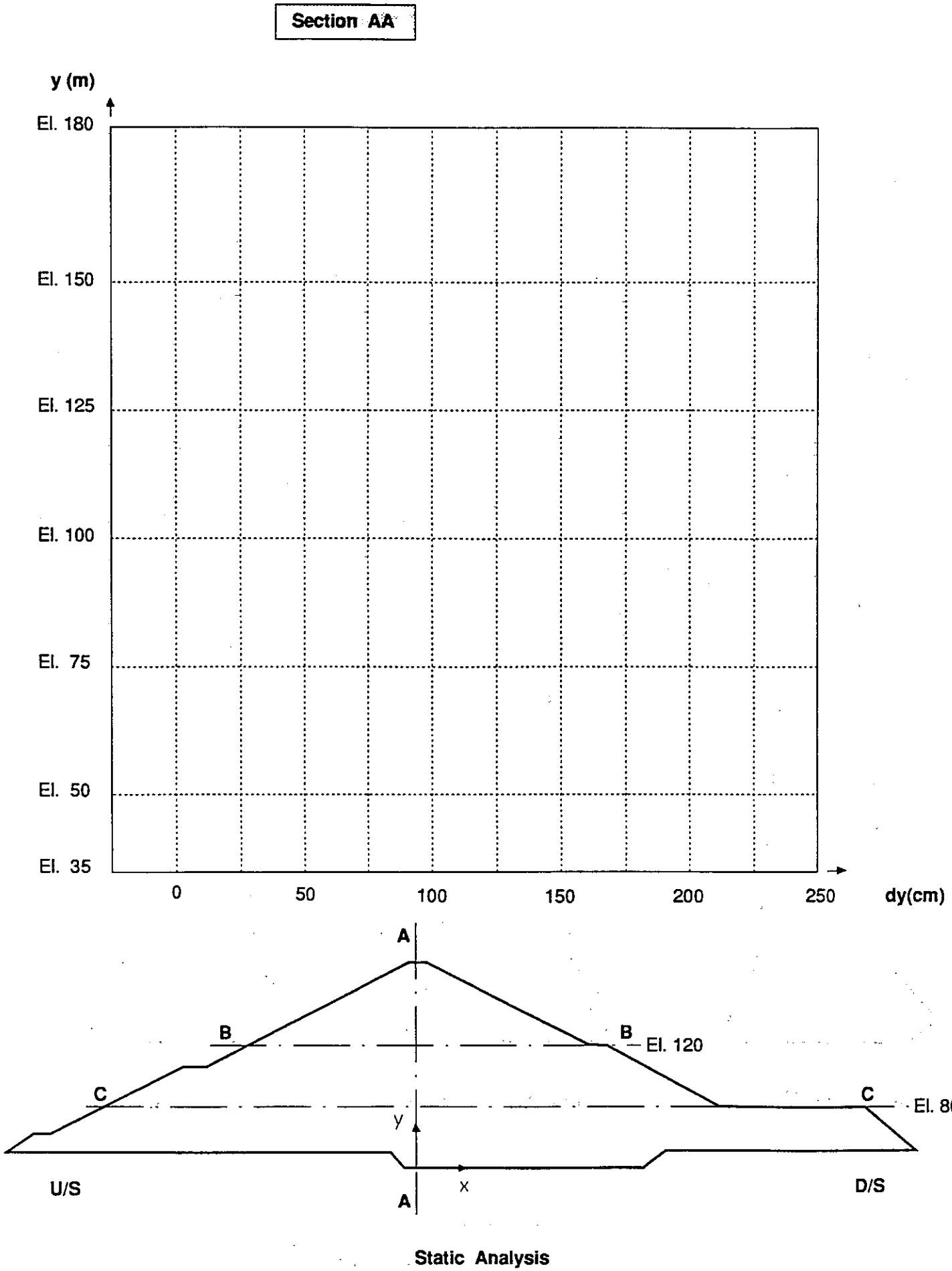

Fig. 6 : 3rd Benchmark Workshop - Theme B1
Template for the settlements

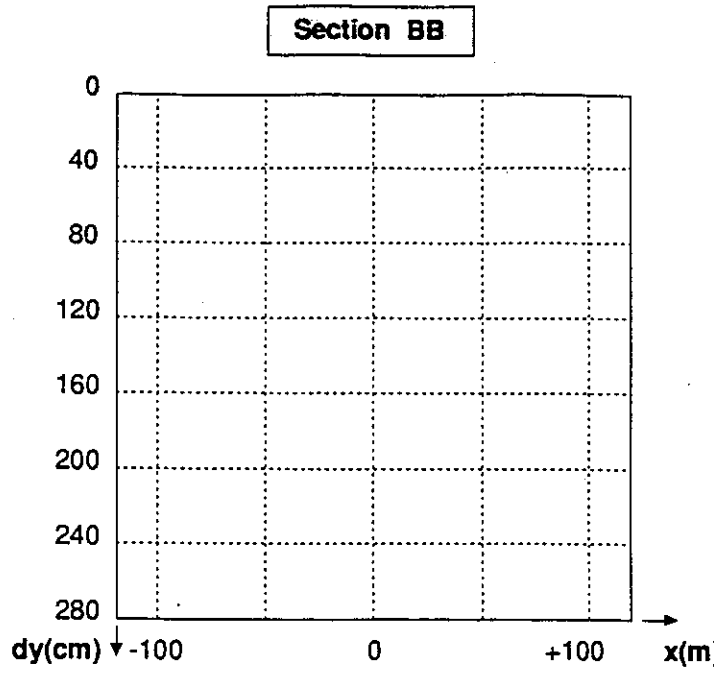

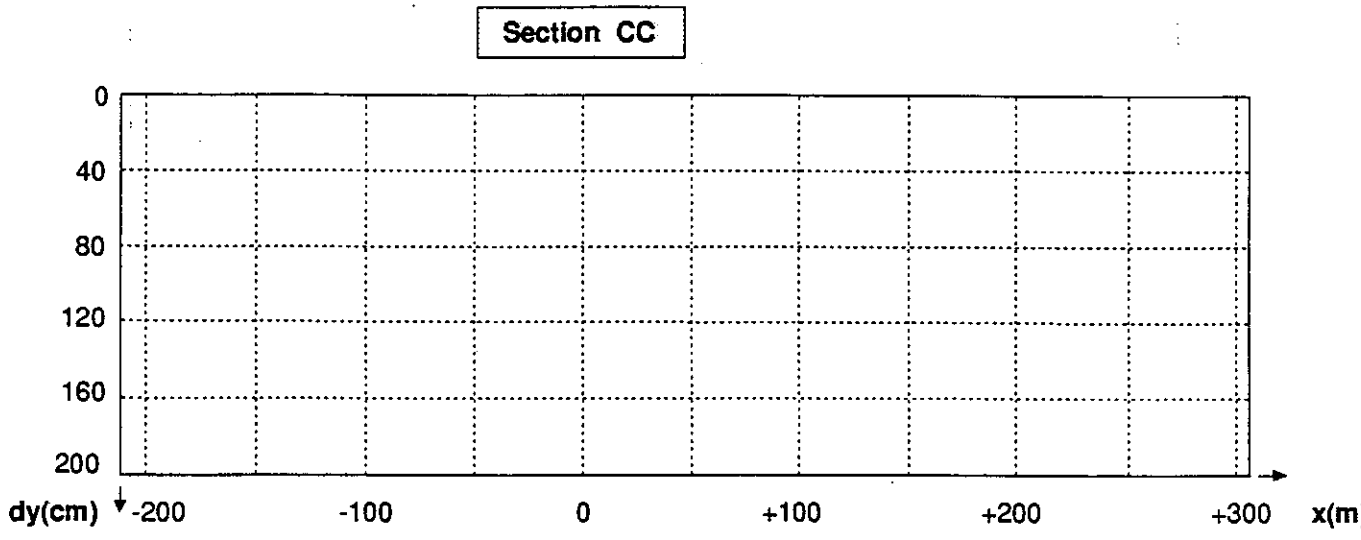

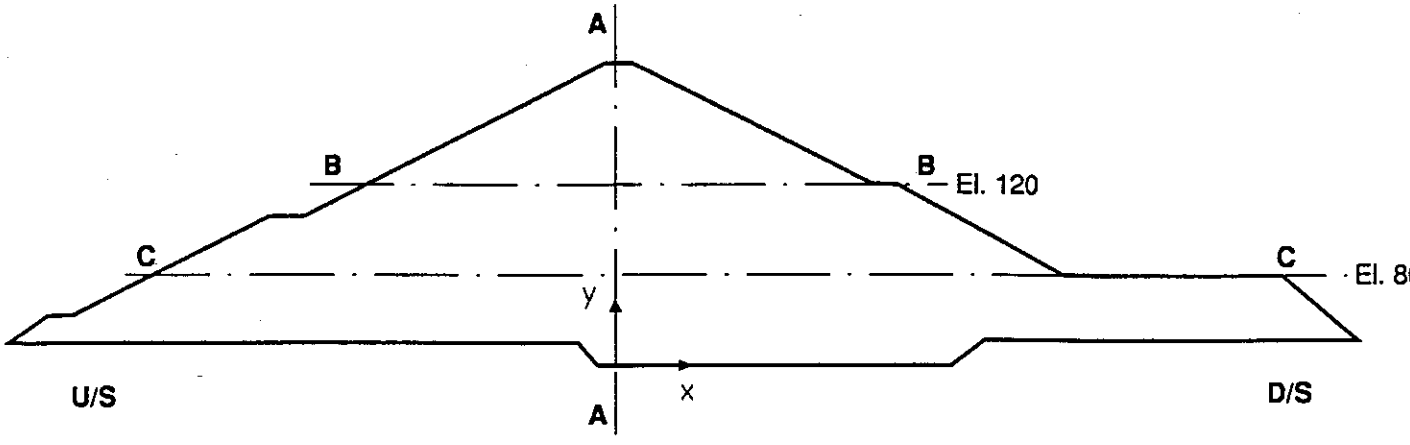

Fig. 7 : 3rd Benchmark Workshop - Theme B1
Template for the settlements

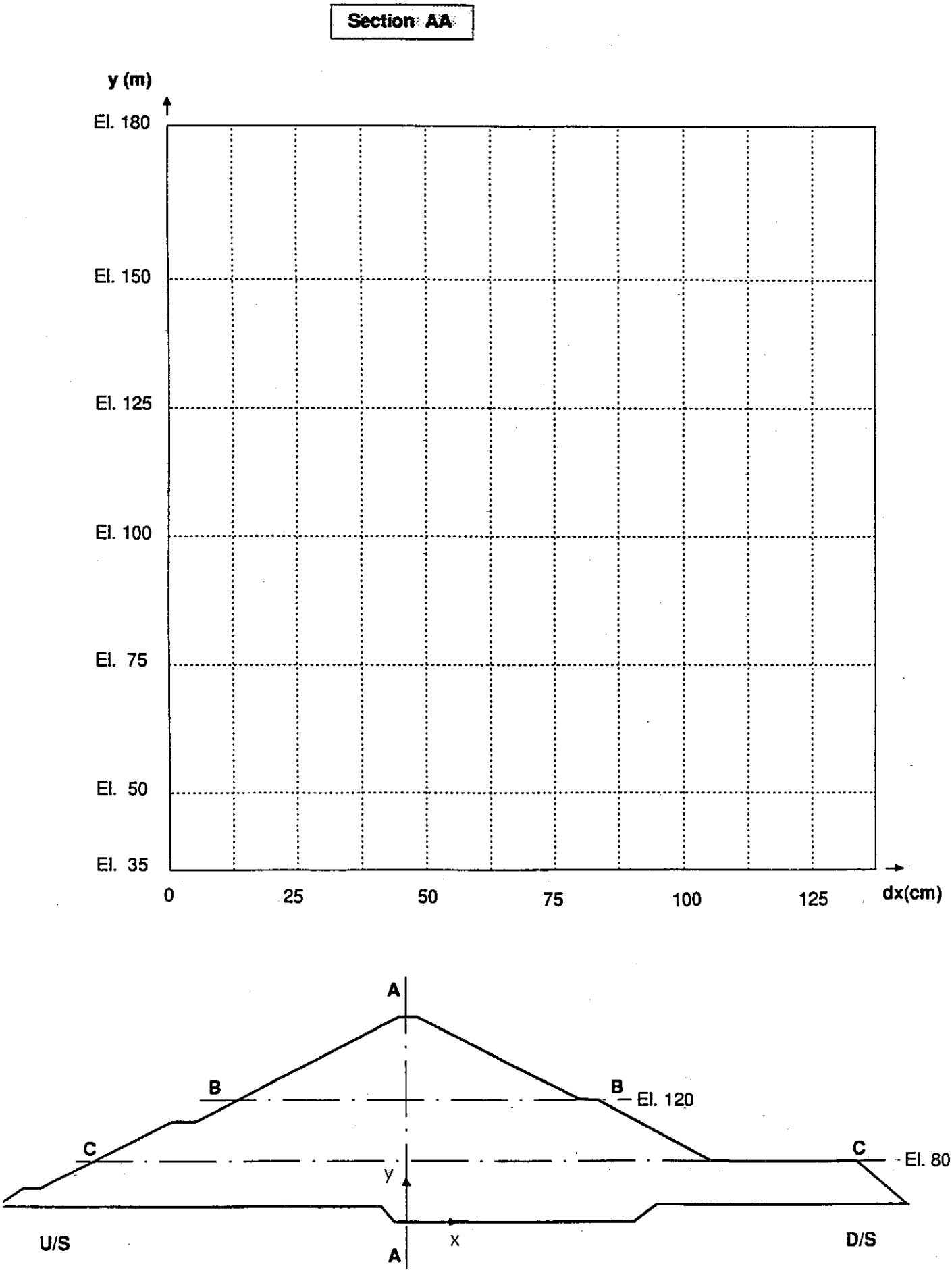

Fig. 8 : 3rd Benchmark Workshop - Theme B1
Template for the horizontal displacements

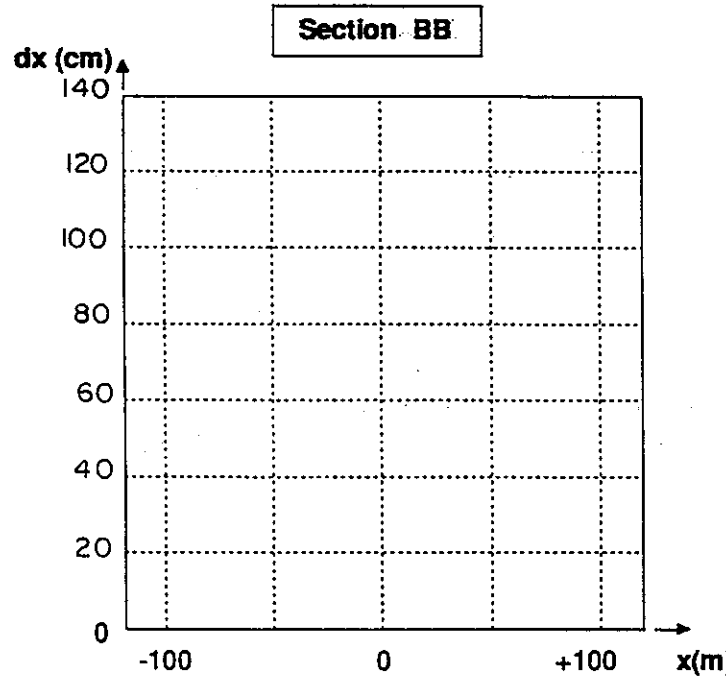

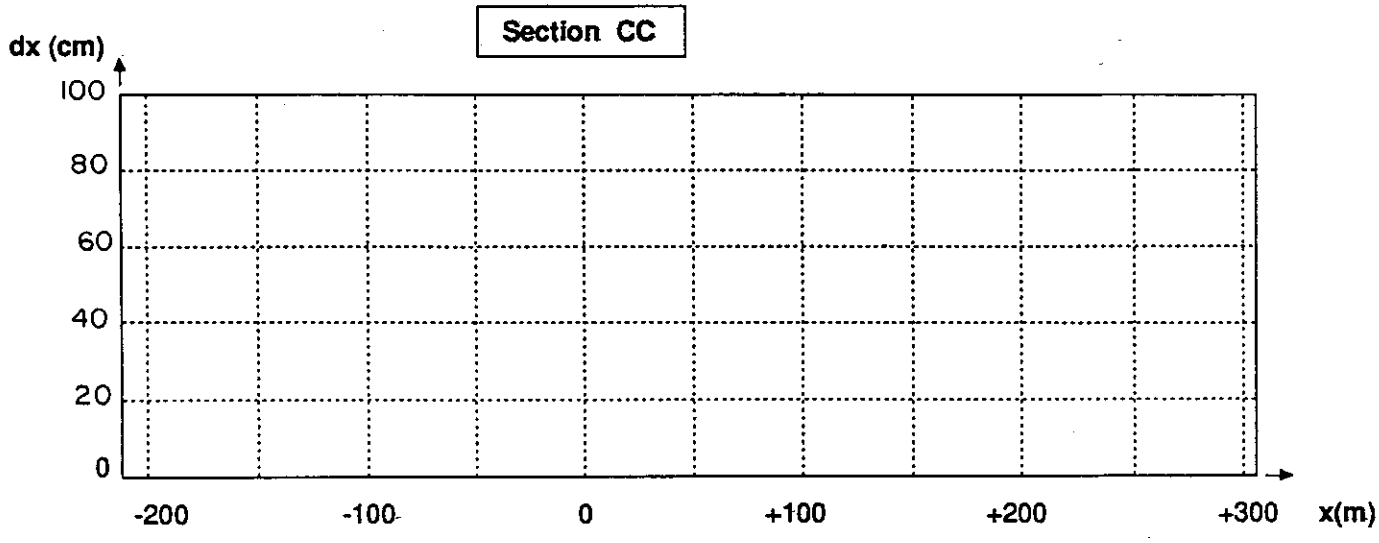

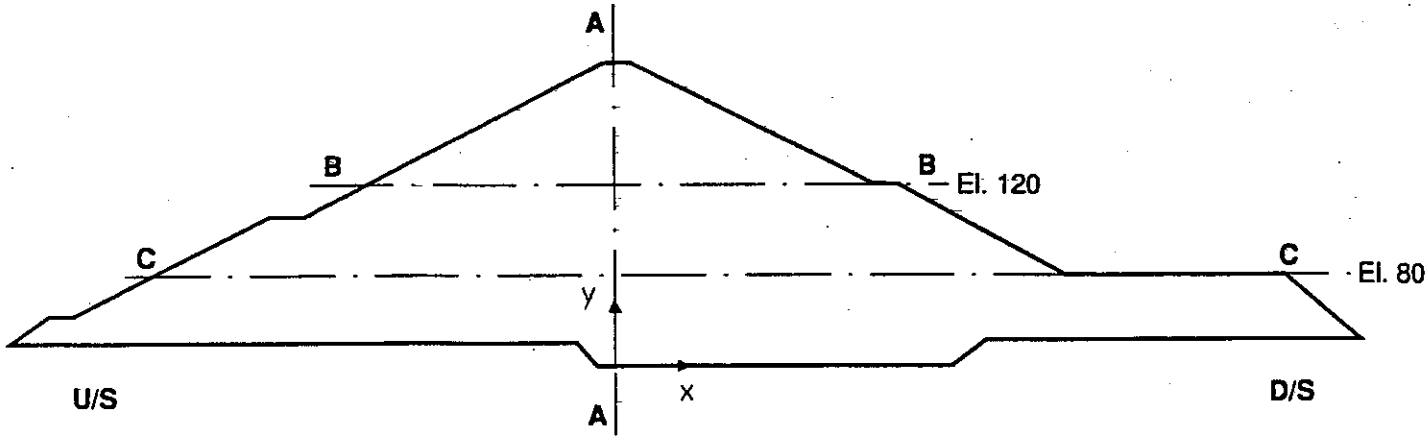

Fig. 9 : 3rd Benchmark Workshop - Theme B1
Template for the horizontal displacements

Third ICOLD Benchmark Workshop on Numerical Analysis of Dams
Paris (France), September 29-30, 1994

ADDENDUM
to Theme B1
Evaluation of pore pressure and settlements of an embankment dam under static loadings

The Mohr Coulomb constitutive model cannot be implemented analytically in finite element programs. Usually, it is integrated by using a numerical algorithm or its yield surface is simplified, or a simpler constitutive model is used (like Drücker Prager model). Therefore discrepancies in the results of finite element computations may be due to the numerical implementation of the constitutive model used by each participant. In order to quantify these discrepancies, it is required to provide the results of a drained triaxial test and an undrained triaxial test with the same following characteristics, **for the core material only** :

- confining pressure $\sigma_3 = 0.5$ MPa,
- amplitude of axial strain : 0 to 10 %.

The following results must be given

- for the drained triaxial test :
  - deviatoric stress ($q = \sigma_1 - \sigma_3$) vs. axial strain ε_1 curve,
  - volumetric strain (ε_v) vs. axial strain ε_1 curve,
  - the value of the maximum deviatoric stress q_{max},
  - the value of the minimum volumetric strain ε_v^e,
  - the value of the axial strain ε_1^e when $\varepsilon_v = \varepsilon_v^e$

- for the undrained triaxial test :
  - deviatoric stress ($q = \sigma_1 - \sigma_3$) vs. axial strain ε_1 curve,
  - pore pressure (u) vs. axial strain ε_1 curve,
  - deviatoric stress ($q = \sigma_1 - \sigma_3$) vs. mean effective stress $p' = (\sigma'_1 + 2\,\sigma'_3) / 3$ curve,
  - the value of the deviatoric stress q at $\varepsilon_1 = 10\%$,
  - the value of the excess pore pressure u at $\varepsilon_1 = 10\%$,
  - the value of the maximum excess pore pressure u_{max} ,
  - the value of the axial strain ε_1^e when $u = u_{max}$,
  - the value of the deviatoric stress q when $u = u_{max}$.

NOTES

NOTES

Third Benchmark Workshop on
NUMERICAL ANALYSIS OF DAMS
Gennevilliers, France, September 29-30, 1994

THEME B1

Evaluation of pore pressure and settlements of an embankment dam under static loadings

SYNTHESIS

&

COMPARISON OF RESULTS

Third Benchmark Workshop on Numerical Analysis of Dams
Gennevilliers (France) - September 29-30, 1994

Theme B1 :

EVALUATION OF PORE PRESSURE AND SETTLEMENTS OF AN EMBANKMENT DAM UNDER STATIC LOADINGS

SYNTHESIS

O.OZANAM*, G. LA BARBERA**

**Coyne et Bellier, Bureau d'Ingénieurs Conseils*
9, Allée des Barbanniers - F-92632 Gennevilliers CEDEX - France
*** ISMES S.p.A.*
Viale Giulio Cesare, 29 - I - 24124 Bergamo BG - Italy

Seven contributions were received for theme B1. Four of them are issued by French companies or laboratories. These contributions can be divided into three groups :

⇒ those devoted to theme B1 :

- GEFDYN used by Coyne et Bellier - fully coupled analysis [5];
- OMEGA used by ISMES and ENEL - fully coupled analysis [2];
- PECPLAS used by Ecole Centrale de Lille - uncoupled and partially coupled analysis [7];
- S.I.C.3 used by CEMAGREF - partially coupled analysis [1];

⇒ those devoted to theme B2 :

- GEFDYN used by EDF/CNEH - 2 applications in fully coupled analysis (paper inserted in section B1) [3];
- MATLOC used by the Civil Engineering Institute of Bucharest - fully coupled analysis (paper inserted in section B2) [6];

⇒ one extra contribution :

- GEFDYN used by Harza - fully coupled analysis in the core [4].

The extra contribution was accepted because it deals with exactly the same problem as that proposed in theme B1, but with another dam. Therefore it is not included in the comparison of results.

The contributions devoted to theme B2 are included here either because the participants did not have sufficient time to perform the whole static and dynamic analysis proposed for theme B2 or because the Committee considered that sufficient interesting results on their static computations were provided by the authors. In both cases, the constitutive model and parameters sets used in the computations are different from those proposed in the Benchmark specifications. This will explain some discrepancies.

The contributions devoted to theme B1 used either the Mohr Coulomb plasticity criterion (Coyne et Bellier, Ecole Centrale de Lille) or an equivalent plasticity criterion (ISMES by using a Drücker Prager model with an equivalent friction angle, CEMAGREF by using the C.J.S. elastoplastic model, which is a regularized approximation of the Mohr Coulomb model).

1. MAIN ASSUMPTIONS OF EACH PARTICIPANT

1.1 Numerical model

Table 1 summarizes the main numerical features adopted by each participant for each computation phase. Three main families of methods can be seen:

- *fully coupled analysis*, in which the mechanical equilibrium and the balance equation of the fluid contain the coupled terms and are solved at the same time in order to provide results in terms of displacements and pore pressure;
- *partially coupled analysis*, in which the pore pressure distribution is first computed by using a flow balance equation and secondly introduced as external forces in the mechanical equilibrium; some iterations between these two computations could be performed in order to improve the coupling;
- *uncoupled analysis*, in which the pore pressure distribution is not taken into account; only the mechanical equilibrium is solved and results are displacement.

Inside the family relative to the fully coupled analyses, different approaches are proposed:

- *fully coupled analysis in the whole dam*, and results in terms of displacements and *pore pressure* (EDF/CNEH);
- *fully coupled analysis in the core* only and uncoupled analysis elsewhere with results in terms of displacements and *pore pressure* (Coyne et Bellier, CEI of Bucharest);
- *fully coupled analysis in the core* (and filters) only without transient flow during impounding and uncoupled analysis elsewhere with results in terms of displacements and *excess pore pressure* (ISMES/ENEL).

With such fully coupled analyses the simulation of the different phases is performed continuously with the same numerical model and software.

The partially coupled analysis was used by the CEMAGREF at each phase and by Ecole Centrale de Lille at the steady state phase. With this type of analysis, the method depends on the loading at each phase:

- during the construction phase, a coupled analysis is performed with the assumption of a fully undrained core material; thus the excess pore pressure in the core is deduced from the volumetric strain and the displacement generated by the placing of each layer is computed according to the mechanical equilibrium, to the elastoplastic Mohr Coulomb model, and to the « undrained » excess pore pressure.
- during impounding, the displacement generated is first computed with the assumption of undrained core material as previously; then the volumetric strain variation is introduced in the flow equation, which provides the transient pore pressure distribution in the whole dam; lastly the displacement is corrected by taking the pore pressure distribution into account.
- at the steady state, the pore pressure distribution in the whole dam is computed with the flow equation and then introduced as an external force in the mechanical equilibrium in order to compute displacements which take into account the pore pressure.

The uncoupled analysis on the whole dam was used by the Ecole Centrale de Lille for the construction phase only: for the placing of each layer, the displacement is computed according to the mechanical equilibrium with the assumption of fully drained materials.

Table 1 : Recapitulative table of the different methods used for theme B1

software	company	mesh	constit. model	phases			
				constr.	1st consolid	impounding	steady state
GEFDYN	EDF CNEH	standard	DP(a) +H	(U,P)	-	ditto	ditto
GEFDYN	EDF CNEH	standard	Hyp(na) +H	(U,P)	-	ditto	ditto
GEFDYN (1)	Coyne et Bellier	standard	M C(na)	core : (U,P) elsewhere : (U)	ditto	ditto	ditto
MATLOC	CEI Bucharest	less refined	Duncan Chang	core : (U,P)	ditto	ditto	ditto
OMEGA (2)	ISMES ENEL	standard	D P(a)	core, filters : (U,ΔP) elsewhere : (U)	ditto	ditto	ditto
PECPLAS	ECLille	quadr. only	M C(na)	(U)	-	-	(P) → (U)
S.I.C.3 (3)	CEMA GREF	standard	C.J.S. (na)	core : (P) → (U) elsewhere : (U)	-	(U_0) → (P) → (U)	(P) → (U)
GEFDYN	Harza	other dam	H(dam) +D P(F)	core : (U,P) elsewhere : (U)	ditto	ditto	ditto

(1) saturated/unsaturated material
(2) no transient seepage
(3) no transient flow - unsaturated material
(a) associated flow rule

MC : Mohr Coulomb constitutive model
DP : Drücker Prager constitutive model
H : Hujeux/Aubry constitutive model
(na) no associated flow rule

(U,P) coupled model with displacement and pore pressure as unknowns
(U,ΔP) coupled model with displacement and excess pore pressure as unknowns
(U) purely mechanical model with displacement as unknown

1.2 Hydraulic boundary conditions

Table 2 summarizes the boundary conditions adopted by each participant (if they are known) :

- on the upstream (U/S) and downstream (D/S) faces of the core in the case of a coupled analysis in the core only,
- on the upstream (U/S) and downstream (D/S) faces of the dam in the case of a coupled or partially coupled analysis in the whole dam.

These boundary conditions are the most important factors in coupled computations. All participants have adopted the assumption of an impervious foundation (except the extra contribution of Harza). The boundary conditions are of three main types (Fig. 1):

- the pore pressure is imposed at a specific value; usually this value is set either to zero (p=0), if there is no water outside the coupled zone, or to the hydrostatic pressure ($p=p_{hyd}$) if there is water under hydrostatic conditions outside the coupled zone; this boundary condition means that flow can occur through the boundary (inside or outside flow); this flow exists certainly if there is water outside the coupled zone, but it is more uncertain if not (especially during construction).
- no flow is imposed (ϕ=0); this assumption seems to be reasonable during construction and impounding (upstream above water level and downstream), but it is too pessimistic for the steady state.
- seepage boundary conditions correspond to variable boundary conditions as a fonction of the pore pressure inside the coupled zone and the water pressure outside it; if there is no water outside, no flow is imposed if the material is unsaturated, or the pore pressure is imposed at zero (atmospheric pressure) if the material is saturated; if there is water outside, the hydrostatic pressure is imposed at the pore pressure; this simple algorithm is summarized by the sketch drawn in Figure 1.

The boundary conditions adopted by ISMES cannot exactly be attached to one of these three cases. Indeed, during the construction phase, the boundary condition of no excess pore pressure corresponds exactly to the condition of pore pressure set to zero. But during the impounding and the steady state phases, the same boundary condition is used, with the additional assumption of hydrostatic pore pressure in upstream rockfill and in the core. This means that :

- during impounding the boundary condition is $p=p_{hyd}$ on upstream and downstream faces,
- at the steady state the core is fully saturated, i.e. the downstream core face is impervious. This is equivalent to a no flow boundary condition on the downstream face of the core.

It also implies that the mechanical hydrostatic pressure is fully applied on this downstream core face. This boundary condition, which seems to be relatively too pessimistic, will then be the source of the main discrepancies obtained on the displacement curves (see section 2).

The coupled zone adopted in the computation is either the whole dam or the core. Pratically, it would be sufficient to restrict the coupled zone to the core only, because the pore pressure in the permeable upstream shoulders is known *a priori* and the downstream shoulders are usually dry. In fact, with some software it may be easier to enlarge the coupled zone to the whole dam, in order to have a kind of seepage boundary condition at the core faces due to the contrast of permeabilities between the core and filter materials.

Table 2 also indicates the permeability coefficients and the horizontal/vertical ratio used in each computation. This ratio mainly influences the pore pressure distribution at the steady state.

Table 2 : Recapitulative table of the hydraulic boundary conditions used for theme B1

software	company	permeab. in m/s	coupled zone	phases			
				constr.	1st consolid	impounding	steady state
GEFDYN	EDF CNEH	$k_H=k_V$ $=2.10^{-10}$	dam	U/S : p=0 D/S : p=0	-	U/S : $p=p_{hyd}$ D/S : p=0	ditto
GEFDYN	EDF CNEH	$k_H=3k_V$ $=6.10^{-10}$	dam	U/S : p=0 D/S : p=0	-	U/S : $p=p_{hyd}$ D/S : p=0	ditto
GEFDYN	Coyne et Bellier	$k_H=4k_V$ $=8.10^{-10}$	core	U/S : seepage D/S : seepage	ditto	U/S : $p=p_{hyd}$ D/S : seepage	ditto
MATLOC	CEI Bucharest	$k_H=k_V$ $=8.10^{-10}$	core	?			
OMEGA	ISMES ENEL	$k_H=4k_V$ $=8.10^{-10}$	core	U/S : $\Delta p=0$ D/S : $\Delta p=0$	ditto	ditto + $p=p_{hyd}$ in the core	ditto + $p=p_{hyd}$ in the core
PECPLAS	ECLille	$k_H=4k_V$ $=8.10^{-10}$	dam	-	-	-	U/S : $p=p_{hyd}$(U/S) D/S : $p=p_{hyd}$(D/S)
S.I.C.3	CEMA GREF	$k_V=4k_H$ $=8.10^{-10}$	dam	U/S : $\phi=0$ D/S : $\phi=0$	-	U/S : $p=p_{hyd}$ D/S : $\phi=0$	ditto
GEFDYN	Harza	$k_H=k_V$ $=1.10^{-8}$	core	U/S : seepage D/S : seepage	ditto	U/S : $p=p_{hyd}$ D/S : seepage	ditto

p : pore pressure
p_{hyd} : hydrostatic pore pressure
Δp : excess pore pressure
ϕ : flow
k_V vertical permeability
k_H horizontal permeability

2. COMPARISON OF RESULTS

No comparison of effective stress distribution will be performed because it is needless. Indeed the total stresses should be approximately identical for all participants, because they depend on the material densities and on the geometry of the earthfill and it is sufficient to compare the pore pressure to evaluate the results of each contribution.

2.1 Triaxial tests

The Mohr Coulomb constitutive model cannot be implemented analytically in finite element programs. Usually, it is integrated by using a numerical algorithm or its yield surface is simplified, or a simpler constitutive model is used (like the Drücker Prager model). Therefore discrepancies in the results of finite element computations may be due to the numerical implementation of the constitutive model used by each participant. In order to quantify these discrepancies, it is required to provide the results of a drained triaxial test and an undrained triaxial test with the following characteristics, for the core material only :

- confining pressure $\sigma_3 = 0.5$ MPa,
- amplitude of axial strain : 0 to 10%.

Typical curves for **drained triaxial tests** are represented in Fig. 2 : deviatoric stress ($q=\sigma_1 - \sigma_3$) vs. axial strain (ε_1) and volumetric strain (ε_v) vs. axial strain. The comparison is performed on the values obtained at some particular points of these curves :

- the value of the maximum deviatoric stress q_{max},
- the value of the minimum volumetric strain ε_v^e,
- the value of the volumetric strain at 10% of axial strain,
- the value of the axial strain ε_1^e, when $\varepsilon_v = \varepsilon_v^e$, elastic limit.

The different values obtained by the participants are represented in Figure 3. No significant differences can be observed for the maximum deviatoric stress, the elastic limit of the axial strain and the minimum volumetric strain, because these values depend mainly on the elastic characteristics of the constitutive model and also on the plastic yield criterion. The small discrepancies are due to the precision of the provided values; some of them have been rounded. The influence of the numerical implementation of the plastic flow rule is obvious on the volumetric strain at 10% of axial strain, because this value depends on the associated or non-associated character of the flow rule and on the dilatancy angle. Therefore ISMES, which uses an associated flow rule, obtains a large dilatancy (11%). Coyne et Bellier, which tested two different implementations of the Mohr Coulomb model, and the Ecole Centrale de Lille obtain values (resp. 0.81% and 0.8%) very close to the analytical solution (0.84%). With the C.J.S. non-associated constitutive model CEMAGREF obtains a slightly larger volumetric strain (1.3%).

Typical curves for **undrained triaxial tests** are represented in Fig. 4 : deviatoric stress ($q=\sigma_1 - \sigma_3$) vs. axial strain (ε_1), volumetric strain (ε_v) vs. axial strain and deviatoric stress vs. mean effective stress ($p' = (\sigma'_1 + 2\,\sigma'_3)/3$). The comparison is performed on the values obtained at some particular points of these curves :

- the value of the deviatoric stress q_{max} at $\varepsilon_1 = 10\%$,
- the value of the excess pore pressure u_f at $\varepsilon_1 = 10\%$,

- the value of the maximum excess pore pressure u_{max} ,
- the value of the axial strain ε_1^e when $u=u_{max}$,
- the value of the deviatoric stress q_e when $u=u_{max}$.

The different values obtained by the participants are represented in Figure 5. As in the case of the drained triaxial test, the only significant discrepancy comes from the associated flow rule used by ISMES. It is clearly readable on the deviatoric stress and the excess pore pressure at an axial strain of 10%. One inexplicable difference concerns the deviatoric stress q_e computed by the Ecole Centrale de Lille; it is probably a misprint.

In Table 1 the associated character of the constitutive law is given for each contribution. Only two computations have been performed with an associated flow rule.

The large dilatancy generated by the standard associated Mohr Coulomb model is one of its well known drawbacks. This will have an influence on the computed displacements and excess pore pressure presented by ISMES, in addition to their particular hydraulic boundary conditions.

2.2 Pore pressure distribution

The comparison of pore pressure distribution in the core is rich in information: form of the contour lines, gradient of pore pressure, maximum pore pressure. Figures 6 to 11 represent the pore pressure contour lines in the core provided in each contribution and Table 3 the maximum computed values.

Table 3 : Maximum pore pressure computed in the core at each loading phase

software	company	permeability in m/s	maximum pore pressure (MPa)		
			end of construction	end of impounding	end of consolidation
GEFDYN	EDF/CNEH	$k_H=k_V=2.10^{-10}$	2.0	1.6	1.3
GEFDYN	EDF/CNEH	$k_H=3k_V=6.10^{-10}$	1.3	1.4	1.3
GEFDYN	Coyne et Bellier	$k_H=4k_V=8.10^{-10}$ init. saturated	0.9	1.2	1.3
GEFDYN	Coyne et Bellier	$k_H=4k_V=8.10^{-10}$ init. unsaturated	1.1	1.2	1.3
OMEGA	ISMES ENEL	$k_H=4k_V=8.10^{-10}$	0.9	1.3**	1.3
S.I.C.3	CEMAGREF	$4k_H=k_V=8.10^{-10}$	1.0	1.2	1.3

** the minimum pore pressure at the core base is 0.7 MPa (instead of nearly zero)

The influence of the ratio between horizontal and vertical permeability coefficients on the pore pressure distribution at the end of impounding and at the steady state is noticeable in Figures 6 and 7 (EDF/CNEH) and 11.

The initial saturation taken into account by Coyne et Bellier ($S_0=0.96$ or $S_0=1$) has an influence during construction and slightly during impounding. This influence decreases with time and loading history. An initial degree of saturation less than 1 induces higher pore pressure during construction (Fig. 8 and 9), because of the lowest permeability in the unsaturated zone and of the no flow boundary condition at the unsaturated core faces.

ISMES presents the results in terms of excess pore pressure (Fig. 10). Therefore the contour lines at the end of construction are similar to those obtained by the other participants, but at the end of impounding they are completely different. In fact they have the same symmetrical shape as those obtained during construction but in terms of negative excess pore pressure instead of positive excess pore pressure. This is fully explained by the symmetrical boundary conditions chosen ($\Delta p=0 \Rightarrow p=p_{hyd}$ on both upstream and downstream core faces): the same inside flow is computed on both faces.

The results obtained by CEMAGREF (Fig. 11) are close to those provided by Coyne et Bellier, with two restrictions :

- the different permeability ratio ($k_V=4k_H$), which induces a different steady state,
- some numerical or graphical disturbances appear at the end of the construction phase.

2.3 Displacements along lines AA, BB and CC

Horizontal and vertical displacements were provided at the end of each phase along 3 main lines of the dam :

- line AA: vertical centre core line,
- line BB: horizontal line at elevation 120,
- line CC: horizontal line at elevation 80.

In each figure the available curves have been drawn and some points of other participants (CEI Bucharest, ECLille) have been superimposed.

a) end of construction

First the comparison of the settlement curves (Fig.12) computed by the participants, who used the specification data of theme B1, shows that :

- all the curves have approximately the same bell-shape,
- the largest settlements are computed by ISMES (180 cm maximum), because of the hydraulic boundary condition of zero pore pressure on the core faces, which allows the water to flow more rapidly,
- the smallest settlements are computed by CEMAGREF (135 cm maximum), because of the undrained core assumption, which induces larger excess pore pressure and therefore less consolidation effect,
- the intermediate settlements are computed by Coyne et Bellier (168 cm maximum), by using seepage boundary conditions, which automatically adapt the boundary condition to a no-flow or zero pore pressure condition, depending on the core state.

The other results obtained with different parameter sets and constitutive models can be compared to the 3 previous results:

- those of EDF/CNEH computed with the Drücker Prager model are very close to Coyne et Bellier's results, even if the boundary conditions are close to those of ISMES; the main reason is the low permeability used in both horizontal and vertical directions ($k_V=k_H$), which slows down the water flow and reduces the soil movement;
- those of EDF/CNEH computed with the hyperbolic model is close to CEMAGREF's results, even if the permeability ratio was increased ($k_H=3k_V$); the main reason is the completely different parameter set used in the rockfills.

- those of CEI of Bucharest are close to Coyne et Bellier's results, but insufficient information is provided by the authors on the boundary conditions (because the paper is devoted to theme B2);

The horizontal displacement curves, represented in Figure 13, present no scattering: the maximum displacement is around 12 cm, except for the results of CEI of Bucharest, which are very close to zero.

The same remarks are also available for sections BB and CC (Fig. 14 and 15), in which it clearly appears that the origin of the discrepancies comes from the core and that rockfill behaviour is more similar.

b) end of impounding

Contrary to the construction phase, the vertical displacements (settlements) are more homogeneous (Fig. 16a). This means that the settlements generated during impounding balance the discrepancies observed during construction. Figure 16b represents the settlements which occur between the end of construction and the end of impounding. This figure clearly shows that in the core :

- the incremental vertical displacement computed by CEMAGREF is settlement, (+15cm) because of the dissipation of pore pressure generated during the construction phase,
- a small up movement is computed by Coyne et Bellier (-7 cm) because of the buoyancy forces applied in the upstream shoulder,
- a large up movement is computed by ISMES (-50 cm) because of the buoyancy forces applied in the upstream shoulder and in the core, but also because of the dilatancy effect due to the associated flow rule of the Mohr Coulomb model, which amplifies the phenomenon.

The effect of the buoyancy forces applied in the upstream shoulder during impounding is also clearly readable in Figures 18a and 18b. This normal numerical result is not representative of the observed rockfill settlements during impounding. No coherent constitutive model is presently available to deal with this phenomenon properly.

The main discrepancies concern the horizontal displacements (Fig. 17) and especially in the upper half of the core. Indeed the curves are identical from elevation 35 to elevation 100. But above elevation 100:

- Coyne et Bellier and CEMAGREF obtain very similar bell-shaped curves, with a crest downstream displacement of 75 to 80 cm and a maximum displacement of 120 cm;
- ISMES obtains a very large horizontal downstream displacement at the crest (125 cm), which is slightly smaller than the maximum displacement (135 cm); this very large crest movement is due to the assumption of a fully saturated core and to the fact that the mechanical horizontal hydrostatic pressure is consequently applied on the downstream core face; this is confirmed by the horizontal displacement curves drawn along line BB, as shown in Figure 19;
- the points provided by CEI of Bucharest are in agreement with the results of Coyne et Bellier and CEMAGREF, with a slightly larger displacement at the crest (92 cm)
- the horizontal displacements provided by EDF are either half of the values computed by Coyne et Bellier and CEMAGREF (with the hyperbolic model) or similar in the bottom half part of the core and surprisingly large (160 cm) at the crest with the Drücker Prager model; in this last case the curve is no longer bell-shaped; these discrepancies are mainly explained by the different parameter sets and constitutive model used by the participants.

c) end of consolidation

The settlement profiles (Fig. 20a) are similar to those obtained at the end of impounding. The incremental settlements (Fig. 20b), that occur only during the consolidation phase, correspond:

- either to down movement (positive increment), which is coherent with a dissipation of the positive excess pore pressure generated during the construction,
- or to up movement (negative increment), which is coherent with the global increase of pore pressure due to the water inflow, induced by the reservoir impounding - this last computed movement is in agreement with the measured data.

In Figure 20a the curve computed by Ecole Centrale de Lille has been added. The smallest settlements could be explained either by the partially coupled approach, which does not take account of the effect of the skeleton deformation on the pore pressure distribution, or by a different ratio of permeability (not indicated in the paper);

The discrepancies at the end of impounding already observed on the horizontal displacement curves are slightly amplified during consolidation (Fig.21a and 21b). The displacement provided by the Ecole Centrale de Lille is very large at the crest (116cm) and the curve is like those provided by ISMES and EDF/CNEH (with Drücker Prager).

Figure 22 points out the large step obtained by ISMES on the settlement profiles in sections BB and CC at the downstream core boundary; this results from the assumption of a fully saturated core and therefore from the hydrostatic mechanical pressure applied on the downstream core face. Another remark could be made: the settlements in rockfill computed by EDF/CNEH with both constitutive models are very large (142 cm and 180cm) in the downstream shoulders and larger than those obtained in the core. The same phenomenon is also observed on the curve in section CC provided by ISMES.

2.4 Computation time

The computation time was provided by only some of the participants. As shown in table 4, these times vary from 4' with MATLOC to more than 4 hours with GEFDYN.

Table 4 : Computation time used by each participant

software	company	Authors	Hardware	CPU time
GEFDYN	Coyne et Bellier	O.Ozanam, B. Tardieu	HP9000/715	4h24' (MC2D) 8h12' (MC 3D)
MATLOC	CEI Bucharest	A. Popovici, I. Toma, R. Sarghiuta	AT486DX 33MHz	4'
OMEGA	ISMES-ENEL	G. La Barbera, A. Bani, G. Mazza'	CONVEX	21'
S.I.C.3	CEMAGREF	L. Guellouz, S. Bonelli	DEC Alpha 3000	2h47'

3. CONCLUSION

The comparison of the results clearly shows the large influence of the hydraulic boundary conditions and of the methodology used to modelize impounding.

Available in situ measurements [9,10,11,12] will be used to select the most credible results from the whole set of results. In particular, the form of the curves along vertical and horizontal sections after some months of consolidation shows that the large settlement in downstream shoulders does not exist in situ.

The comparison with in situ measurements is restricted by :

- the assumption of an impervious foundation - in reality, the permeability of the core is of the order of magnitude of 10^{-9} -10^{-10} m/s and the permeability of the rock close to the rock surfaces is probably of the order of magnitude of one lugeon, which is equivalent to 10^{-7}m/s; as a rule, the rock, even grouted, is less watertight than a clay core; in the next workshop this aspect should be dealt with-,
- the « striction » of rockfill during impounding, which is not modelized by the present constitutive models, because the mechanism is not clearly known.

In addition, the monitored section is not the section of maximum height used in the computation. This has a great influence on the settlements during construction. Figure 24b, which presents the theoretical settlement curves at the end of construction for the monitored section and for the computed section, points out that the settlement at elevation 80 in the core can be doubled when the height of the section varies from 120m to 145m. In order to reduce the effect of the section, the data measured at the end of construction has been corrected according to the following method.
The extrapolation proposed by O. Ozanam et al. [8] is made on maximum settlements along a centre vertical line as a function of embankment height during dam construction (Fig. 24a). Then the form of the settlement curve along the centre line is assumed to be parabolic. Extrapolated values put on the figures 12 to 15 are deduced from the parabolic curve at the end of construction drawn in Fig.24b. At the other stages (impounding and consolidation), the extrapolated settlement is obtained by adding the extrapolated value at the end of construction with the measured displacement increase after the end of construction.

In any case, the hydromechanical coupling in the core is an important phenomenon which cannot be neglected. The boundary conditions on the core faces should be :

- during impounding, hydrostatic pore pressure on the upstream face and pore pressure set to zero (and not « excess pore pressure set to zero ») on the upstream face above the water level and on the downstream face.
- during construction, no-flow generates too large an excess pore pressure and too small a settlement, and pore pressure set to zero induces the contrary result.

The seepage boundary conditions proposed by Coyne et Bellier seem to provide a realistic intermediate solution.

Concerning mechanical behaviour, the highly dilatant associated Mohr Coulomb model should be avoided and modified in order to allow a non-associated flow rule by introducing a dilatancy angle different from the friction angle.

In order to define a reference range of results for this type of analysis, the results of CEMAGREF, Coyne et Bellier and the Civil Engineering Institute of Bucharest could be considered as the most credible.

REFERENCES

[1] GUELLOUZ L., BONELLI S. (1994) : Evaluation of pore pressure and settlements of an embankment dam under static loadings (software S.I.C.3) - 3rd Benchmark Workshop on Numerical Analysis of Dams-Theme B1 - Gennevilliers (France) - September 29-30, 1994.

[2] LA BARBERA G., BANI A., MAZZA' G. (1994) : Evaluation of pore pressure and settlements of an embankment dam under static loadings (software OMEGA) - 3rd Benchmark Workshop on Numerical Analysis of Dams-Theme B1 - Gennevilliers (France) - September 29-30, 1994.

[3] LAIGLE F., FRY J.J., MAGNIN P. (1994) : Static analysis of El Infiernillo dam (software GEFDYN and UDAM) - 3rd Benchmark Workshop on Numerical Analysis of Dams -Theme B1 - Gennevilliers (France) - September 29-30, 1994.

[4] MARTIN P. P., SENGUPTA A. (1994) : Numerical analysis of Bath County Upper Reservoir dam (software GEFDYN) - 3rd Benchmark Workshop on Numerical Analysis of Dams -Theme B1 - Gennevilliers (France) - September 29-30, 1994.

[5] OZANAM O., TARDIEU B. (1994) : Evaluation of pore pressure and settlements of an embankment dam under static loadings: GEFDYN analysis - 3rd Benchmark Workshop on Numerical Analysis of Dams-Theme B1 - Gennevilliers (France) - September 29-30, 1994.

[6] POPOVICI A., TOMA I., SARGHIUTA R. (1994) : Nonlinear seismic analysis of an embankment dam (software MATLOC) - 3rd Benchmark Workshop on Numerical Analysis of Dams -Theme B2 - Gennevilliers (France) - September 29-30, 1994.

[7] SHAHROUR I., MROUEH H. (1994) : Analysis of the behaviour of an embankment dam using PECPLAS finite element program - 3rd Benchmark Workshop on Numerical Analysis of Dams -Theme B1 - Gennevilliers (France) - September 29-30, 1994.

[8] OZANAM O., LACROIX F., de BONNECHOSE E. (1992) : Static and dynamic coupled analyses of El Infiernillio dam - 2nd Benchmark Workshop on Numerical Analysis of Dams - Theme B - Bergamo (Italy) - July 16-17, 1992.

[9] MARSAL R.J. and RAMIREZ de ARELLANO L. : *El Infiermillo Dam - Observations during the Construction Period and First Filling of the Reservoir* - CFE, Mexico, 1965.

[10] MARSAL R.J., RAMIREZ de ARELLANO L., GUZMAN M.A. and ADAMA H.Z. : *El Infiernillo, in Behaviour of Dams built in Mexico* - Contribution to the XII ICOLD, UNAM/CFE, Mexico, (1976) - Chap. 7.

[11] F.G. VALENCIA : *Efectos en la presa El Infiernillo, Michoagan.* Chapter 4 - CFE Document.

[12] E. MORENOS, J.M. CAMPOS (1980) : *Behaviour records of El Infiernillo and La Villita dams from construction to March 1979.* Chapter 5 in "Performance of El Infiernillo and La Villita dams in Mexico including the earthquake of March 14, 1979". CFE - Mexico.

Third Benchmark Workshop on Numerical Analysis of Dams
Gennevilliers (France) - September 29-30, 1994

Theme B1 :

EVALUATION OF PORE PRESSURE AND SETTLEMENTS OF AN EMBANKMENT DAM UNDER STATIC LOADINGS

SYNTHESIS

FIGURES

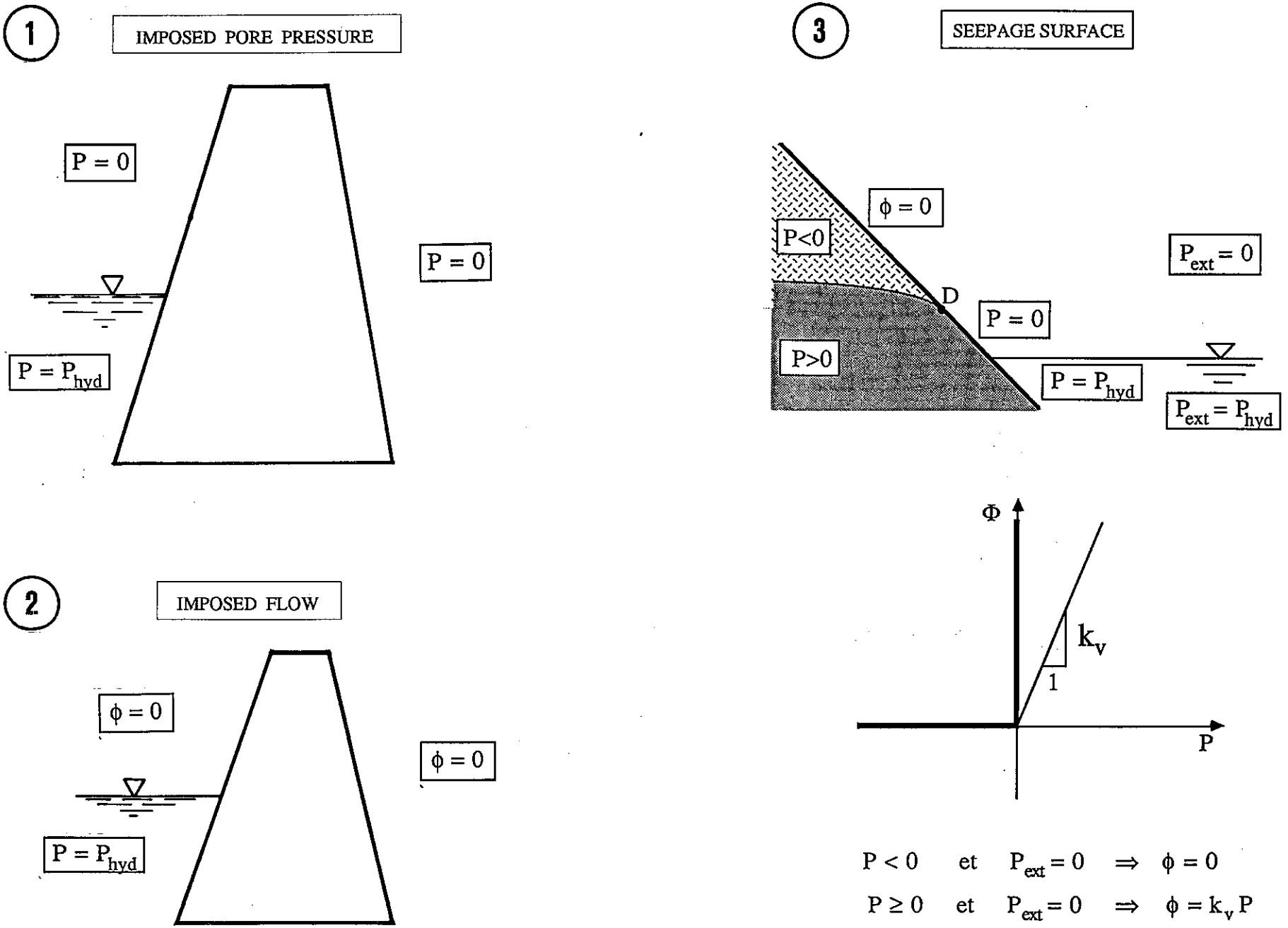

HYDRAULIC BOUNDARY CONDITIONS
THE THREE USUAL CONDITIONS FOR ROCKFILL DAMS

Fig. 1

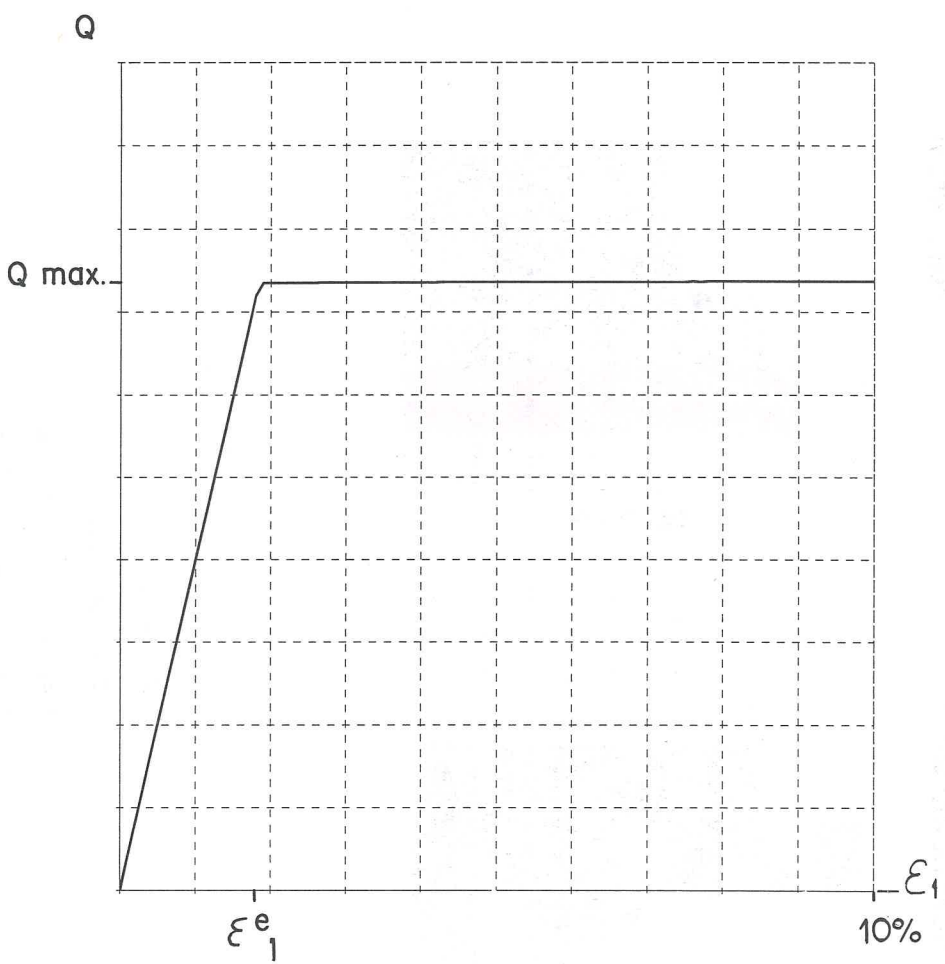

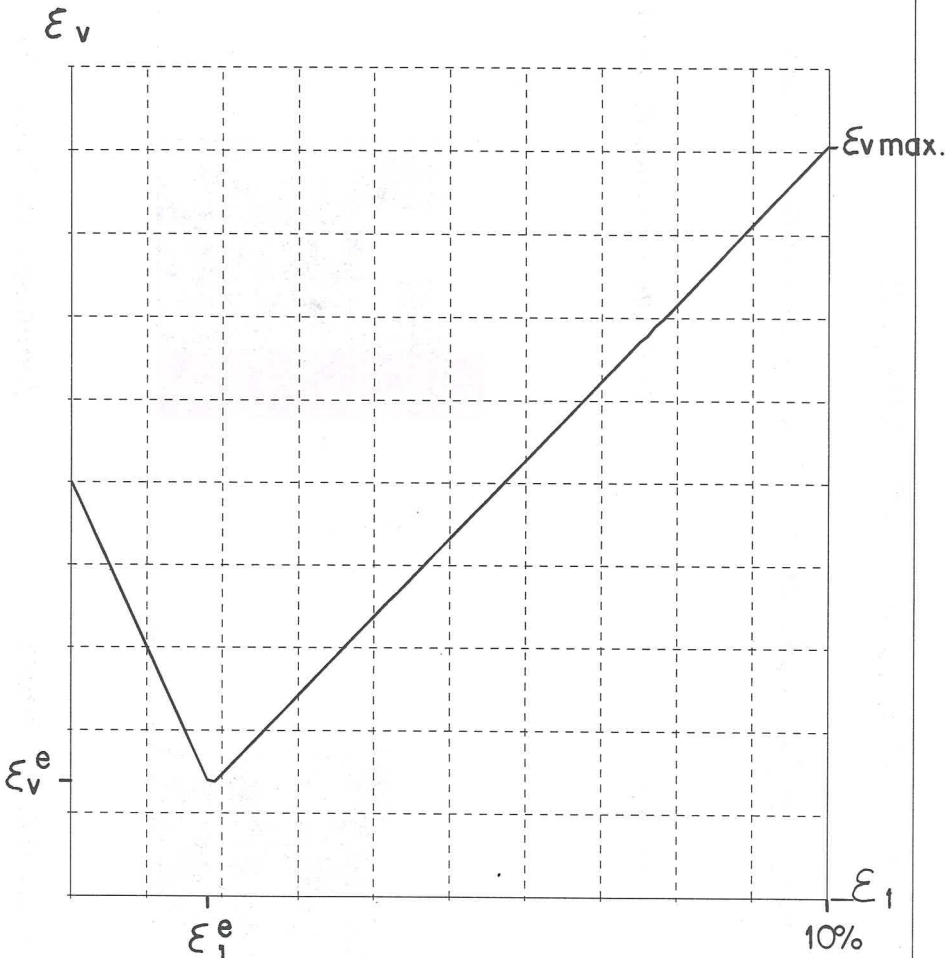

DRAINED TRIAXIAL TEST - SIG3=0.5 MPA

CORE MATERIAL - MOHR COULOMB 2D - (Q,EPS1) - (EPSV,EPS1) CURVES

Fig. 2

3rd. ICOLD 1994 - STATIC ANALYSIS

Drained triaxial test sample calculated by different Authors

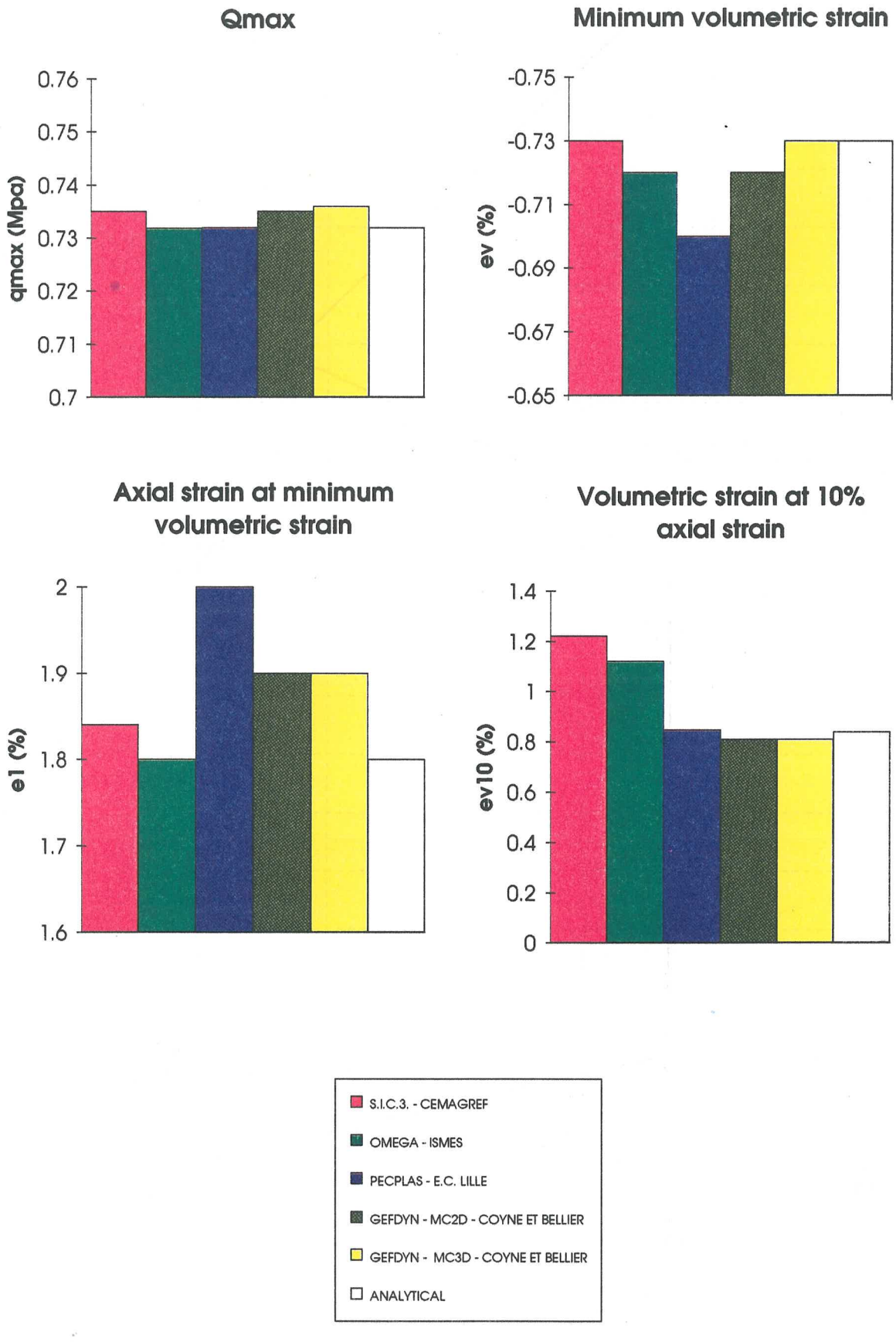

Fig. 3

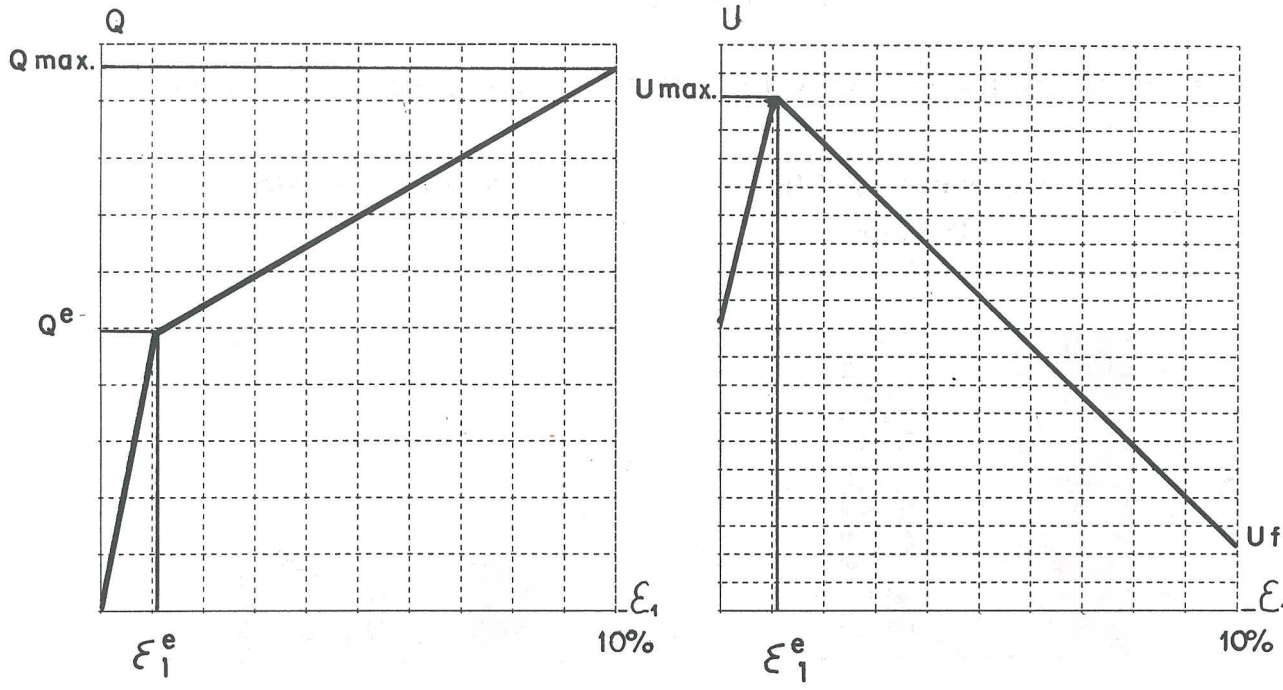

UNDRAINED TRIAXIAL TEST - SIG3=0.5 MPA
CORE MATERIAL - MOHR COULOMB 2D - (Q,EPS1) - (U,EPS1) CURVES

24/06/1994 | COYNE ET BELLIER | GEFDYN | EL INFIERNILLO DAM (MEXICO)
3RD BW - CIGB 94 | THEME B1 | NUMERICAL ANALYSIS OF DAMS

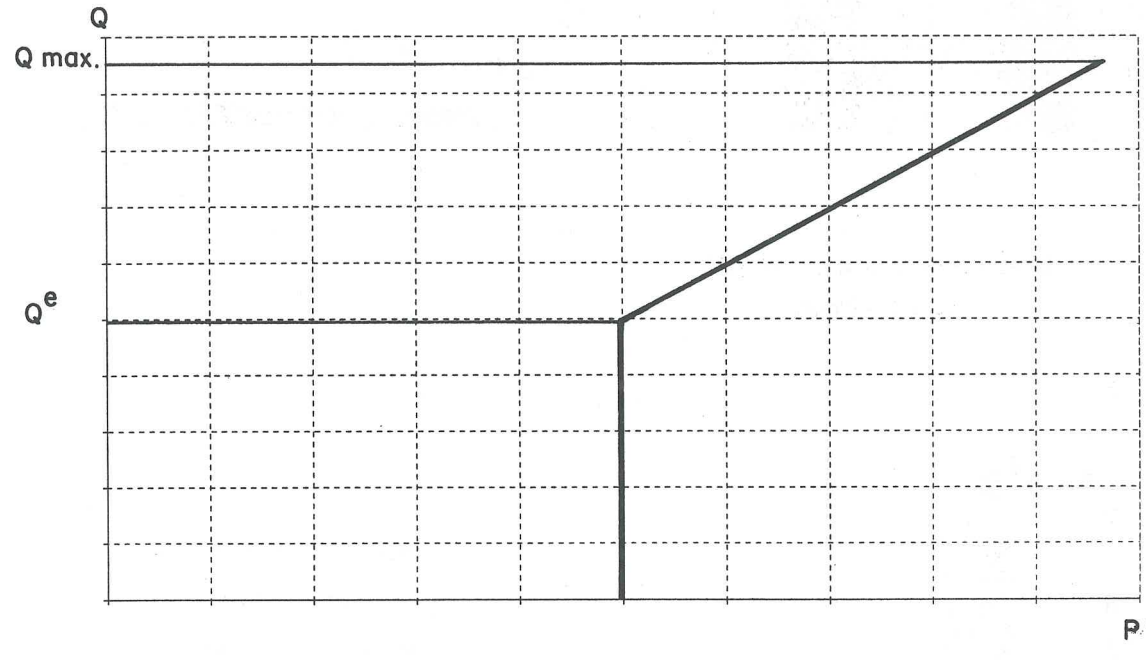

UNDRAINED TRIAXIAL TEST - SIG3=0.5 MPA
CORE MATERIAL - MOHR COULOMB 3D - (Q,P') CURVE

Fig. 4

3rd. ICOLD 1994 - STATIC ANALYSIS

Undrained triaxial test sample calculated by different Authors

Deviatoric stress when u=umax

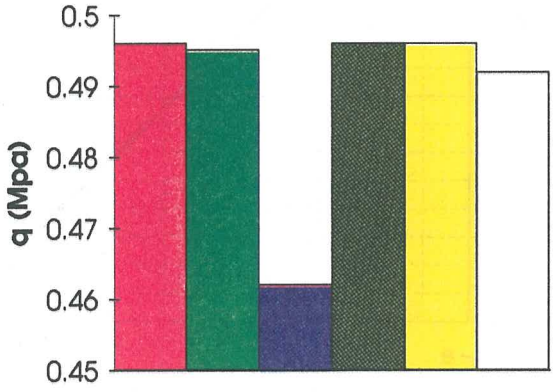

Axial strain at u=umax

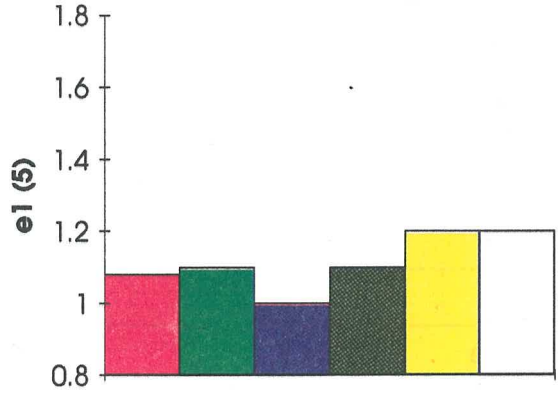

Maximum excess pore pressure

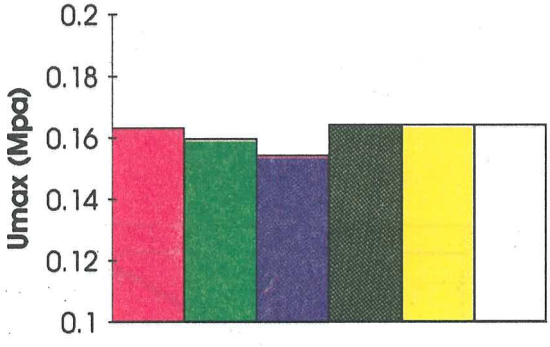

Excess pore pressure at 10% axial strain

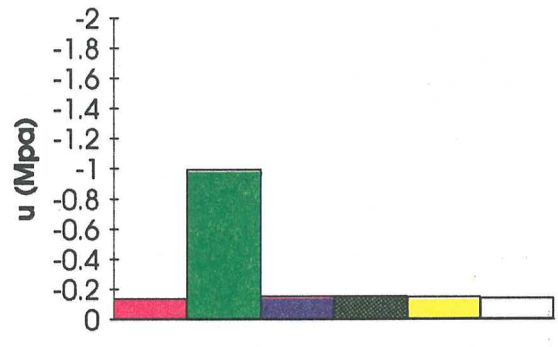

Deviatoric stress at 10% axial strain

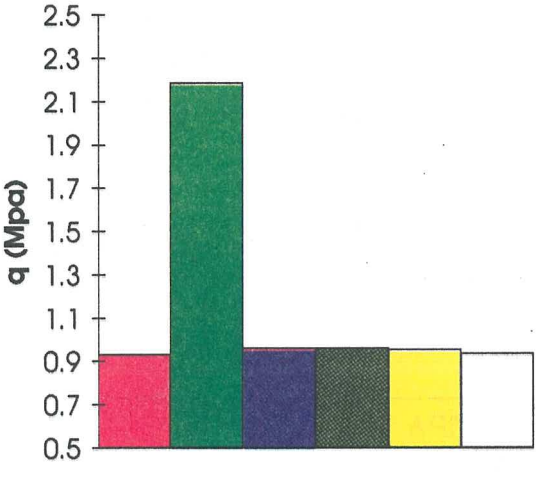

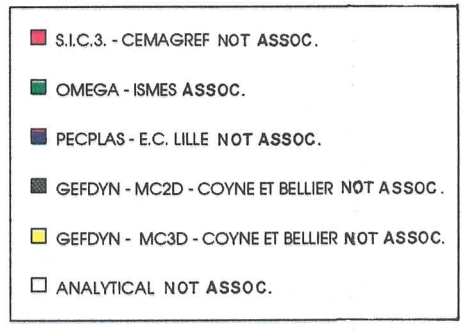

Fig. 5

PORE PRESSURES DISTRIBUTION
ZOOM ON THE CORE REGION

EDF / CNEH - GEFDYN
$k_h = k_v$

EL INFIERNILLO Dam -STATIC ANALYSIS

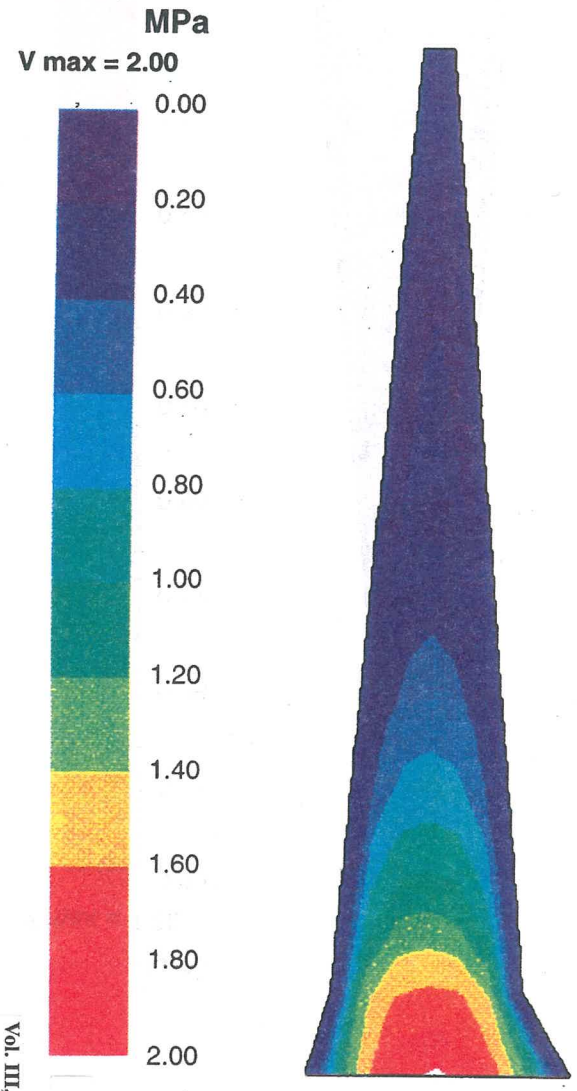

End of Construction

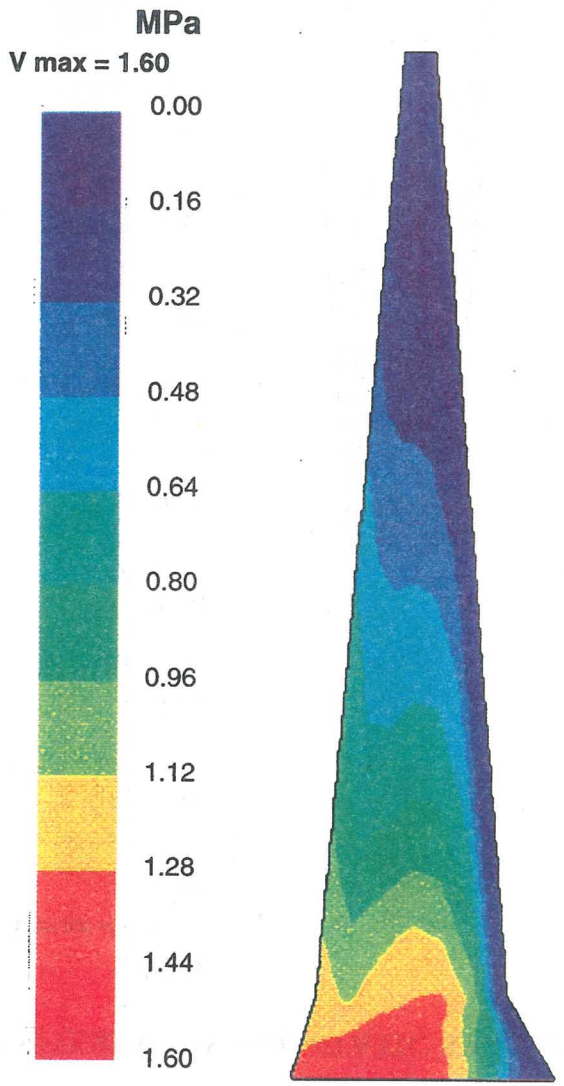

End of Impounding

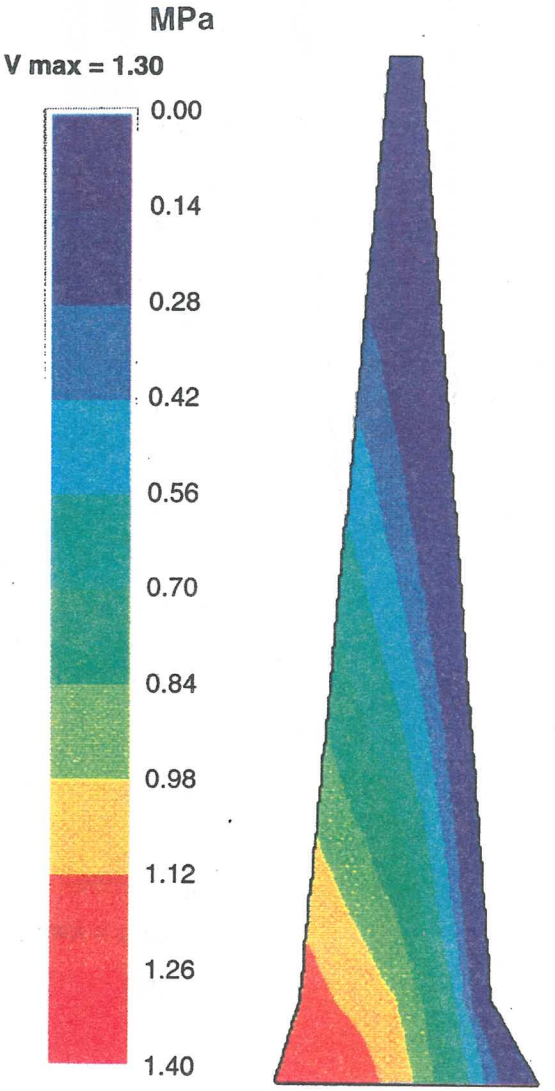

End of Consolidation

Fig. 6

PORE PRESSURES DISTRIBUTION
ZOOM ON THE CORE REGION

EDF / CNEH - GEFDYN
$k_H = 4\ k_V$

EL INFIERNILLO Dam -STATIC ANALYSIS

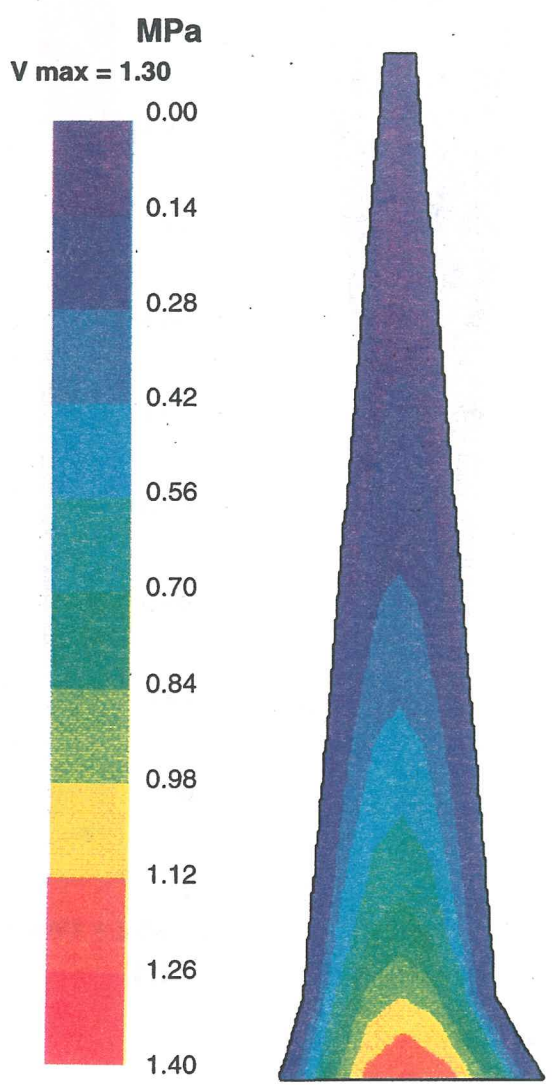

End of Construction

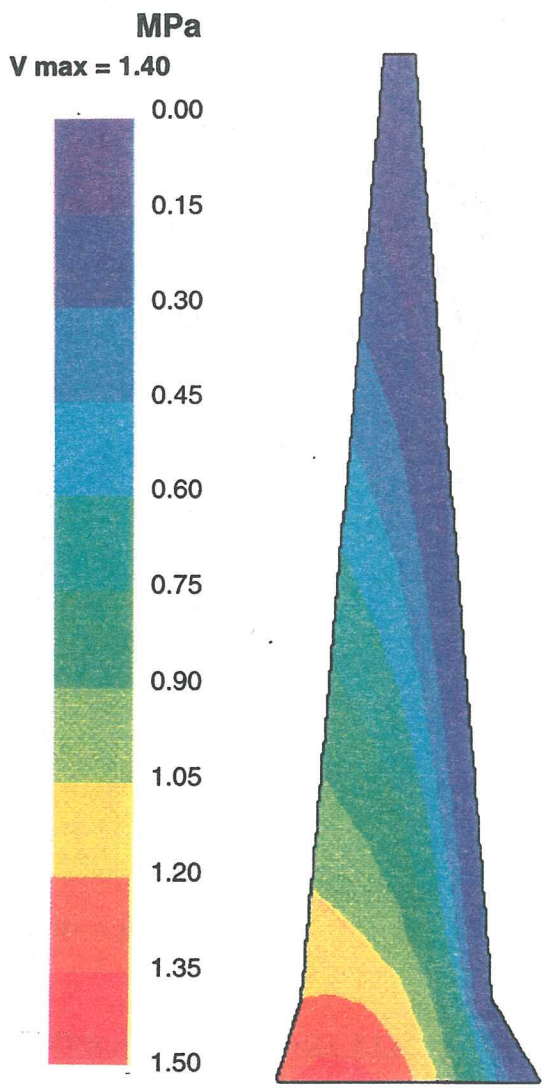

End of Impounding

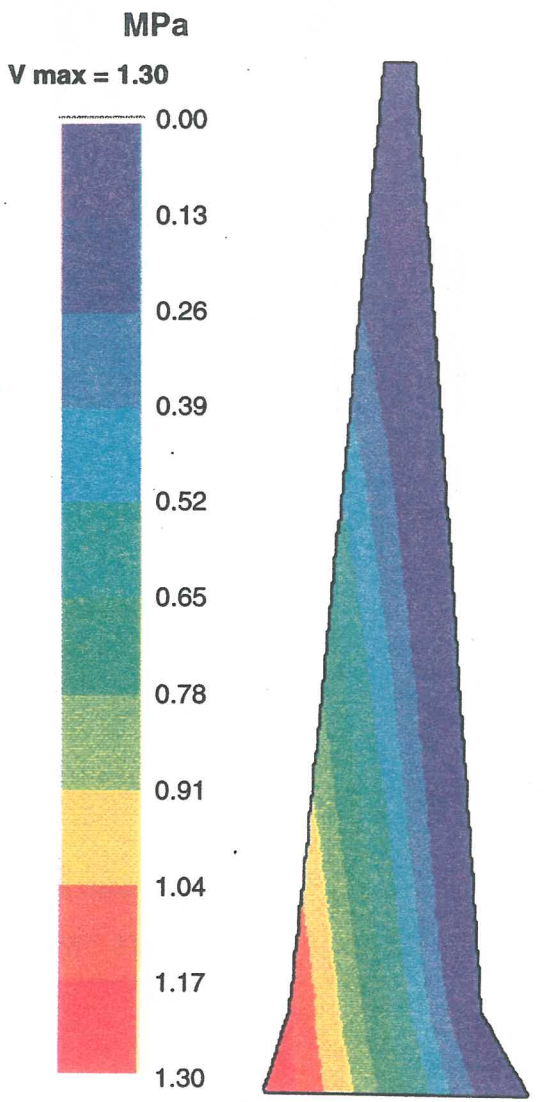

End of Consolidation

Fig. 7

GEFDYN - COYNE ET BELLIER
Unsaturated case

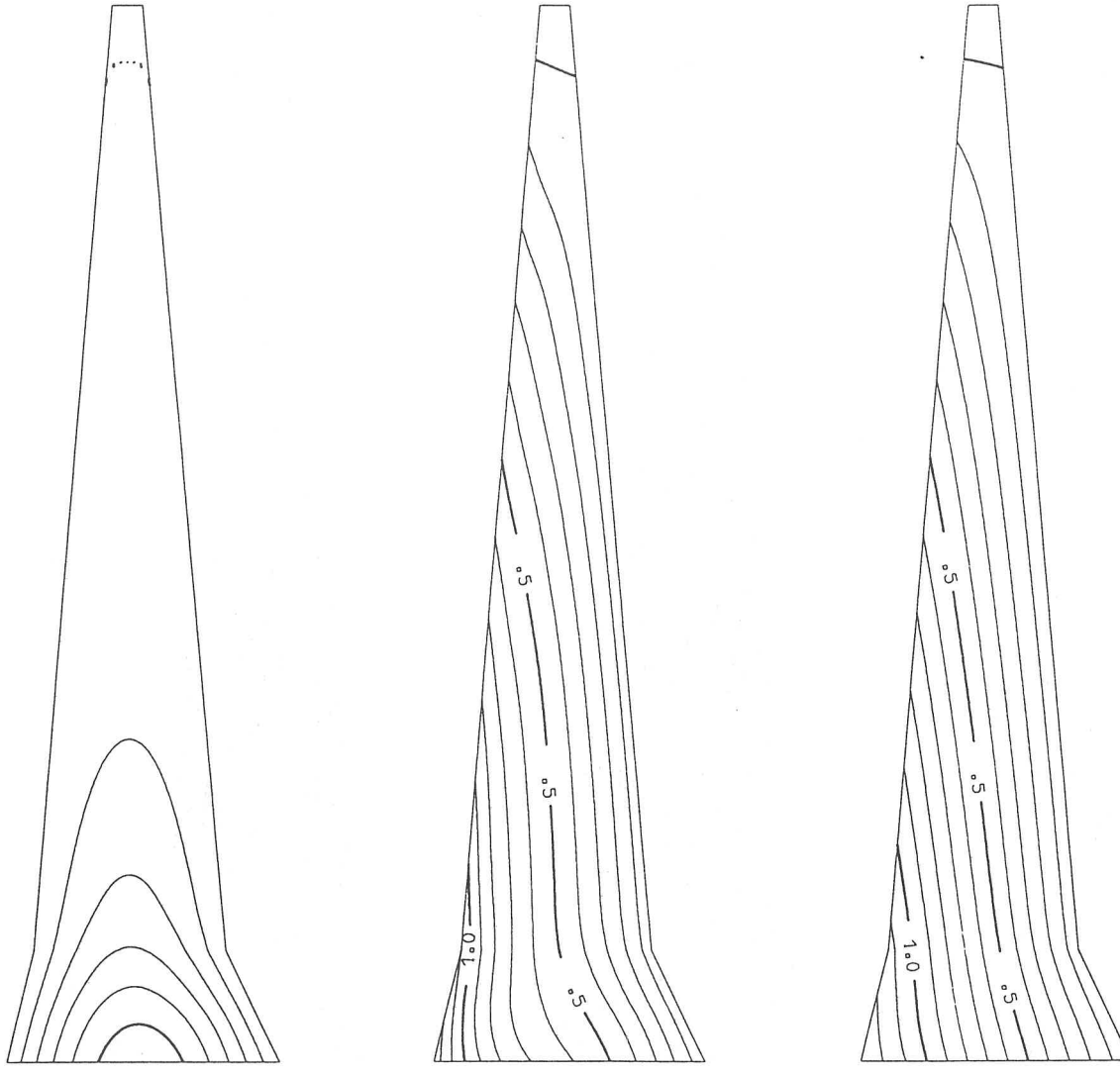

End of first consolidation period

End of dam impounding

End of second consolidation period

GEOMETRICAL SCALE : .00100

Pore pressure contour lines
saturated case (+Mohr Coulomb 2D)

Fig. 8

GEFDYN - COYNE ET BELLIER
Saturated case

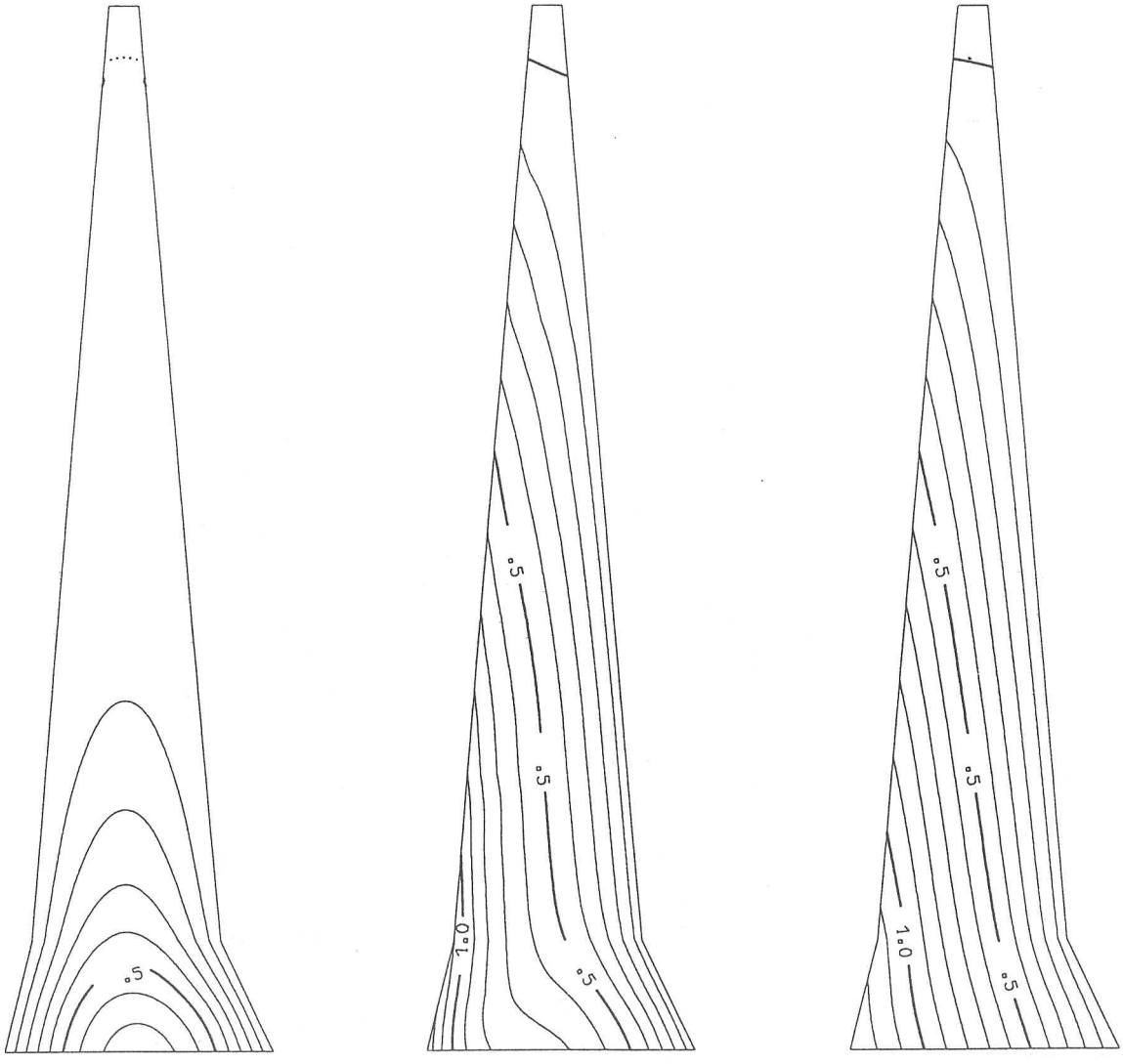

End of first consolidation period

End of dam impounding

End of second consolidation period

GEOMETRICAL SCALE : .00100

Pore pressure contour lines
unsaturated case (+Mohr Coulomb 3D)

Fig. 9

3rd. ICOLD 1994 - STATIC ANALYSIS

EXCESS PORE WATER PRESSURE DISTRIBUTION

DRUCKER-PRAGER MODEL

OMEGA - ISMES - ENEL

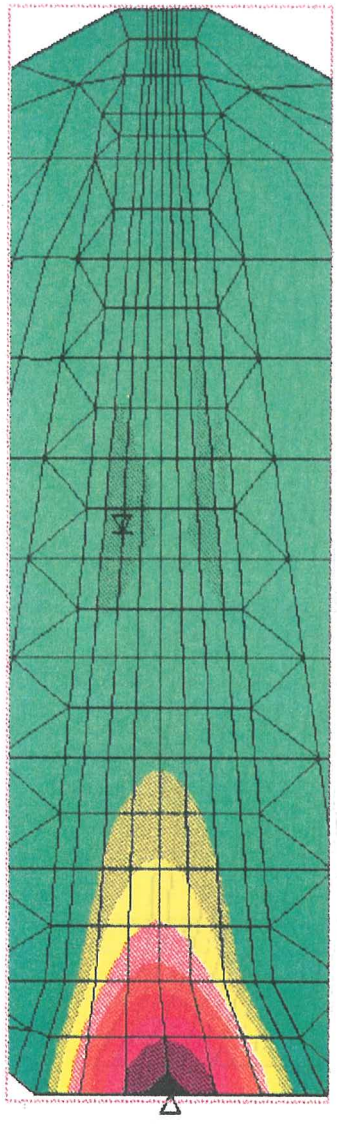

VMIN = -0.5702E-02

VMAX = 0.8283E+00

End of Construction

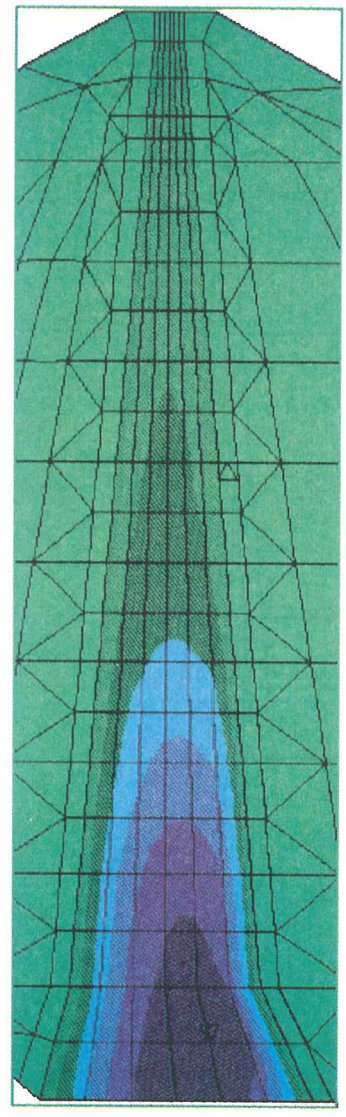

VMIN = -0.6073E+00

VMAX = 0.1246E-06

End of Impounding

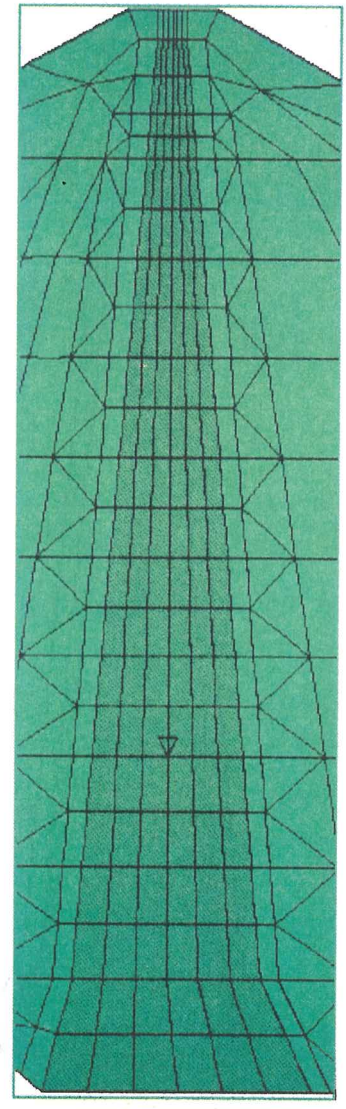

VMIN = -0.4333E-01

VMAX = 0.0000E+00

End of Consolidation

SCALE: (MPa)

0.9000E+00
0.8000E+00
0.7000E+00
0.6000E+00
0.5000E+00
0.4000E+00
0.3000E+00
0.2000E+00
0.1000E+00
-0.1490E-07
-0.1000E+00
-0.2000E+00
-0.3000E+00
-0.4000E+00
-0.5000E+00
-0.6000E+00

Fig. 10

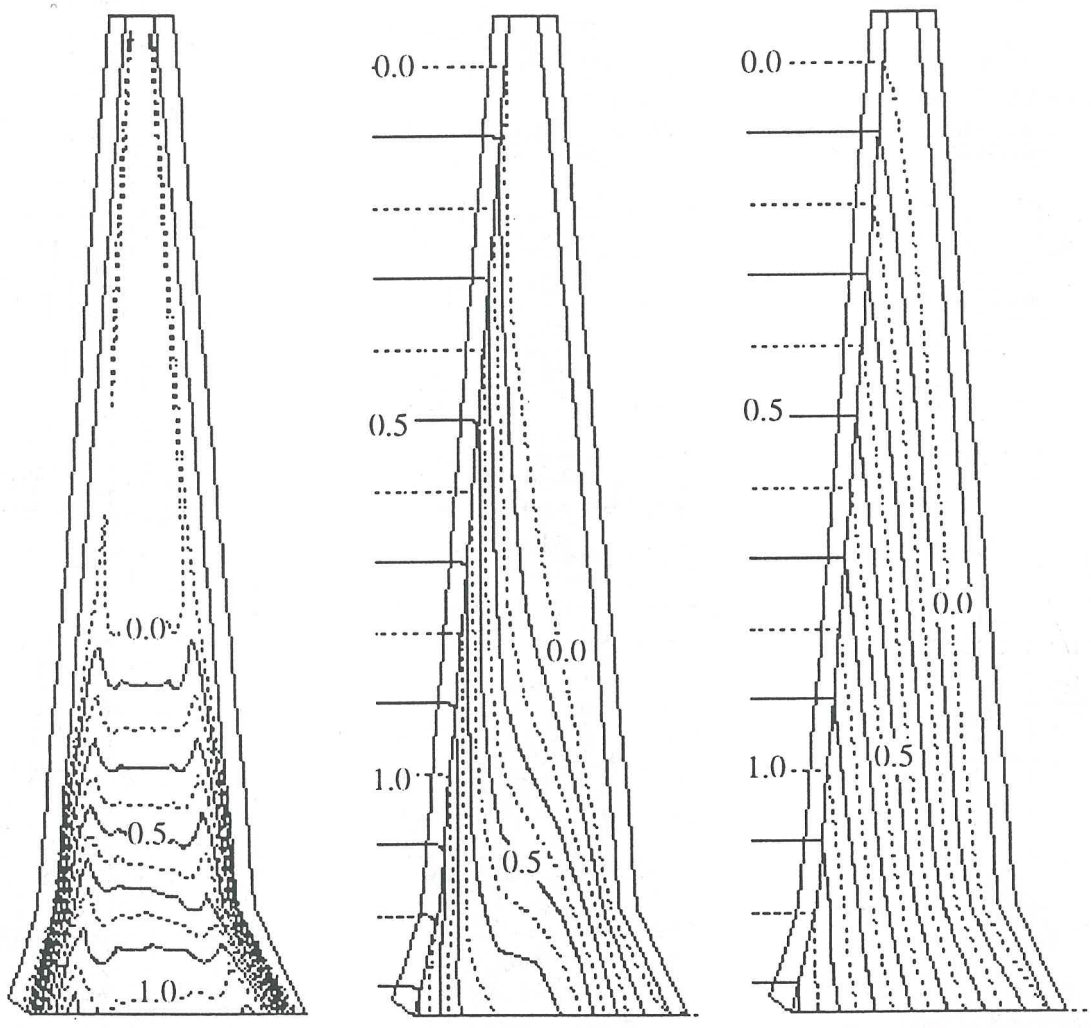

Pore pressure u_w in the core (MPa) (compression positive)
Quasi-static analysis

3rd. ICOLD 1994 - STATIC ANALYSIS
COMPARISON OF RESULTS

SETTLEMENTS PROFILE AT THE END OF CONSTRUCTION PHASE

SECTION A-A

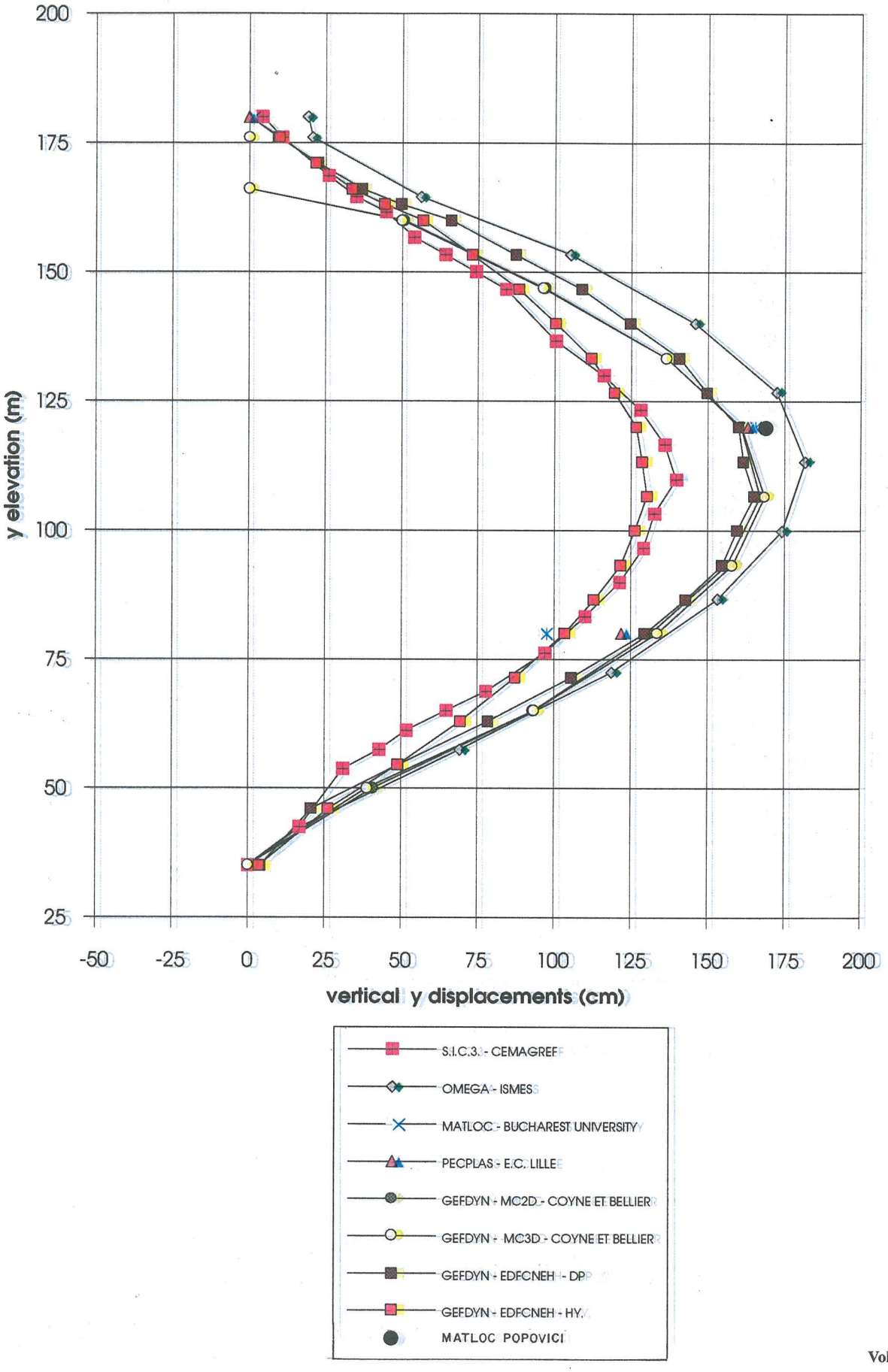

Fig. 12

3rd. ICOLD 1994 - STATIC ANALYSIS
COMPARISON OF RESULTS

HORIZONTAL DISPLACEMENTS AT THE END OF CONSTRUCTION PHASE

SECTION A-A

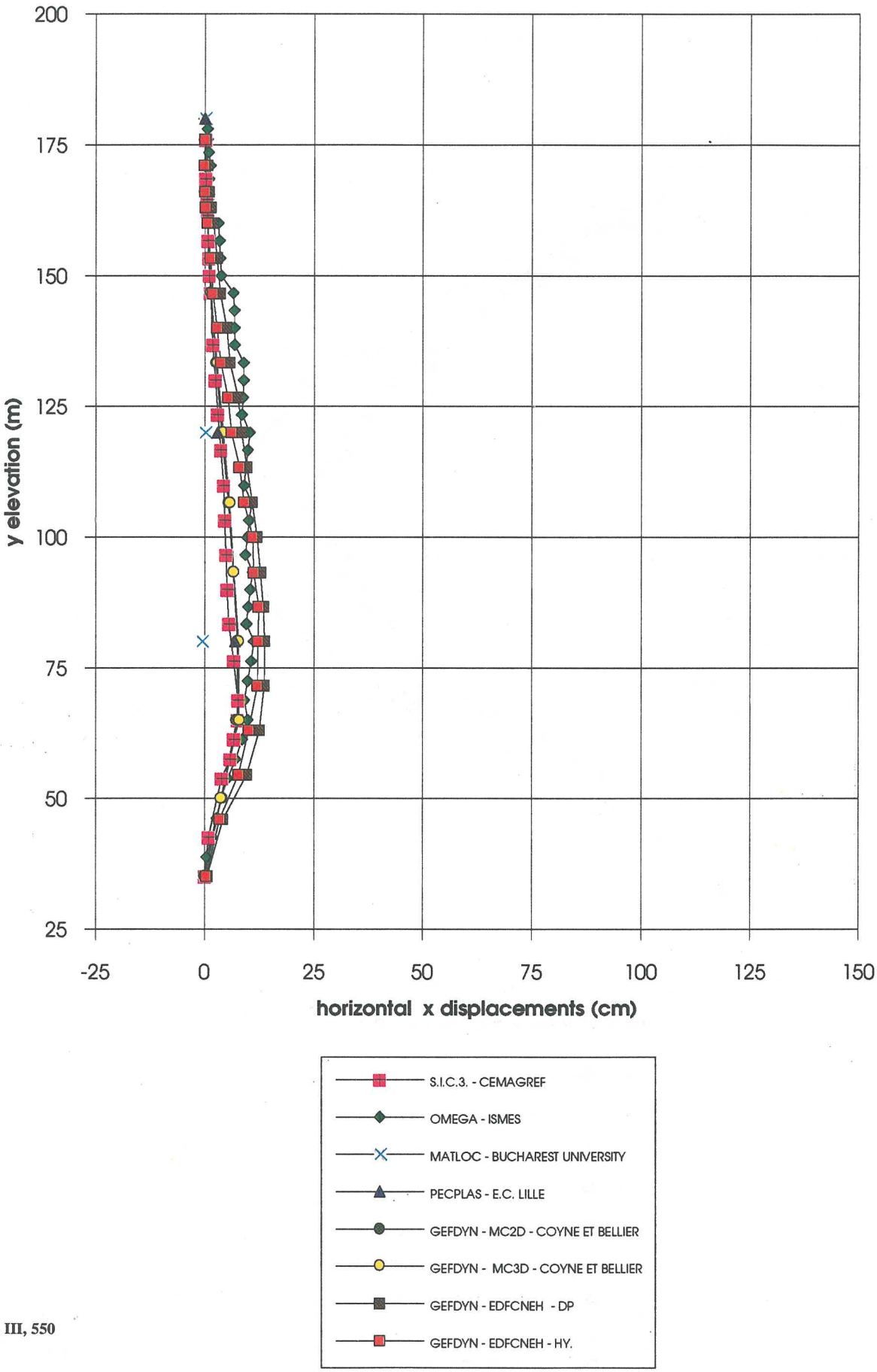

Fig. 13

SETTLEMENTS PROFILE AT THE END OF CONSTRUCTION PHASE

SECTION B-B

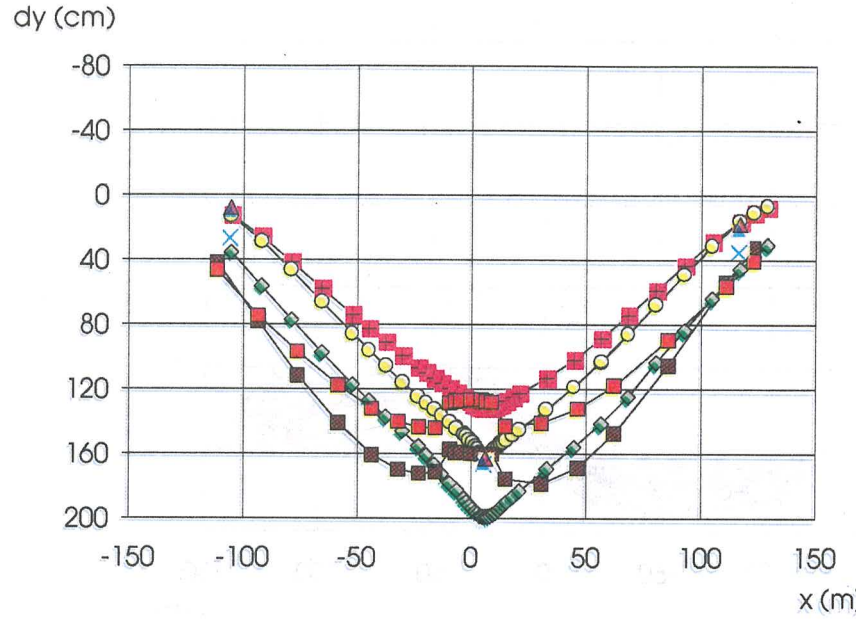

SECTION C-C

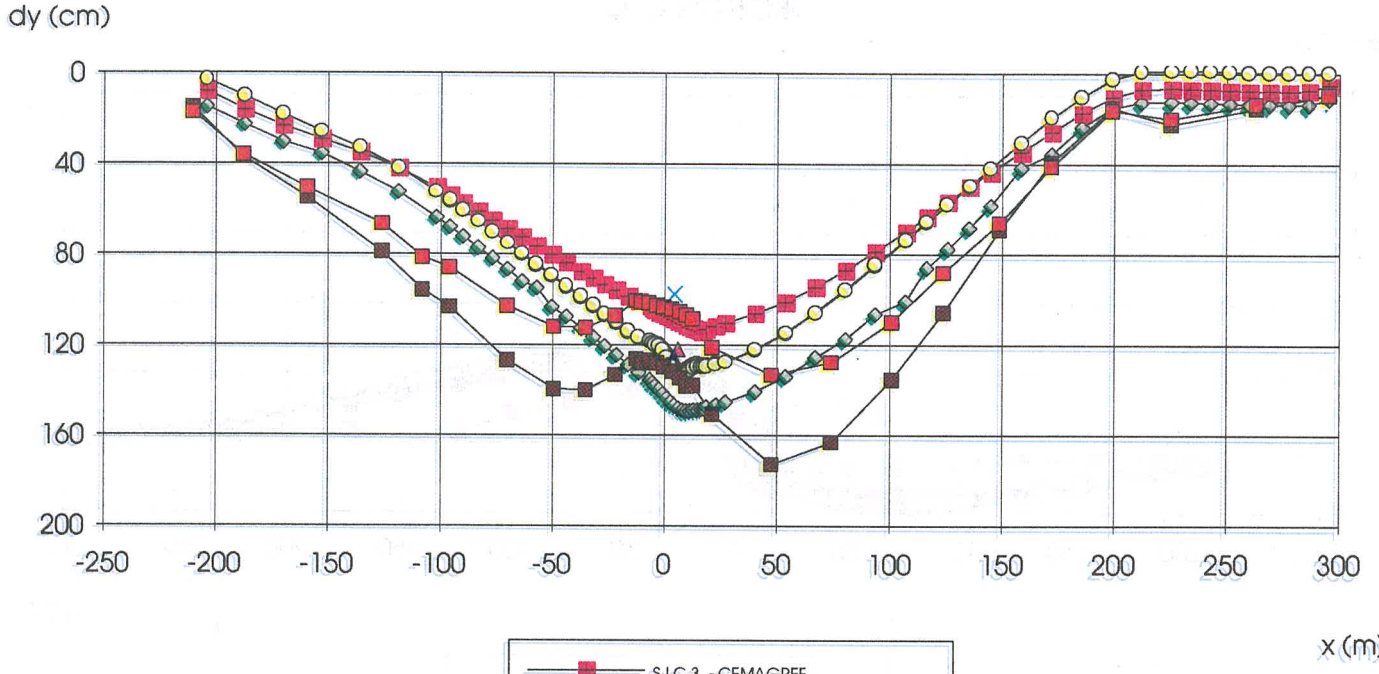

Fig. 14

3rd. ICOLD 1994 - STATIC ANALYSIS
COMPARISON OF RESULTS

HORIZONTAL DISPLACEMENTS AT THE END OF CONSTRUCTION PHASE

SECTION B-B

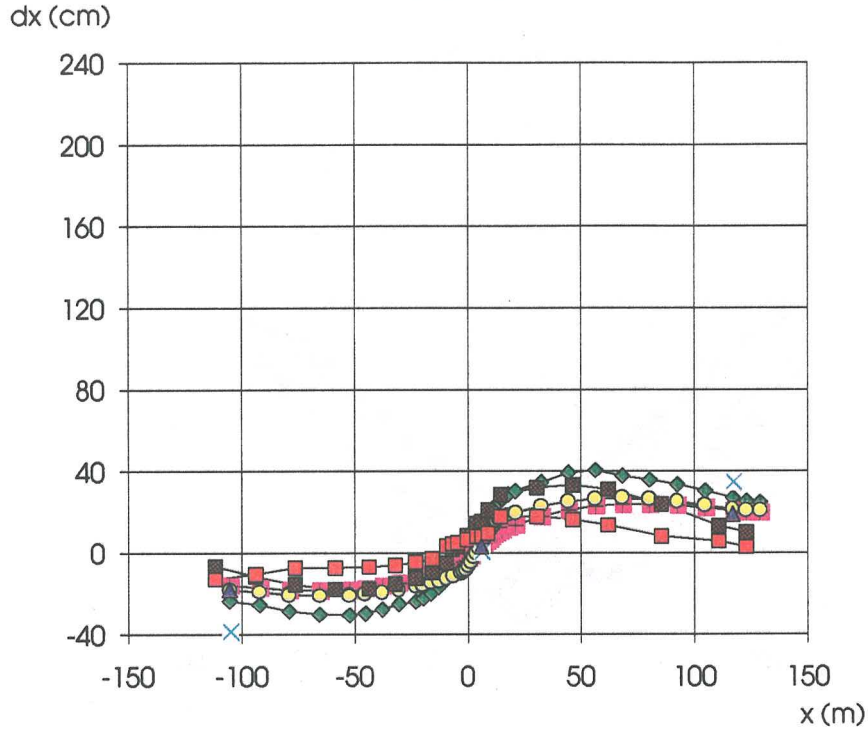

SECTION C-C

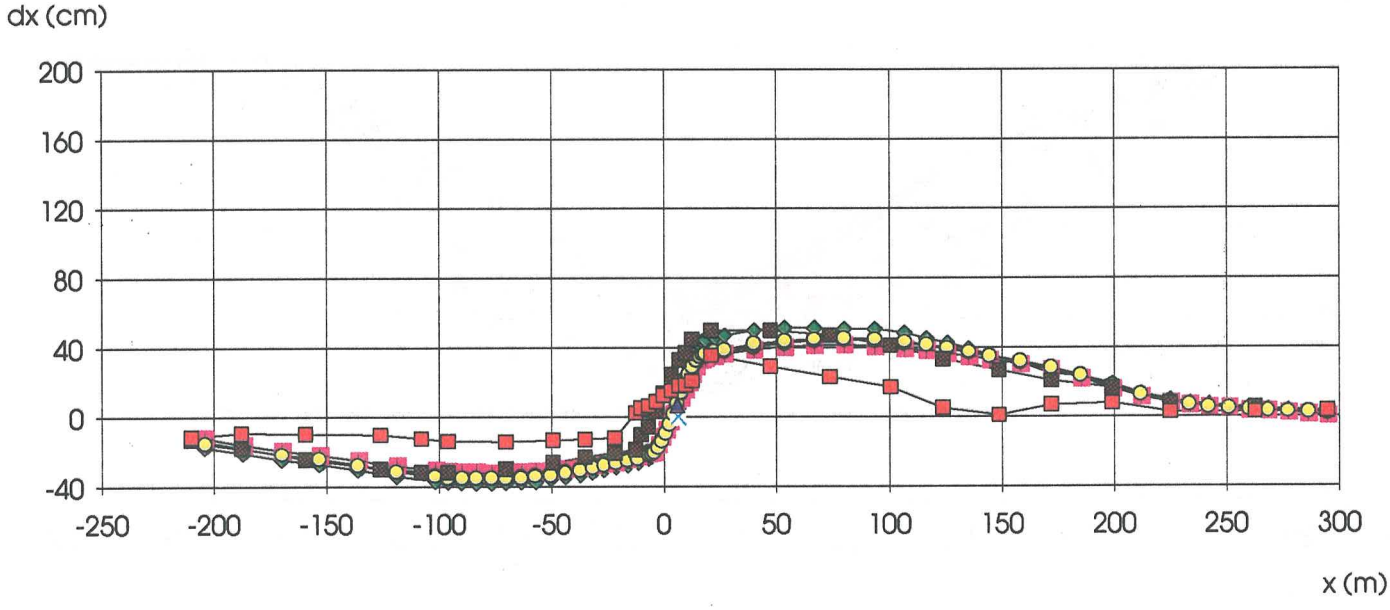

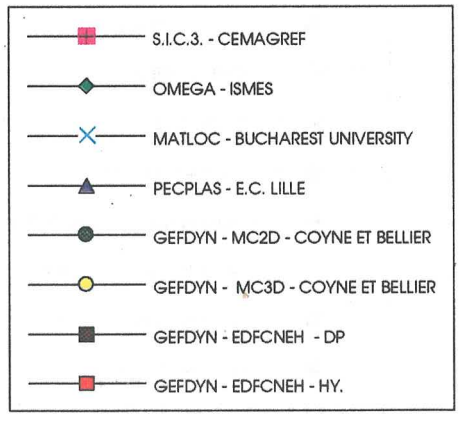

Fig. 15

3rd. ICOLD 1994 - STATIC ANALYSIS
COMPARISON OF RESULTS

SETTLEMENTS PROFILE AT THE END OF IMPOUNDING PHASE

SECTION A-A

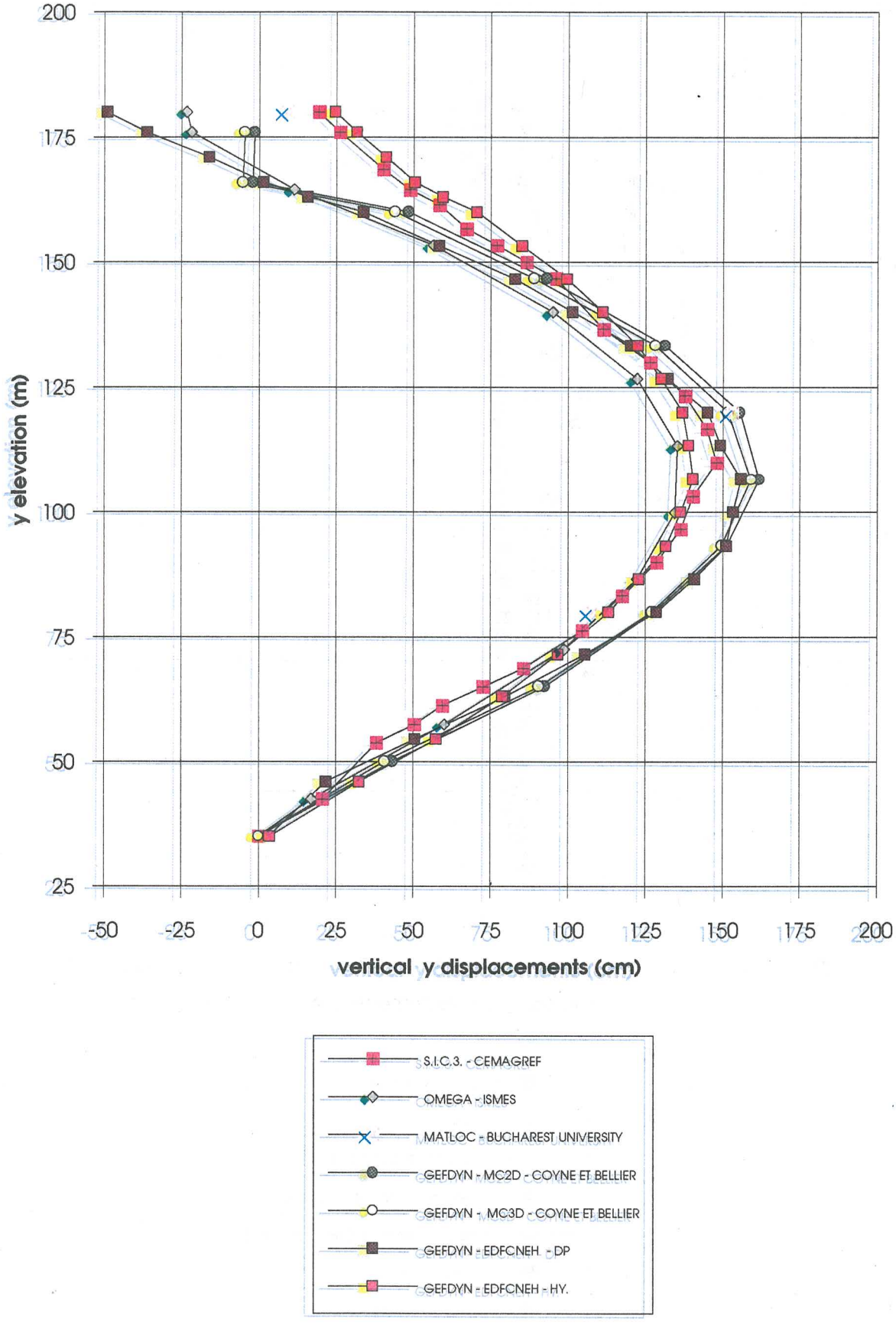

Fig. 16a

3rd. ICOLD 1994 - STATIC ANALYSIS
COMPARISON OF RESULTS

INCREMENTAL SETTLEMENTS: TOTAL SETTLEMENTS AT THE END OF IMPOUNDING - TOTAL SETTLEMENTS AT THE END OF CONSTRUCTION

SECTION A-A

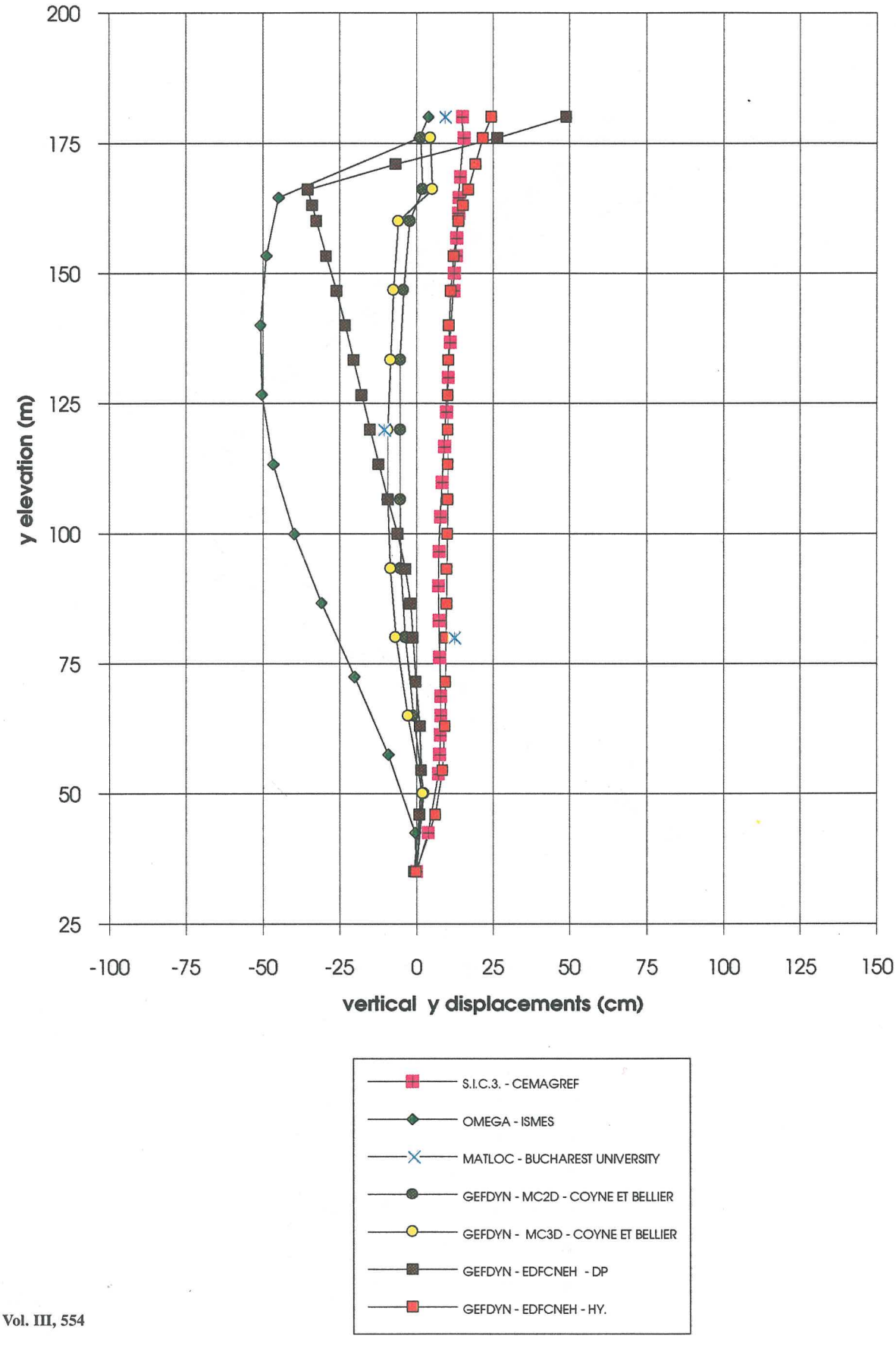

Fig. 16b

3rd. ICOLD 1994 - STATIC ANALYSIS
COMPARISON OF RESULTS

HORIZONTAL DISPLACEMENTS AT THE END OF IMPOUNDING PHASE

SECTION A-A

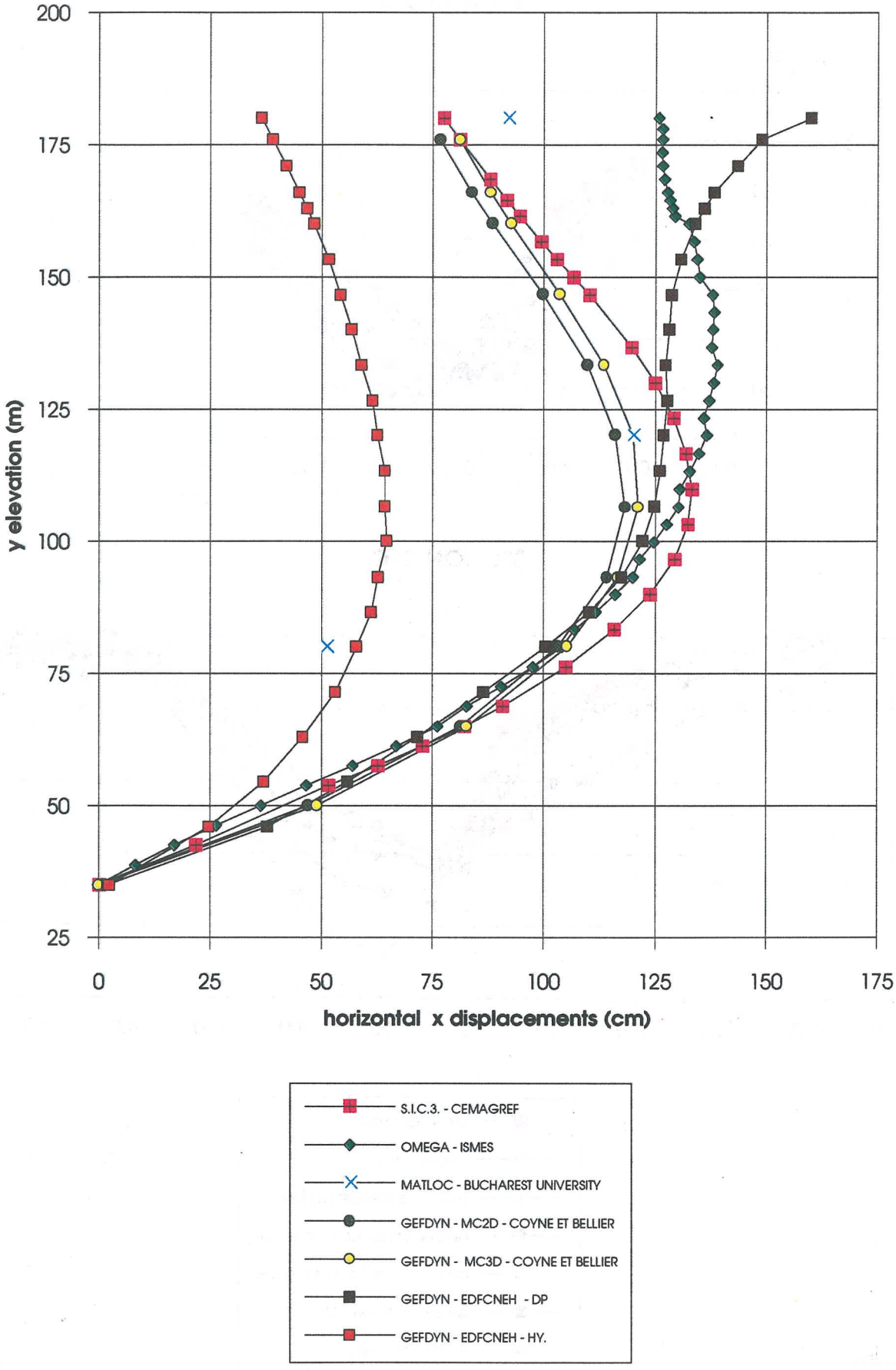

Fig. 17

3rd. ICOLD 1994 - STATIC ANALYSIS
COMPARISON OF RESULTS

SETTLEMENTS PROFILE AT THE END OF IMPOUNDING PHASE

SECTION B-B

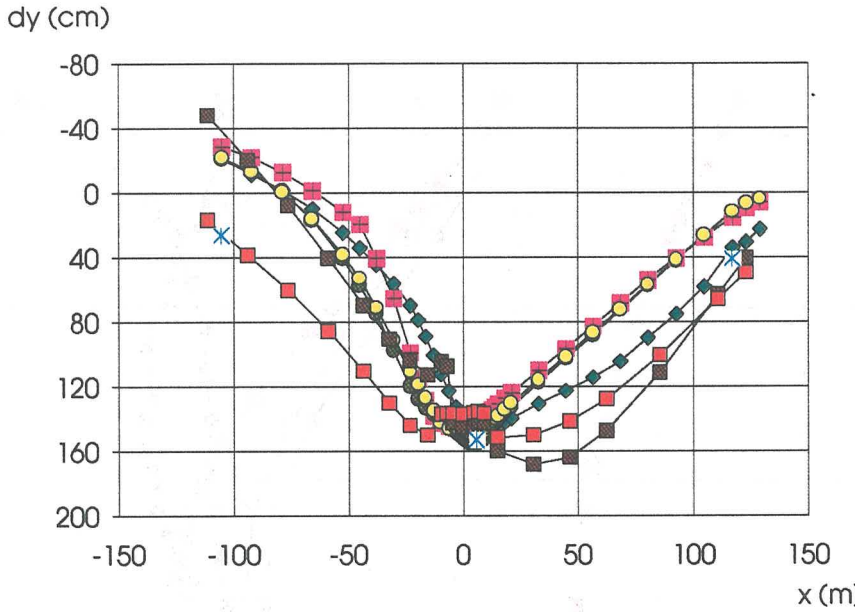

SECTION C-C

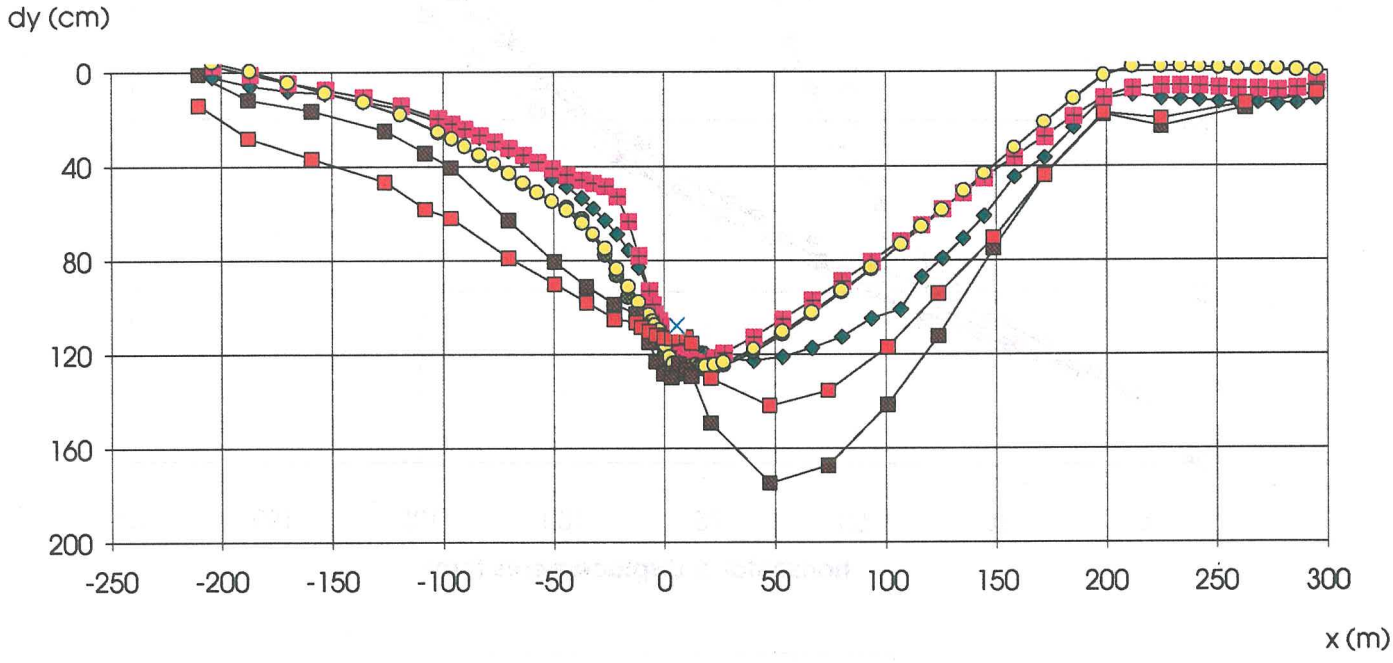

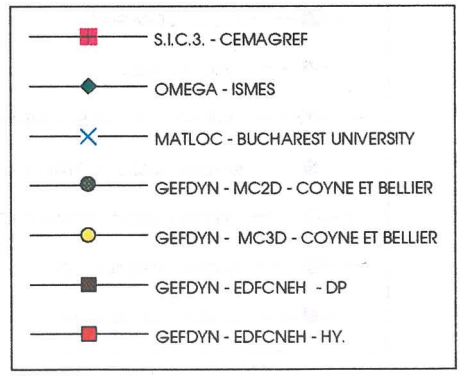

Fig. 18a

INCREMENTAL SETTLEMENTS: TOTAL SETTLEMENTS AT THE END OF IMPOUNDING - TOTAL SETTLEMENTS AT THE END OF CONSTRUCTION

SECTION B-B

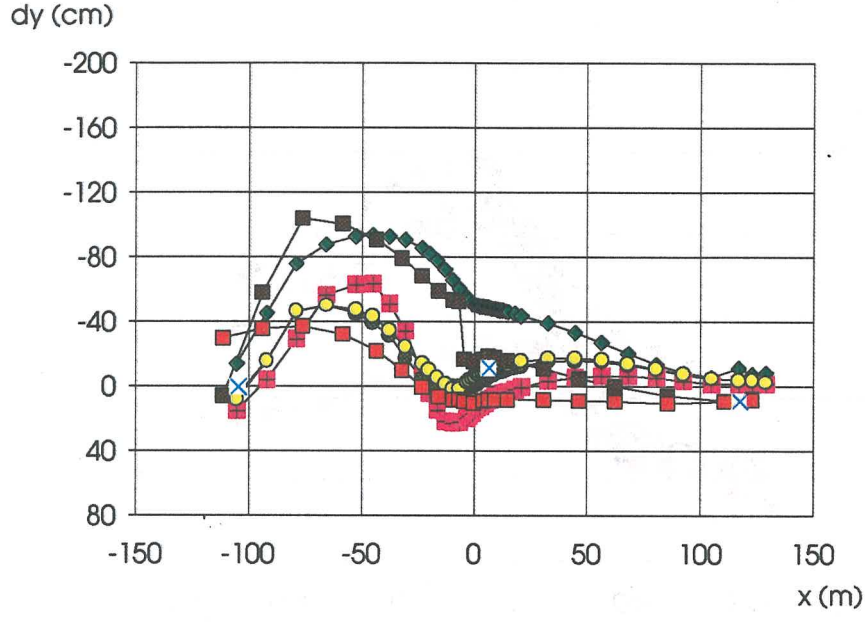

SECTION C-C

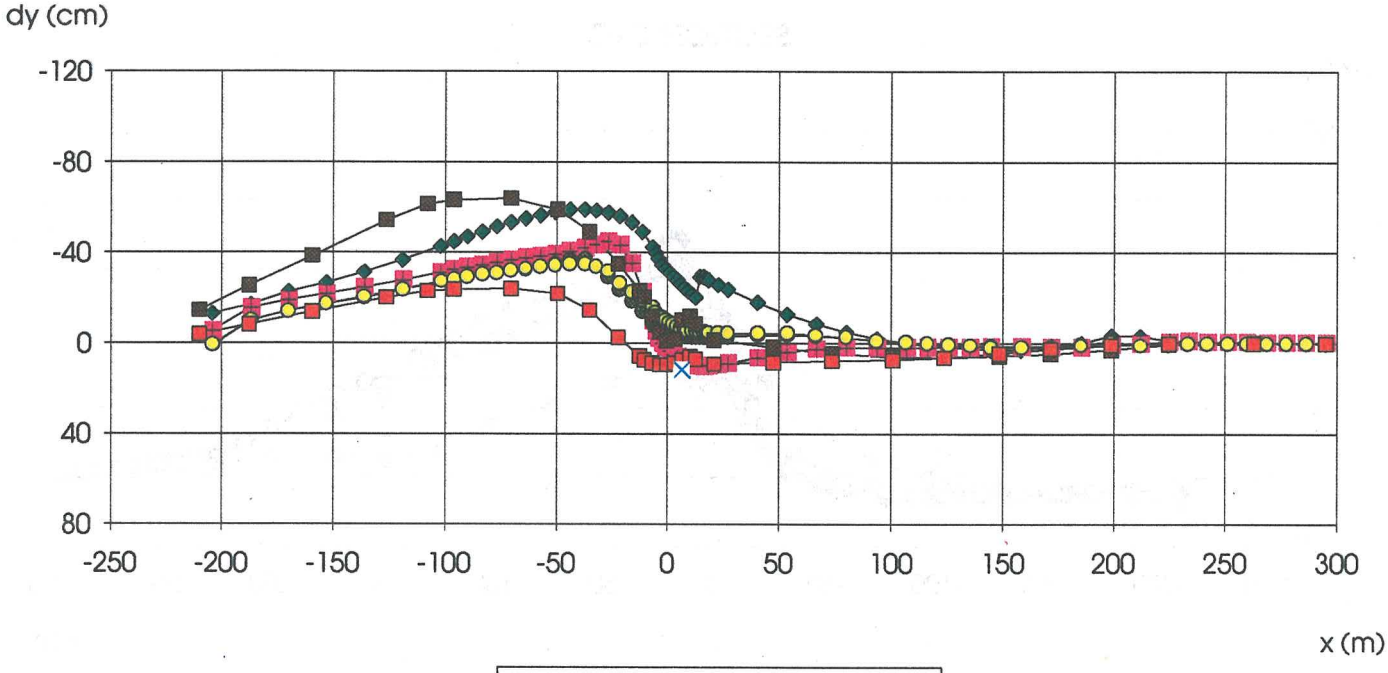

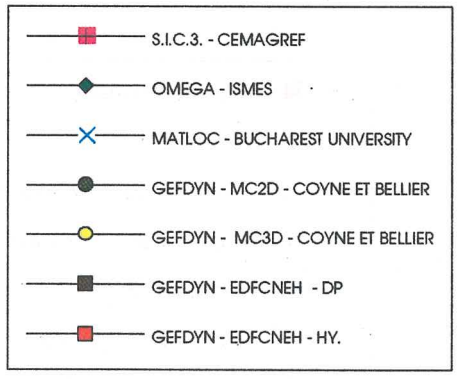

Fig. 18b

3rd. ICOLD 1994 - STATIC ANALYSIS
COMPARISON OF RESULTS

HORIZONTAL DISPLACEMENTS AT THE END OF IMPOUNDING PHASE

SECTION B-B

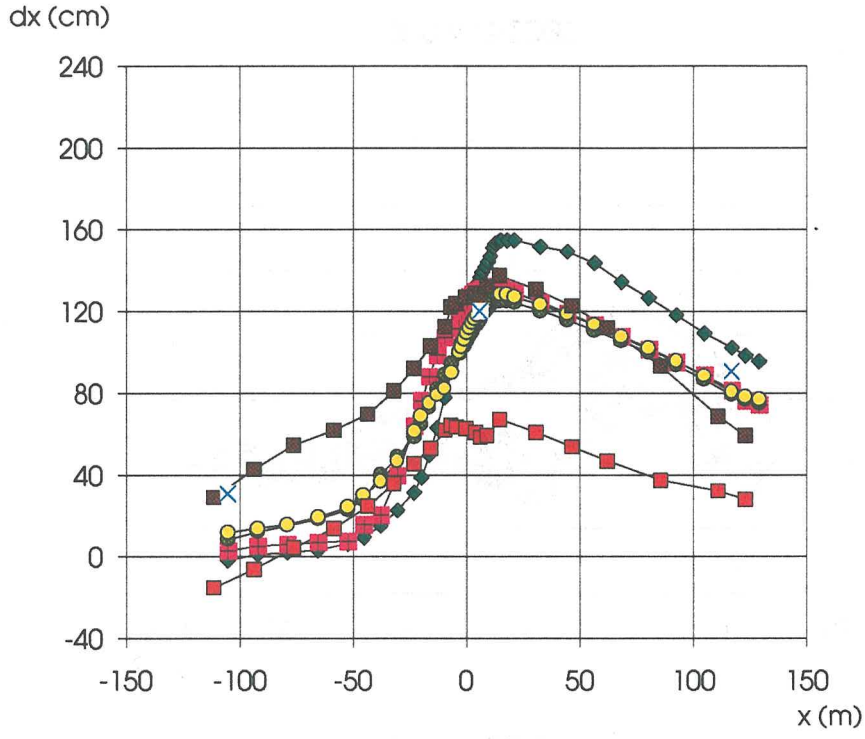

SECTION C-C

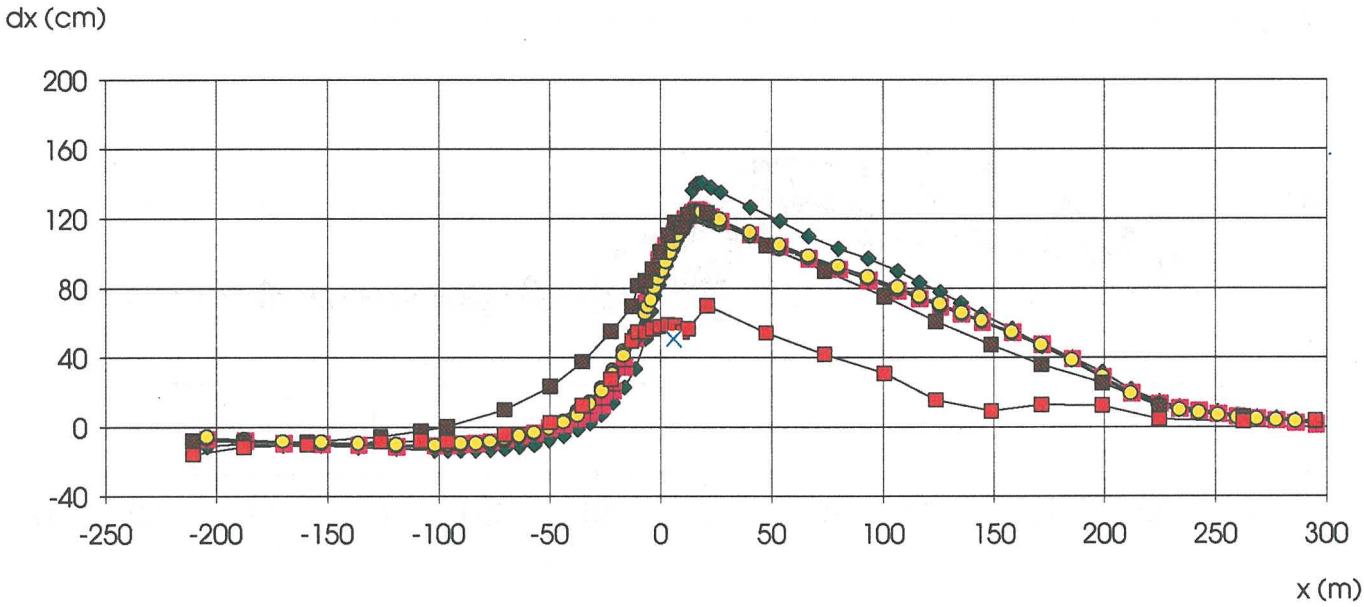

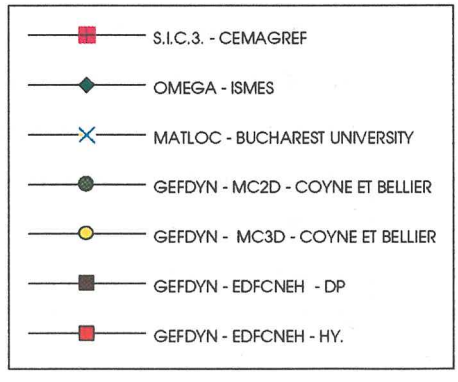

Fig. 19

3rd. ICOLD 1994 - STATIC ANALYSIS
COMPARISON OF RESULTS

SETTLEMENTS PROFILE AT THE END OF CONSOLIDATION PHASE

SECTION A-A

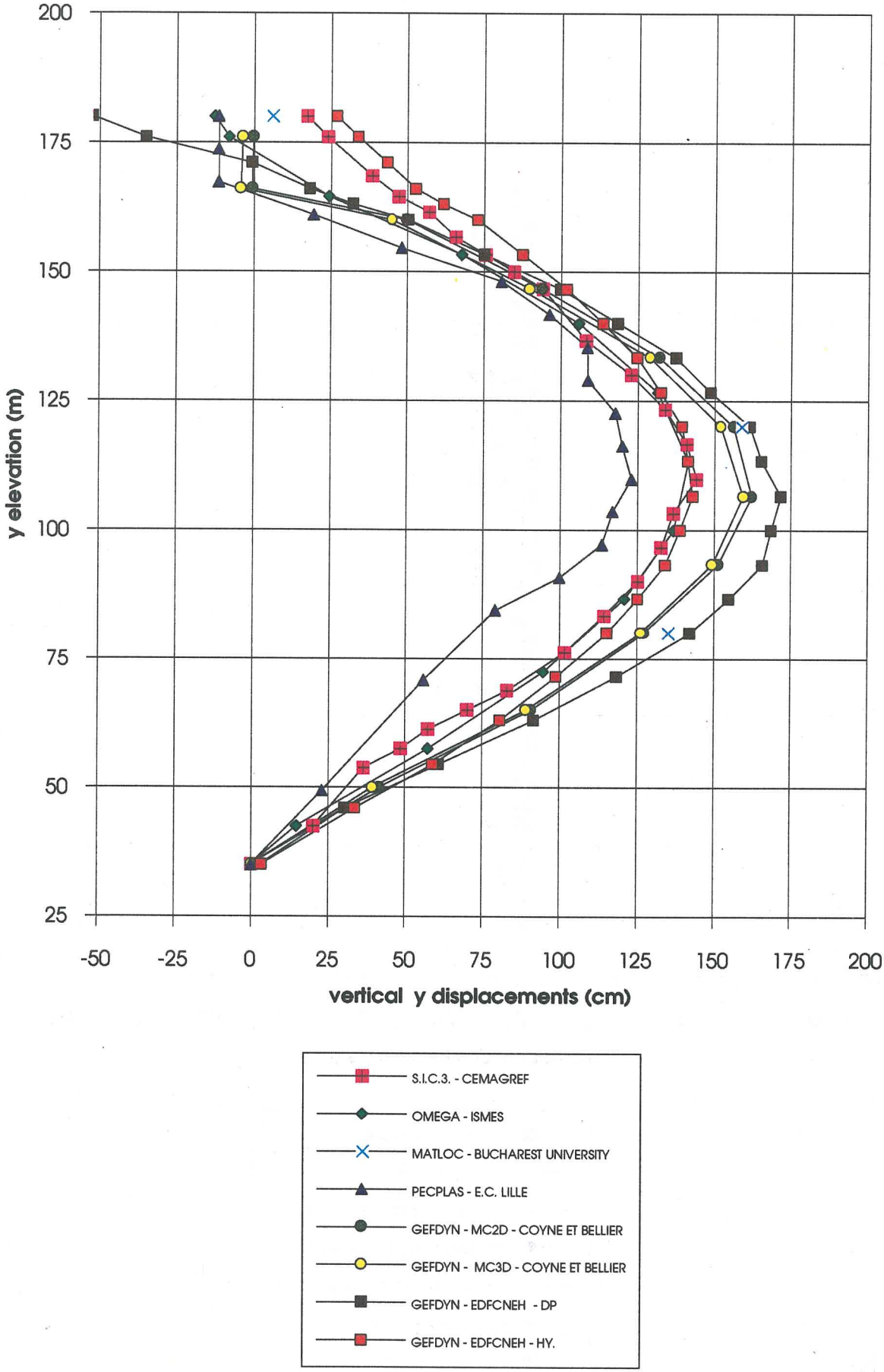

Fig. 20a

3rd. ICOLD 1994 - STATIC ANALYSIS
COMPARISON OF RESULTS

INCREMENTAL SETTLEMENTS: TOTAL SETTLEMENTS AT THE END OF CONSOLIDATION - TOTAL SETTLEMENTS AT THE END OF IMPOUNDING

SECTION A-A

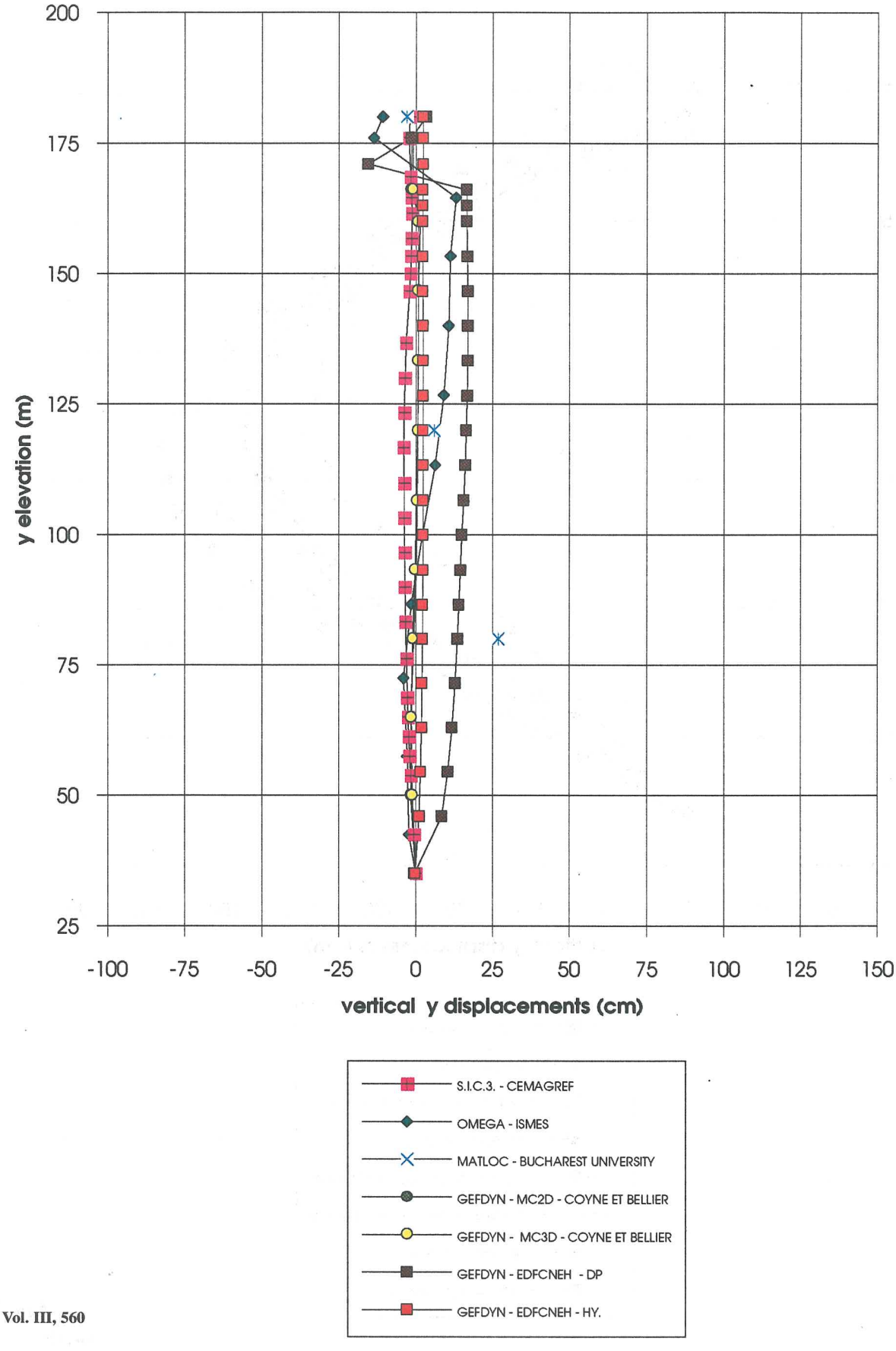

Fig. 20b

3rd. ICOLD 1994 - STATIC ANALYSIS
COMPARISON OF RESULTS

HORIZONTAL DISPLACEMENTS AT THE END OF CONSOLIDATION PHASE

SECTION A-A

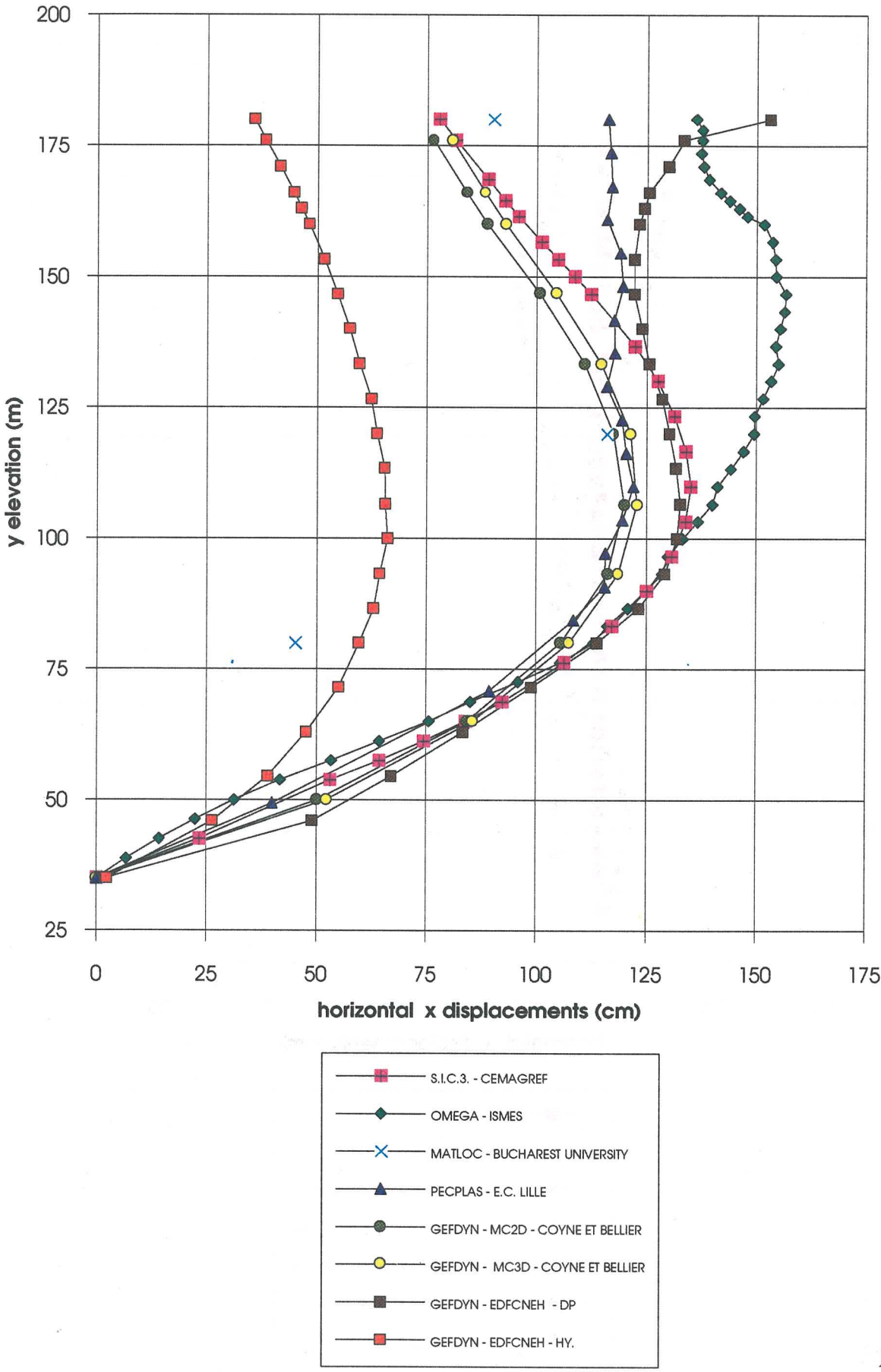

Fig. 21a

3rd. ICOLD 1994 - STATIC ANALYSIS
COMPARISON OF RESULTS

INCREMENTAL HORIZONTAL DISPLACEMENTS: TOTAL HORIZONTAL DISPL. AT THE END OF CONSOLIDATION - TOTAL HORIZONTAL DISPL. AT THE END OF IMPOUNDING

SECTION A-A

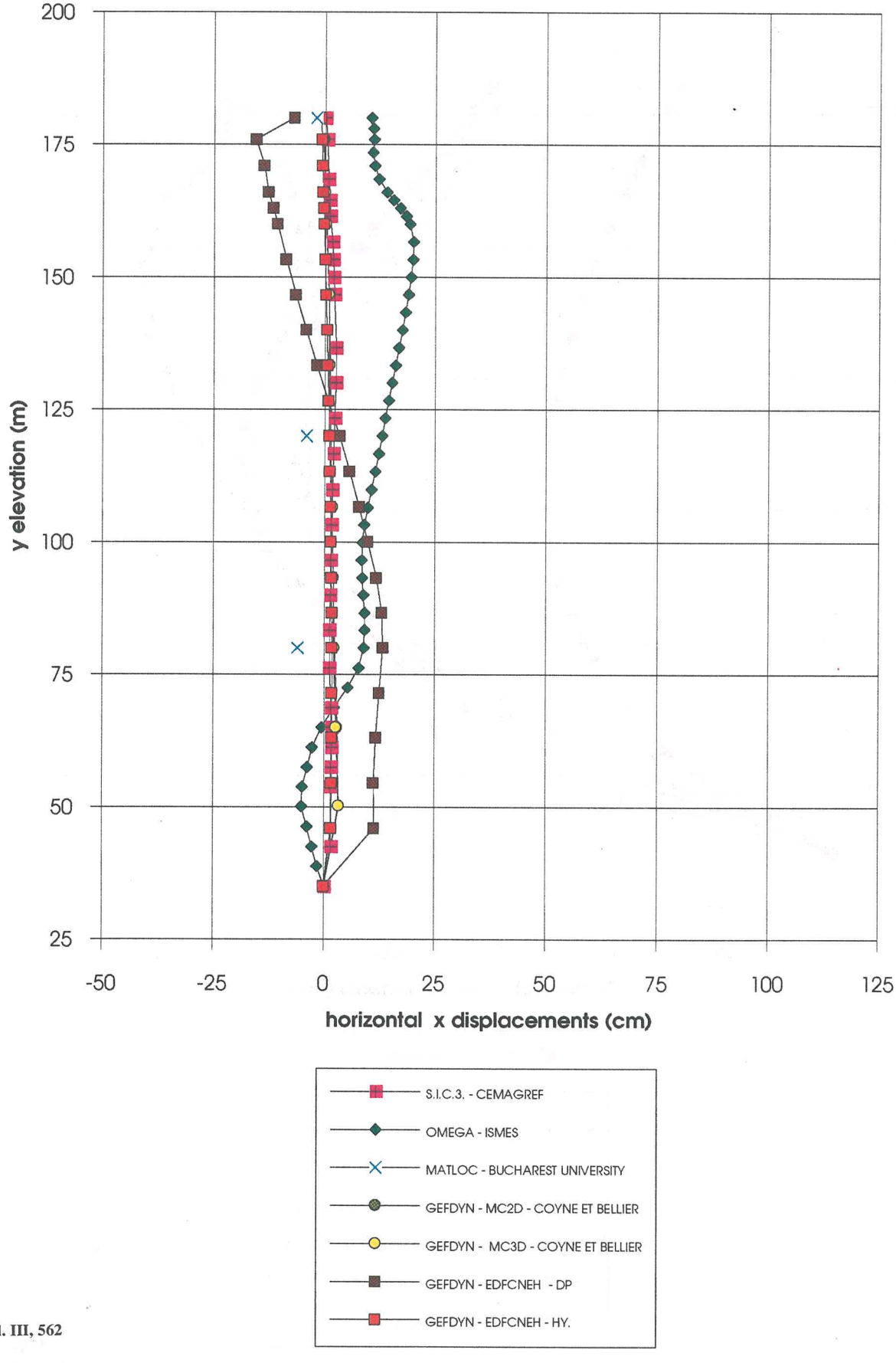

Fig. 21b

3rd. ICOLD 1994 - STATIC ANALYSIS
COMPARISON OF RESULTS

SETTLEMENTS PROFILE AT THE END OF CONSOLIDATION PHASE

SECTION B-B

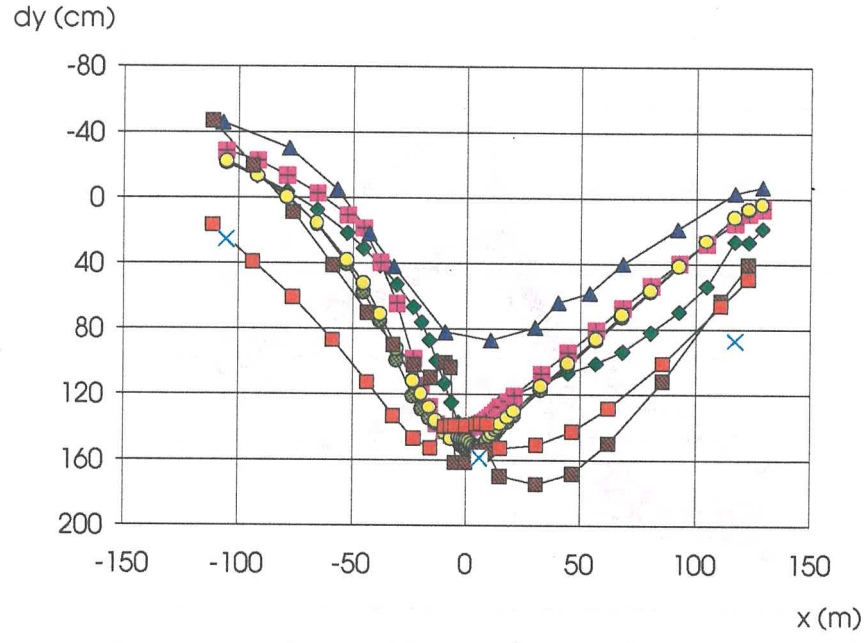

SECTION C-C

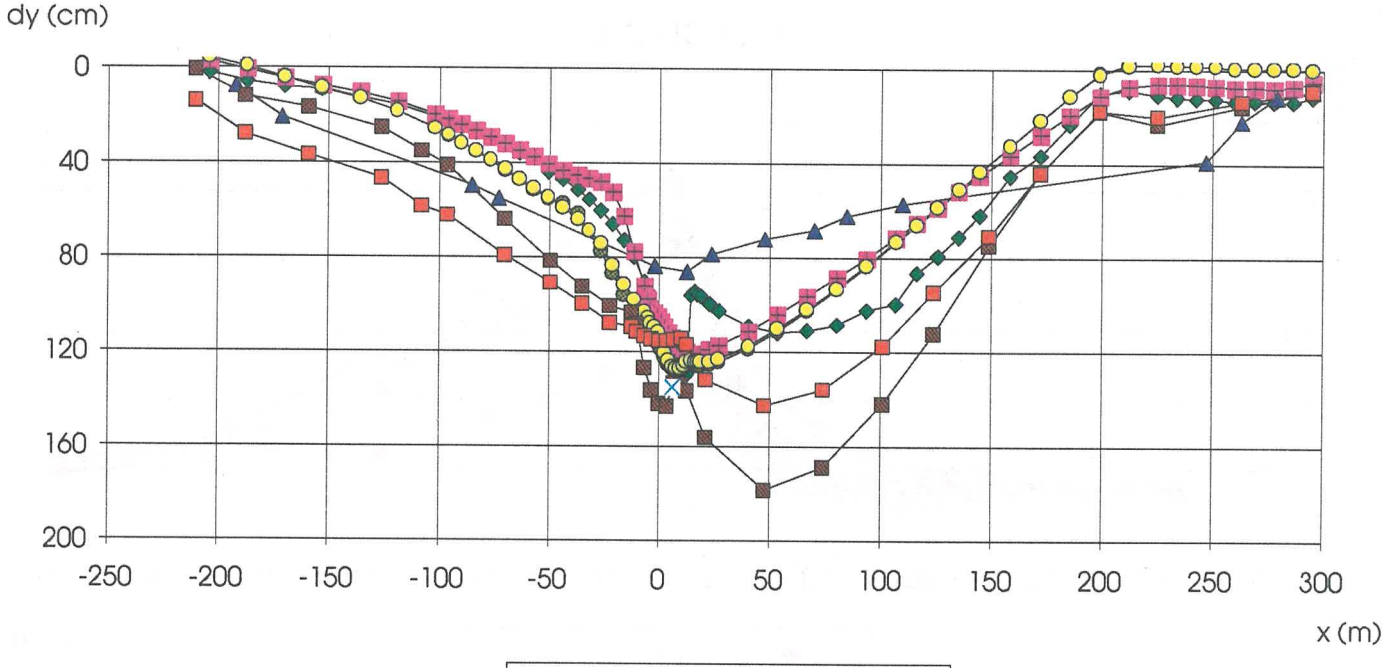

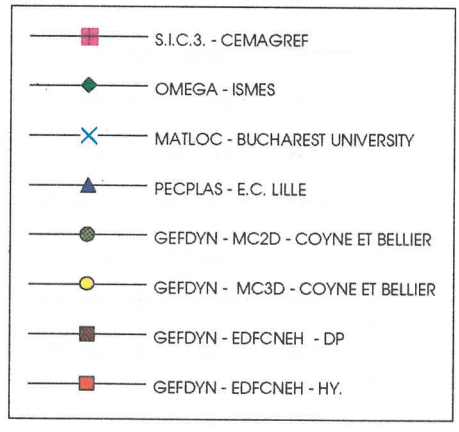

Fig. 22

3rd. ICOLD 1994 - STATIC ANALYSIS
COMPARISON OF RESULTS

HORIZONTAL DISPLACEMENTS AT THE END OF CONSOLIDATION PHASE

SECTION B-B

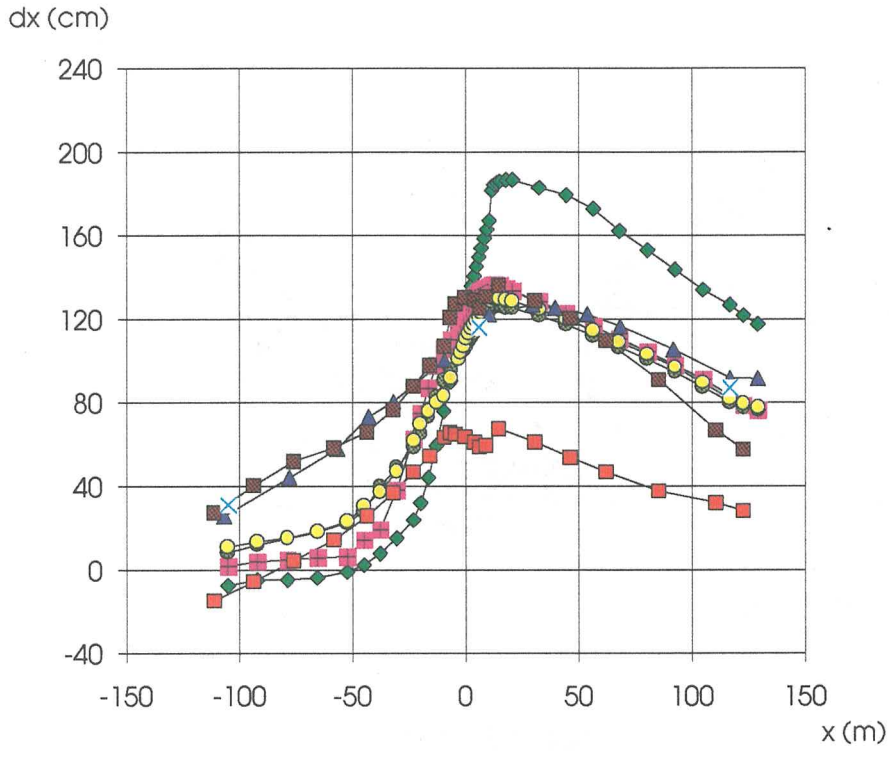

SECTION C-C

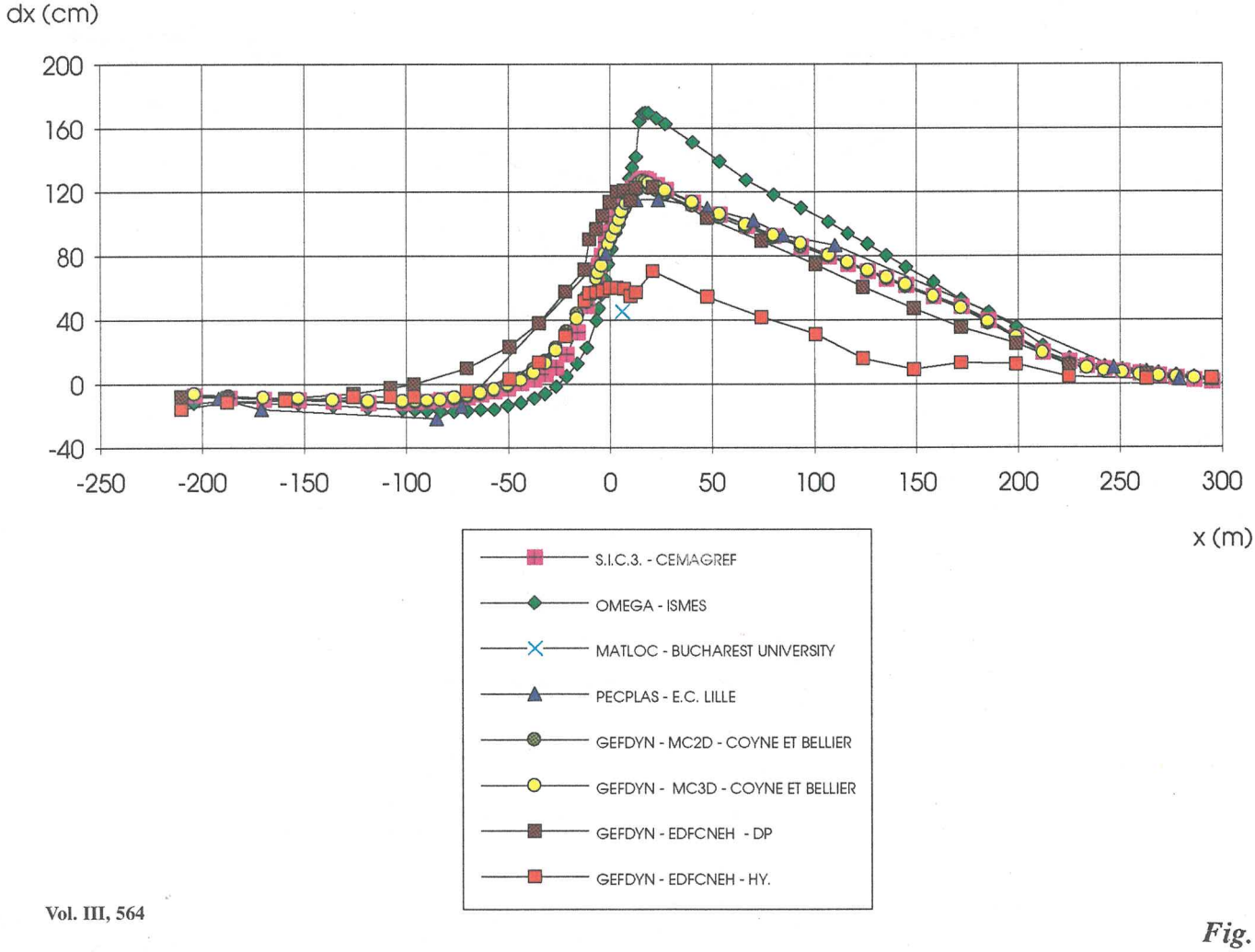

Fig. 23

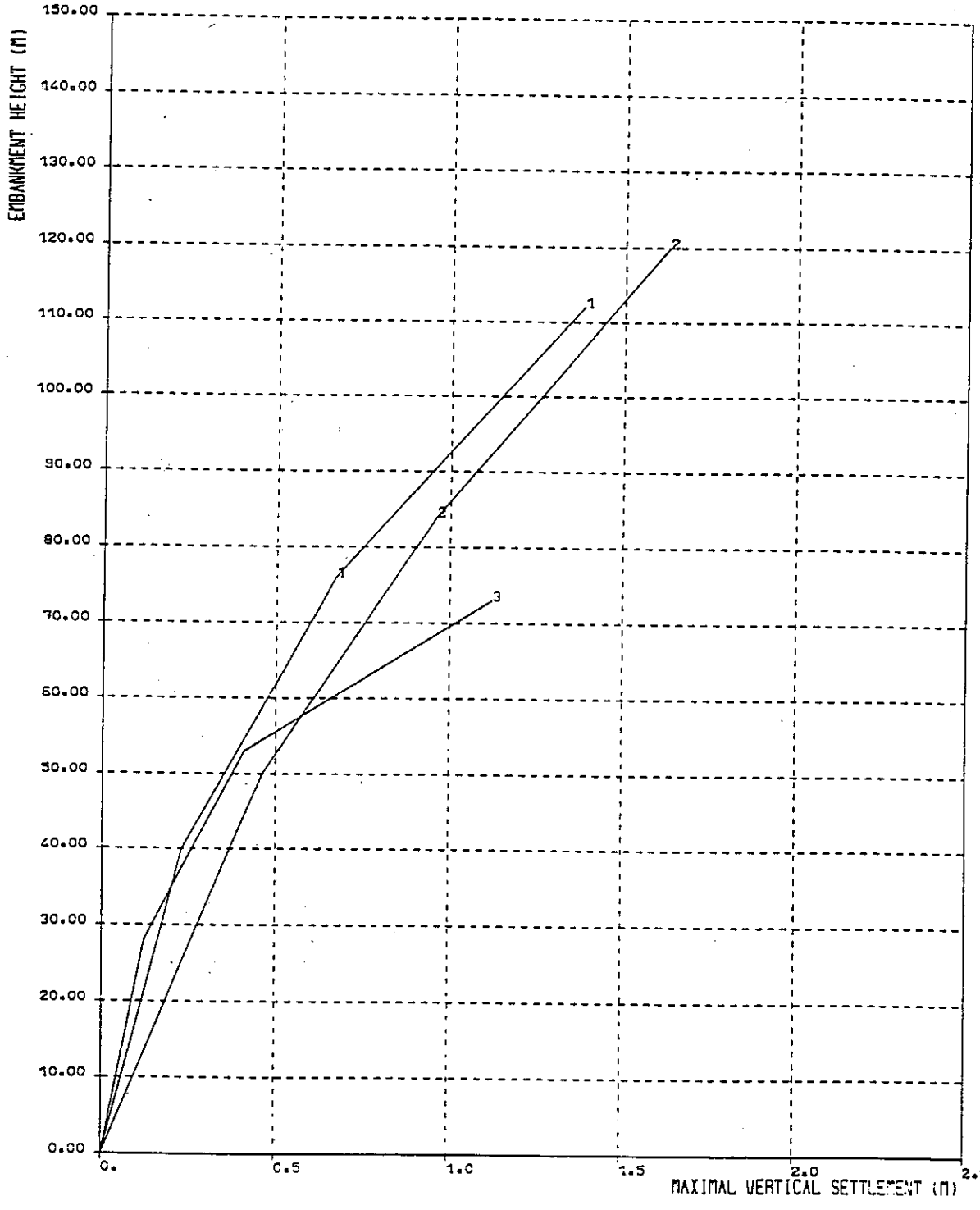

1 D1 (U/S ROCKFILL)
2 I1 (CORE)
3 D3 (D/S ROCKFILL)

EL INFIERNILLO - MAX. VERTICAL SETTLEMENT

VALUES OBSERVED AT THE END OF CONSTRUCTION

Fig. 24 a

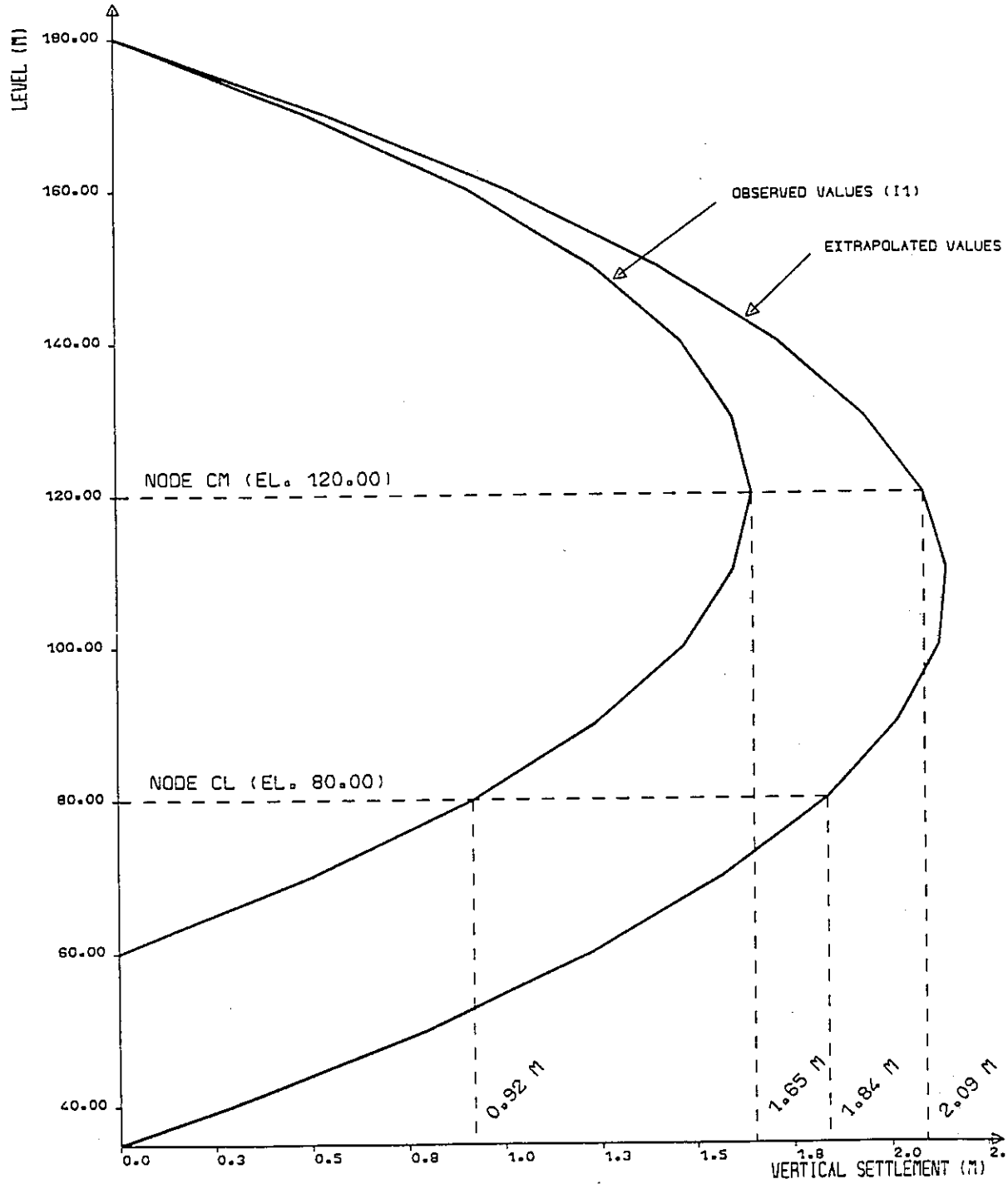

SETTLEMENTS IN THE CORE - CONSTRUCTION PE

OBSERVED VALUES (I1) AND EXTRAPOLATED SETTLEMENTS

Fig. 24b

Third Benchmark Workshop on Numerical Analysis of Dams
Gennevilliers (France) - September 29-30, 1994

Theme B1 :

EVALUATION OF PORE PRESSURE AND SETTLEMENTS OF AN EMBANKMENT DAM UNDER STATIC LOADINGS

SYNTHESIS

APPENDIX : COMPARISON OF RESULTS

COMPLEMENTARY TABLES AND DRAWINGS

3rd-.ICOLD 1994 - STATIC ANALYSIS
Comparison of results

Horizontal displacements (cm)

End of Conctruction

		Points of the dam section				
Authors	Utilized models	CC	CM	CL	UM	DM
S.I.C.3 - CEMAGREF	Mohr-Coulomb	0	3	6	-16	20
OMEGA - ISMES	Drucker-Pruger	0	10	11	-24	27
MATLOC - U.BUCHAREST	Duncan-Chang	0	0	-1	-39	34
GEFDYN - COYNE ET BELLIER	Mohr-Coulomb 2D	0	4	8	-18	21
	Mohr-Coulomb 3D	0	4	8	-18	21
GEFDYN - EDFCNEH	Drucker-Pruger	0	8	14	-7	13
	Hyperbolic	0	6	12	-13	6
PECPALS - E.C. LILLE	Mohr-Coulomb	0	3	7	-18	19

End of Impounding

		Points of the dam section				
Authors	Utilized models	CC	CM	CL	UM	DM
S.I.C.3 - CEMAGREF	Mohr-Coulomb	77	130	111	2	81
OMEGA - ISMES	Drucker-Pruger	126	137	104	-2	102
MATLOC - U.BUCHAREST	Duncan-Chang	92	120	51	31	91
GEFDYN - COYNE ET BELLIER	Mohr-Coulomb 2D	76	116	103	8	79
	Mohr-Coulomb 3D	81	120	105	12	81
GEFDYN - EDFCNEH	Drucker-Pruger	160	127	101	29	69
	Hyperbolic	36	63	58	-15	32
PECPALS - E.C. LILLE	Mohr-Coulomb	-	-	-	-	-

End of Consolidation

		Points of the dam section				
Authors	Utilized models	CC	CM	CL	UM	DM
S.I.C.3 - CEMAGREF	Mohr-Coulomb	77	132	112	2	83
OMEGA - ISMES	Drucker-Pruger	136	150	113	-8	127
MATLOC - U.BUCHAREST	Duncan-Chang	90	116	45	31	87
GEFDYN - COYNE ET BELLIER	Mohr-Coulomb 2D	76	117	106	8	80
	Mohr-Coulomb 3D	81	121	108	11	82
GEFDYN - EDFCNEH	Drucker-Pruger	153	130	114	27	67
	Hyperbolic	36	64	60	-15	32
PECPALS - E.C. LILLE	Mohr-Coulomb	116	119	103	26	92

3rd-.ICOLD 1994 - STATIC ANALYSIS
Comparison of results

Vertical displacements (cm)

End of Conctruction

Authors	Utilized models	Points of the dam section				
		CC	CM	CL	UM	DM
S.I.C.3 - CEMAGREF	Mohr-Coulomb	-4	-132	-109	-13	-16
OMEGA - ISMES	Drucker-Pruger	-19	-199	-148	-36	-45
MATLOC - U.BUCHAREST	Duncan-Chang	0	-164	-96	-25	-32
GEFDYN - COYNE ET BELLIER	Mohr-Coulomb 2D	0	-161	-131	-14	-16
	Mohr-Coulomb 3D	0	-161	-134	-14	-16
GEFDYN - EDFCNEH	Drucker-Pruger	0	-160	-130	-42	-54
	Hyperbolic	0	-127	-103	-47	-56
PECPALS - E.C. LILLE	Mohr-Coulomb	-	-163	-122	-8	-18

End of Impounding

Authors	Utilized models	Points of the dam section				
		CC	CM	CL	UM	DM
S.I.C.3 - CEMAGREF	Mohr-Coulomb	-19	-141	-117	28	-15
OMEGA - ISMES	Drucker-Pruger	23	-150	-122	22	-34
MATLOC - U.BUCHAREST	Duncan-Chang	-9	-153	-108	-26	-41
GEFDYN - COYNE ET BELLIER	Mohr-Coulomb 2D	1	-156	-128	21	-12
	Mohr-Coulomb 3D	5	-152	-127	22	-12
GEFDYN - EDFCNEH	Drucker-Pruger	49	-145	-129	48	-63
	Hyperbolic	-25	-137	-113	-17	-66
PECPALS - E.C. LILLE	Mohr-Coulomb	-	-	-	-	-

End of Consolidation

Authors	Utilized models	Points of the dam section				
		CC	CM	CL	UM	DM
S.I.C.3 - CEMAGREF	Mohr-Coulomb	-17	-137	-113	28	-15
OMEGA - ISMES	Drucker-Pruger	13	-158	-119	22	-26
MATLOC - U.BUCHAREST	Duncan-Chang	-6	-159	-135	-26	-87
GEFDYN - COYNE ET BELLIER	Mohr-Coulomb 2D	0	-156	-127	21	-12
	Mohr-Coulomb 3D	4	-152	-126	22	-12
GEFDYN - EDFCNEH	Drucker-Pruger	52	-162	-142	47	-63
	Hyperbolic	-27	-139	-115	-17	-66
PECPALS - E.C. LILLE	Mohr-Coulomb	11	-123	-79	45	-8

3rd-.ICOLD 1994 - STATIC ANALYSIS
Comparison of results

Pore Pressure (Mpa)

End of Conctruction

		Points of the dam section				
Authors	Utilized models	CC	CM	CL	UM	DM
S.I.C.3 - CEMAGREF	Mohr-Coulomb	-	-0.15	0.20	-0.85	-0.85
OMEGA - ISMES	Drucker-Pruger	0.00	0.01	0.09	0.00	0.00
MATLOC - U.BUCHAREST	Duncan-Chang	-	-	-	-	-
GEFDYN - COYNE ET BELLIER	Mohr-Coulomb 2D	0.01	0.08	0.26	-	-
	Mohr-Coulomb 3D	0.01	0.08	0.27	-	-
GEFDYN - EDFCNEH	Drucker-Pruger	0.00	0.25	0.59	0.00	0.00
	Hyperbolic	0.00	0.19	0.48	0.00	0.00
PECPALS - E.C. LILLE	Mohr-Coulomb	-	-	-	-	-

End of Impounding

		Points of the dam section				
Authors	Utilized models	CC	CM	CL	UM	DM
S.I.C.3 - CEMAGREF	Mohr-Coulomb	-0.12	0.37	0.52	0.49	-0.72
OMEGA - ISMES	Drucker-Pruger	0.00	0.37	0.57	0.48	0.00
MATLOC - U.BUCHAREST	Duncan-Chang	-	-	-	-	-
GEFDYN - COYNE ET BELLIER	Mohr-Coulomb 2D	-0.06	0.26	0.45	0.48	-
	Mohr-Coulomb 3D	-0.05	0.27	0.47	0.48	-
GEFDYN - EDFCNEH	Drucker-Pruger	0.00	0.33	0.68	0.48	0.00
	Hyperbolic	0.00	0.33	0.68	0.48	0.00
PECPALS - E.C. LILLE	Mohr-Coulomb	-	-	-	-	-

End of Consolidation

		Points of the dam section				
Authors	Utilized models	CC	CM	CL	UM	DM
S.I.C.3 - CEMAGREF	Mohr-Coulomb	-0.12	0.40	0.59	0.49	-0.72
OMEGA - ISMES	Drucker-Pruger	0.00	0.49	0.89	0.48	0.00
MATLOC - U.BUCHAREST	Duncan-Chang	-	-	-	-	-
GEFDYN - COYNE ET BELLIER	Mohr-Coulomb 2D	-0.07	0.24	0.44	0.48	-
	Mohr-Coulomb 3D	-0.07	0.25	0.46	0.48	-
GEFDYN - EDFCNEH	Drucker-Pruger	0.00	0.28	0.62	0.48	0.00
	Hyperbolic	0.00	0.25	0.46	0.48	0.00
PECPALS - E.C. LILLE	Mohr-Coulomb	0.00	0.31	0.70	0.50	0.00

3rd. ICOLD 1994 - STATIC ANALYSIS
Comparison of results
Horizontal displacements (m)

Point CC

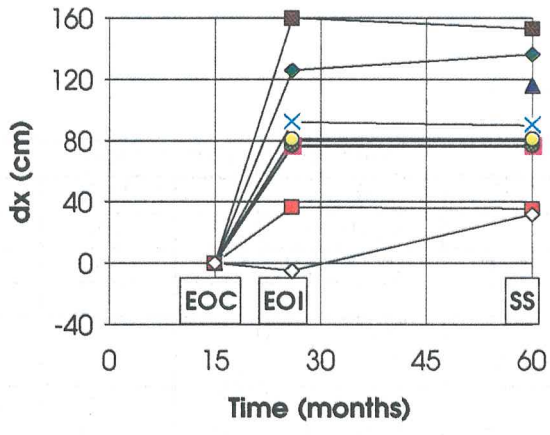

Point CM

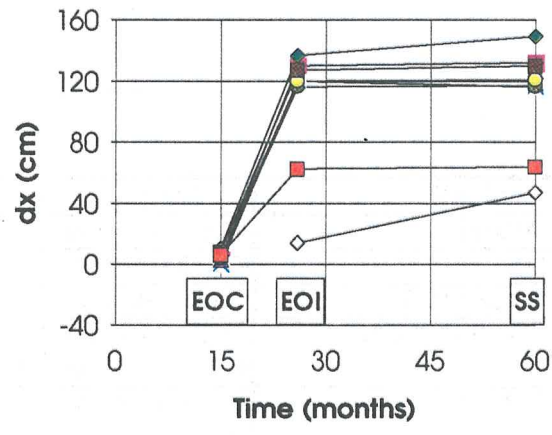

Point CL

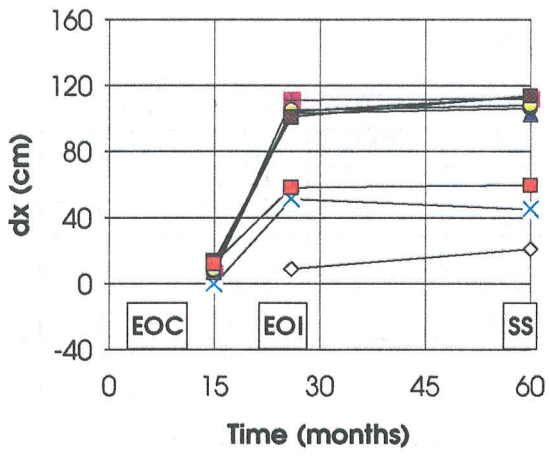

Point UM

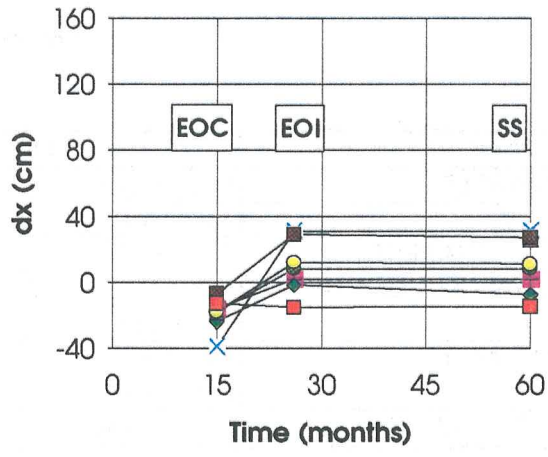

Point DM

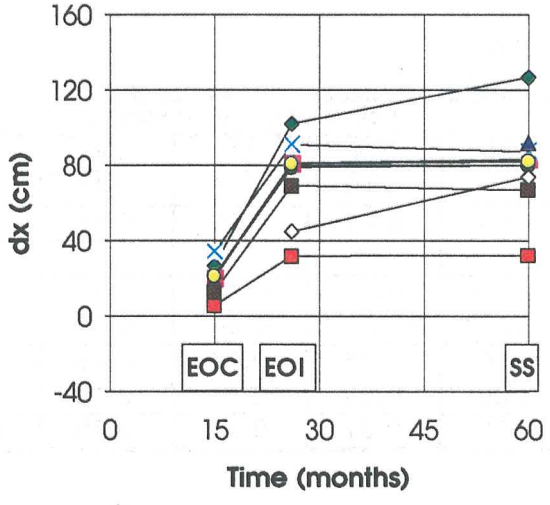

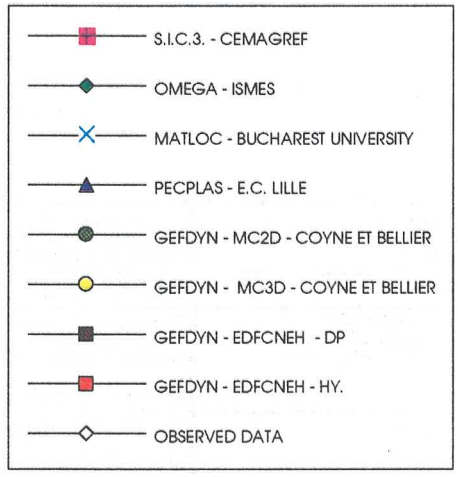

EOC - End Of Construction
EOI - End Of Impounding
SS - Steady State Condition

3rd. ICOLD 1994 - STATIC ANALYSIS
Comparison of results
Vertical displacements (m)

Point CC

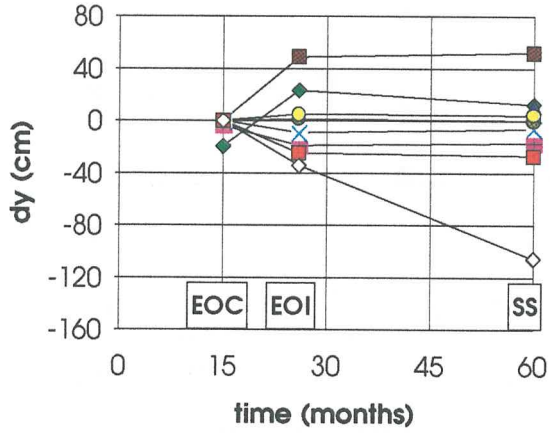

Point CM

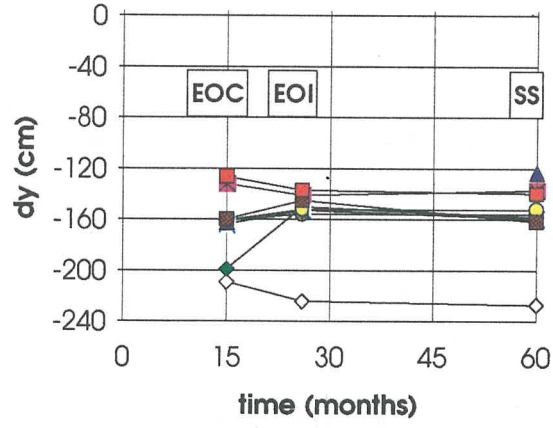

Point CL

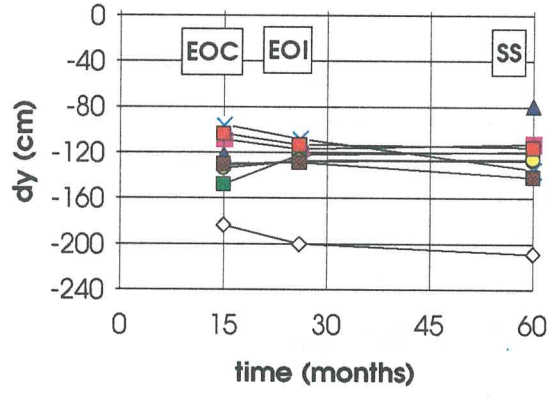

Point UM

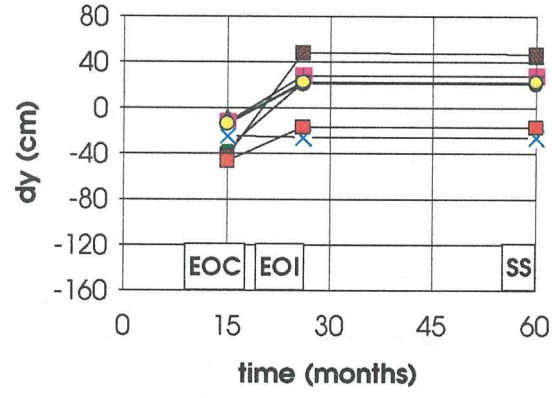

Point DM

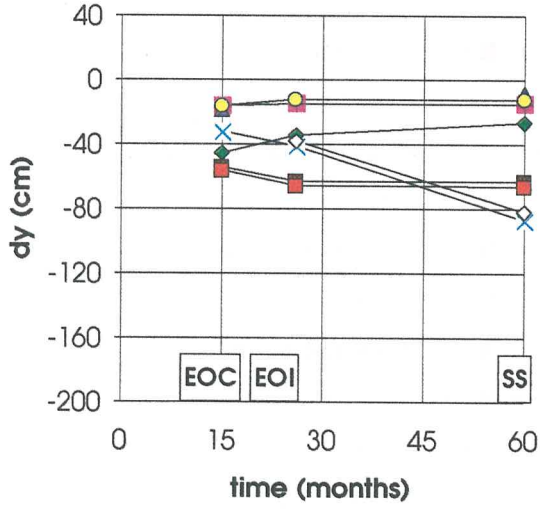

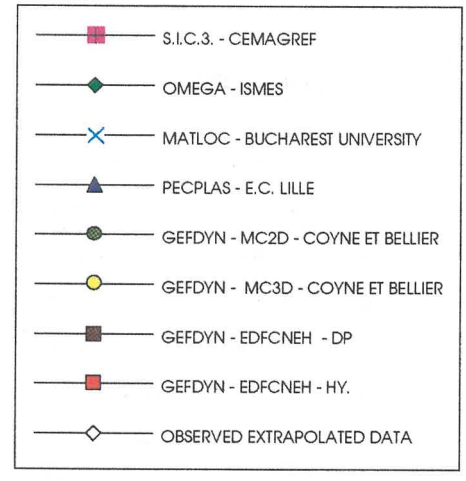

EOC - End Of Construction
EOI - End Of Impounding
SS - Steady State Condition

3rd. ICOLD 1994 - STATIC ANALYSIS
Comparison of results
Pore Pressure (Mpa)

Point CC

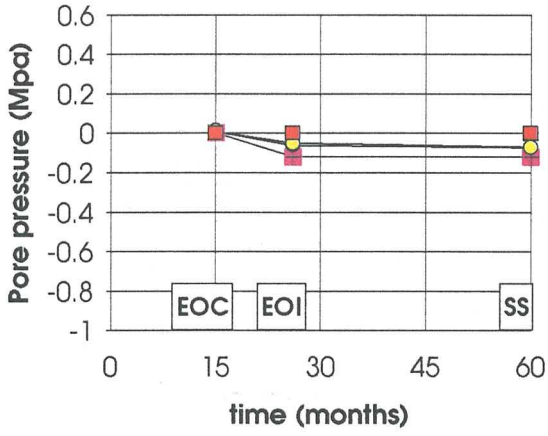

Point CM

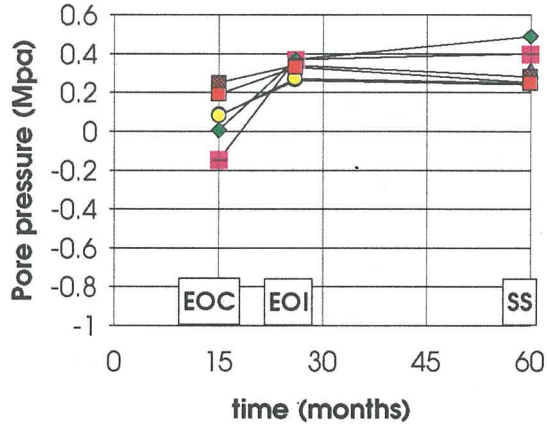

Point CL

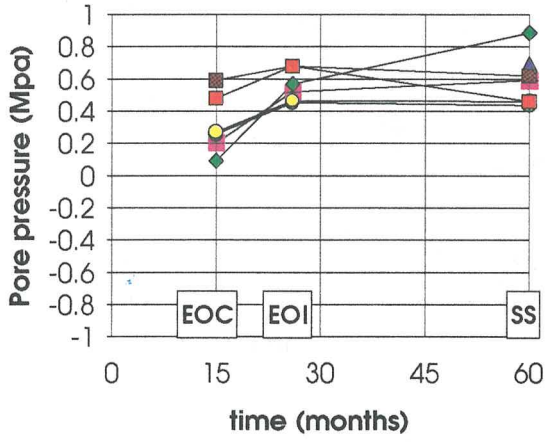

Point UM

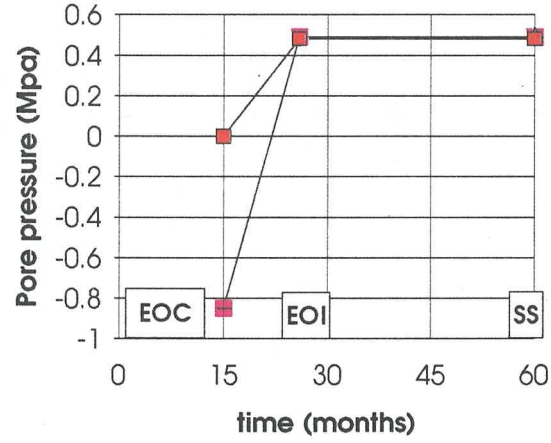

Point DM

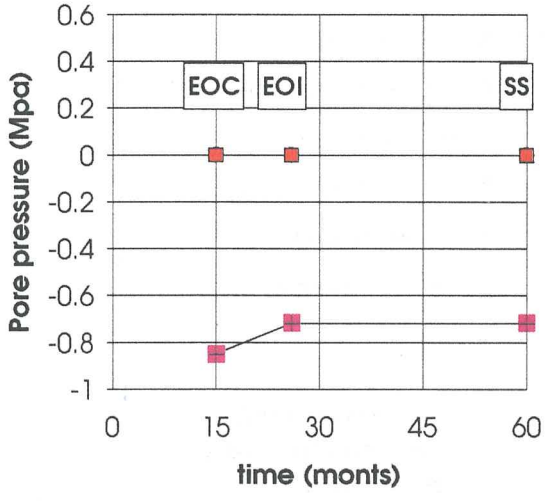

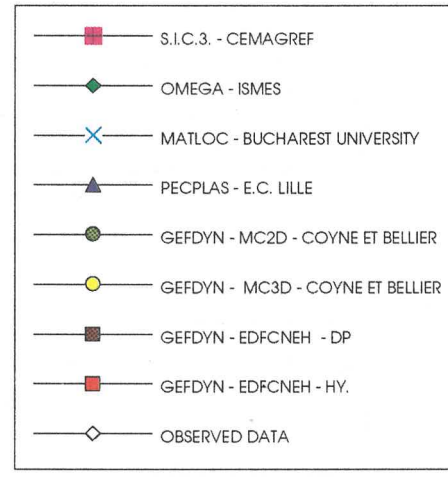

EOC - End Of Construction
EOI - End Of Impounding
SS - Steady State Condition

INCREMENTAL HORIZONTAL DISPLACEMENTS: TOTAL HORIZONTAL DISPL. AT THE END OF IMPOUNDING - TOTAL HORIZONTAL DISPL. AT THE END OF CONSTRUCTION

SECTION A-A

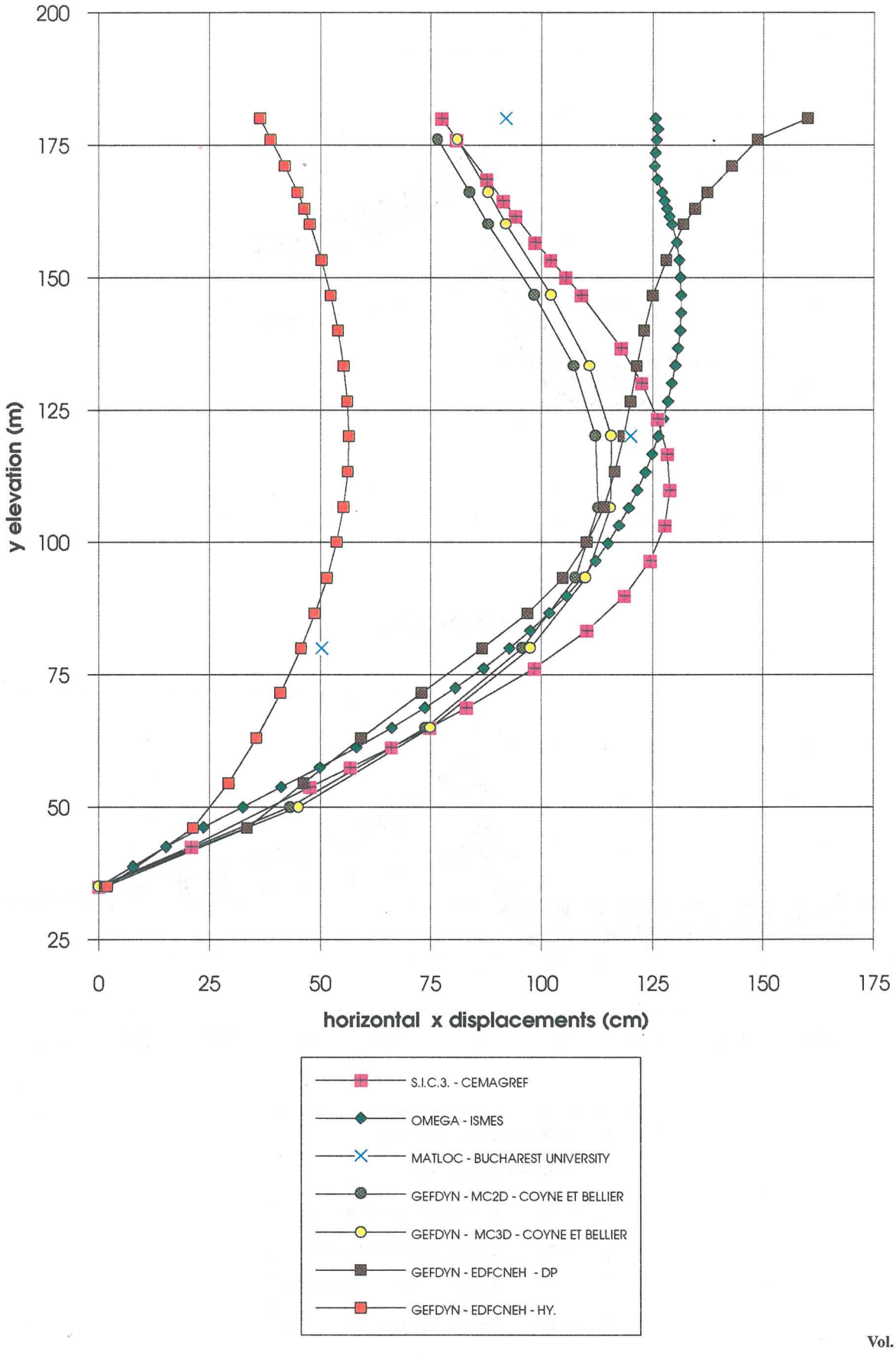

3rd. ICOLD 1994 - STATIC ANALYSIS
COMPARISON OF RESULTS

INCREMENTAL HORIZONTAL DISPLACEMENTS: TOTAL HORIZONTAL DiSPL. AT THE END OF IMPOUNDING - TOTAL HORIZONTAL DISPL. AT THE END OF CONSTRUCTION

SECTION B-B

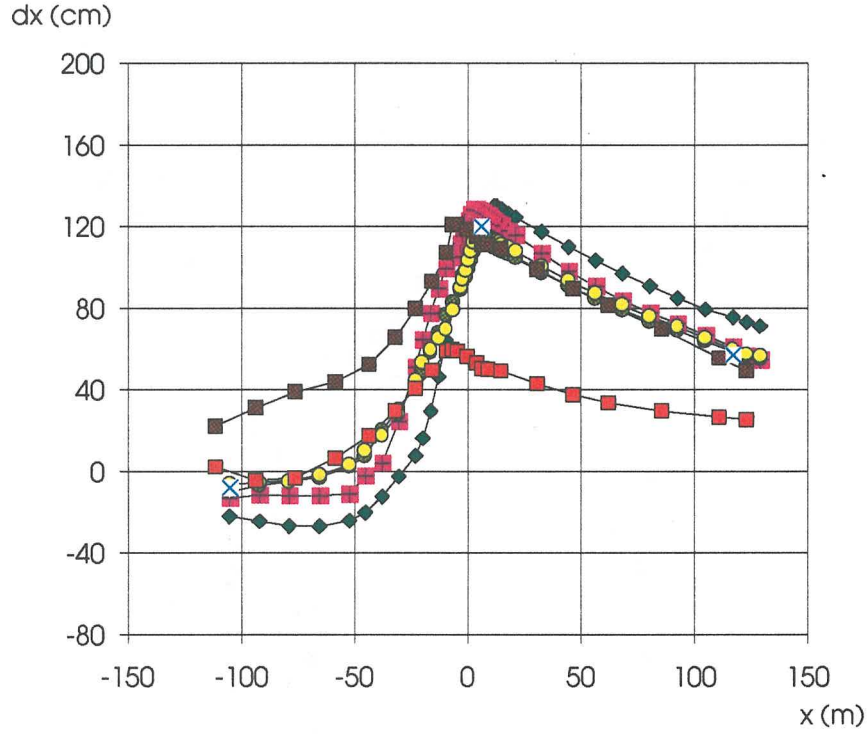

SECTION C-C

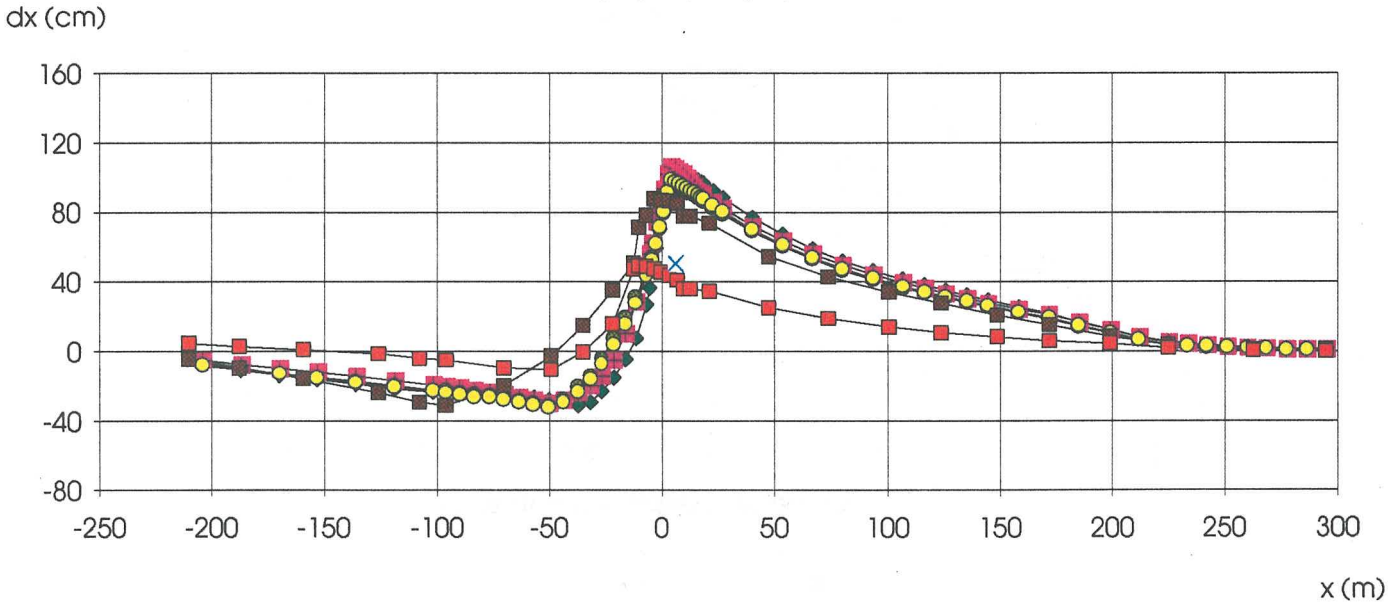

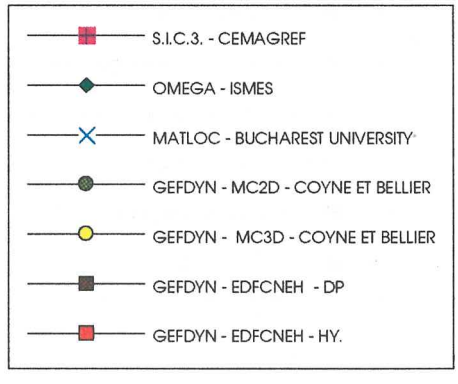

INCREMENTAL SETTLEMENTS: TOTAL SETTLEMENTS AT THE END OF CONSOLIDATION - TOTAL SETTLEMENTS AT THE END OF IMPOUNDING

SECTION B-B

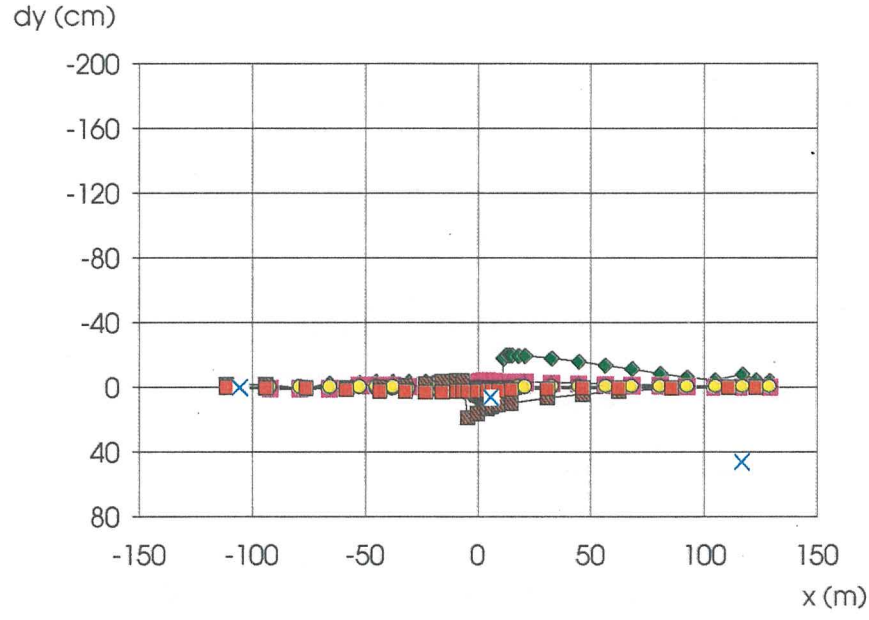

SECTION C-C

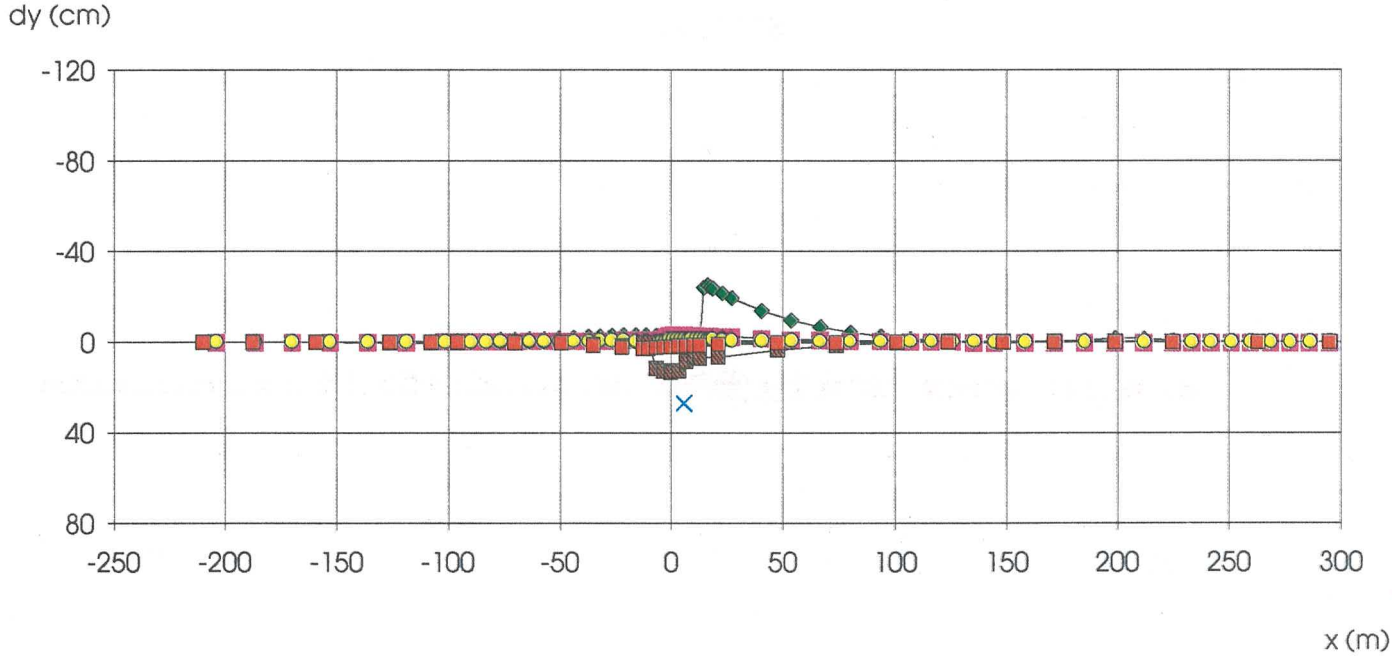

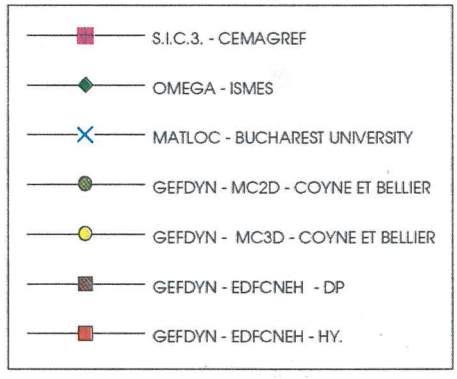

INCREMENTAL HORIZONTAL DISPLACEMENTS: TOTAL HORIZONTAL DISPL. AT THE END OF CONSOLIDATION - TOTAL HORIZONTAL DISPL. AT THE END OF IMPOUNDING

SECTION B-B

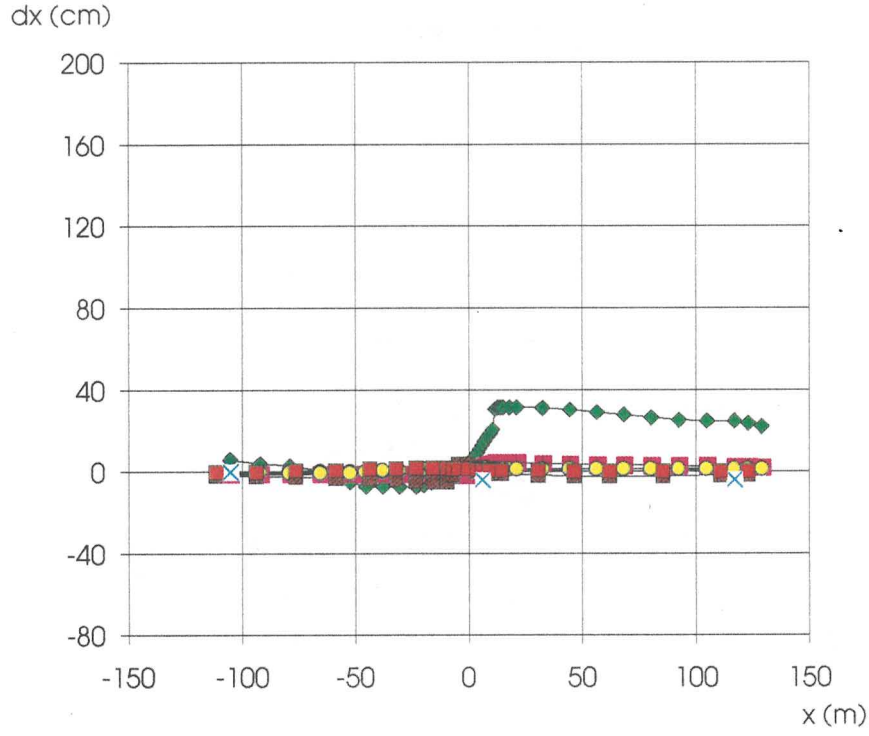

SECTION C-C

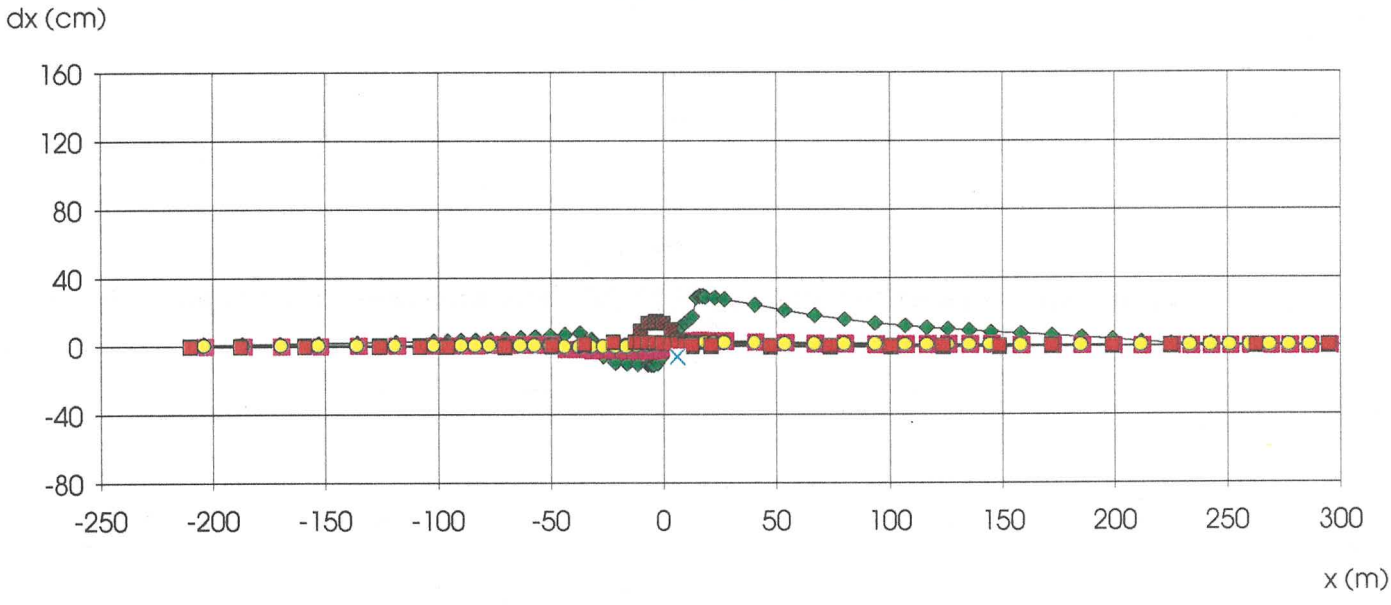

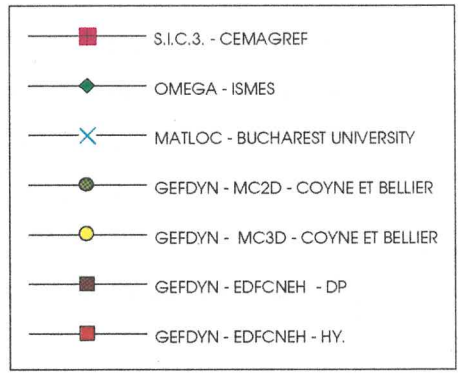

NOTES

NOTES

Third Benchmark Workshop on
NUMERICAL ANALYSIS OF DAMS
Gennevilliers, France, September 29-30, 1994

THEME B1

Evaluation of pore pressure and settlements of an embankment dam under static loadings

PAPERS

. GEFDYN & UDAM : F. Laigle, J.J. Fry, EDF-CNEH, France

. GEFDYN : O. Ozanam, B. Tardieu, Coyne et Bellier, France

. OMEGA : G. La Barbera, A. Bani, G. Mazzà, ISMES SpA and ENEL-CRIS, Italy

. PECPLAS : I. Shahrour, A. Khorshavan, M. Zaher, Ecole Centrale de Lille, France

. S.I.C.3 : L. Guellouz, S. Bonelli, O.Débordes, CEMAGREF, France

. GEFDYN - Bath County Upper Dam : A. Sengupta, Ph. Martin, Harza Eng. Comp., USA

STATIC ANALYSIS OF EL INFIERNILLO DAM .

François LAIGLE, Jean Jacques FRY, Philippe MAGNIN.
EDF/CNEH. Savoie Technolac
73 373 Le Bourget du lac Cedex, France.

0/ Preamble:

Analyses presented here correspond to ***a justification approach*** *of constitutive models and parameters identification process. The aim of this study is to compare some numerical results with field measurements, in the case of a well monitored dam, like El Infiernillo dam. We try to define the limitations of some modellings, and the interest of other approaches.*

Under these conditions, this analysis does not exactly correspond to the theme B1, which concerns essentially the ***validation approach*** *of numerical models and the couple user/software. In this case, it's necessary to compare some predictions, obtained with different software, allowing identical assumptions.*

1/ INTRODUCTION:

This paper presents the results of a numerical modelling of the El Infiernillo dam's behaviour, during its construction, impounding, and consolidation period. This work has been undertaken at EDF/CNEH, for the third ICOLD Benchmark Workshop on Numerical Analysis of Dams.

3 analyses were performed , using 2 different software:

The 2 first modellings were made with GEFDYN, which has been developed jointly by EDF/CNEH, COYNE et BELLIER, and ECOLE CENTRALE DE PARIS. In these two cases, constitutive models were changed in shells, filters, and transitions only. In the first test, a Drucker-Prager model was used for these materials. In the second simulation, a hyperbolic model was used. The aim of this comparison was to understand and evaluate the interest of a non-linear approach.

In the last simulation, we used UDAM, which has been developed by EDF/CNEH and ENPC/CERMES. This sofware is based on a three-phases approach of the fill material. Air pressure, water pressure, and displacements are unknown nodal variables, and are calculated by a coupled approach. This software is well suited to reproduce homogeneous clayey fill construction. In this first version, a multiphase material and a drained material could be used together.

For each analysis, more details on material properties, and main assumptions were introduced, and data about state of stresses, settlements, and pore pressures distribution were computed at 3 points in time: End of construction, end of impounding, and end of consolidation.

II/ PRESENTATION OF EACH APPROACH; ASSUMPTIONS

II.1/ TWO-PHASES COUPLED APPROACH OF STATIC BEHAVIOUR.

In this part, two simulations were made with GEFDYN. In this approach, we assumed the saturation of soil, especially in core material. So, only two phases were taken into account :

+ A solid part, corresponding to the skeleton of grains. The behaviour of this solid phase is simulated by a constitutive model presented subsequently.

+ A fluid part corresponding to the free water in soils.

II.1.1/ MESH- BOUNDARY CONDITIONS.

Linear elements with three or four nodes only were used. The final purpose was to simulate the dynamic behaviour of this dam, so the dimension elements might respect a criterion on the maximum length. Mesh is shown at figure 1. This final mesh is constituted by 442 volumetric elements. Other specific elements are used on boundaries:

+ Paraxial elements under the foundation. These elements are necessary if we want to absorb waves on the boundary, and avoid the effect of wave reflection on the mesh's limits.

+ Interface elements, between mesh and paraxial elements. These elements present only numerical function.

+ Loading elements which allow the application of mechanical sollicitation during the impounding , on the upstream shell.

II.1.2/ CONSTITUTIVE EQUATIONS:

Two static approaches were performed with GEFDYN, and only constitutive model of the shell materials were modified. The following models have been adopted for each simulation:

+ **Core**: In these two cases, an elastoplastic model was used to simulate the clay's behaviour. This model is the HUJEUX model, which has been adopted by COYNE et BELLIER during the second Bechmark Workshop in Bergamo (1992). All parameters have been estimated again, with laboratory tests, such as oedometer, and triaxial test. These parameters are listed in table 1, and fitting of triaxial and oedometer curves have been drawn on figure 2.

a/ Simulation C1

+ In a first approach (Simulation C1), DRUCKER-PRAGER model is used, **in shells**, and other parts of the dam.

Initialy, we made an identification of HUJEUX model parameters, for each material, with laboratory test results. Figures 3 and 4 present some fitting of triaxials tests on shoulder and filter, made with HUJEUX model, but this last computation of El Infiernillo dam is not presented here. In this paper, only computations which respect all convergence criteria, will be analysed. With an elastoplastic model, like HUJEUX model, in shoulders, and particulary in filters, we met lot of numerical problems, due essentially to large shear strains between filters and core (Shear strain > 5% locally, in filters and core) and, perhaps, an imperfect modelling of the contact between core and filters. These shear strains are large when relative stiffnesses between core and shoulders are very different.

Parameters	Core
K	50 MPa
G	23 MPa
n	0,50
Φ	26°
Ψ	26°
b	0,80
β	28
$\mathbf{P_{ci}}$	0,200 MPa
d	1,80
a	0,001
acyc	0,0005
α	1,50
c	0,02
$\mathbf{c_{cyc}}$	0,01
m	2
$\mathbf{r_{iso}}$	0,01
$\mathbf{r_{ela}}$	0,01
$\mathbf{r_{hyst}}$	0,08
$\mathbf{r_{mbl}}$	0,30

Table 1: Hujeux model parameters for clay

The DRUCKER-PRAGER model parameters are the following:

+ The friction angle Φ.
+ The characteristic angle of dilatancy: Ψ
+ The cohesion which is chosen equal to zero in these granular materials.
+ The Young's modulus E.
+ The Poisson's ratio ν.

These values are defined according to the laboratory results, or to field measurements, such as settlement and strain, for example. Φ and Ψ were chosen with triaxial tests, when the Young's modulus was defined with settlement measurements in transitions and rockfill shells. The parameters sets used in this computation, for each material of shells, are given in table 2.

Parameters	Filters	Transitions	Shoulders
E	250 MPa	65 MPa	35 MPa
ν	0,30	0,30	0,30
Φ	36°	41°	41°
Ψ	33°	39°	39°
C	0	0	0

Table 2: Parameters of DRUCKER-PRAGER model. Simulation C1.

In this approach, the rockfill behaviour is essentially elastic and linear, with an unloading young's modulus which is the same as the loading modulus. We 'll see subsequently, that, with these asumptions, some results are not acceptable, at the end of consolidation, and during the impounding. In fact, we could see that during the impounding, an important swelling of upstream shell may appear.

b/ Simulation C2

+ In a second time, an hyperbolic model was adopted for all materials, without clay core (Simulation C2). This model has been obtained using specific values for HUJEUX model parameters. In the original model of ECP, four mechanisms are considered: Three deviatorics mechanisms, and one isotropic mechanism. In this case, with hyperbolic model, we assume that isotropic mechanism is not active. Concerning deviatoric mechanisms, the assumptions are the following:

- No volumetric hardening. The parameter b is taken equal to zero, and the value of Pc is no longer considered.
- No volumetric plastic strain. We concider that we work in the hysteretic domain, so there isn't volumetric plastic strain. Irreversible behaviour is reproduced with a unloading initial modulus which is given by a_{cyc} value.

The parameter sets are given in table 3.

Parameters	Core	Filter	Transition	Compacted and dumped shoulder
K	50 MPa	90 MPa	75 MPa	30 MPa
G	23 MPa	120 MPa	84 MPa	56 MPa
n	0,50	0	0	0
Φ	26°	44°	41°	41°
Ψ	26°	44°	39°	39°
b	0,80	0	0	0
β	28	*	*	*
P_{ci}	0,200 MPa	*	*	*
d	1,80	*	*	*
a	0,001	0,002	0,0045	0,006
acyc	0,0005	0,002	0,0045	0,006
α	1,50	*	*	*
c	0,02	0,0001	0,0001	0,0001
c_{cyc}	0,01	0,0001	0,0001	0,0001
m	2	*	*	*
r_{iso}	0,01	1.	1.	1.
r_{ela}	0,01	0	0	0
r_{hyst}	0,08	1.	1.	1.
r_{mbl}	0,30	1.	1.	1.

Table 3: Parameters of the simulation C2, with hyperbolic model.

Figure 5 shows some fitting of triaxial test curves on compacted shoulder, using this hyperbolic model.

II.1.3/ PERMEABILITY:

Permeabilities in rockfills, and filters, are important, relative to the clay's permeability in the core. The permeability of clay has been modified between the two approaches. Values used are in Table 4 and 4.bis:

material	Core	Filter	Transition	Compacted and dumped shoulder
k_{wv} (m/s)	2.10^{-10}	8.10^{-5}	7.10^{-4}	7.10^{-4}
k_{wh} (m/s)	2.10^{-10}	8.10^{-5}	7.10^{-4}	7.10^{-4}

Table 4: Permeabilities for the C1 simulation.

material	Core	Filter	Transition	Compacted and dumped shoulder
k_{wv} (m/s)	2.10^{-10}	8.10^{-5}	7.10^{-4}	7.10^{-4}
k_{wh} (m/s)	6.10^{-10}	8.10^{-5}	7.10^{-4}	7.10^{-4}

Table 4 bis: Permeabilities for the C2 simulation.

II.2/ PARTIALLY SATURATED APPROACH OF CORE BEHAVIOUR.

UDAM sofware makes possible the forecasting of pore pressure increase during construction of earthfill dam in clay, and permits evaluation of the influence of saturation on this water pressure evolution. Its used is really justifiable for clayey fills dams, during their construction.

In one aim of validation. it seemed interesting to apply this unsaturated approach to rockfill dams, and to compare with others sofware results.

The initial version did not allow the simulation of impounding phase. Some modifications have been introduced during this work, but this new version remain incomplete. Coupled approach was only used in core. Shell's behaviour was considered uncoupled, so without water pressure. This limitation should not be forgotten when interpreting results.

Materials may be concidered unsaturated in core, and the effects of suction's variations (which characterize the difference between air pressure and water pressure) on mechanical and hydraulic behaviour are taken into account. Different phases are:

- Solid part.
- Fluid part, which is the water. This fluid phase is not necessary continuous in soil, and we don't apply Bishop's theory of effective stress.
- A gas phase, which correspond to the air.

State variables are the void ratio e, and the degree of saturation Sat. Both variables advance independently with stress and suction. This assumption was initialy proposed by Mathias, with the concept of state surfaces. Formulae of each state surface are as follows:

$$e = \frac{(1-e_0)}{\exp\left\{\frac{\left[a_e.\frac{(\sigma-u_a)}{P_{atm}} + b_e\left(1-\frac{(\sigma-u_a)}{\sigma_e}\right).\frac{(u_a-u_w)}{P_{atm}}\right]^{1-m}}{K_b.(1-m)}\right\}} - 1$$

$$Sat = 1-\left[a_s + b_s(\sigma-u_a)\right]\left[1-\exp\left(-c_s(u_a-u_w)\right)\right]$$

e_0 is the initial void ratio, in saturated conditions, with any stress.
u_a: Air pressure.
u_w: Water pressure.
P_{atm}: atmospheric pressure;
σ: Vertical stress.

a_e, K_b and m influence the compressibility of soil, and may be defined from oedometer test, on saturated sample.
b_e characterize the effect of suction, on soil's behaviour.
σ_e is the swelling stress.

With this concept of state surface, the following phenomena are simulated:

+ Collapse or swelling of soil, under constant total stresses, with variation of suction.
+ Evolution of compressibility, versus suction.
+ Evolution of mechanical properties, like friction angle and cohesion.

Mechanical constitutive model is the hyperbolic DUNCAN law, only for shear strains. In fact, volumetric deformations are defined by the void ratio state surface, and the hyperbolic model is only use to compute deviatoric strains. Kb, bulk modulus, and m, parameters of the DUNCAN's law are not used here.

II.2.1/ MESH-BOUNDARY CONDITIONS.

UDAM use, actually, only linear elements with four nodes. It's not possible to introduce triangles. Mesh is shown figure 6, and is constituted of 611 nodes and 552 elements.

There are two kind of materials for one modelling like this. Only core was considered unsaturated, and we used for this clay the three-phase approach. The other materials have a

great permeability, and may be simulated by an uncoupled modelling. In rockfill and filters, we did not take into account this coupling. For these granular materials, the constitutive model was DUNCAN's law, with all parameters.

During construction, we must initialise suction on each layer. Like atmospheric pressure is taken as a reference, initial water pressure is lesser than zero.

Boundary conditions, essentially for unsaturated soil, are not easy to define. We must impose, around the core, some conditions about water pressure and air pressure, during construction, and, what is more difficult, during impounding.

+ Construction: *Air pressure* is zero on the core's limits;
Water pressure:
No flow through limits if this pressure is lesser than zero.
Water pressure is after imposed to zero.

+Impounding: *Air pressure* is equal to water pressure under the reservoir's level.
In this case, suction is null.
On the other boundaries, air pressure is zero.
Water pressure:
water level on the upstream face.
Same conditions as during contruction, on the other limits.

II.2.2/ SOIL PARAMETERS:

All parameters, for each soil, are presented in table 5 and table 6, state surfaces are shown figures 7 and 8.

Void ratio state surface	e_0	a_e	b_e	K_b	σ_e	m
	0,61	0,9	0,57	68 kPa	300kPa	0,5
Degree of saturation state surface	a_s	b_s	c_s			
	1,0	$-1.\ 10^{-7}$	$1.0\ 10^{-6}$			

Table 5: state surface parameters

These parameters may be defined from oedometer tests, with suction control. As we did not have any data about unsaturated behaviour of clay's core, we used the following approach:

- Plasticity index: Ip=20 to 30.

For identical material with Ip=24, we may keep, for optimum Proctor water content, a succion of 170 kPa. **w=wopt ===> Suc=170 kPa.**

For this soil, optimum Proctor water content is about 17,4%. There is a good agreement between El Infiernillo clay and this material, since they have an identical liquid limit, about 40 %. We assume that **wopt=17,4%.**

The average initial water content in core was about 19,3%, so clay was deposited with a water content equal to w=wopt+2, and an average degree of saturation of 94 to 95%.

Initial void ratio was about 0,55.

With these data, we could define some state surface parameters, which might respected the following conditions:

w=wopt=17,4 % ==> Suc=170 kPa ==> Sat= ? ==> e=?
w=wopt+2 ==> Suc= ? ==> Sat=94 to 96%==> e=0,55.

With precedent parameter set, we obtain:

w=wopt=17,4% ==> Suc=170 kPa ==> Sat=90 % ==> e=0,53
w=wopt+2 ==> Suc=95 kPa ==> Sat=94,2% ==> e=0,55

Materials	Core	Filter	Transition	Shouders, compacted and dumper
K_{load}	50.	1800	330	180
K_{unload}	100.	3600	660	360
n	0,65	0,30	0,50	0,50
Φ	25°	41°	41°	41°
C	20 kPa	0	0	0
K_b	State surface	1200	400	220
m	State surface	0,3	0,5	0,6
Rf	0,80	0,7	0,7	0,7

Table 6: Mechanical parameters

II.2.3/ PERMEABILITY:

With the three phase approach, two permeabilities have to be introduced; One for air flow, and another for water flow. Like mechanical properties, these permeabilities vary with the

state of soil, so, with void ratio and degree of saturation. These evolutions are expressed by the two following formulae:

$$\text{Water permeability:} \quad K_w = A.10^{\alpha e}\left(\frac{Sat - S_{ru}}{1 - S_{ru}}\right)^3$$

$$\text{Air permeability:} \quad K_a = B\frac{\gamma_a}{\mu_a}[e(1 - Sat)]^c$$

A and α characterize the water permeability when soil is saturated.
S_{ru} is the residual saturation.
γ_a, and μ_a are air density and air viscosity.
B and c characterize the air permeability evolution.

With following values, water permeability is about 10^{-10} m/s, but vary with the degree of saturation, and void ratio.

A=9. 10^{-12}
α=3.
S_{ru}=0.

B=2. 10^{-7}
c=3.

Ratio kwh/kwv is equal to 3.5.

III/ FIGURES

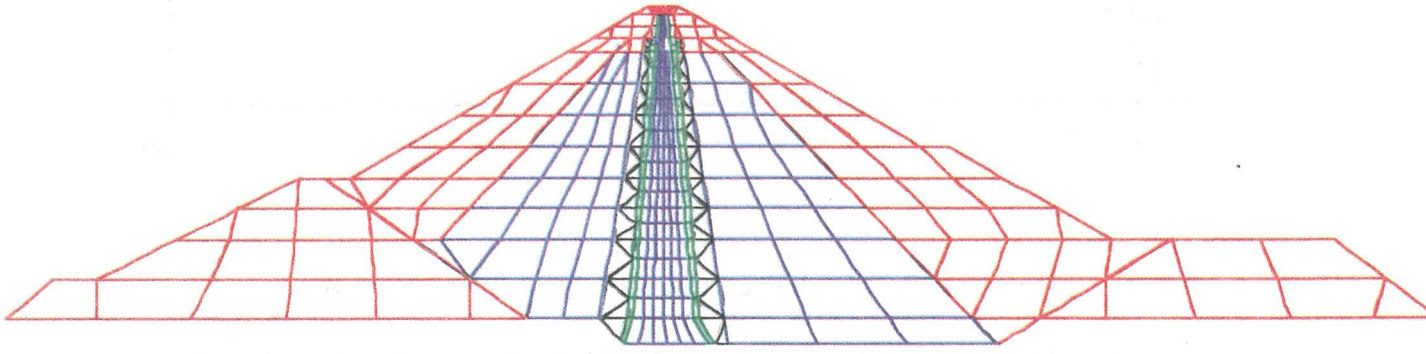

Figure 1: Finit element mesh used with GEFDYN software.

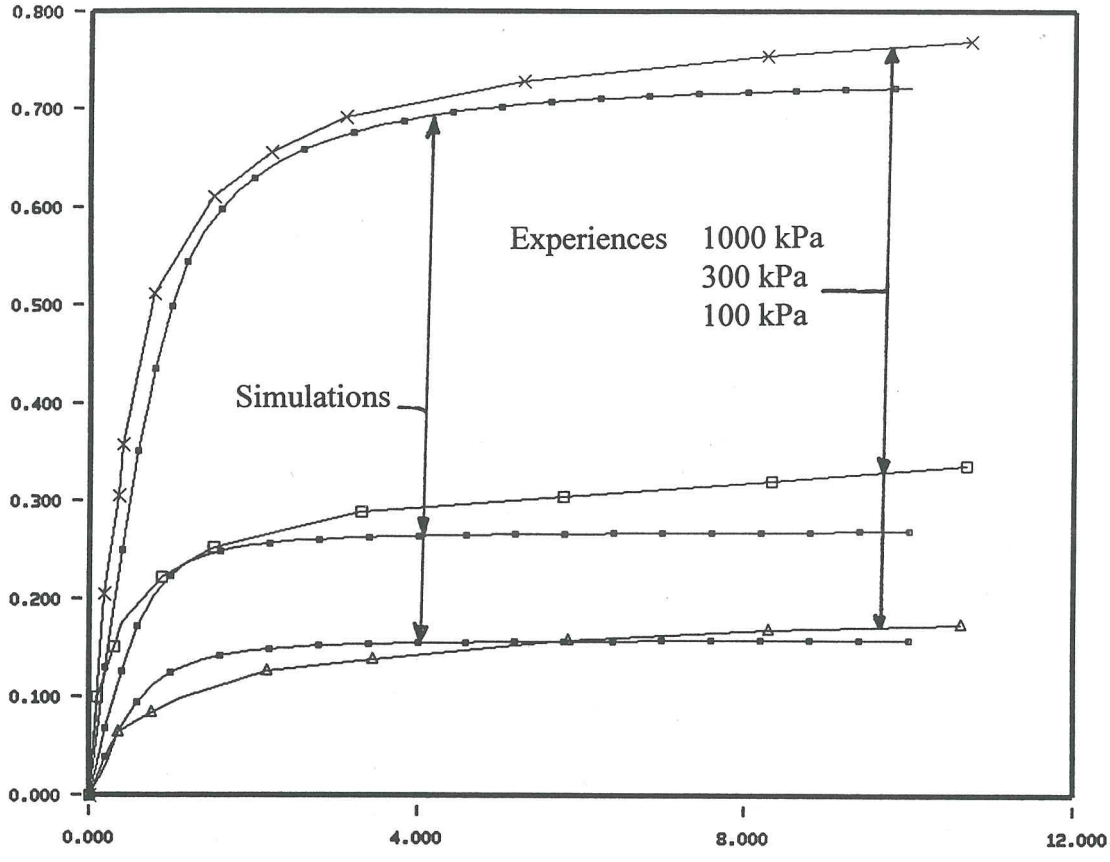

Figure 2a: Core: Undrained triaxial tests simulations on clay.

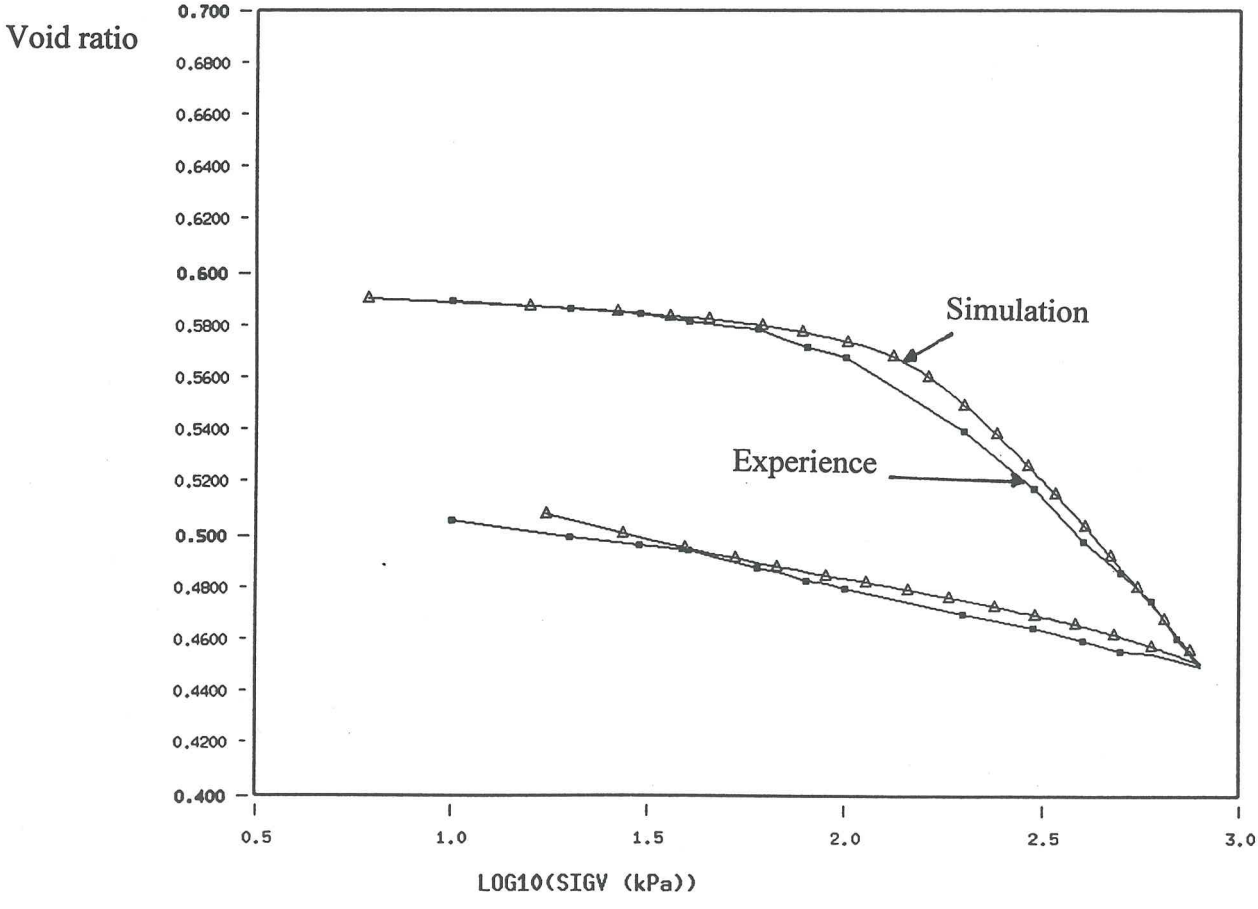

Figure 2b: Core: Oedometer simulation on clay

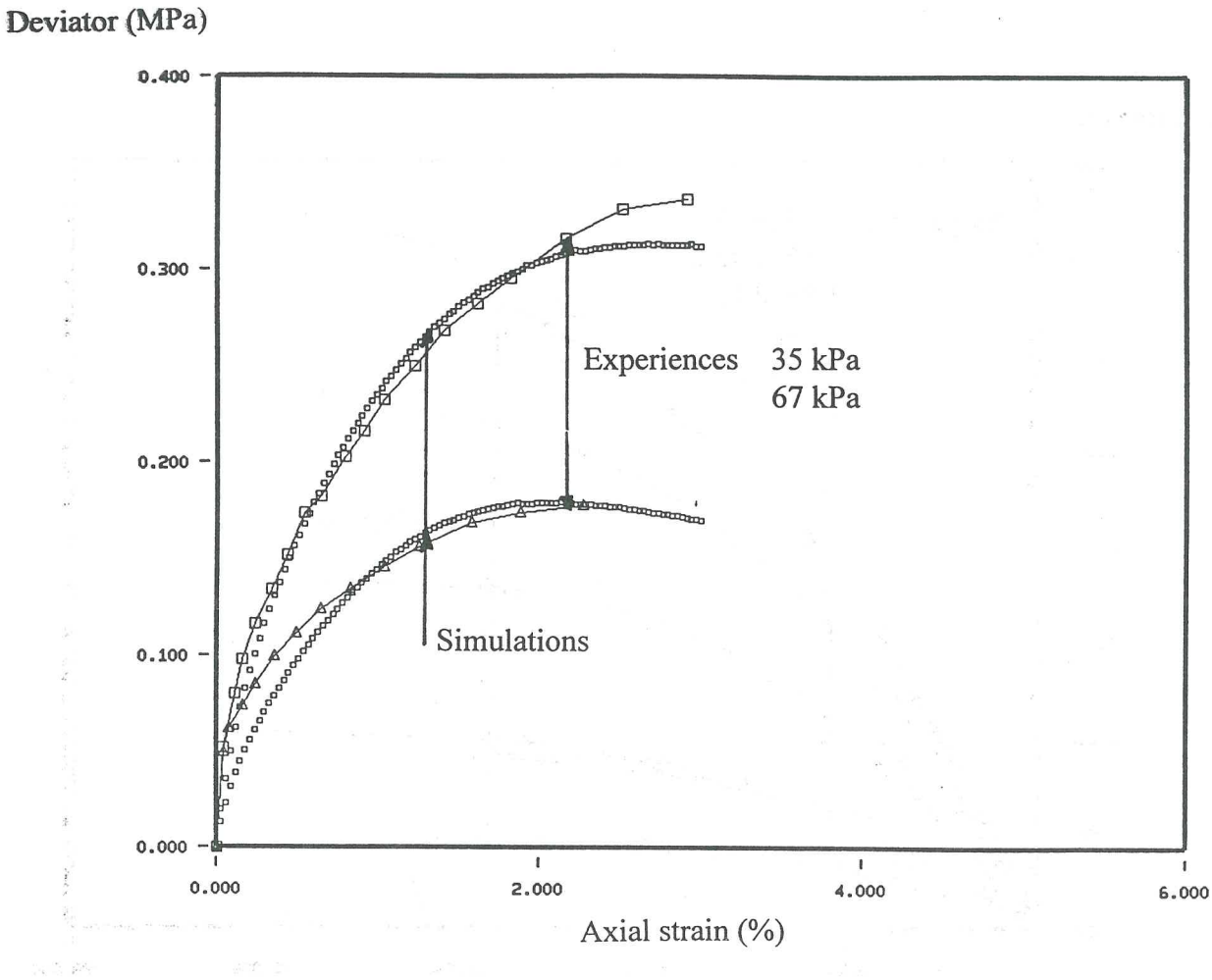

Figure 3a: Filters: Triaxial tests simulations

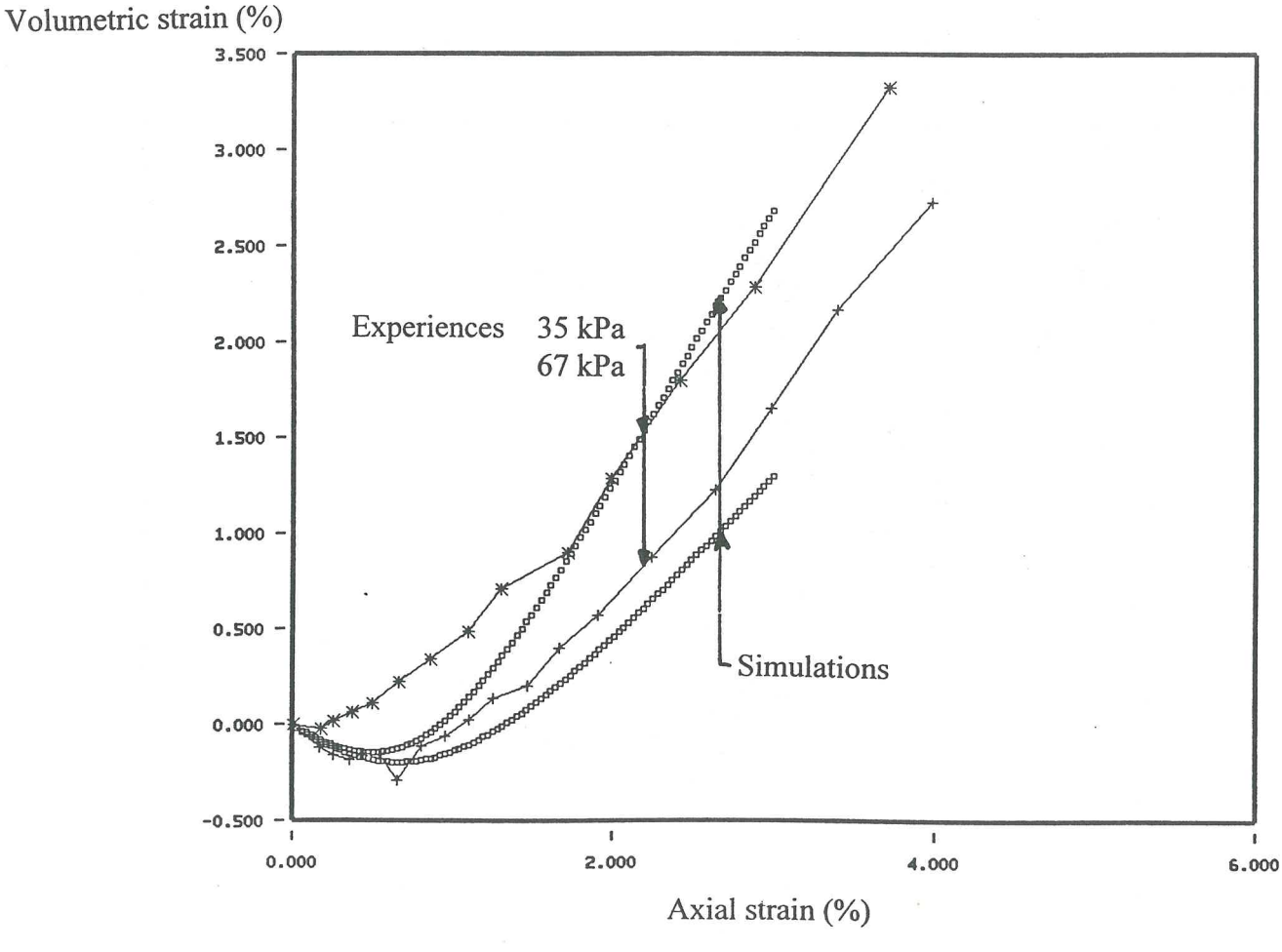

Figure 3b: Filters: Triaxial tests simulations.

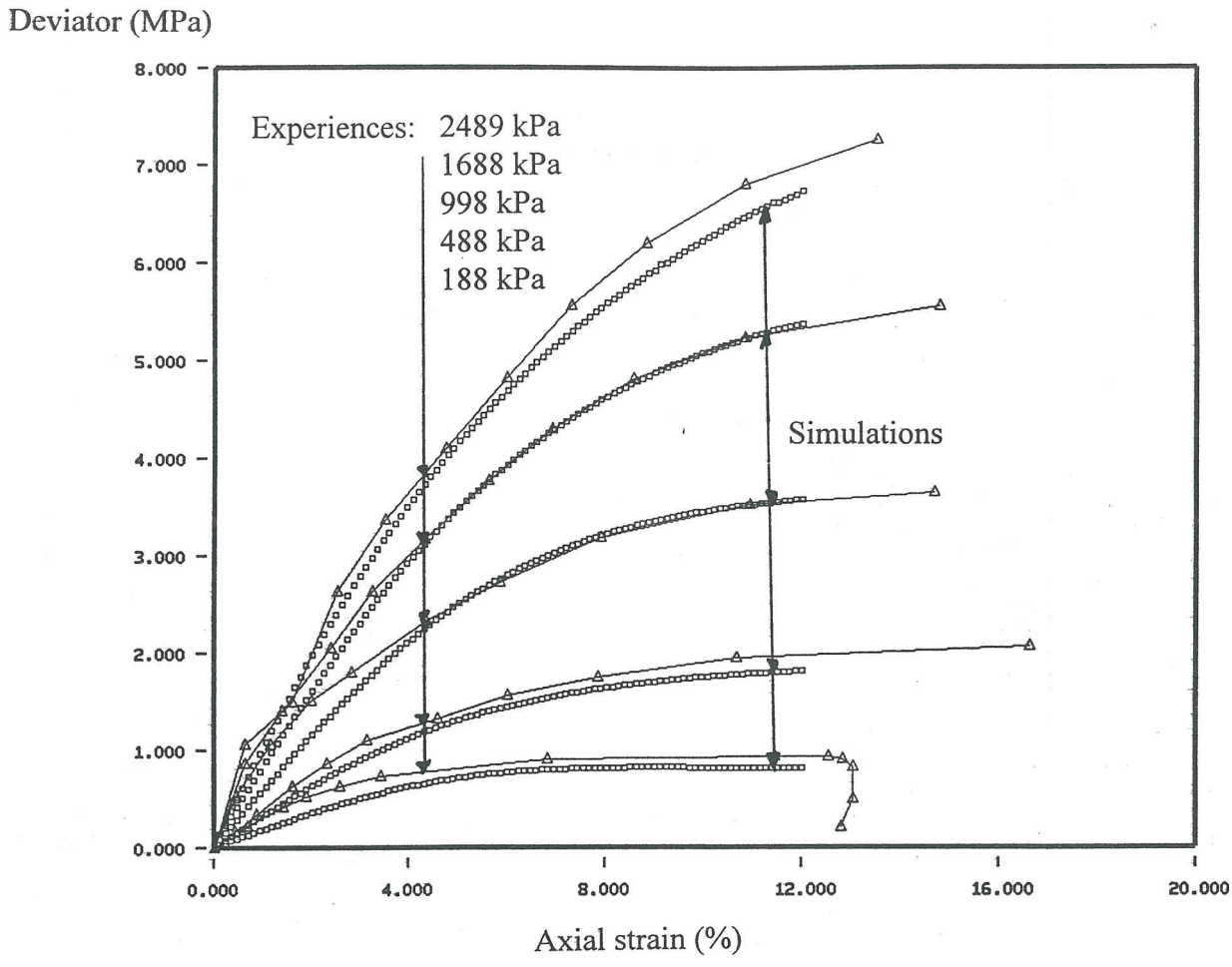

Figure 4a: Dense rockfill : Triaxial tests simulations

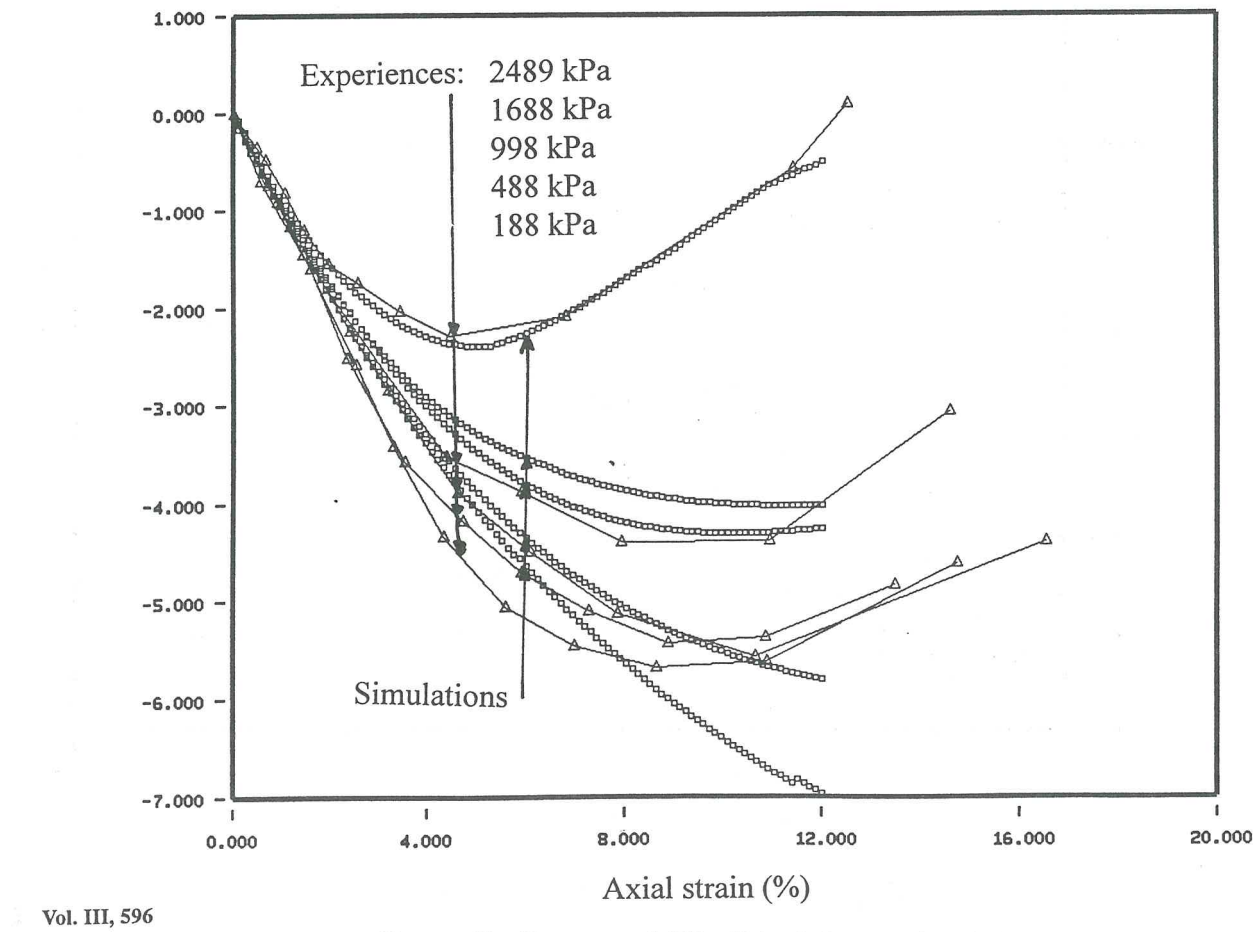

Figure 4b: Dense rockfill : Triaxial tests simulations

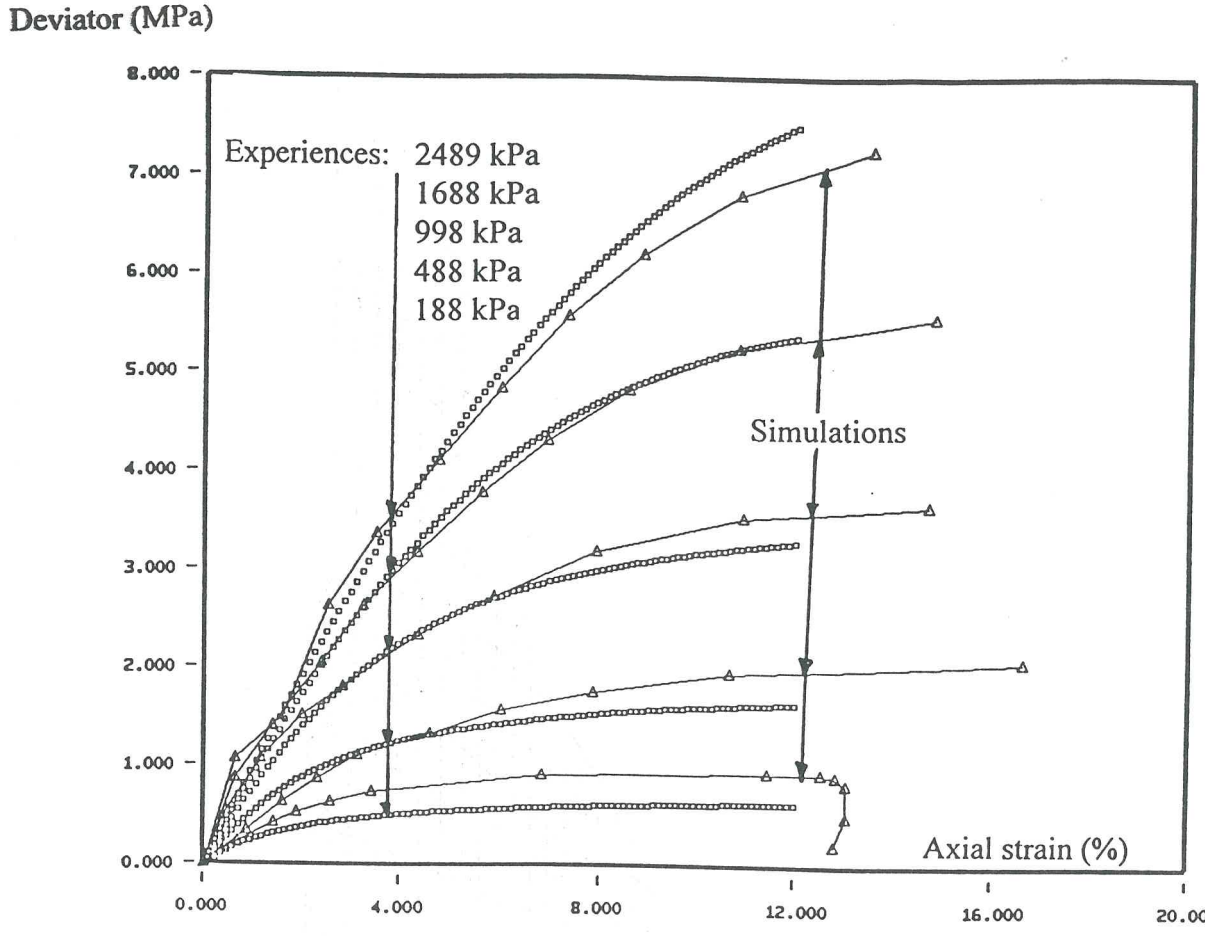

Figure 5a: Dense rockfill : Triaxial tests simulations with hyperbolic model.

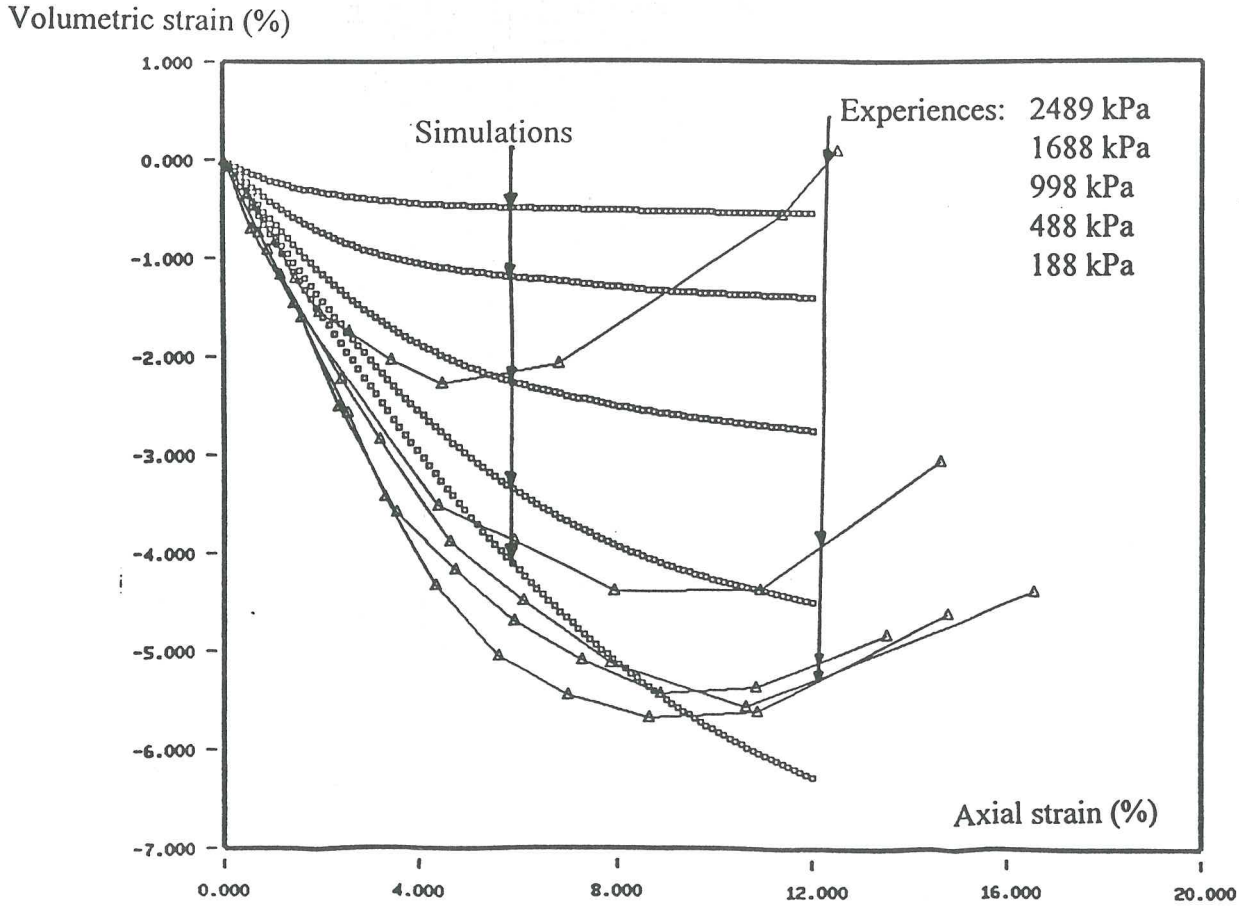

Figure 5b: Dense rockfill : Triaxial tests simulations with hyperbolic model.

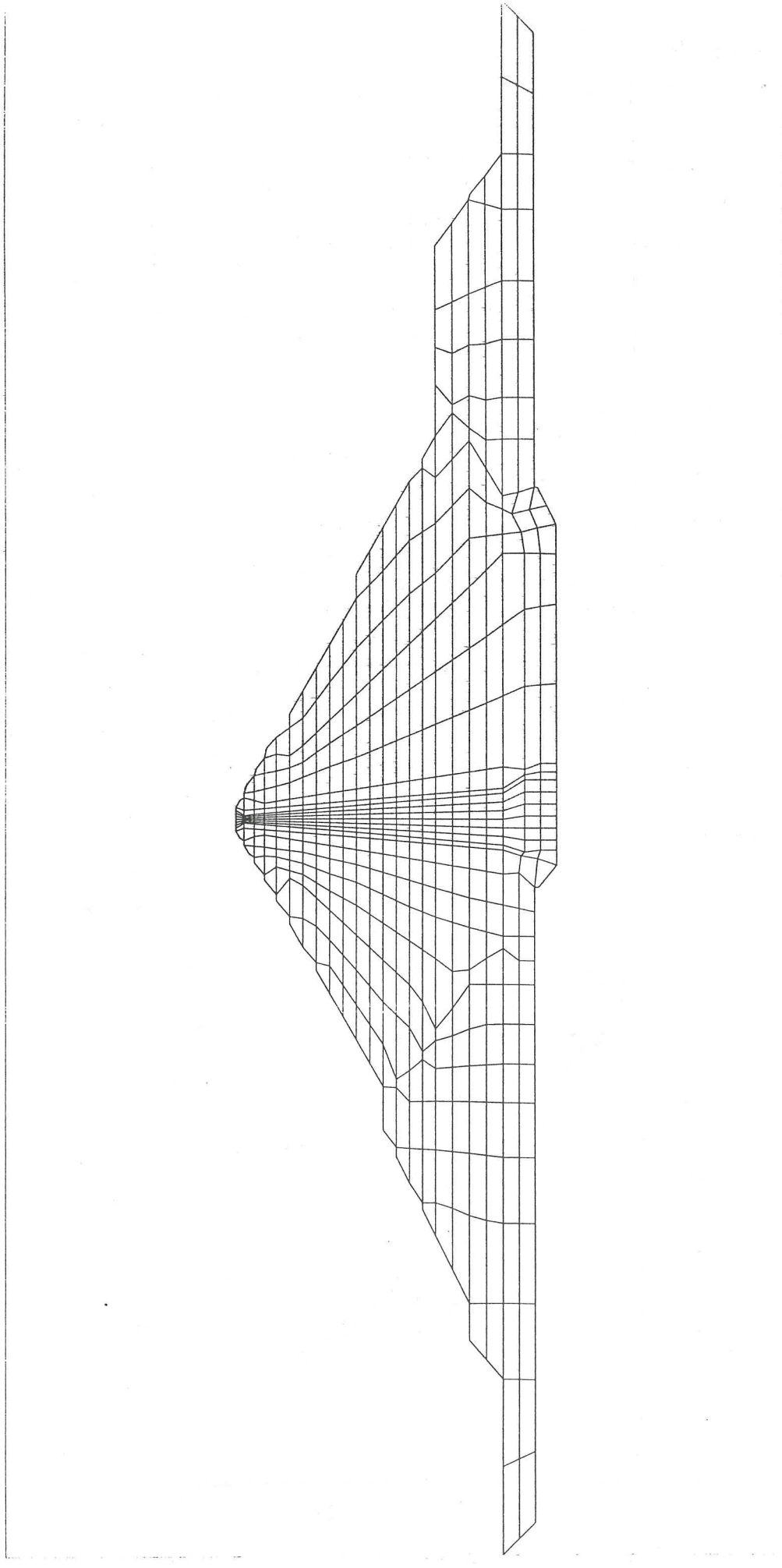

Figure 6: Finit element mesh used with UDAM software.

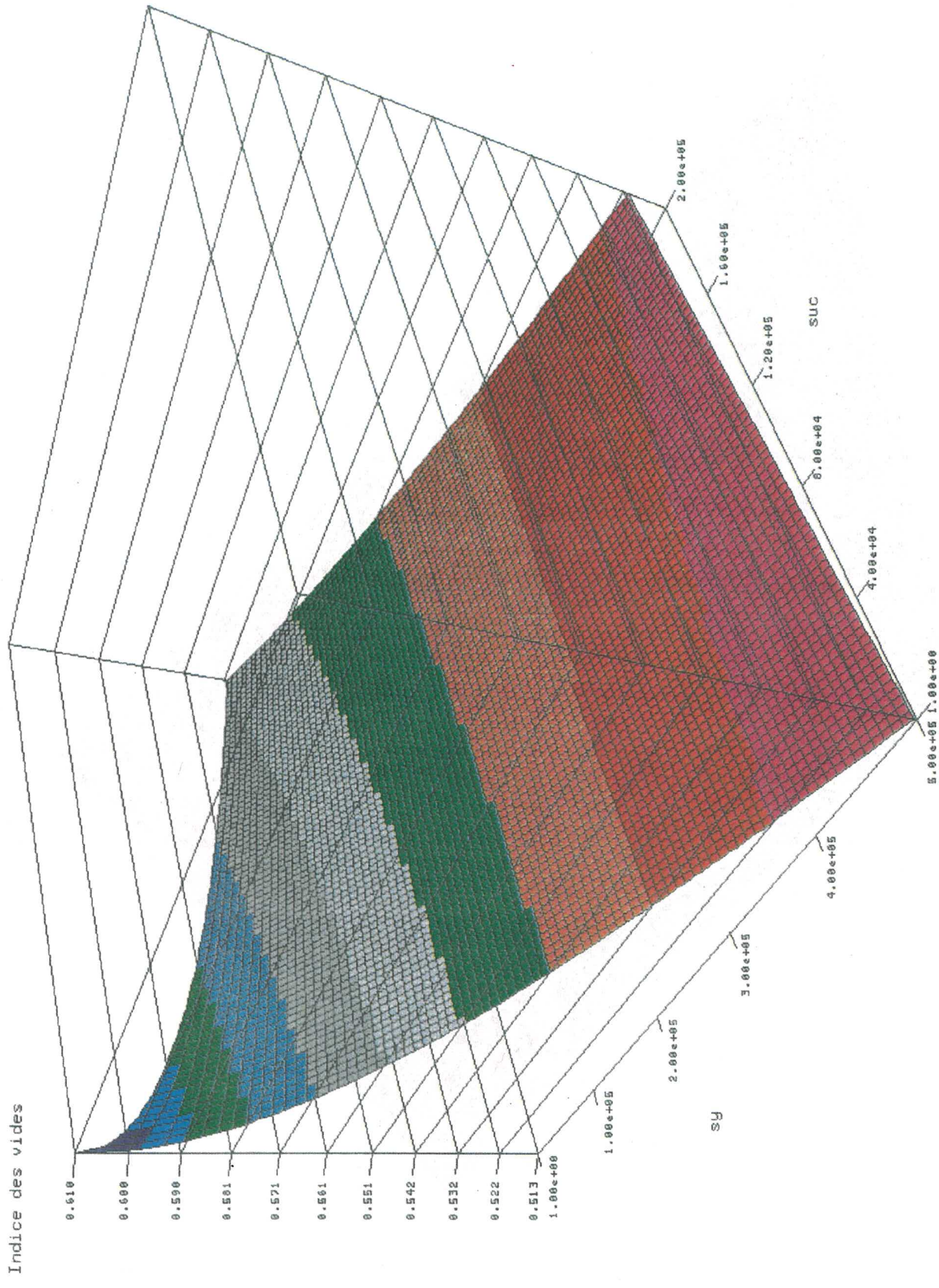

Figure 7: Void ratio state surface

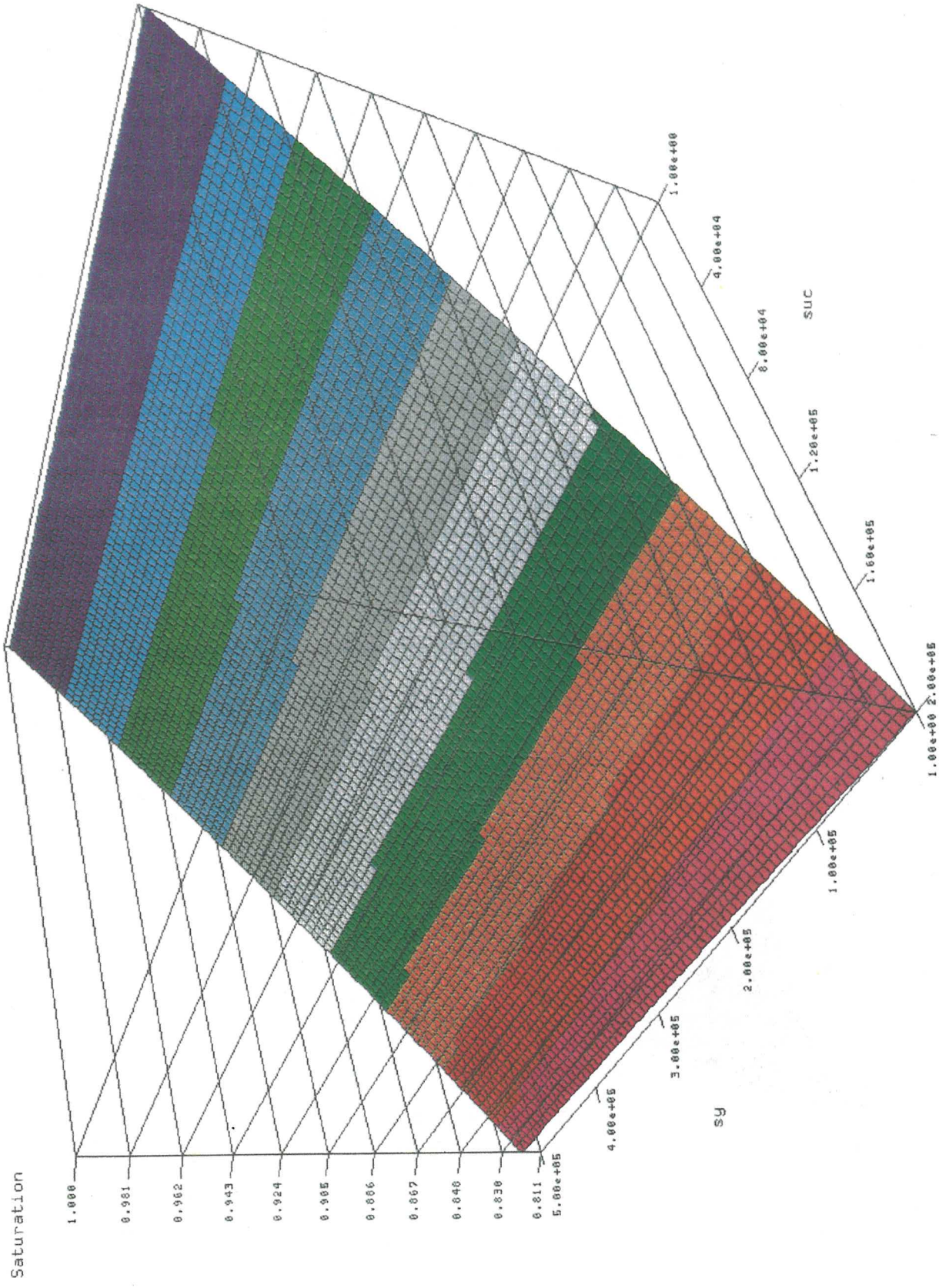

Figure 8: Degree of saturation state surface.

	Points of the Dam section				
	CC	CM	CL	UM	DM
End of construction	0	+ 8.	+ 14.	- 7.	+ 13.
End of Impounding	+ 160.	+ 127.	+ 100.	+ 29.	+ 69.
End of Consolidation	+ 153.	+ 130.	+ 114.	+ 27.	+ 67.

Horizontal Displacements (10^{-2} m)

	Points of the Dam section				
	CC	CM	CL	UM	DM
End of construction	0	- 160.	- 130.	- 42.	- 54
End of Impounding	+49.	- 145.	- 129.	+ 48.	- 63.
End of Consolidation	+52.	- 162.	- 142.	+ 47.	- 63.

Vertical Displacements (10^{-2} m)

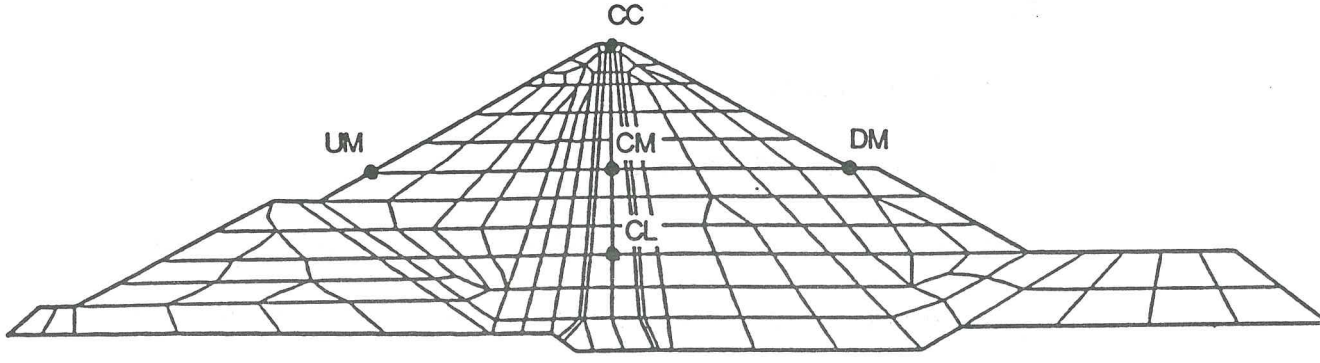

Table 3

Static Analysis

GENERAL SUMMARY : RESULTS OF DISPLACEMENTS AFTER EACH PHASE

IV/ RESULTS

MODELLING C1

+ **Software**: GEFDYN

+ **Two-phase coupled approach.**

+ **Constitutive models:**

Core: Elastoplastic model. HUJEUX.

Filter: Elastic-Plastic model: DRUCKER-PRAGER

Transition: Elastic-Plastic model: DRUCKER-PRAGER

Compacted shoulder : Elastic-Plastic model: DRUCKER-PRAGER

Loose shoulder : Elastic-Plastic model: DRUCKER-PRAGER

PORE PRESSURES DISTRIBUTION
ZOOM ON THE CORE REGION

EL INFIERNILLO Dam -STATIC ANALYSIS

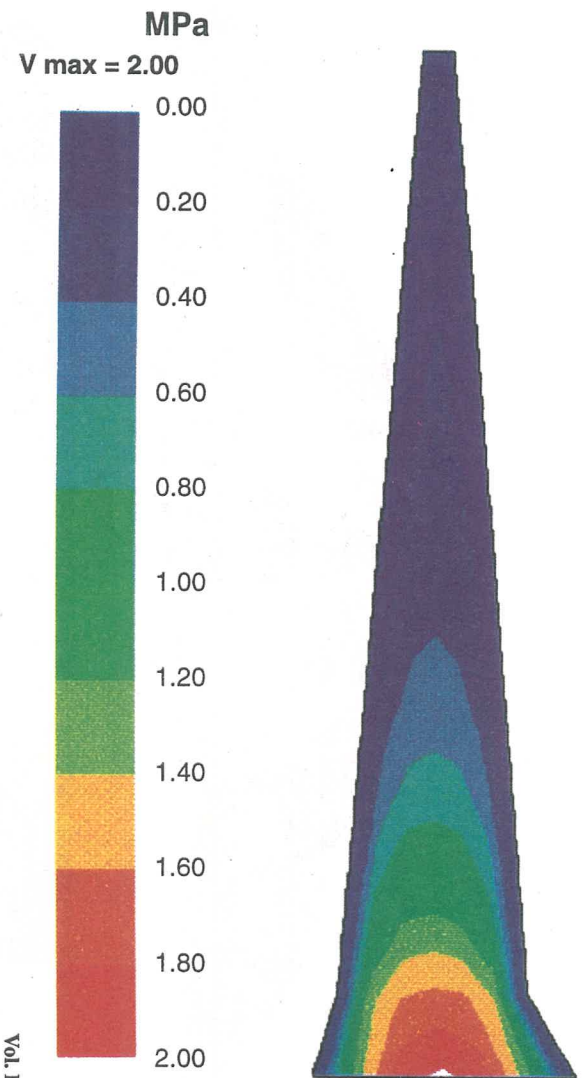

End of Construction

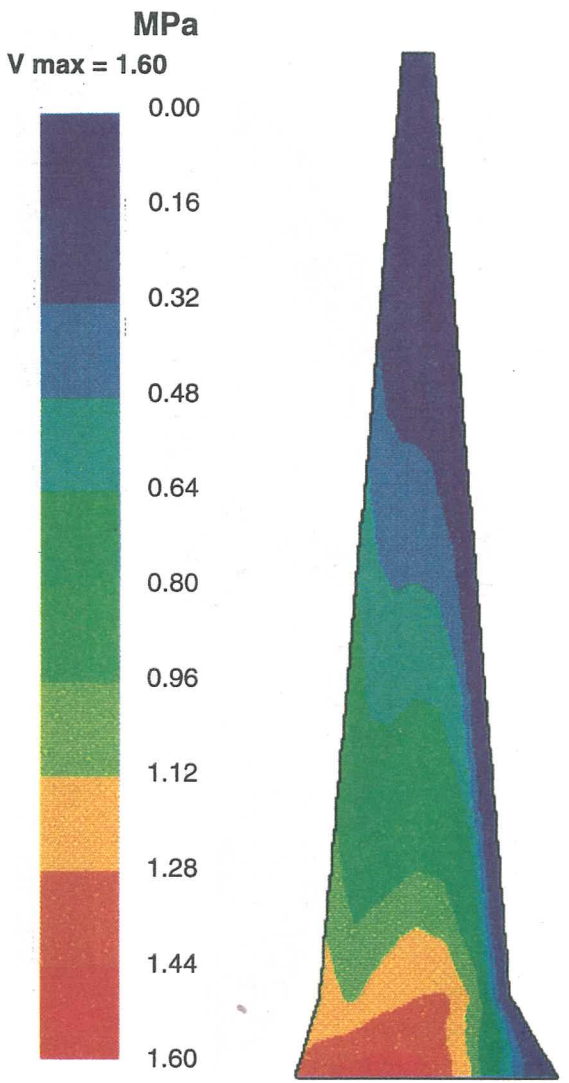

End of Impounding

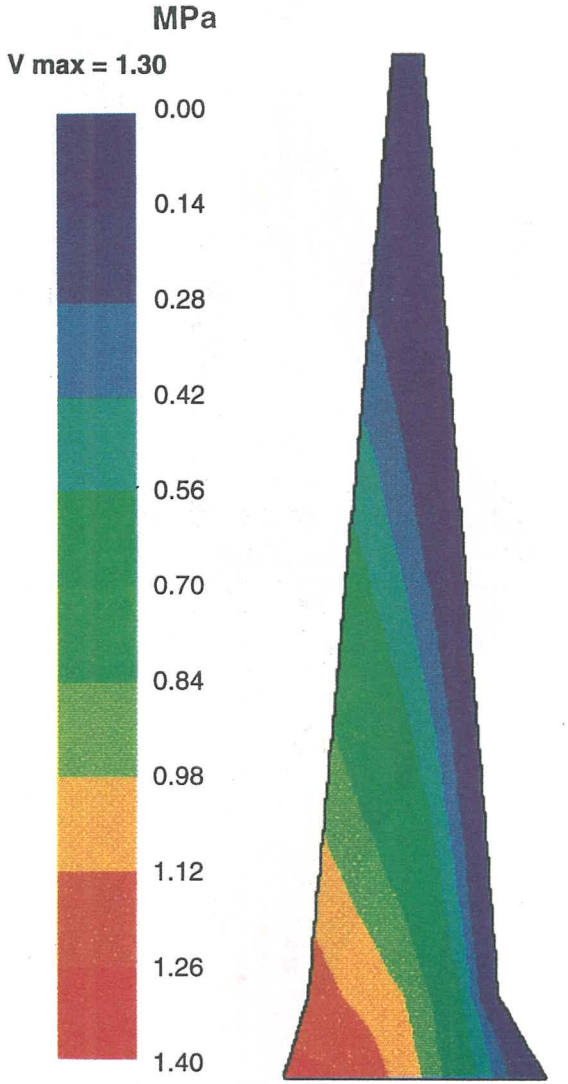

End of Consolidation

VERTICAL STRESSES DISTRIBUTION

EL INFIERNILLO Dam -STATIC ANALYSIS

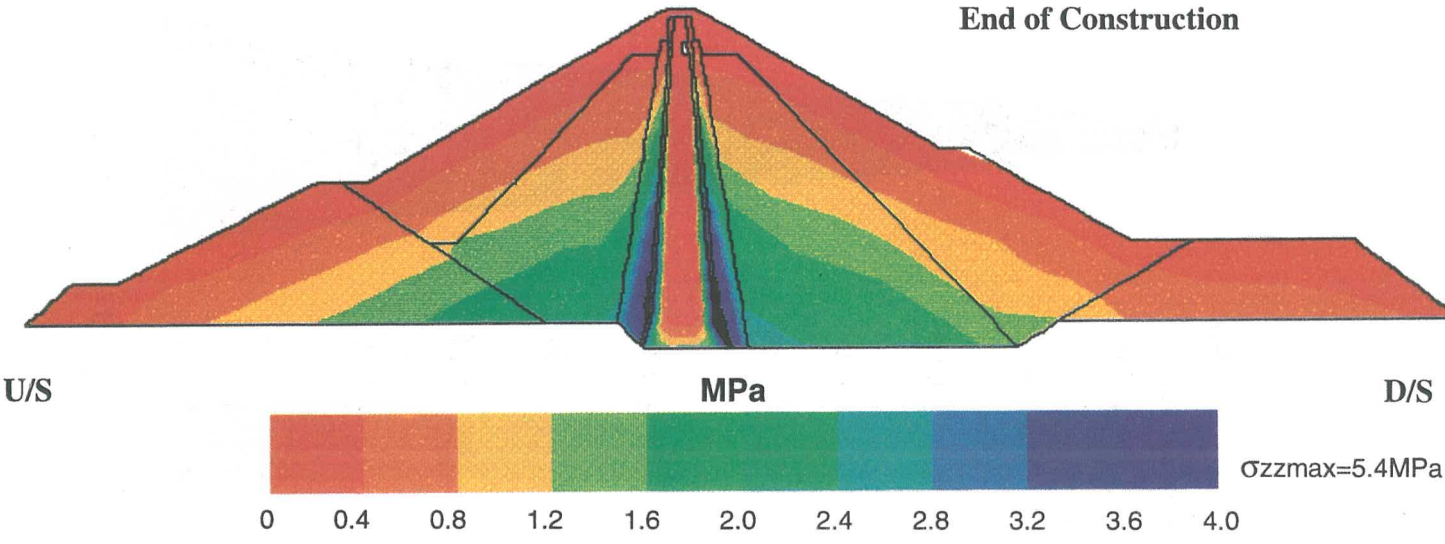

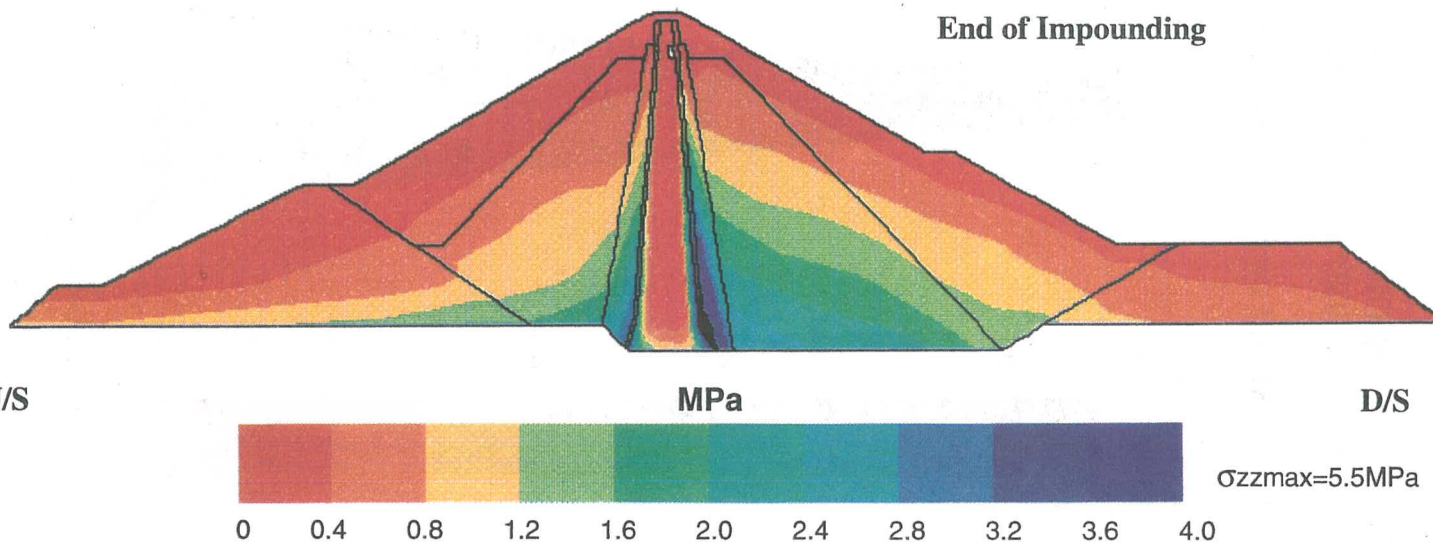

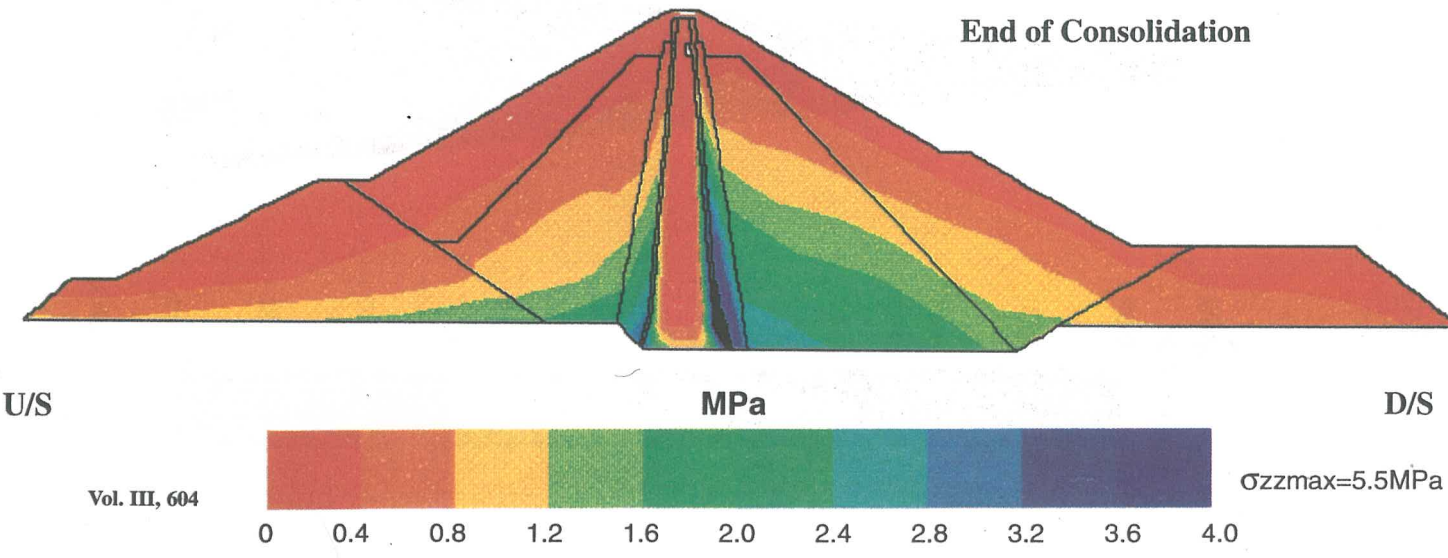

HORIZONTAL STRESSES DISTRIBUTION

EL INFIERNILLO Dam -STATIC ANALYSIS

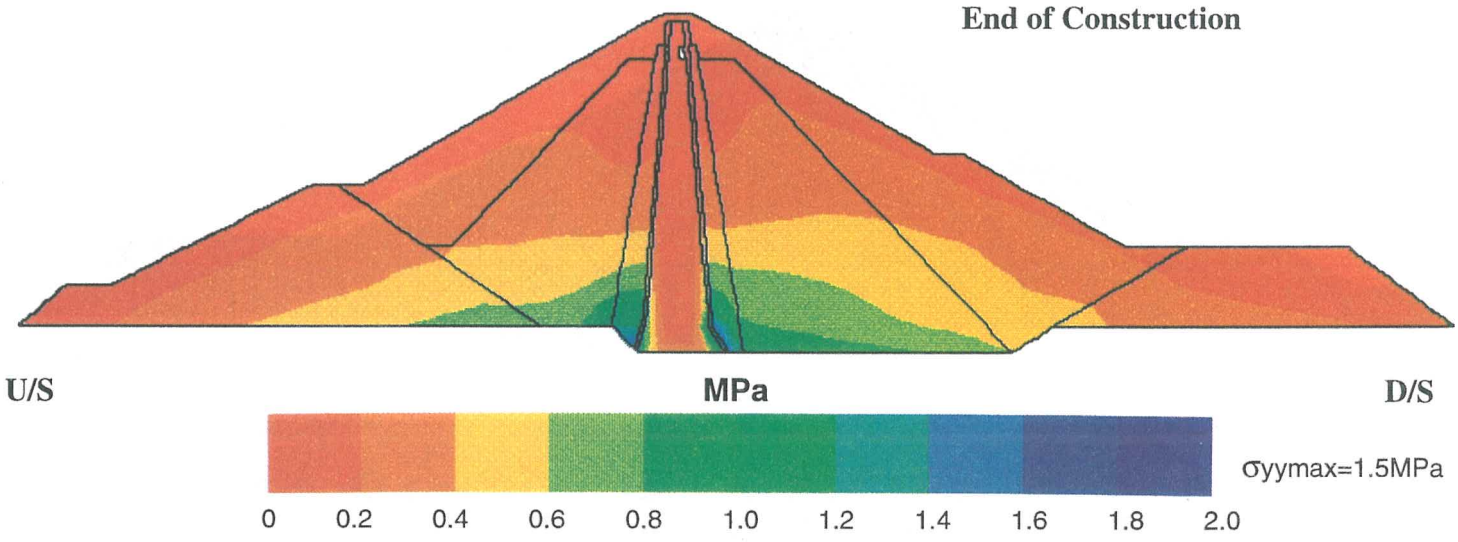

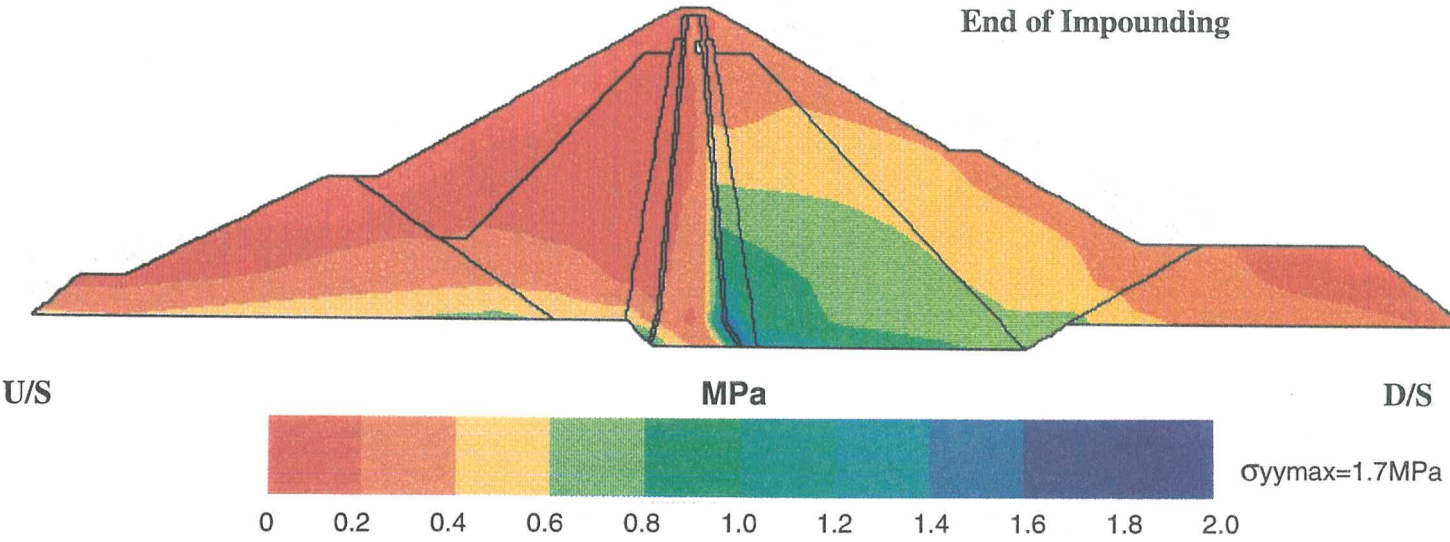

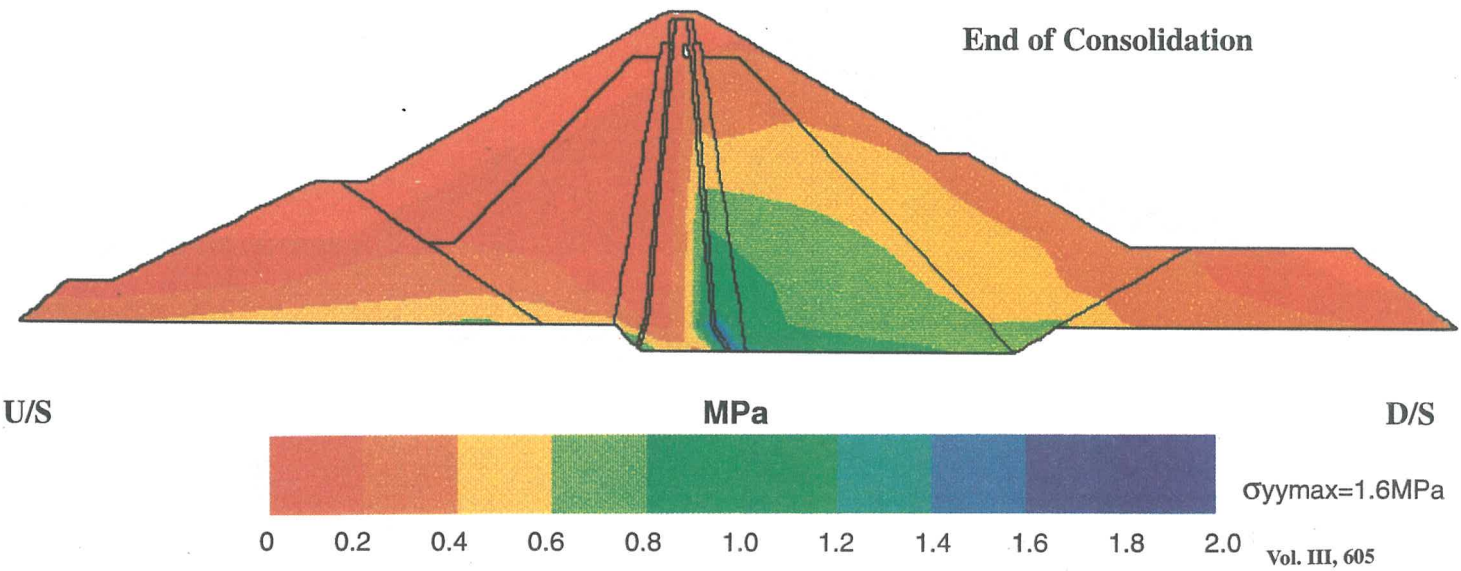

SHEAR STRESSES DISTRIBUTION

EL INFIERNILLO Dam -STATIC ANALYSIS

End of Construction

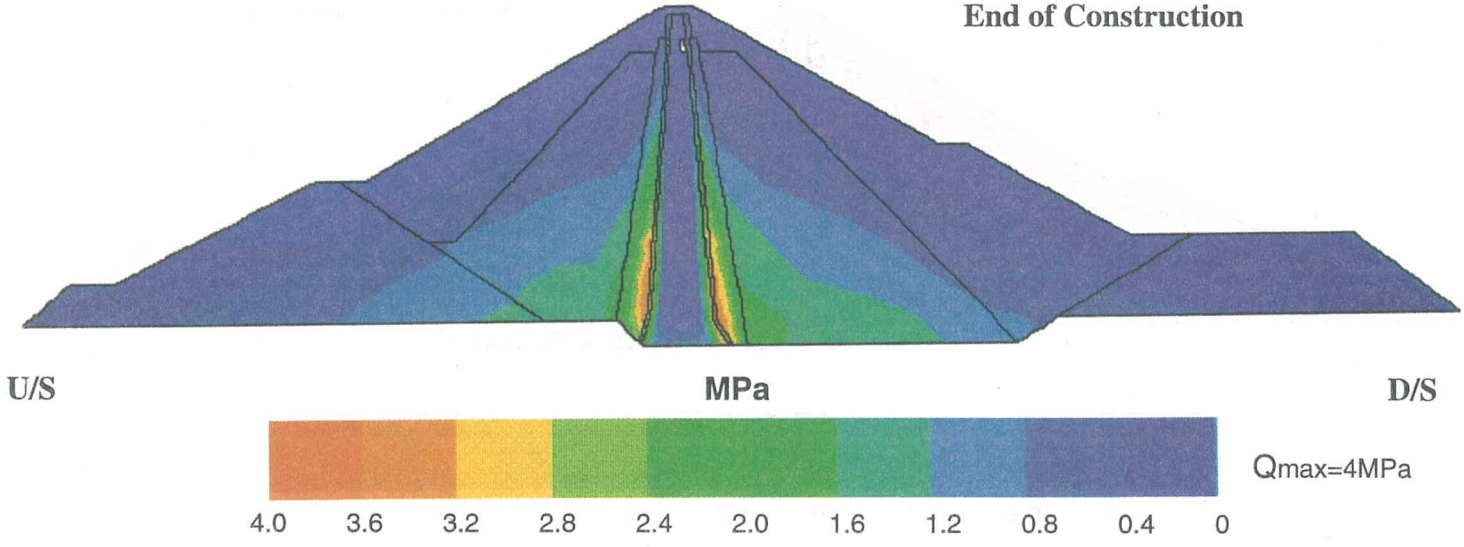

End of Impounding

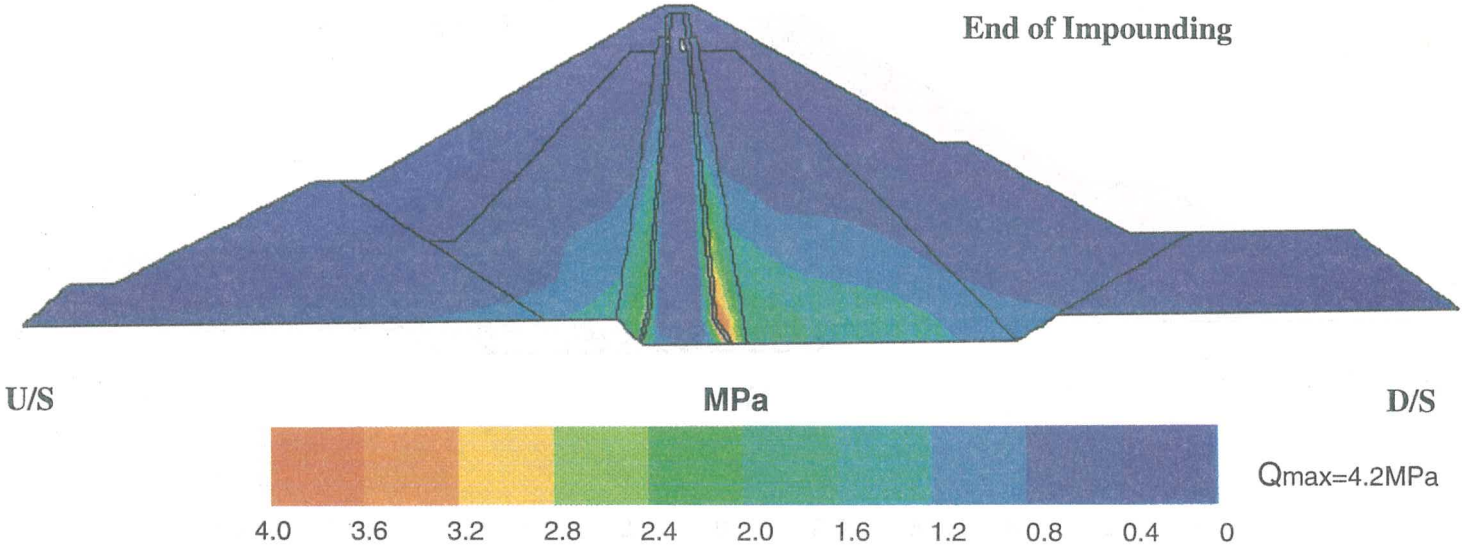

End of Consolidation

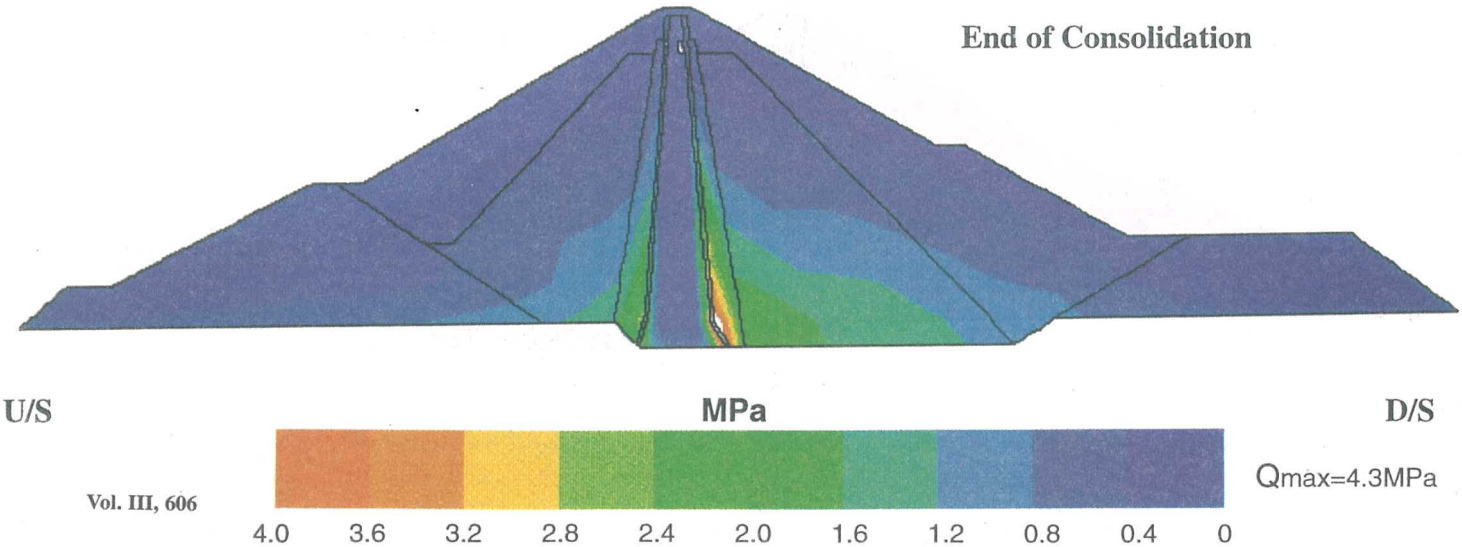

	Points of the Dam section				
	CC	CM	CL	UM	DM
End of construction	0	+ 6.1	+ 12.3	- 13.9	+ 5.5
End of Impounding	+ 36.5	+ 62.6	+ 58.0	- 15.1	+ 32.0
End of Consolidation	+ 35.6	+ 63.7	+ 59.7	- 14.7	+ 32.1

Horizontal Displacements (10^{-2} m)

	Points of the Dam section				
	CC	CM	CL	UM	DM
End of construction	0	- 126.7	- 103.5	- 46.6	- 56.1
End of Impounding	-24.6	- 137.0	- 113.2	- 16.8	- 65.9
End of Consolidation	-27.0	- 139.5	- 115.4	- 17.0	- 66.0

Vertical Displacements (10^{-2} m)

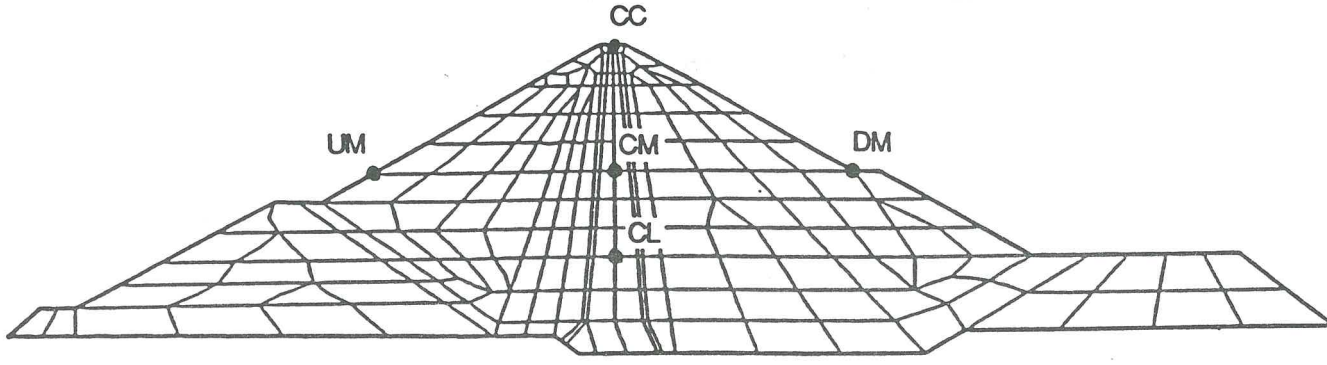

Table 3

Static Analysis

GENERAL SUMMARY : RESULTS OF DISPLACEMENTS AFTER EACH PHASE

RESULTS

MODELLING C2

+ **Software**: GEFDYN

+ **Two-phase coupled approach.**

+ **Constitutive models:**

Core: Elastoplastic model. HUJEUX.

Filter:Hyperbolic model

Transition: Hyperbolic model.

Compacted shoulder : Hyperbolic model.

Loose shoulder : Hyperbolic model.

Section BB

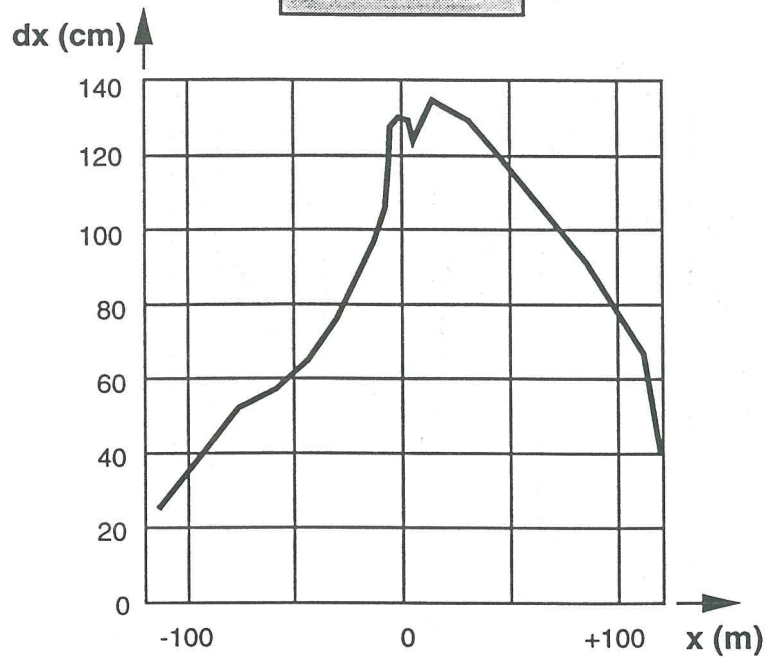

Section CC

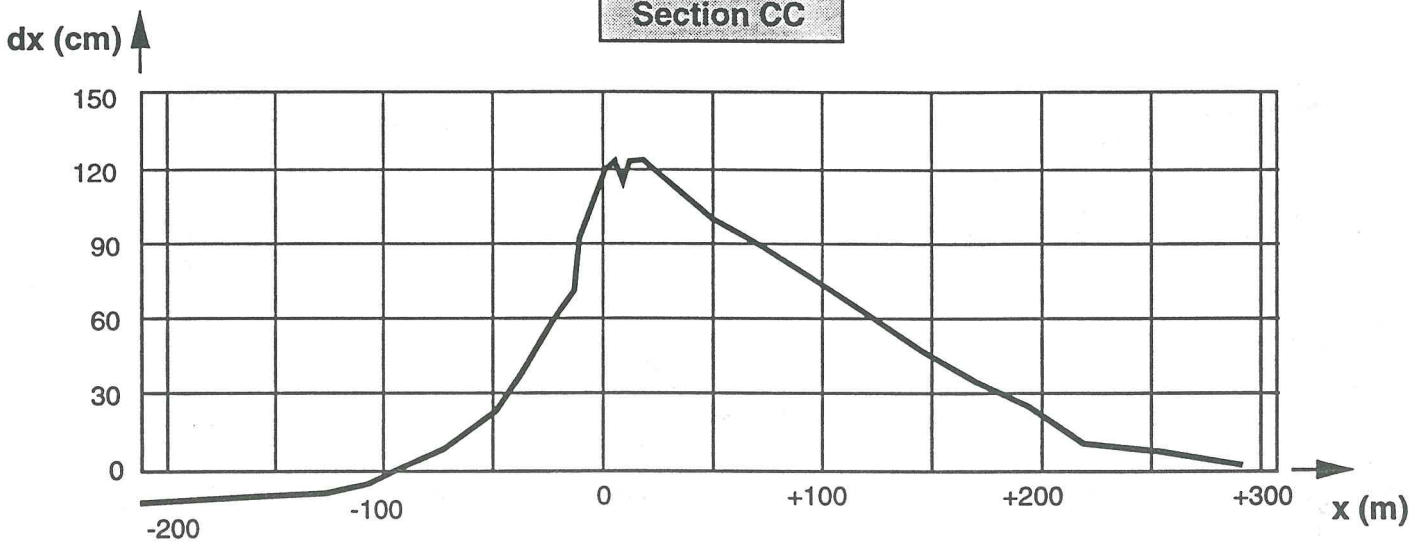

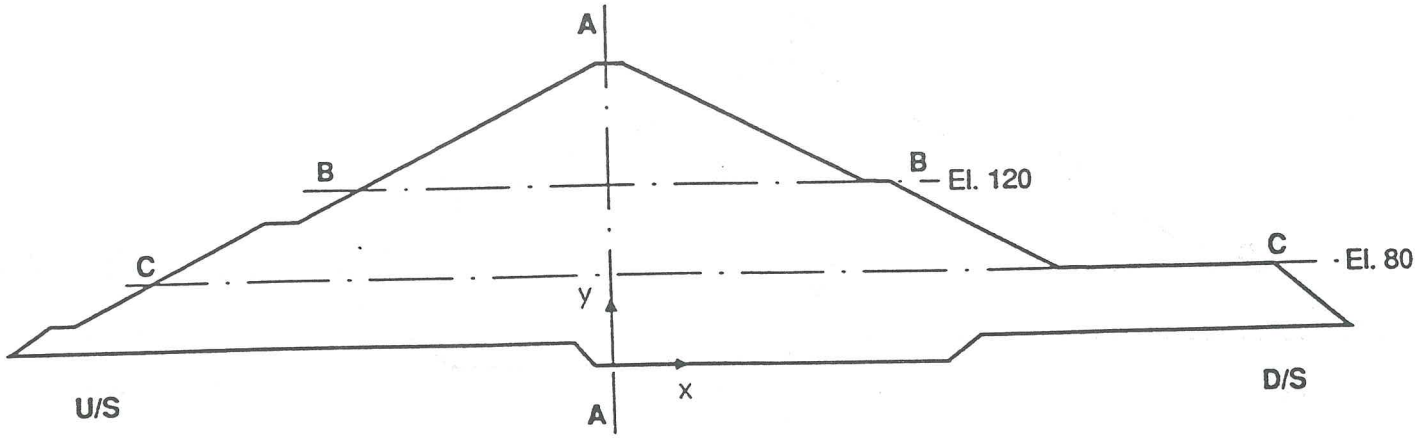

Static Analysis

TEMPLATE FOR THE HORIZONTAL DISPLACEMENTS AT THE END OF THE CONSOLIDATION PHASE

Section BB

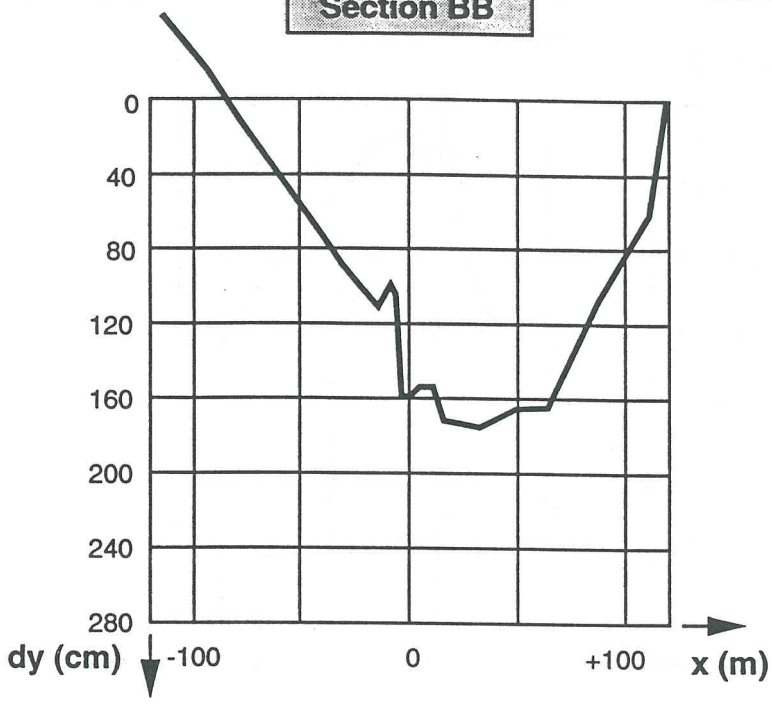

Section CC

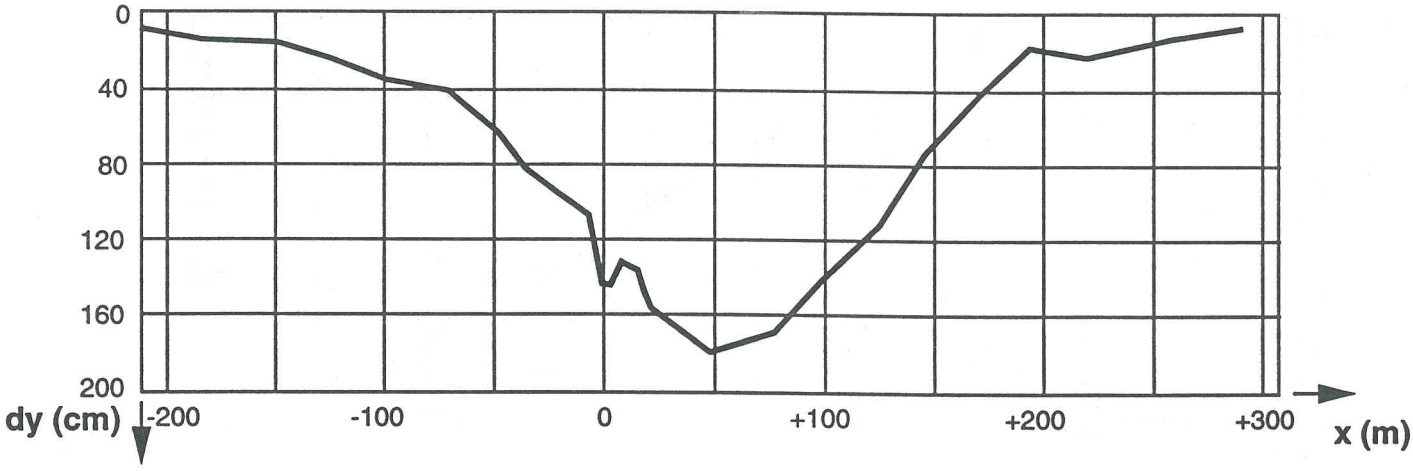

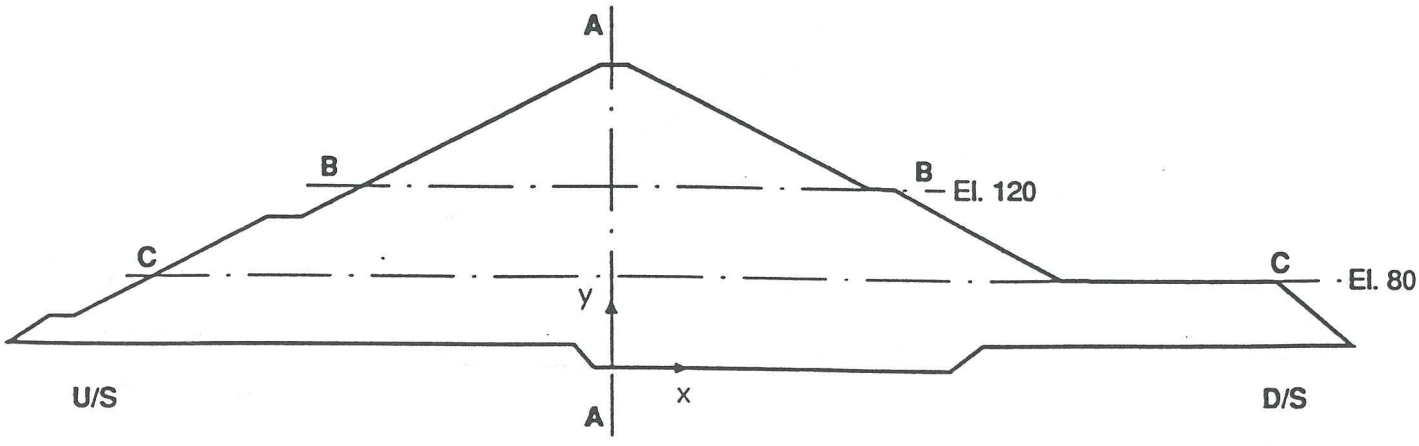

Static Analysis

TEMPLATE FOR THE SETTLEMENTS
AT THE END OF THE CONSOLIDATION PHASE

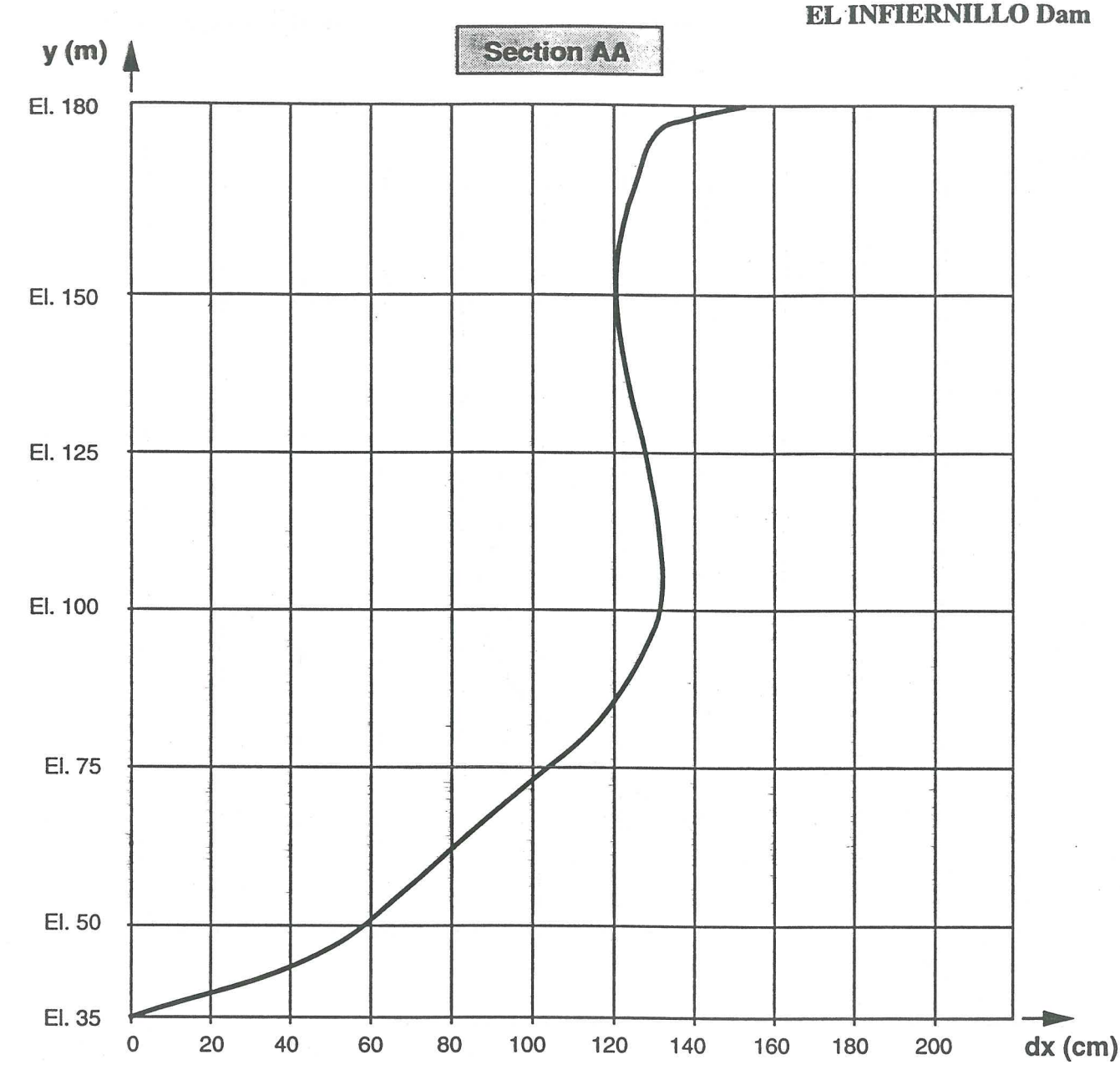

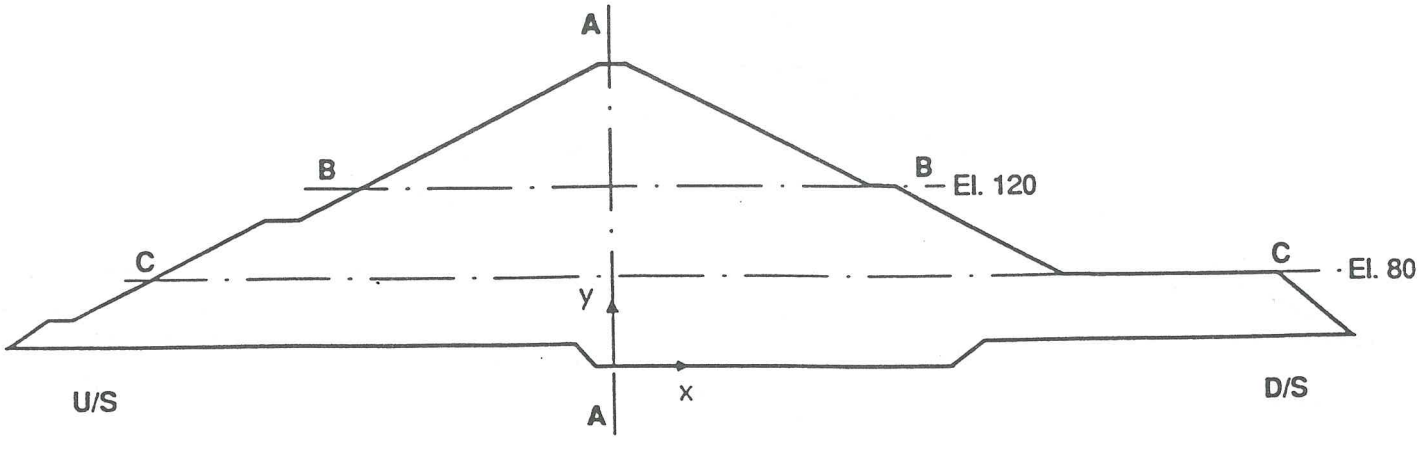

Static Analysis

TEMPLATE FOR THE HORIZONTAL DISPLACEMENTS AT THE END OF THE CONSOLIDATION PHASE

Section AA

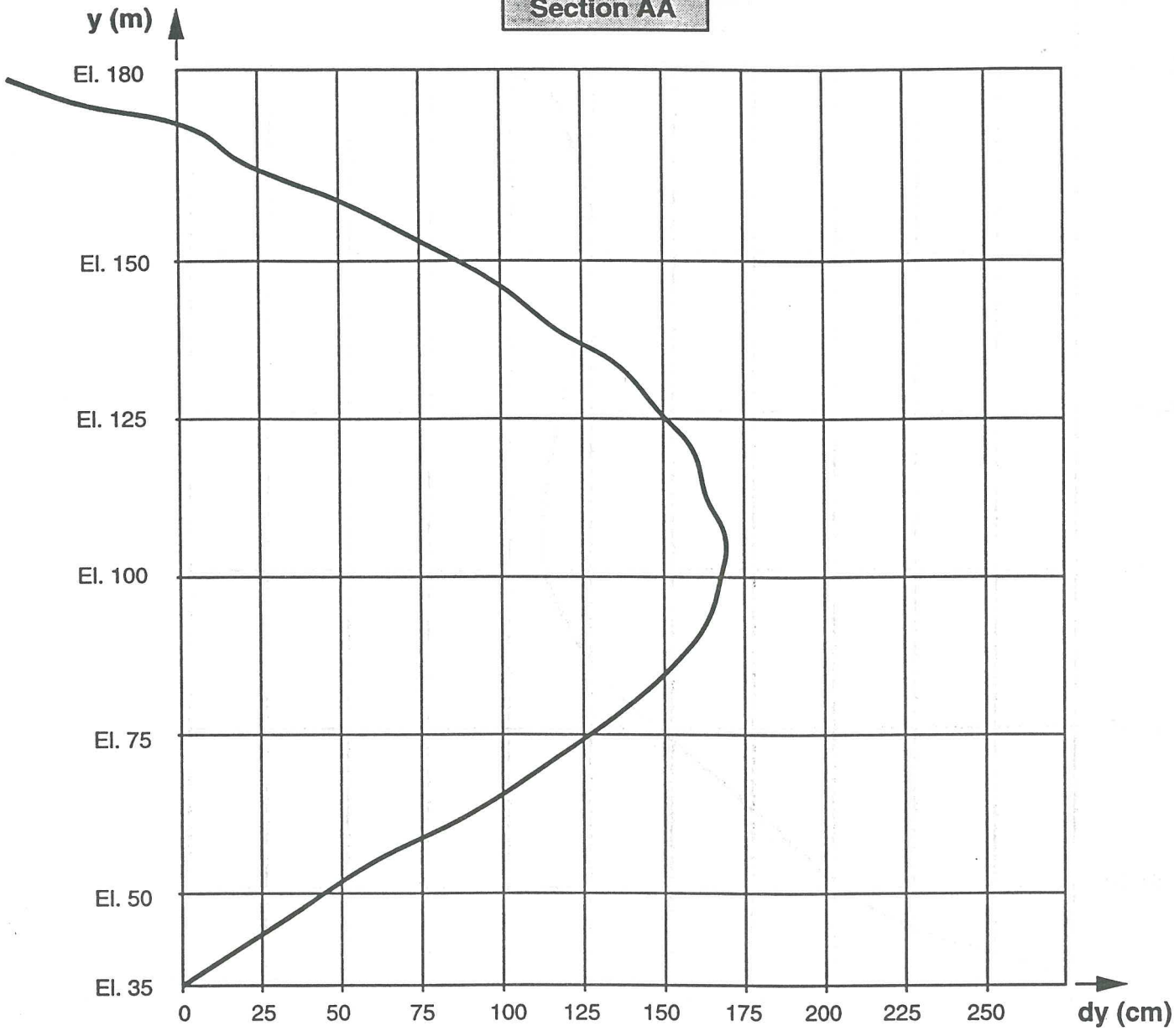

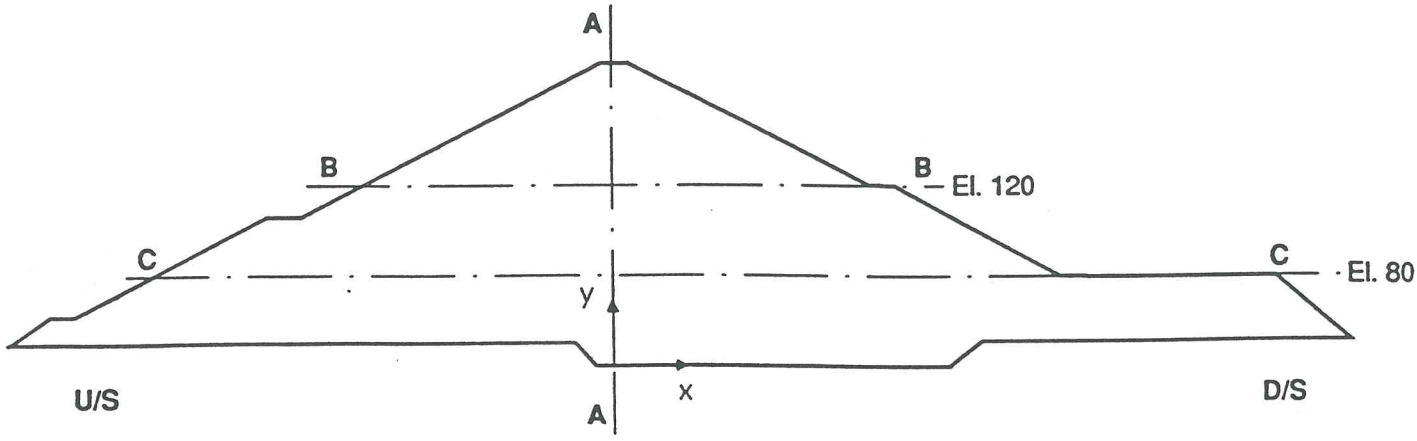

Static Analysis

TEMPLATE FOR THE SETTLEMENTS
AT THE END OF THE CONSOLIDATION PHASE

PORE PRESSURES DISTRIBUTION
ZOOM ON THE CORE REGION

EL INFIERNILLO Dam -STATIC ANALYSIS

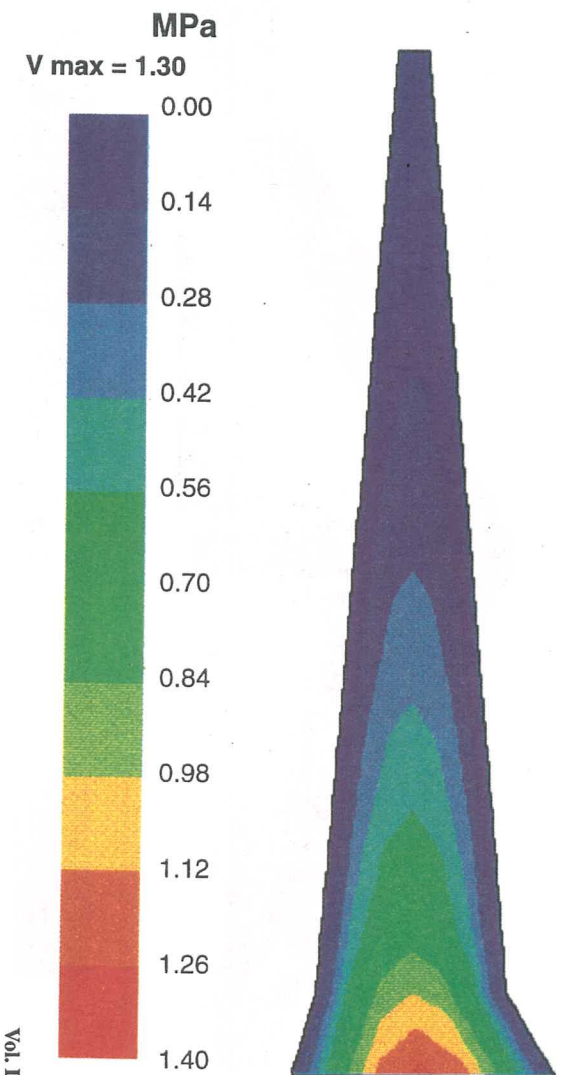

End of Construction

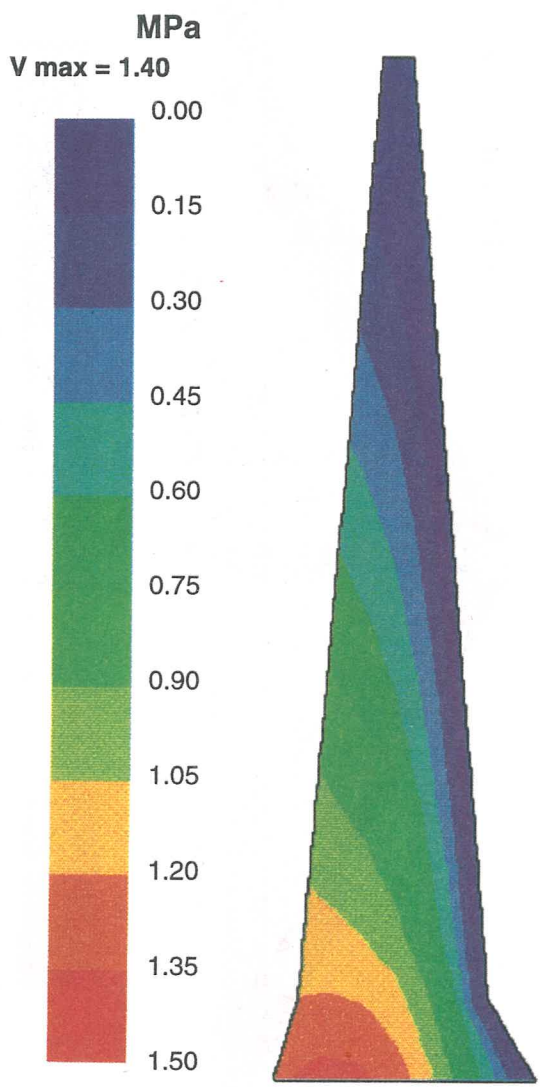

End of Impounding

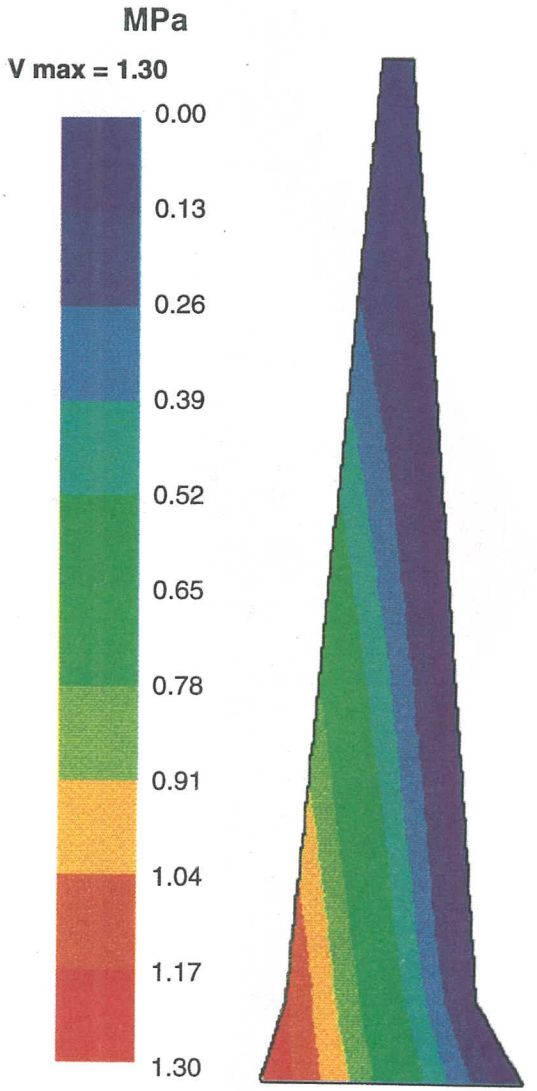

End of Consolidation

VERTICAL STRESSES DISTRIBUTION

EL INFIERNILLO Dam - STATIC ANALYSIS

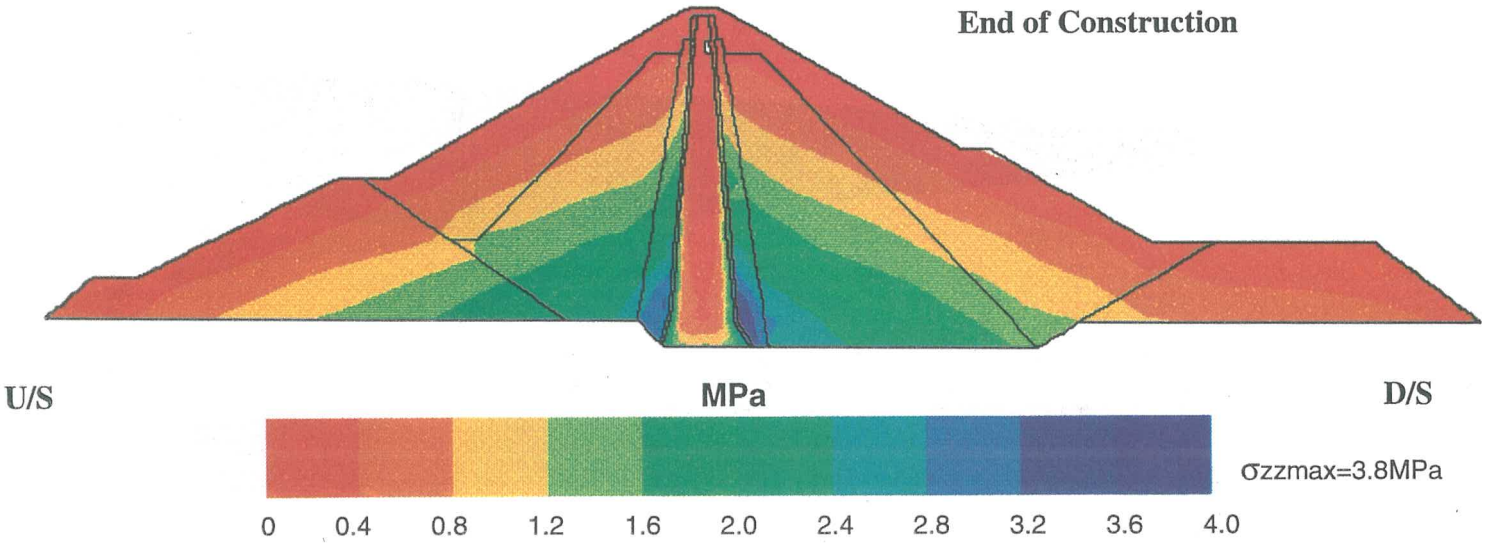

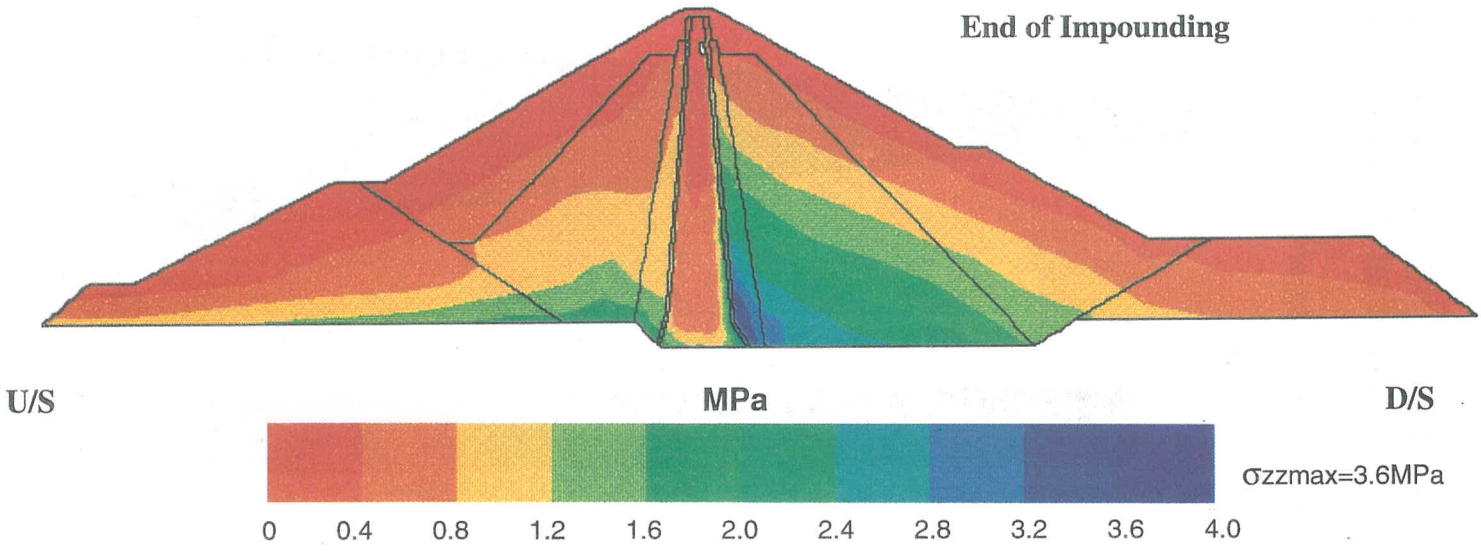

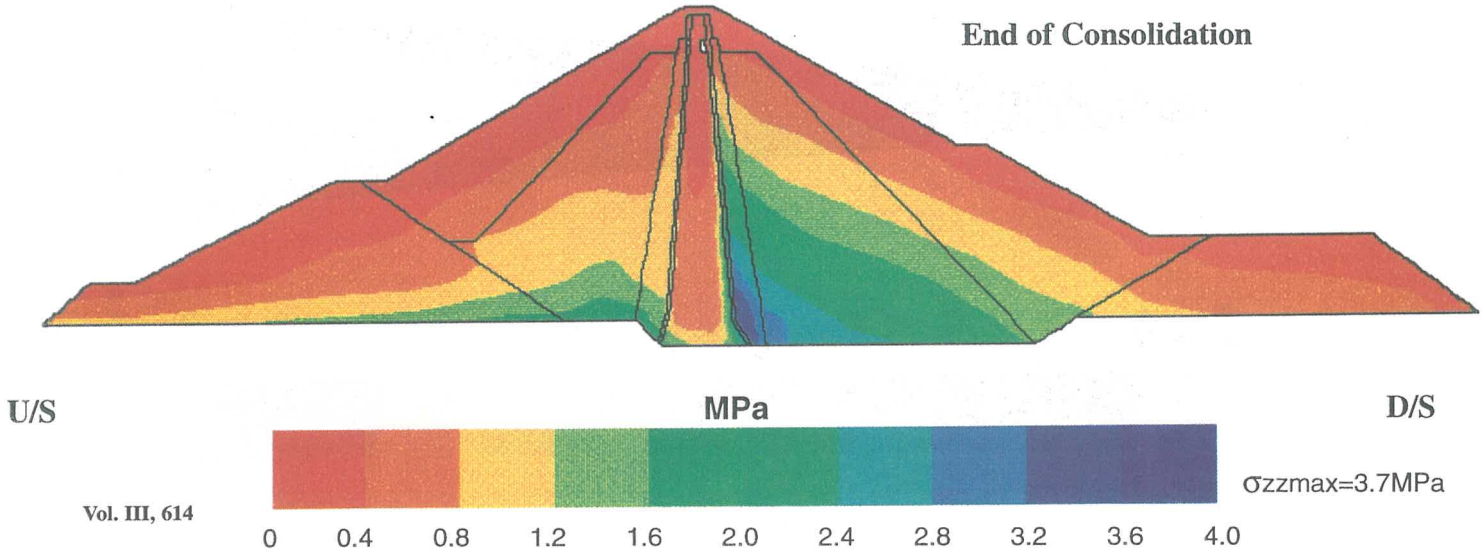

HORIZONTAL STRESSES DISTRIBUTION

EL INFIERNILLO Dam - STATIC ANALYSIS

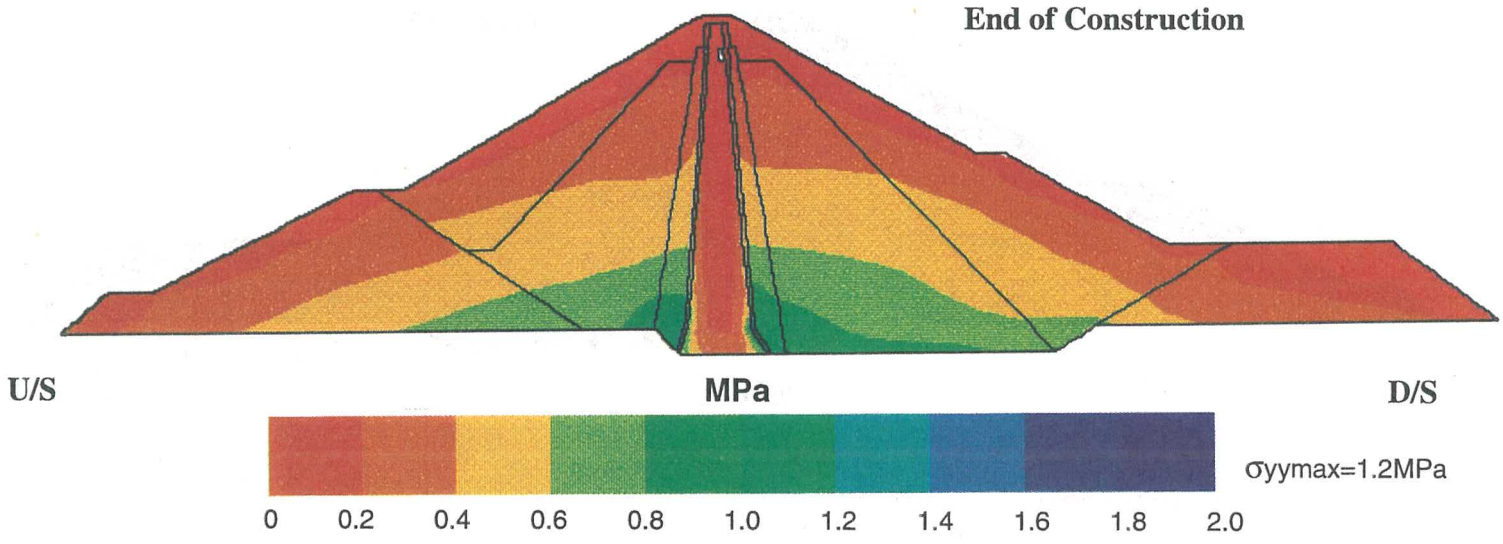

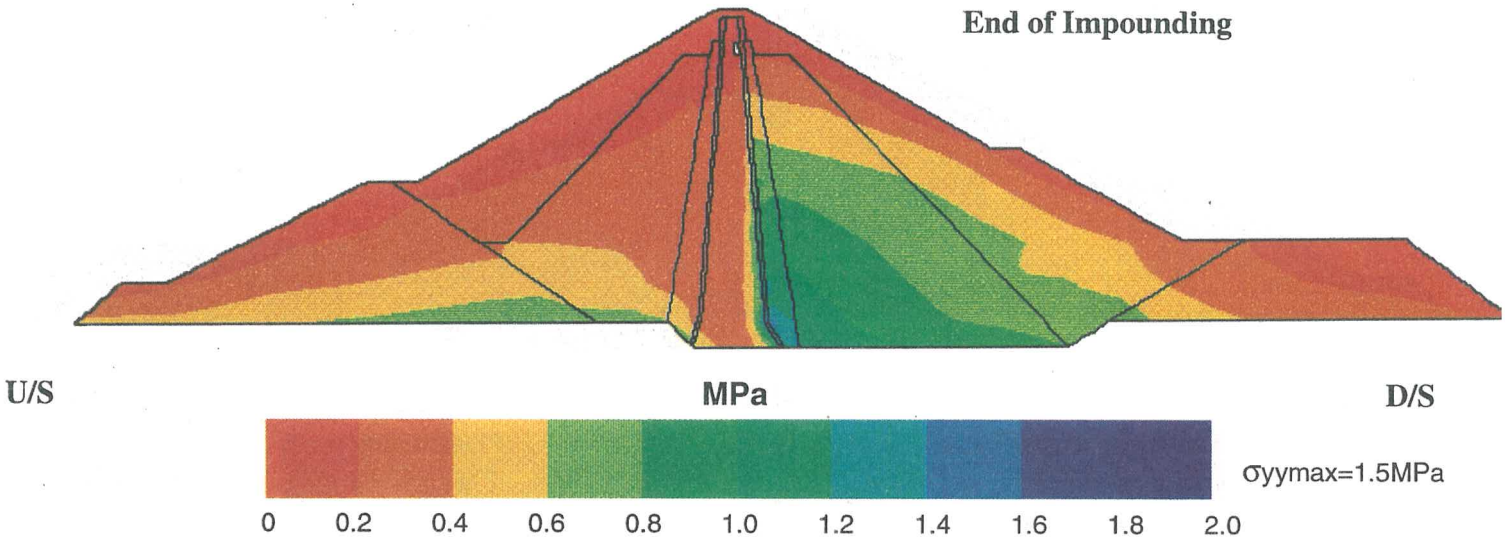

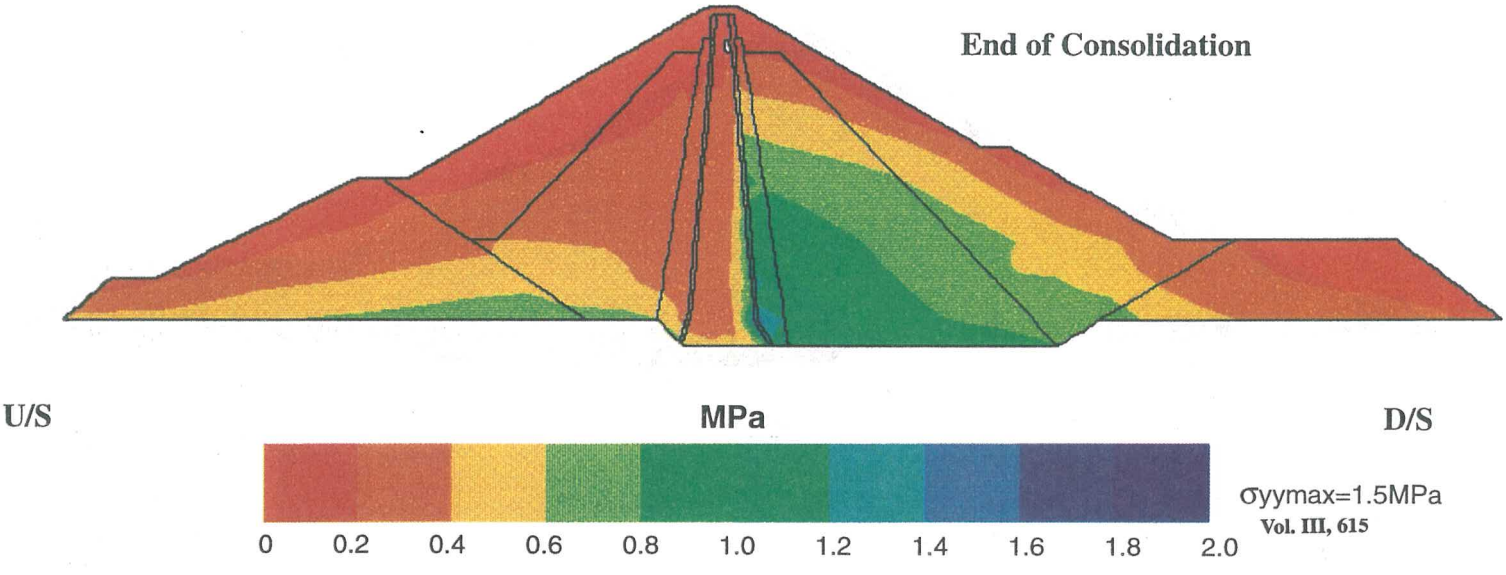

SHEAR STRESSES DISTRIBUTION

EL INFIERNILLO Dam - STATIC ANALYSIS

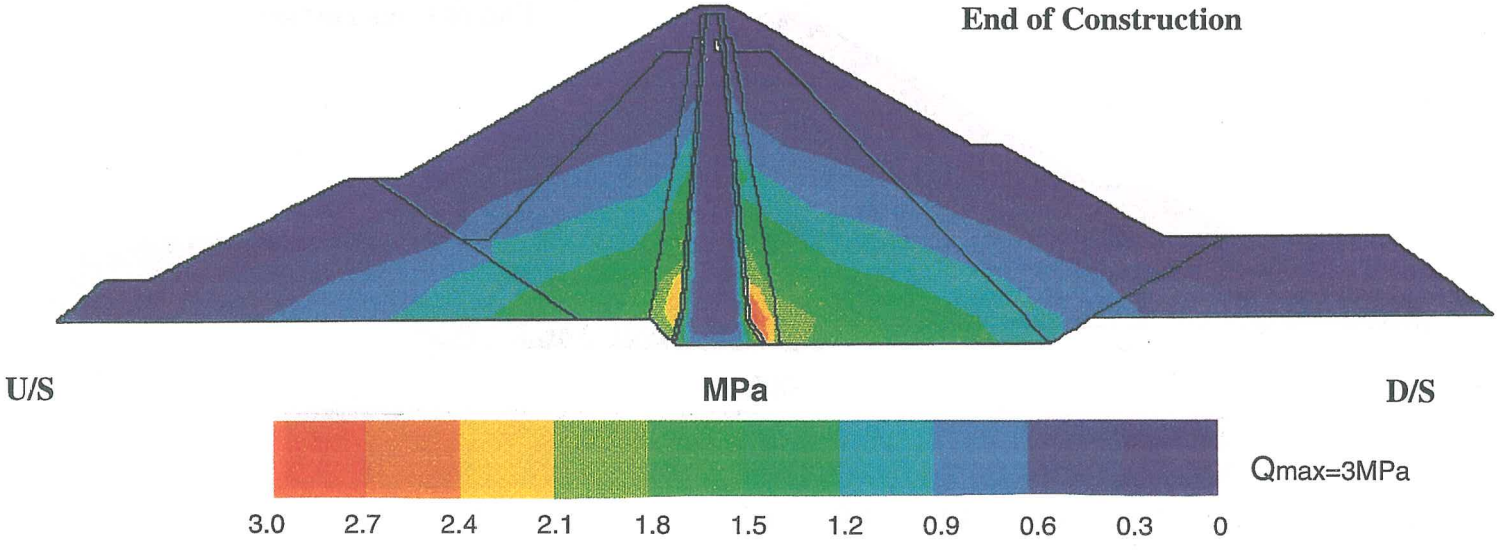

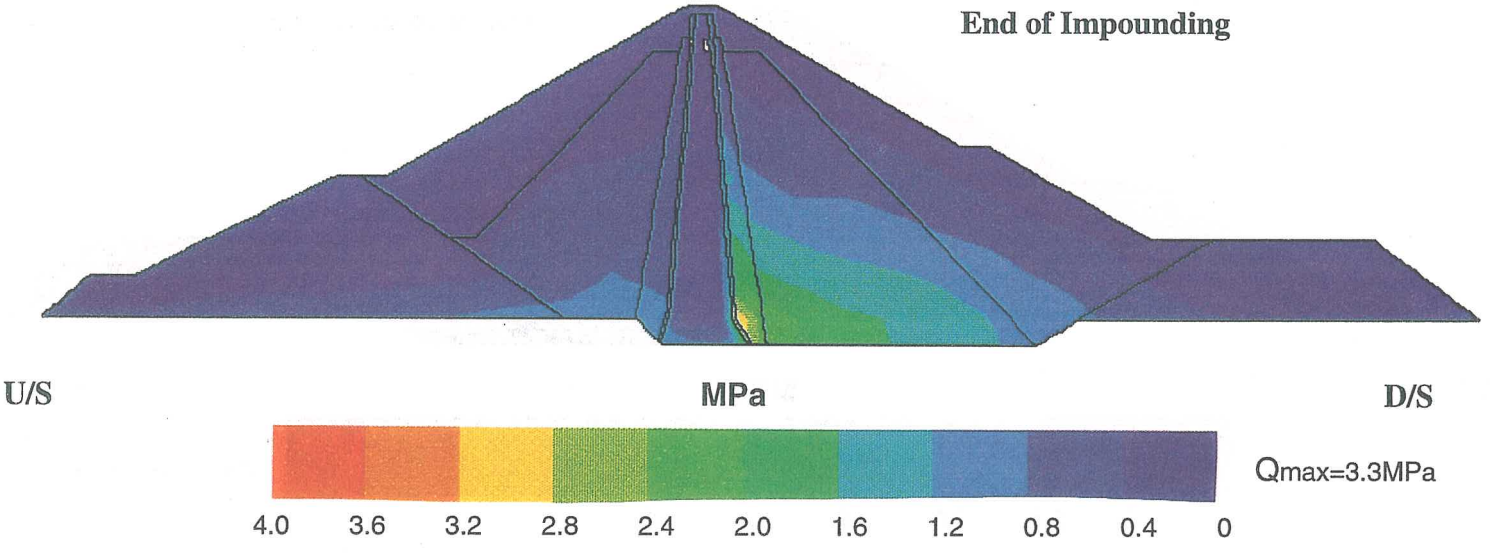

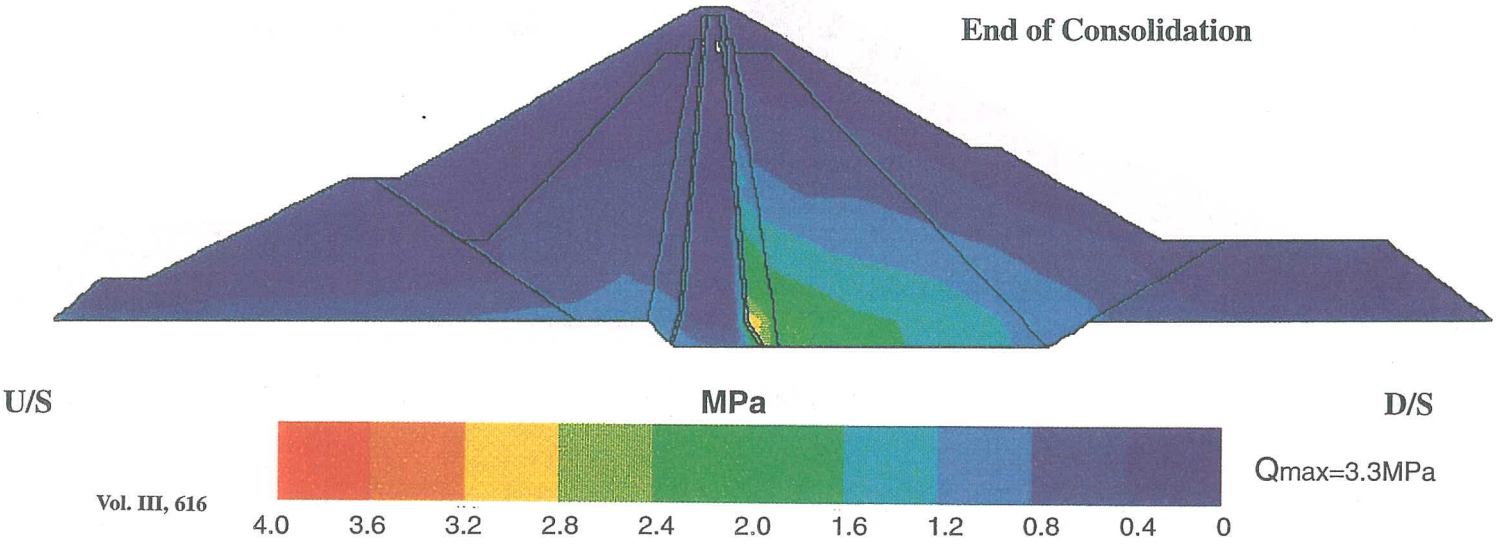

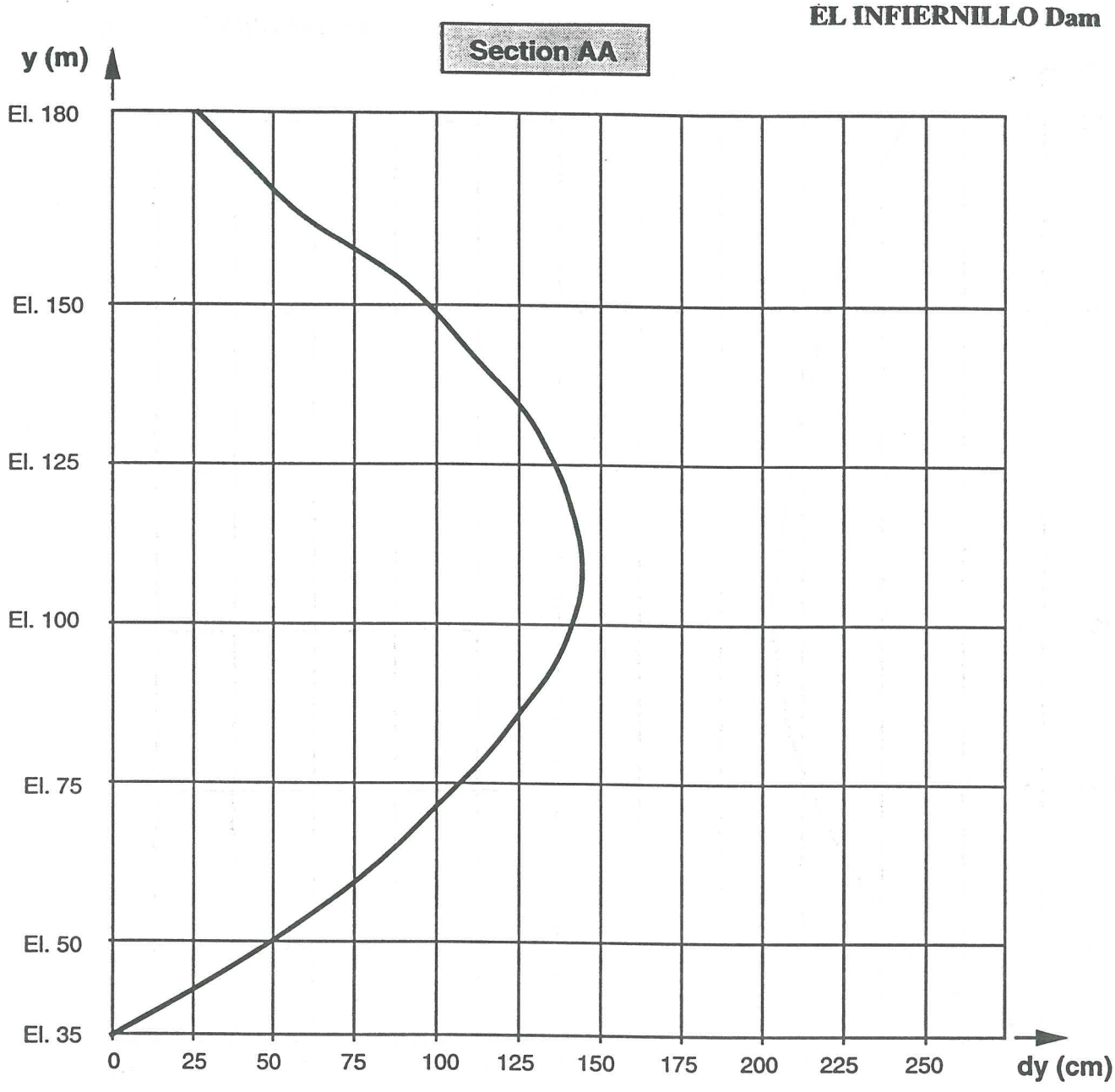

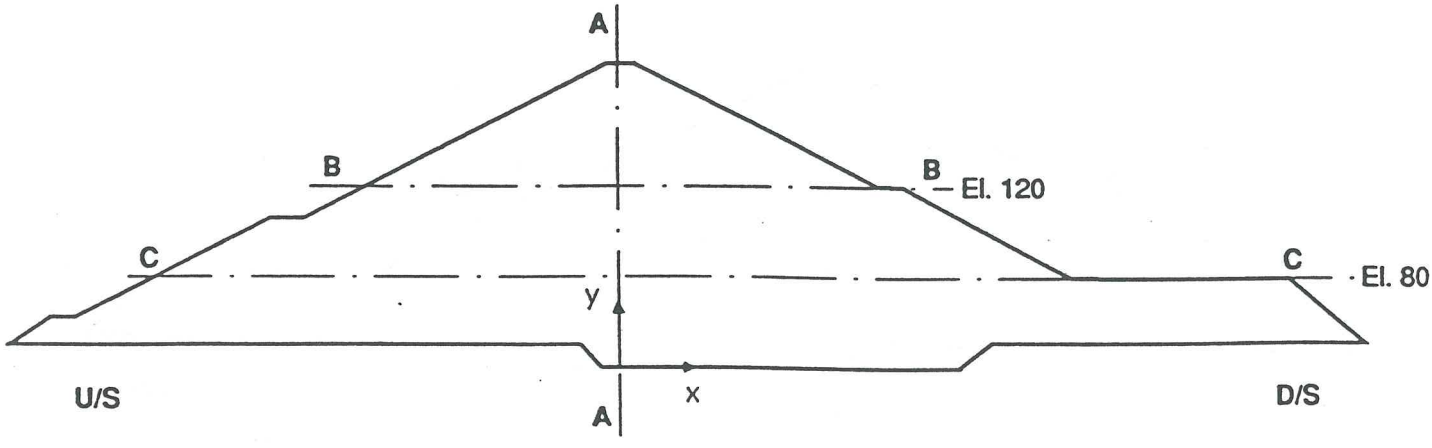

Static Analysis

TEMPLATE FOR THE SETTLEMENTS
AT THE END OF THE CONSOLIDATION PHASE

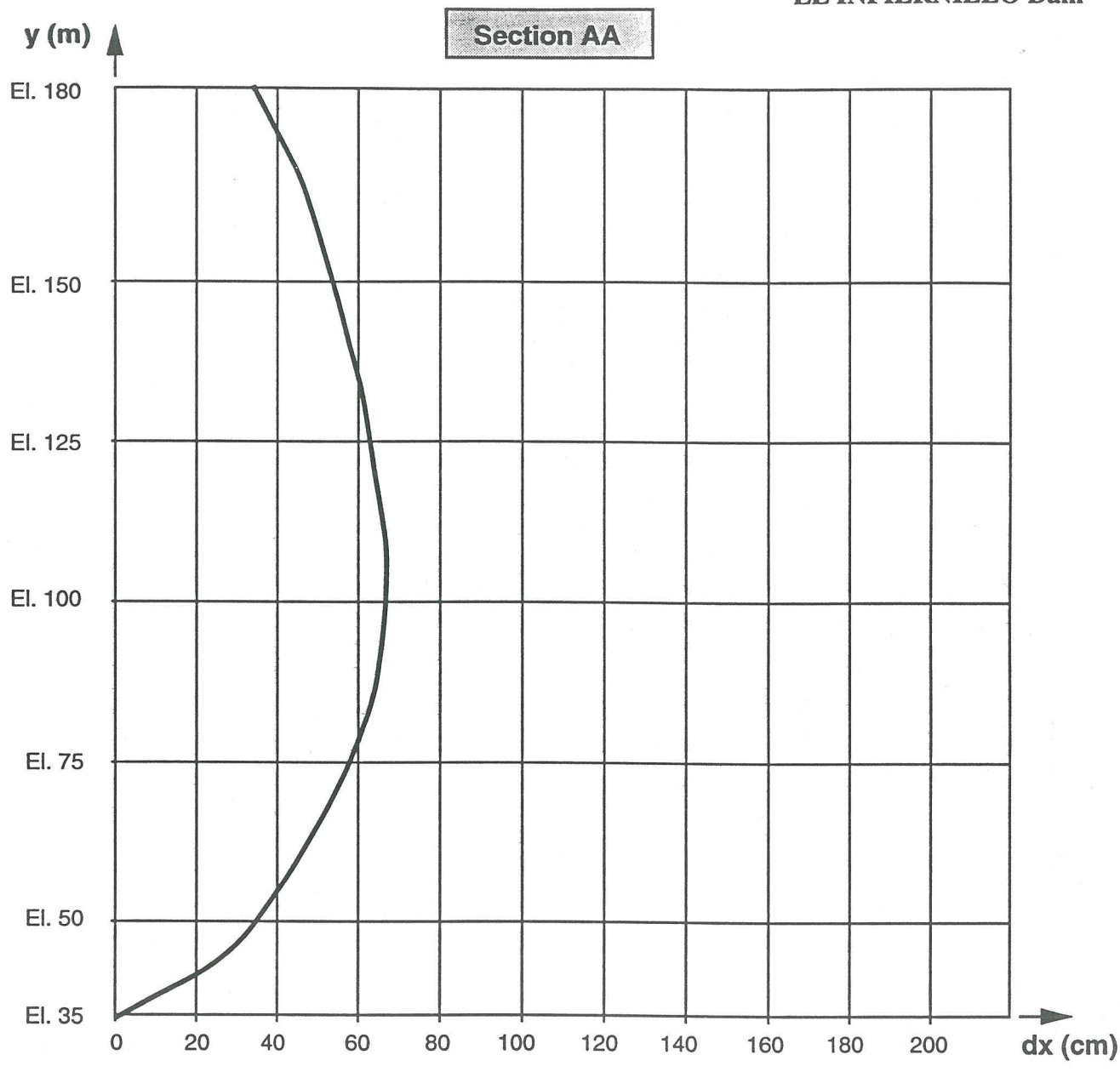

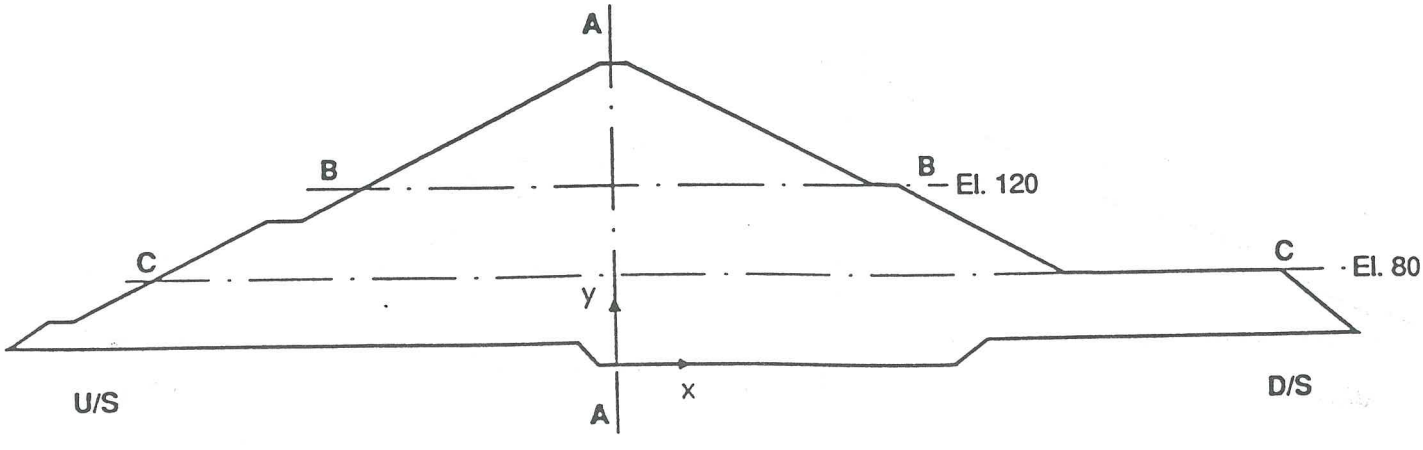

Static Analysis

TEMPLATE FOR THE HORIZONTAL DISPLACEMENTS AT THE END OF THE CONSOLIDATION PHASE

Section BB

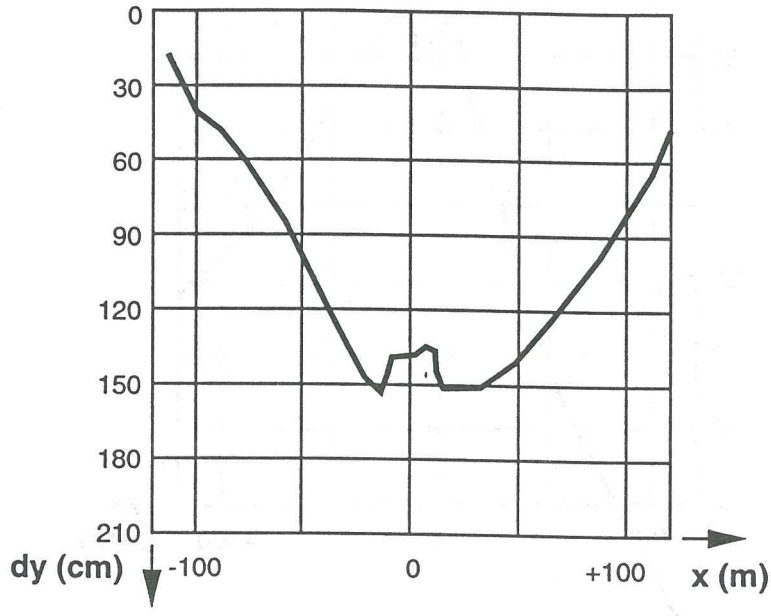

Section CC

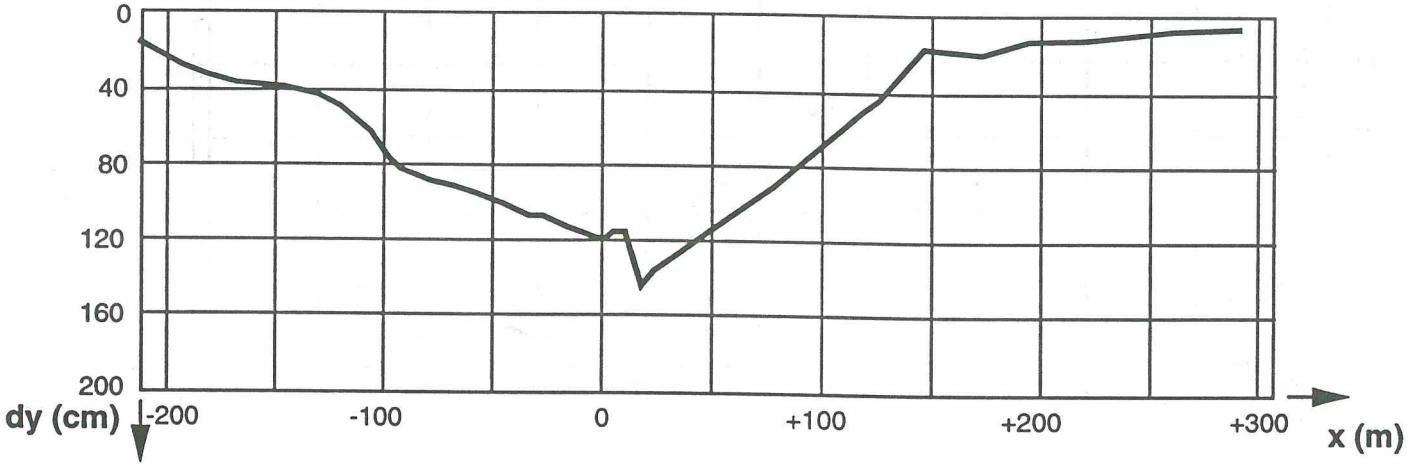

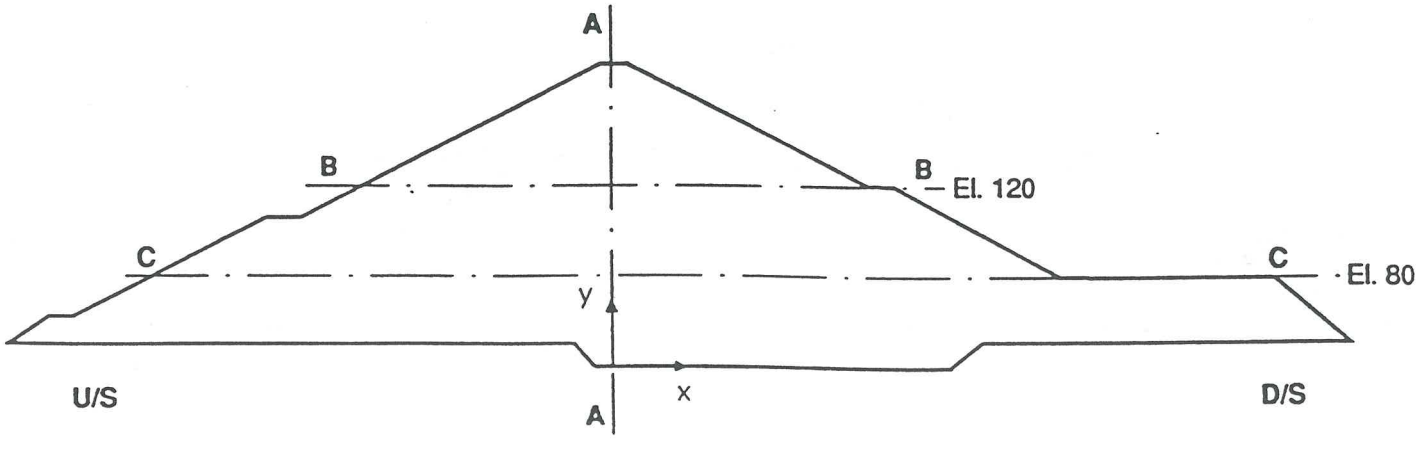

Static Analysis

TEMPLATE FOR THE SETTLEMENTS
AT THE END OF THE CONSOLIDATION PHASE

Section BB

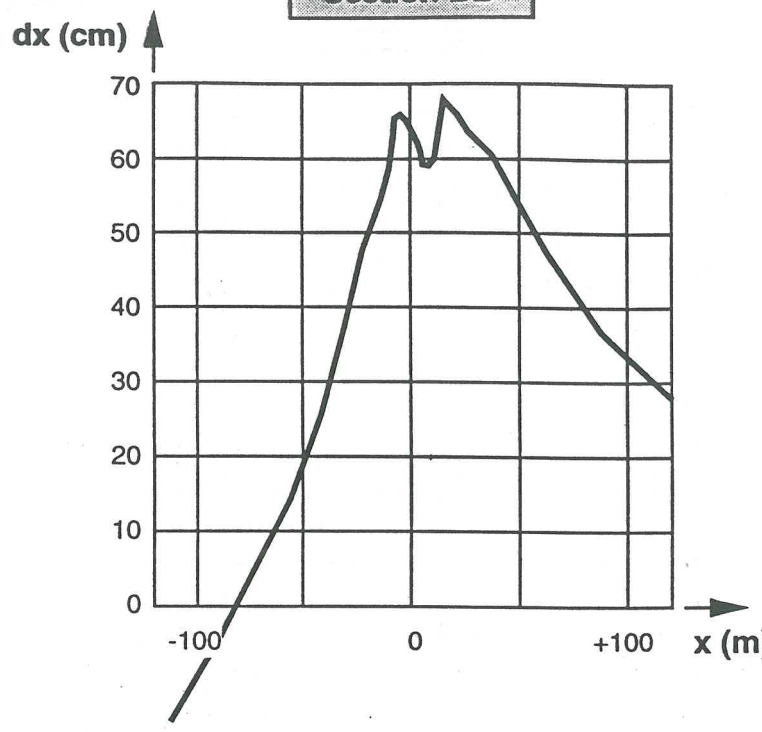

Section CC

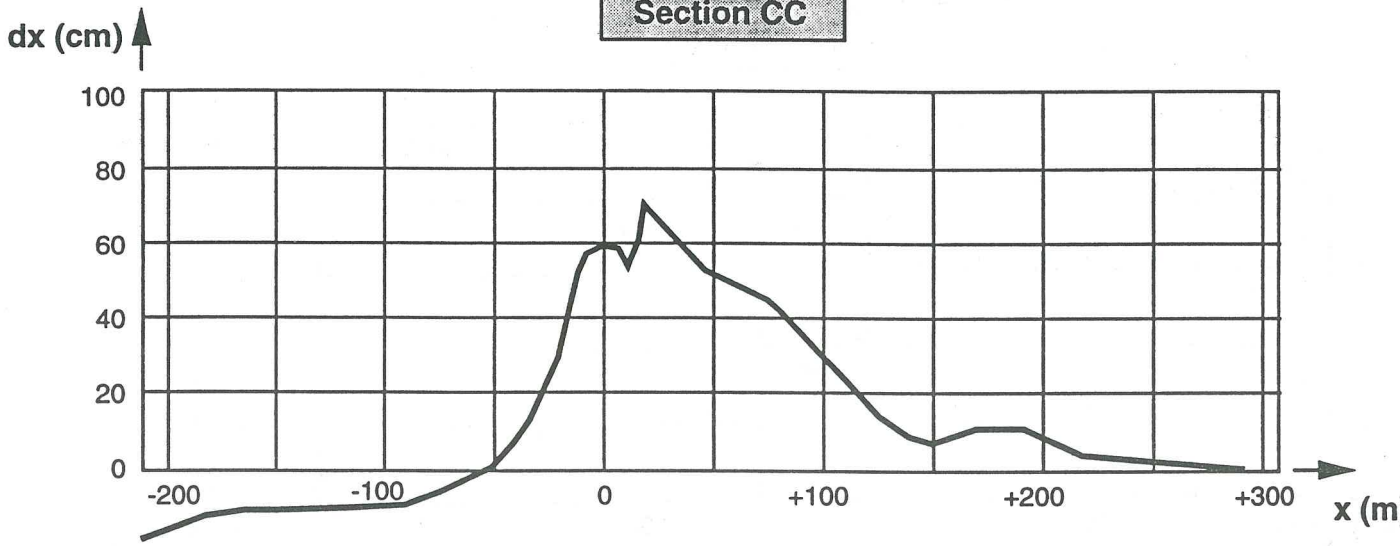

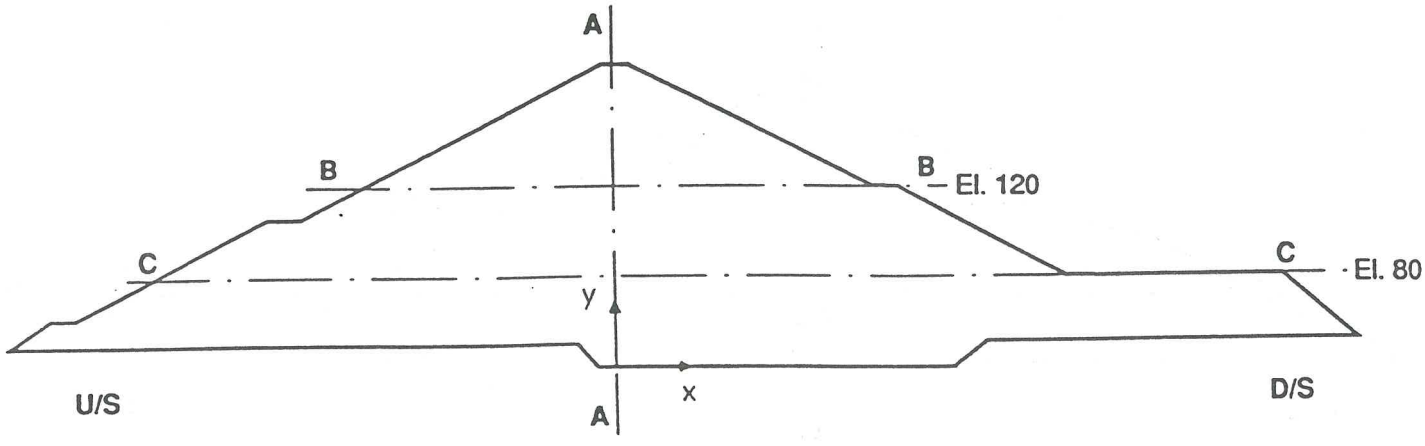

Static Analysis

TEMPLATE FOR THE HORIZONTAL DISPLACEMENTS AT THE END OF THE CONSOLIDATION PHASE

RESULTS

MODELLING C3

+ **Software**: UDAM

+ **Three phase coupled approach.**

+ **Constitutive models:**

Core: State surfaces and Duncan's model for mechanical behaviour.

Filter: Duncan's model.

Transition: Duncan's model.

Compacted shoulder : Duncan's model.

Loose shoulder : Duncan's model.

MODELLING C3

+ **Software**: UDAM

+ **Three phases coupled approach.**

+ **Constitutive models:**

Core: State surfaces and Duncan's model for mechanical behaviour.

Filter: Duncan's model.

Transition: Duncan's model.

Compacted shoulder : Duncan's model.

Loose shoulder : Duncan's model.

	Points of the Dam section				
	CC	CM	CL	UM	DM
End of construction	0	+ 7.0	+ 14.0	- 67.0	+ 67.0
End of Impounding	+ 25.0	+ 34.0	+ 39.0	- 36.0	+ 80.0
End of Consolidation	+ 28.0	+ 41.0	+41.0	- 38.0	+ 86.0

Horizontal Displacements (10^{-2} m)

	Points of the Dam section				
	CC	CM	CL	UM	DM
End of construction	0	- 160.0	- 120.0	- 13.0	+ 2.0
End of Impounding	- 8.0	- 169.0	- 133.0	- 52.0	+ 4.0
End of Consolidation	- 7.0	- 165.0	- 125.0	- 52.0	+ 5.0

Vertical Displacements (10^{-2} m)

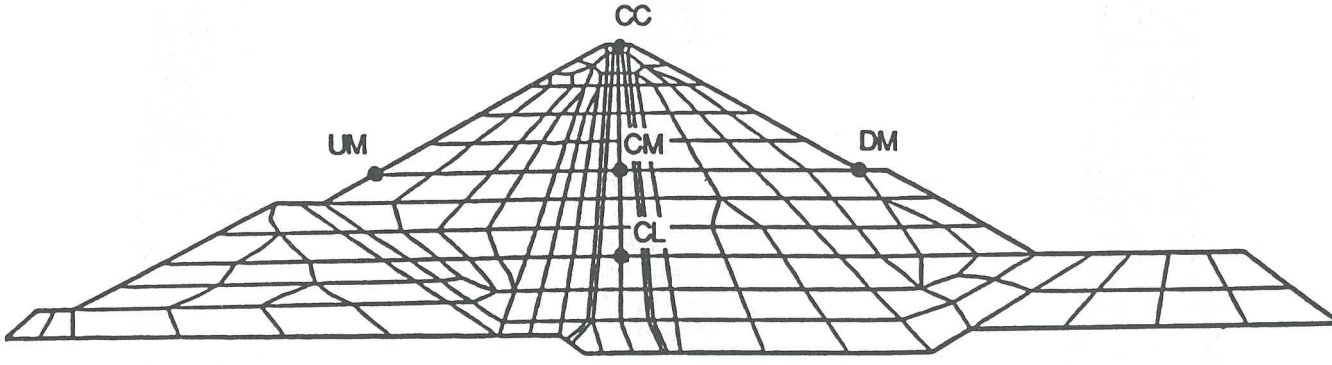

Table 3

Static Analysis

GENERAL SUMMARY : RESULTS OF DISPLACEMENTS AFTER EACH PHASE

UDAM v8.0B

UDAM

Construction Simulation of Earthfill Dams

MAGNIN Philippe 1994

Simulation U8_148.B

EL INFIERNILLO DAM

TEMPLATE FOR PORE PRESSURES DISTRIBUTION
Zoom on The Core Region

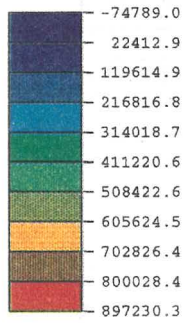

V Min = -74789.0
V Max = 897230.3

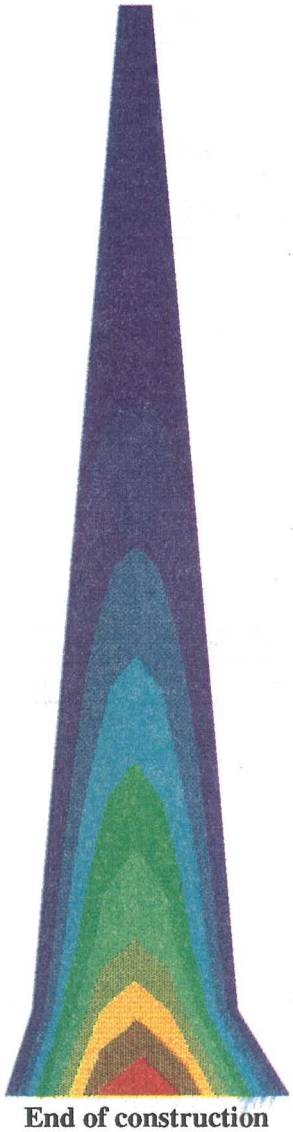

End of construction
(step : 105 time = 449 j)

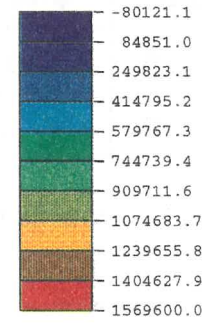

V Min = -80121.1
V Max = 1569600.0

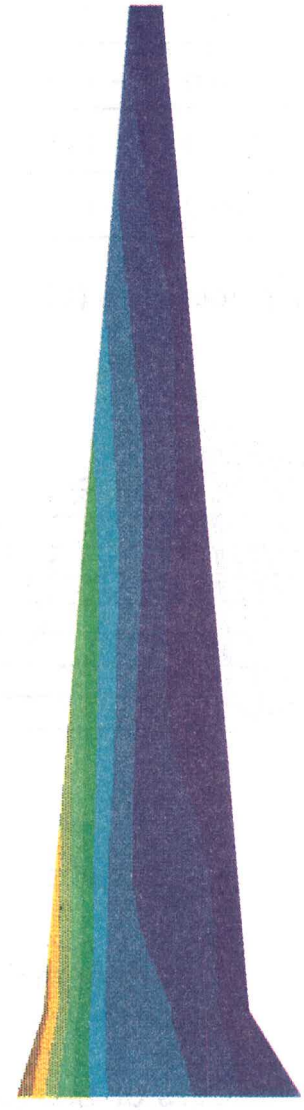

End of impounding
(step : 105 time = 838 j)

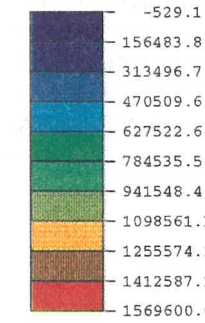

V Min = -529.1
V Max = 1569600.0

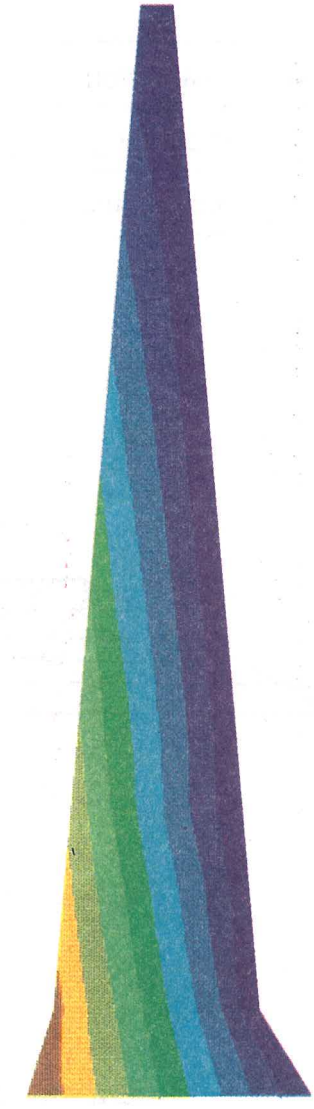

End of consolidation
(step : 105 time = 1370 j)

GRAPHEVIEW v6.0

UDAM v8.0B

UDAM

Simulation of Earthfill Dams

EL INFIERNILLO DAM

HORIZONTAL STRESSES DISTRIBUTION
Dam And Foundation

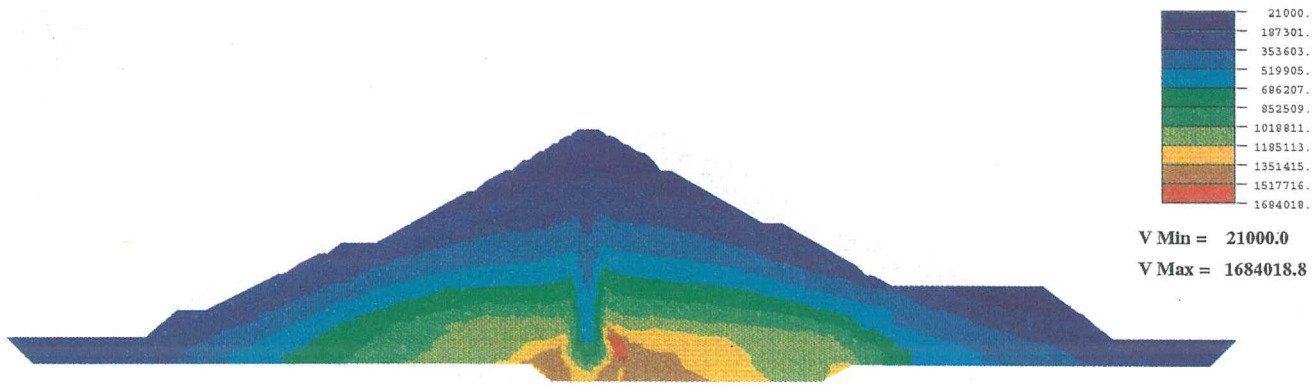

End of construction
(step : 105 time = 449 j)

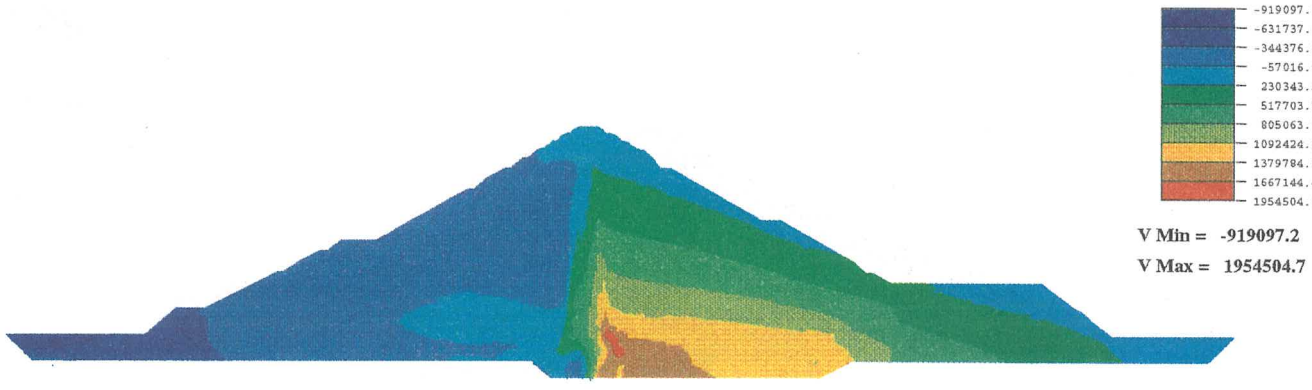

End of impounding
(step : 175 time = 838 j)

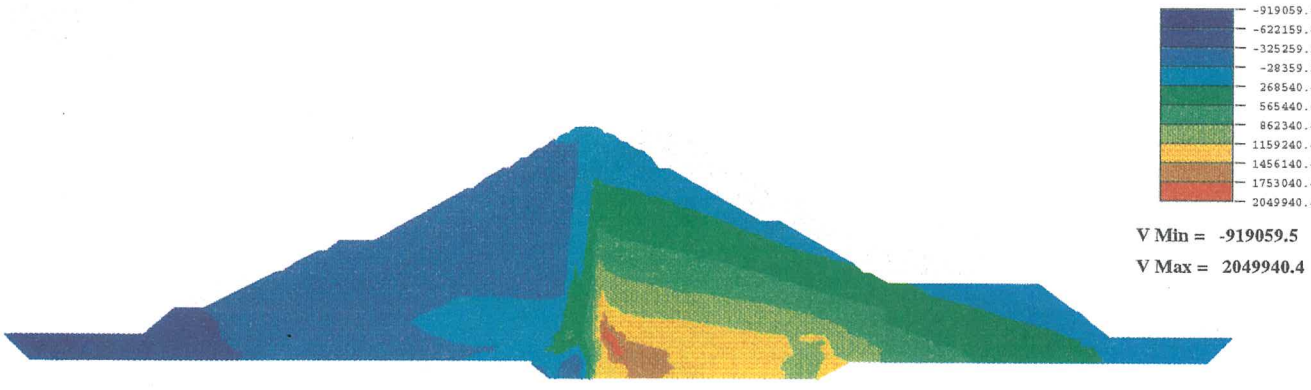

End of consolidation
(step : 360 time = 1370 j)

EL INFIERNILLO DAM

VERTICAL STRESSES DISTRIBUTION
Dam And Foundation

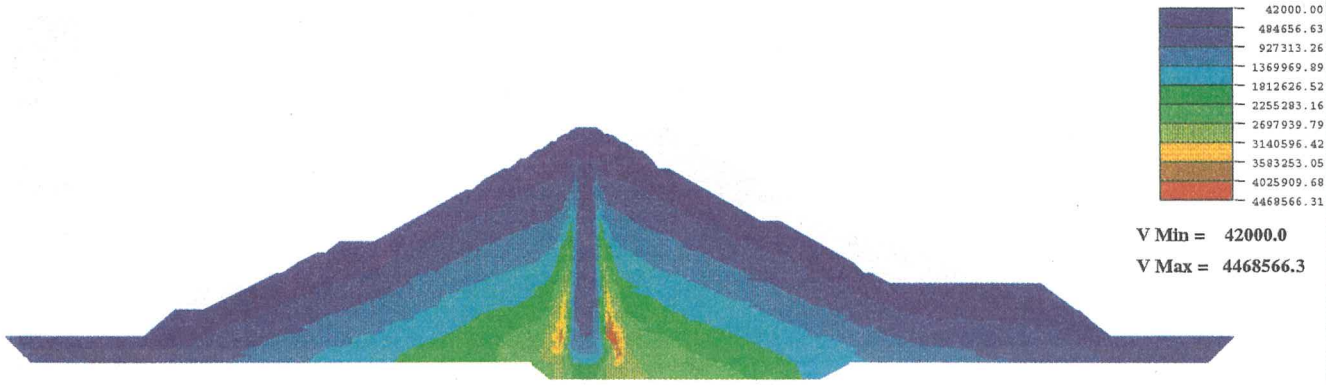

End of construction
(step : 105 time = 449 j)

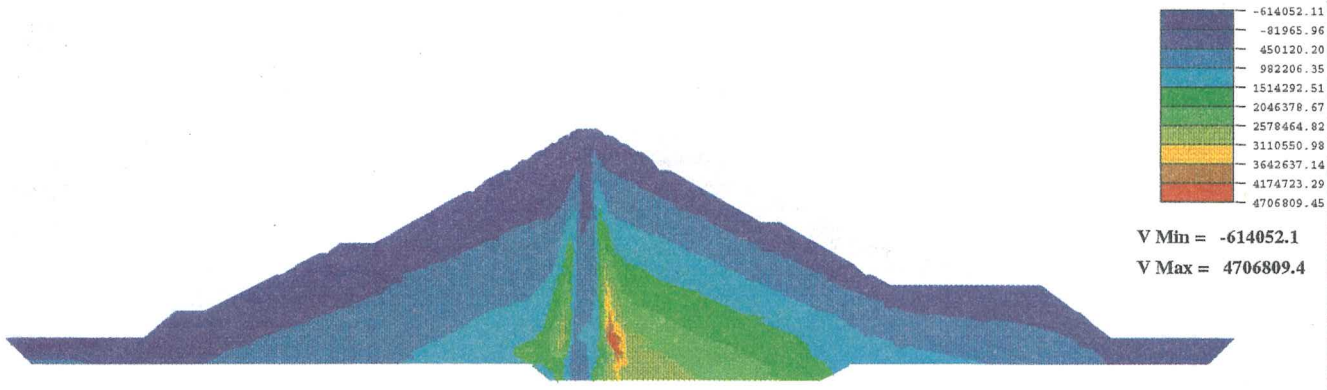

End of impounding
(step : 175 time = 838 j)

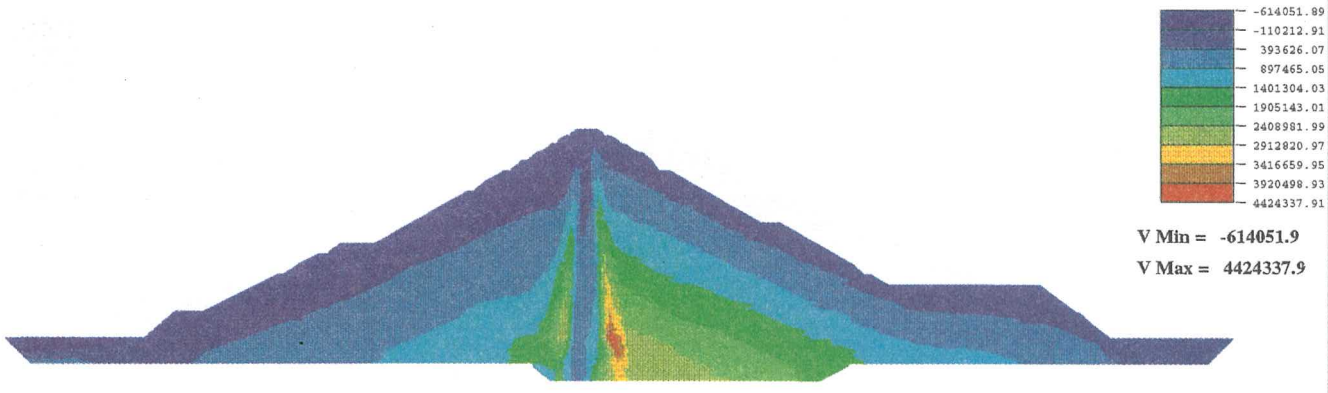

End of consolidation
(step : 360 time = 1370 j)

GRAPHEVIEW v6.0 **UDAM v8.0B**

UDAM

Simulation of Earthfill Dams

MAGNIN Philippe 1994 **Simulation U8_152.B**

EL INFIERNILLO DAM

TEMPLATE FOR PORE PRESSURES DISTRIBUTION
Dam And Foundation

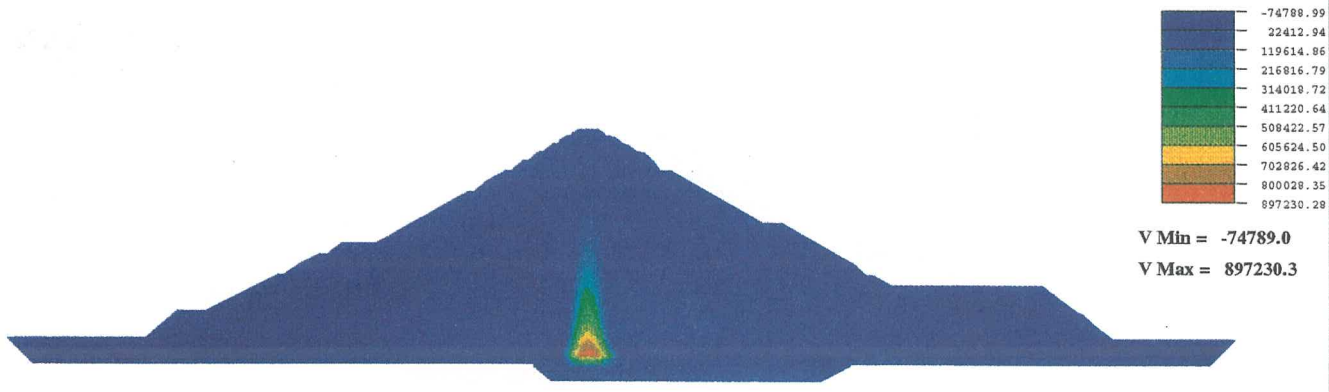

End of construction
(step : 105 time = 449 j)

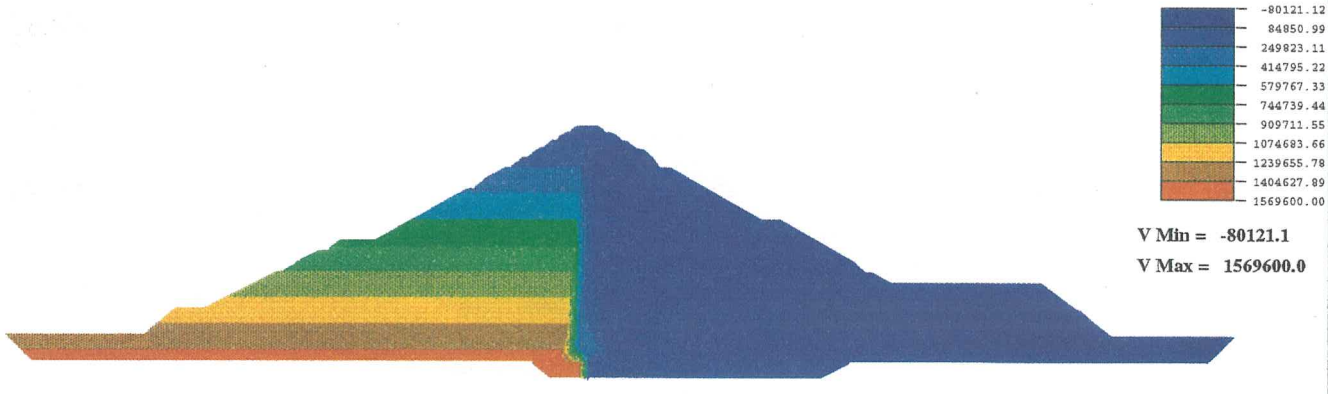

End of impounding
(step : 175 time = 838 j)

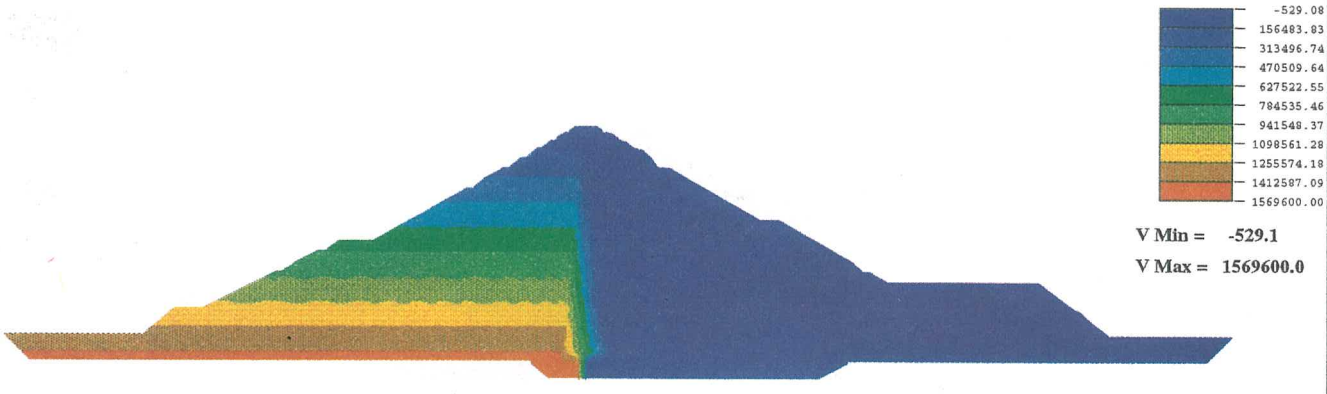

End of consolidation
(step : 360 time = 1370 j)

GRAPHEVIEW v6.0

UDAM

UDAM v8.0B

Simulation of Earthfill Dams

MAGNIN Philippe 1994

Simulation U8_152.B

EL INFIERNILLO DAM

VERTICAL DISPLACEMENTS DISTRIBUTION
Dam And Foundation

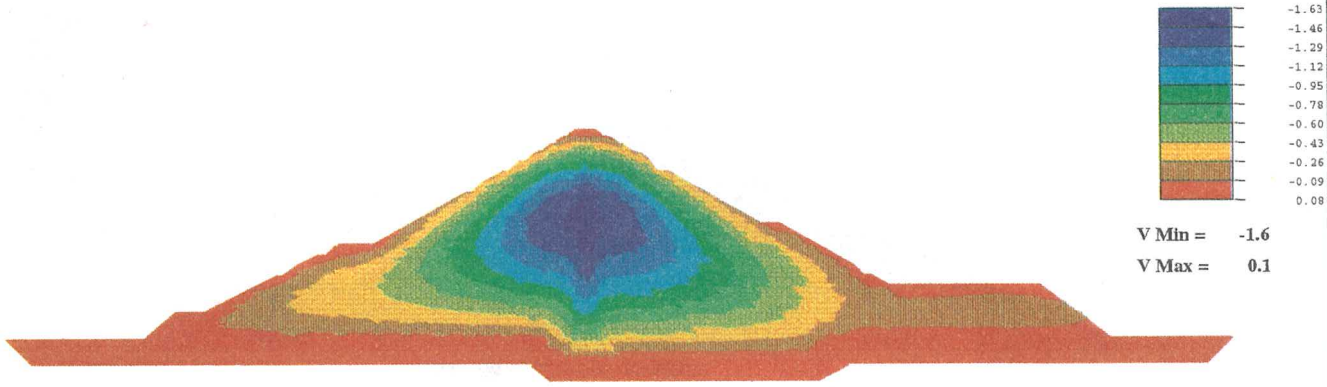

End of construction
(step : 105 time = 449 j)

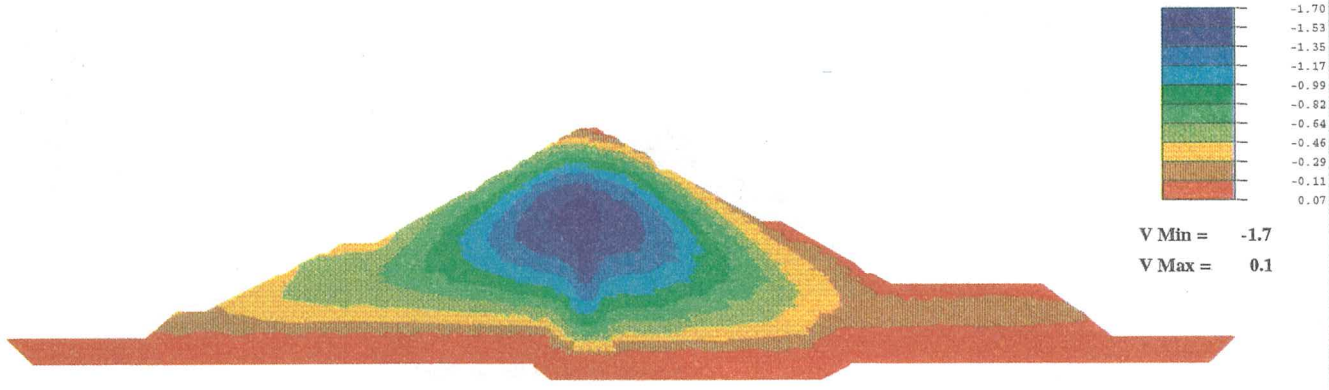

End of impounding
(step : 175 time = 838 j)

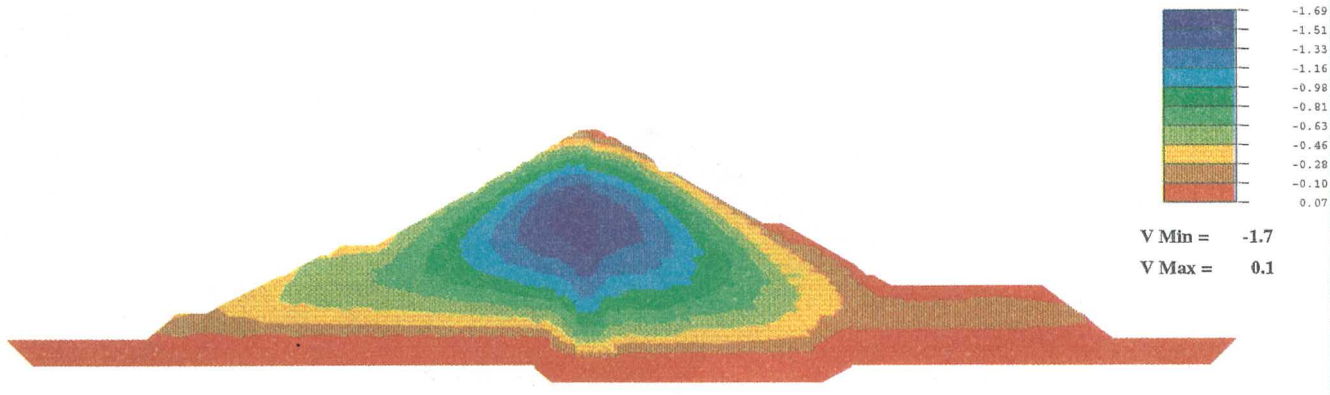

End of consolidation
(step : 360 time = 1370 j)

GRAPHEVIEW v6.0 **UDAM v8.0B**

UDAM

Simulation of Earthfill Dams

MAGNIN Philippe 1994 **Simulation U8_152.B**

EL INFIERNILLO DAM

HORIZONTAL DISPLACEMENTS DISTRIBUTION
Dam And Foundation

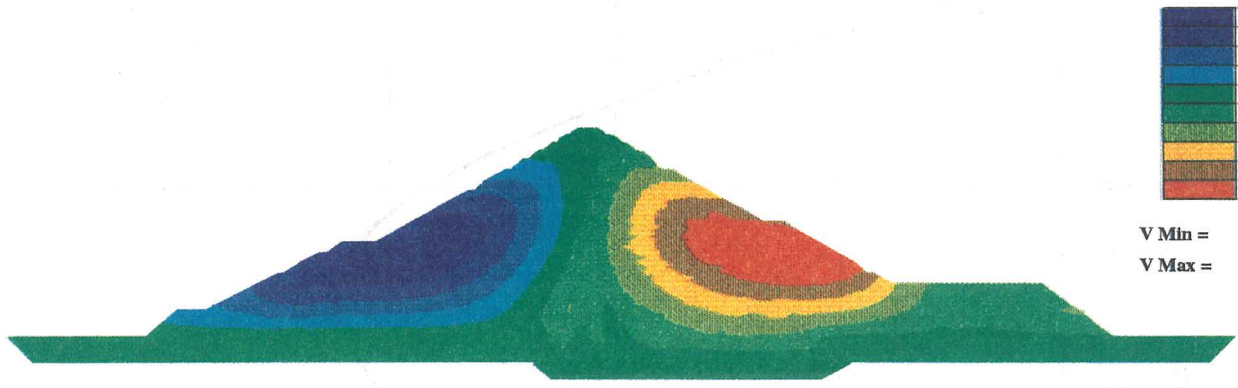

End of construction
(step : 105 time = 449 j)

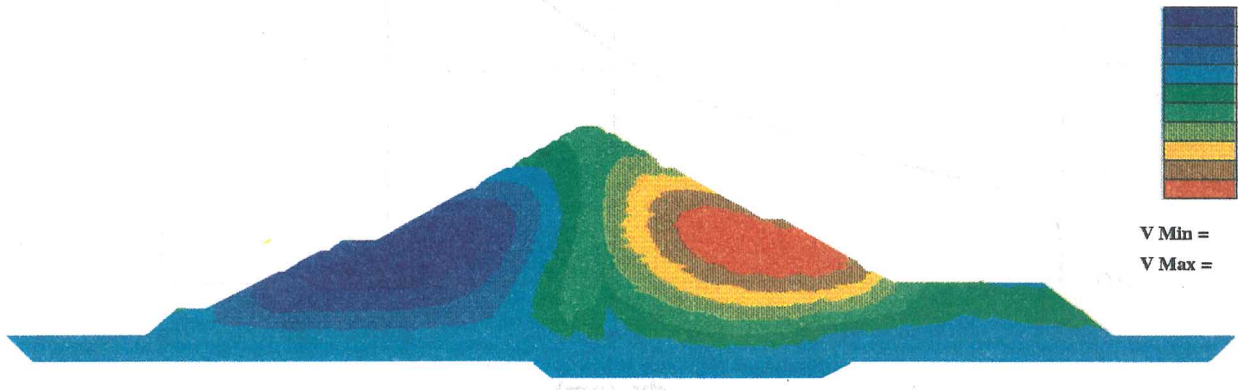

End of impounding
(step : 175 time = 838 j)

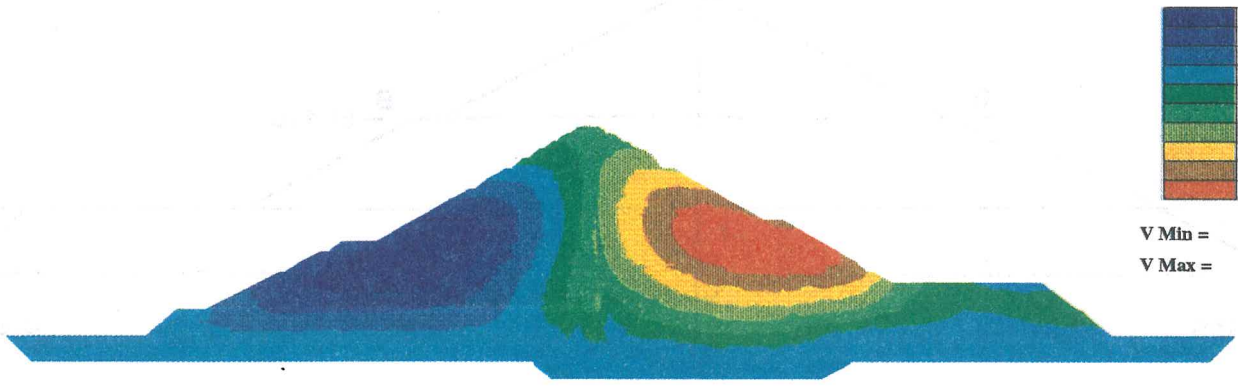

End of consolidation
(step : 360 time = 1370 j)

GRAPHEVIEW v6.0

UDAM

UDAM v8.0B

Simulation of Earthfill Dams

MAGNIN Philippe 1994

Simulation U8_152.B

Section AA

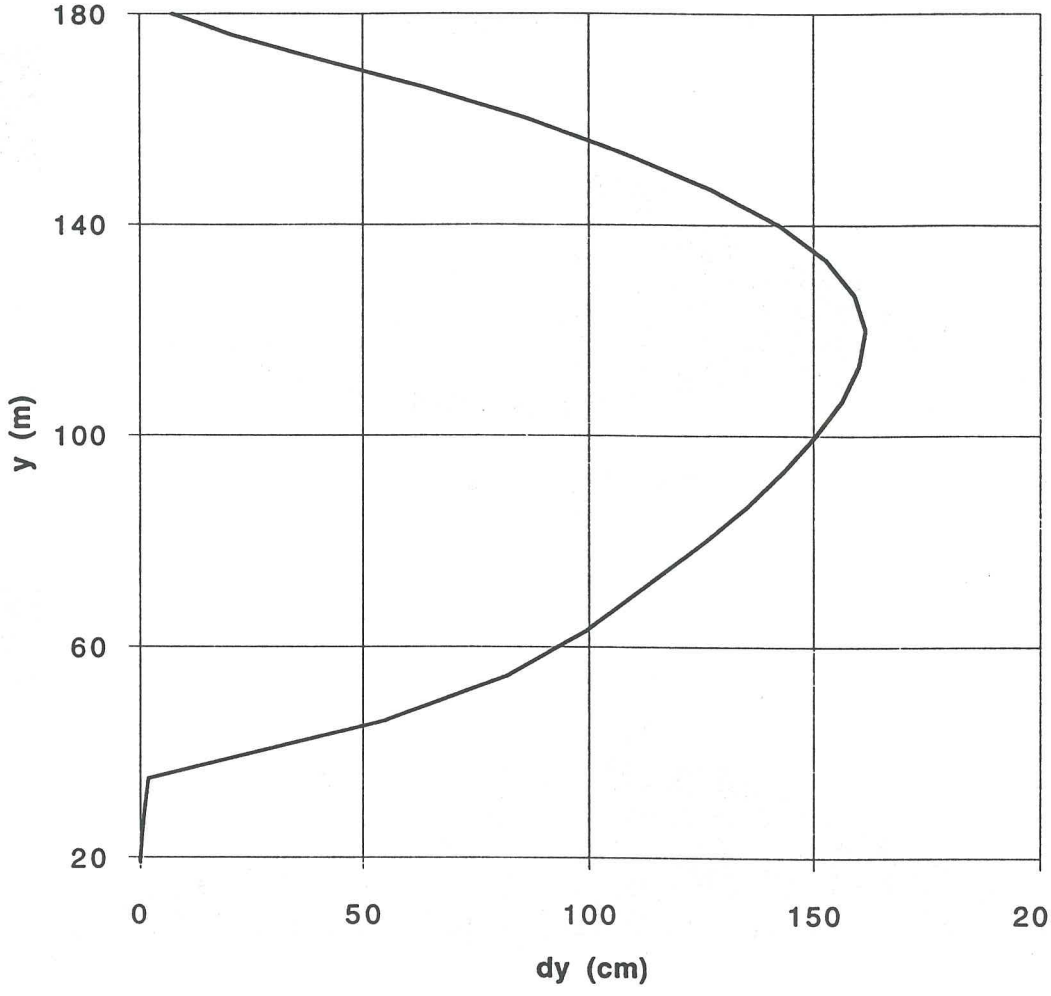

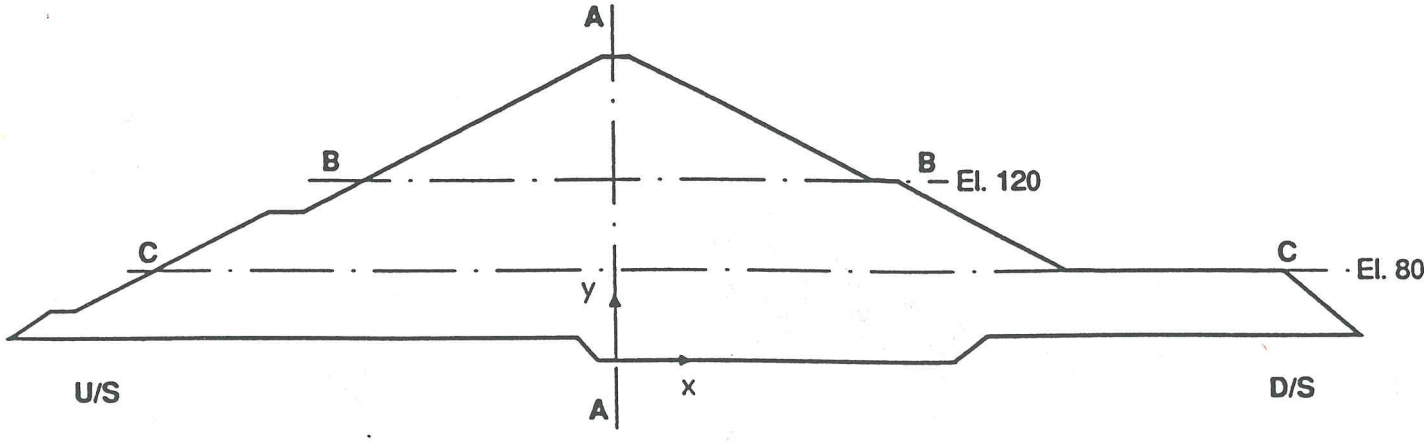

TEMPLATE FOR THE SETTLEMENTS

AT THE END OF THE CONSOLIDATION PHASE

UDAM

Section AA

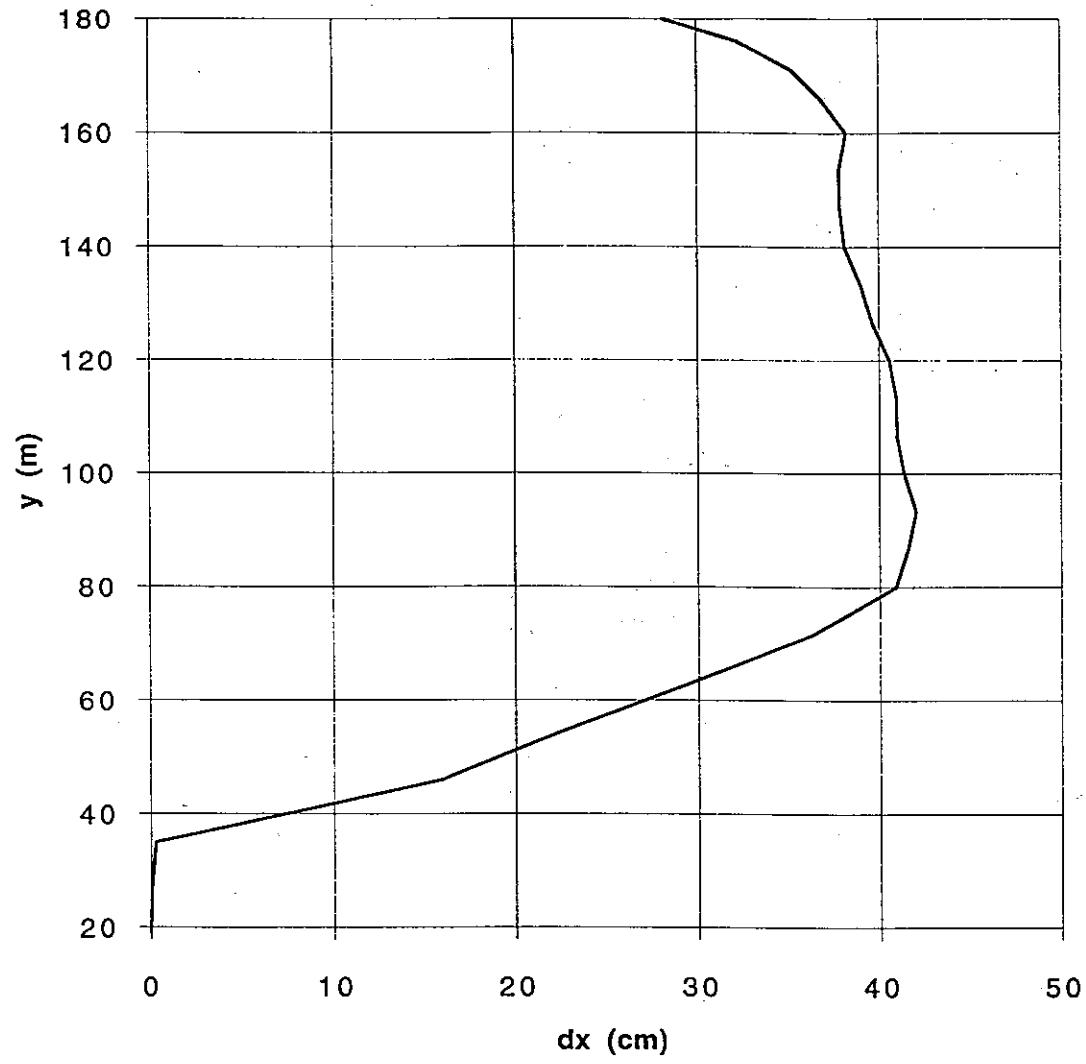

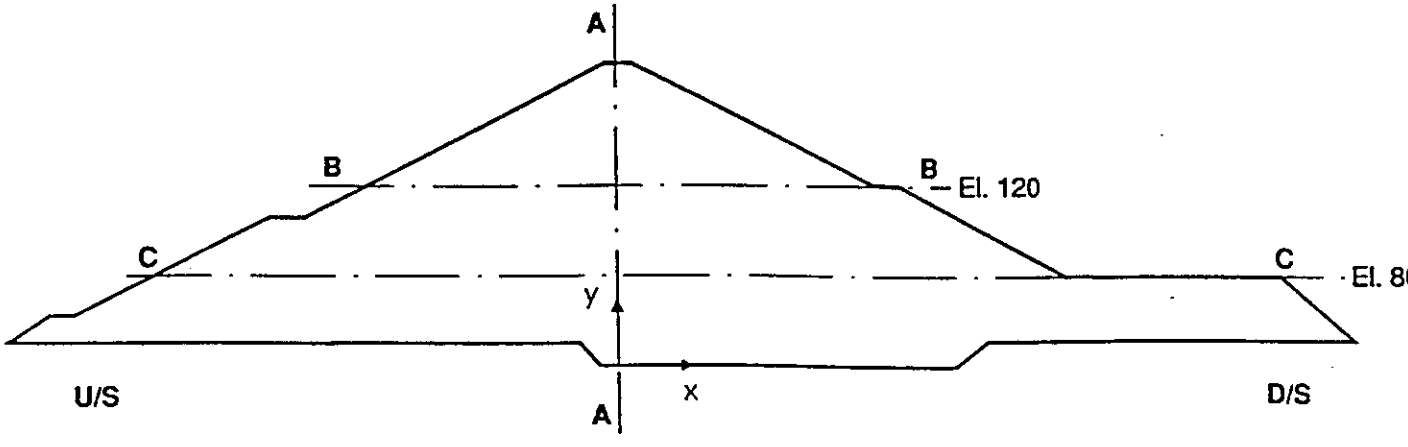

TEMPLATE FOR THE HORIZONTAL DISPLACEMENTS
AT THE END OF THE CONSOLIDATION PHASE

Section BB

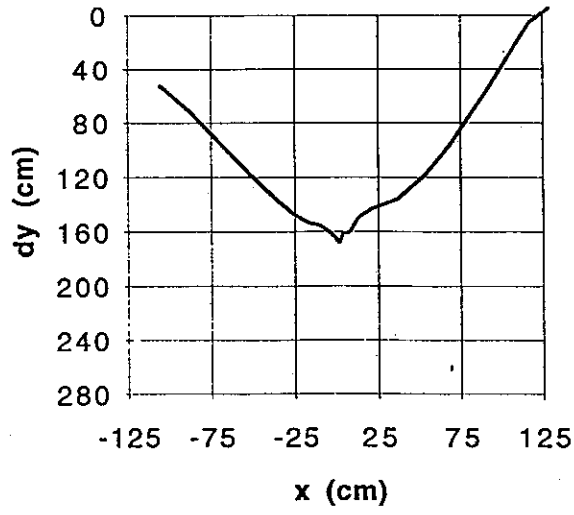

Section CC

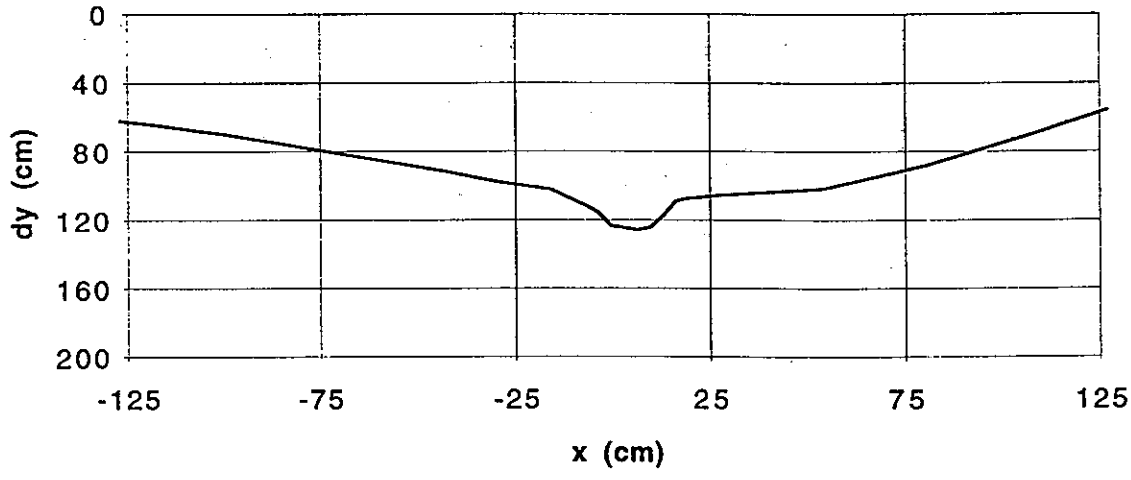

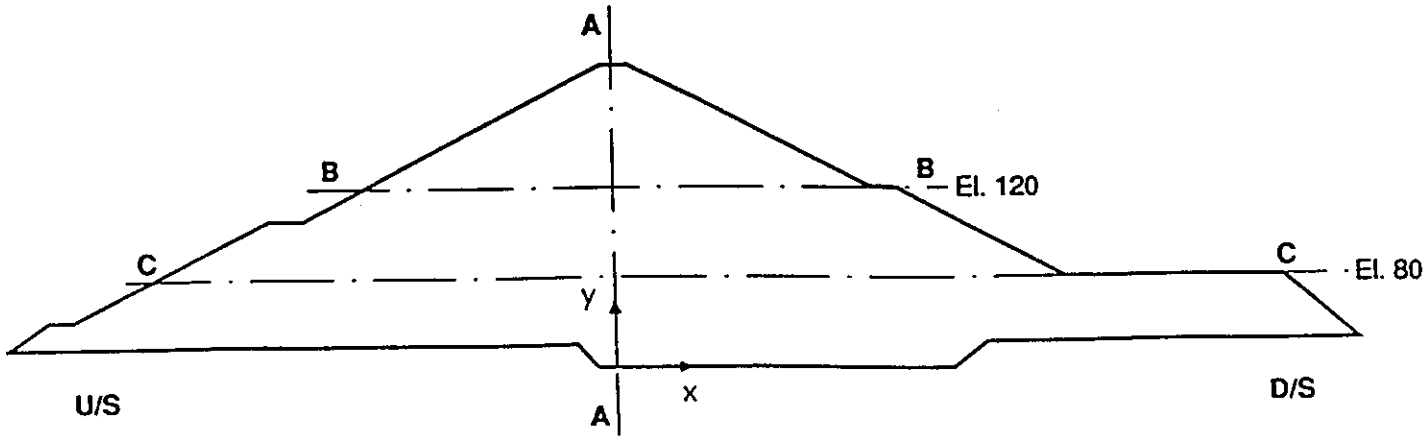

TEMPLATE FOR THE SETTLEMENTS

AT THE END OF THE CONSOLIDATION PHASE

UDAM

Section BB

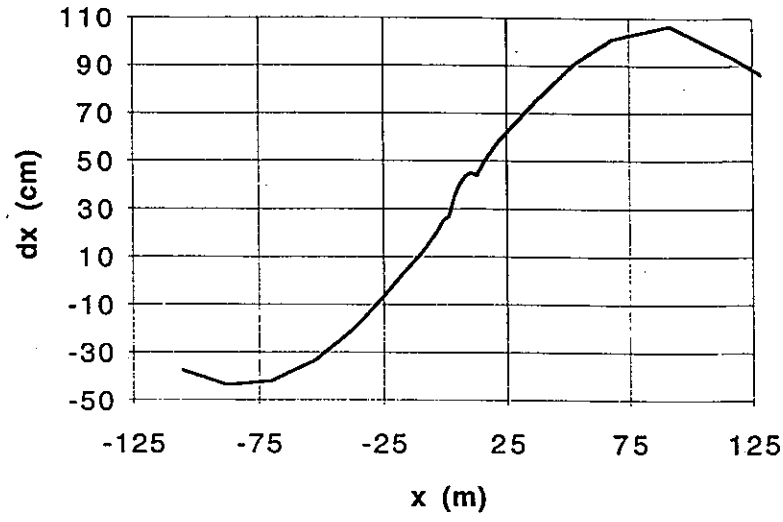

Section CC

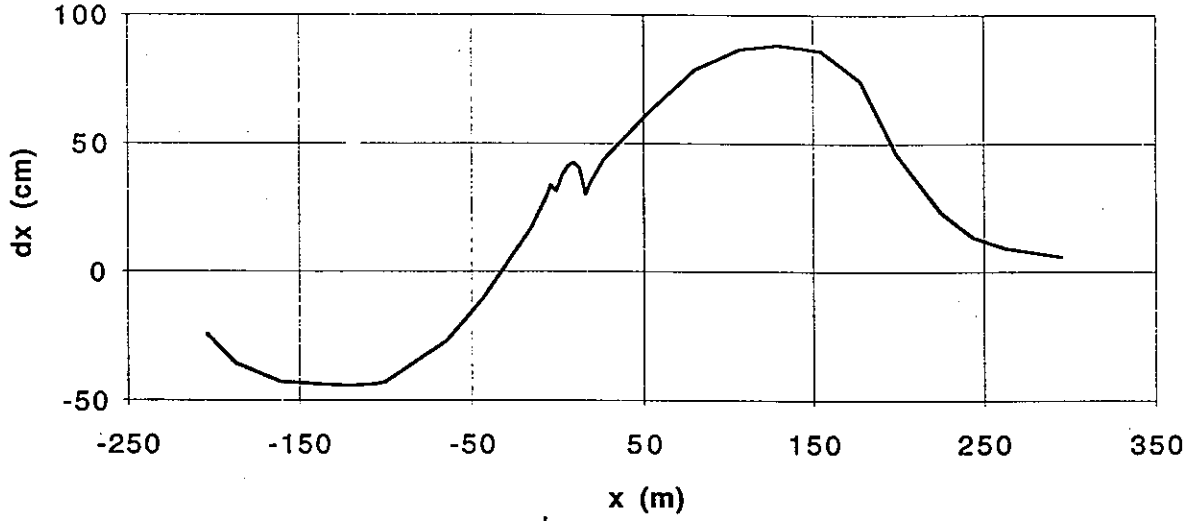

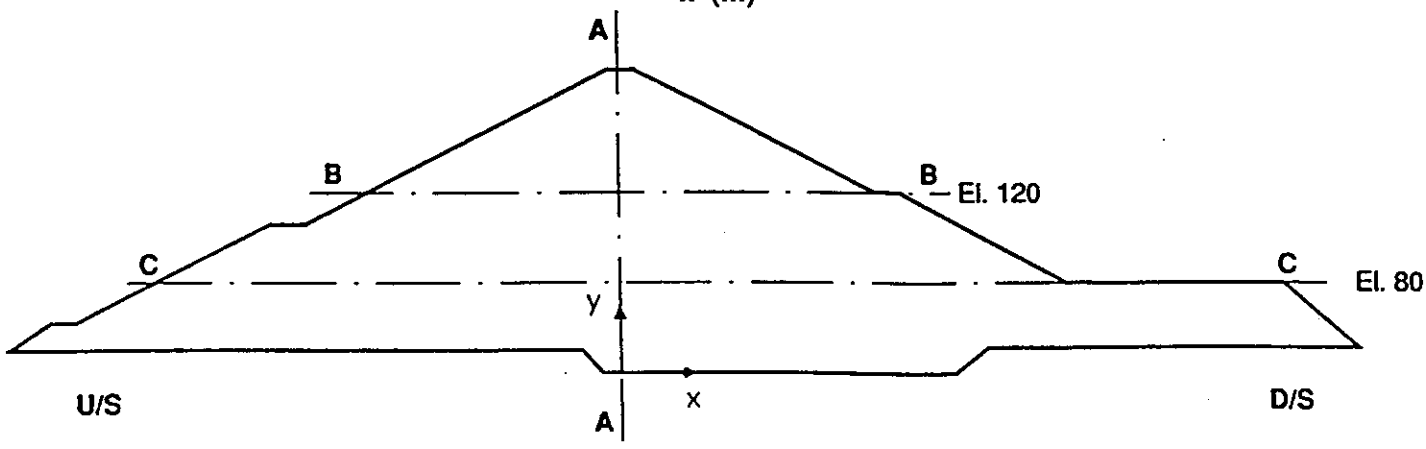

TEMPLATE FOR THE HORIZONTAL DISPLACEMENTS

AT THE END OF THE CONSOLIDATION PHASE

V/ ANALYSIS OF RESULTS

Two kinds of approachs have been retained in this work, that are analysed and discussed separately.

V.1/ TWO-PHASE APPROACH

V.1.1/ Two-Phase approach- Settlements.

With two first simulations with GEFDYN, we wanted to evaluate the interest of a non linear modelling in shells, and essentially during impounding. This phase corresponds with an unloading path for soil, and it seems necessary to take into account two different modulus, on loading and unloading. Some results about settlements show this importance. In fact, if we compare settlements on crest, we establish that, in the first case with an elastic-plastic model such as Drucker-Prager, at the end of impounding, an important swelling appears. At this moment, settlement on crest (Point CC) is about +52 cm. On the contrary, with the non linear approach, this settlement is only -27 cm. Of course, initial modulus are not the same, so it's difficult to compare. But, it seems that the non linearity is essential, even if this modelling is not sufficient to obtain a correct vertical displacement during impounding. A lessening of modulus, or/and friction angle, seems to be a solution, to take into account the alteration and compressibility of wet rockfill.

These remarks are the same about horizontal displacement, which are lesser with the hyperbolic approach. In the first simulation (C1 Drucker-Prager in shells), the maximum horizontal movement is in crest, about 1,60m at the end of impounding. It's an excessive value which may not be acceptable. On the contrary, with the non linear model (C2), this greater horizontal settlement is in core (Point CM), and is about 63 cm at the end of consolidation. On crest, this movement is only about 36 cm.

All these results show that it's essential to simulate rockfill and, of course, clay, with a non linear model.

V.1.2/ Two-phase approach- Stresses.

Vertical stresses and horizontal stresses are shown for every simulation, at different times such as the end of construction, end of impounding, and end of consolidation period. We established that there are strong stresses at base of the dam, in filters and transitions. These stresses are due to a transfer load between the core and the shoulder, and it depends on the relative stiffness of core and rockfill.

In fact, with the DRUCKER-PRAGER model, filters and rockfills are less deformable, and concentration of stresses is important. We obtained, at each time:

+ **End of construction**: σ_z=5,4 MPa and σ_y=1,5MPa, on the dowstream face of the core. On the upstream face, state of stresses are also strong, but decreased during the impounding.

+ **End of impounding**: σ_z=5,5 MPa and σ_y=1,7 MPa, on the downstream face.

+ **End of consolidation**: σ_z=5,5 MPa and σ_y=1,6 MPa, on the downstream face.

In the second simulation, with the hyperbolic model, strains are better simulated, and contrast of rigidity seem less important, in this case, between filters, shoulders, and core. Stresses are lesser than in the first simulation,and are the following:

+ **End of construction**: σ_z=3,8 MPa and σ_y=1,2MPa, on the dowstream face of the core.

+ **End of impounding**: σ_z=3,6 MPa and σ_y=1,5 MPa, on the downstream face.

+ **End of consolidation**: σ_z=3,7 MPa and σ_y=1,5 MPa, on the downstream face.

Shear stress was also presented, in the two approaches. In the two cases, this stress was maximal at the end of impounding, on the downstream face, at the base of core. With an elastic-plastic approach, maximum shear stress was about 4,3 MPa, whereas with the hyperbolic model, maximum shear stress was about 3,3 MPa. This stress evolution may be explained by the modification of relative striffness between core and shoulders.

V.1.3/ Two-phase approach - Pore pressures.

For these two simulations, clay was considered saturated initially. Material properties in core are identical in both cases, and only permeabilities are modified. In the C1 approach, with DRUCKER-PRAGER, permeability is isotropic, and equal to 2.10^{-10}m/s. On the contrary, during the second computation, this permeability isn't isotropic, and the ratio between horizontal and vertical values is about 3, with a vertical permeability equal to 2.10^{-10}m/s.

If we compare maximum pore pressure value at the end of construction, we obtain:

+ u_{wmax}=2,00 MPa in C1 simulation.
+ u_{wmax}=1,30 MPa in C2 simulation.

This difference between these values may be explained by two factors:

+ The modification of permeabilities. It seems to be the major factor.
+ Evolution of transferred load between core and shoulders.

At the end of consolidation, 5 years after impounding, pore pressures are equal to 1,3 MPa

V.1.4/ Conclusion about this two-phase approach:

From these two simulations, it seems that some improvements are necessary to represent correctly the behaviour of rockfill dams, during their construction, but essentially during their impounding. In fact we have shown that a non linear approach, using an elastoplastic constitutive model with hardening, is necessary in core, but also in shoulders.

If we use a linear model in shoulder, we have established that excessive swelling appears during the impounding. This phenomenon is due to:

- No lessening of young modulus, due to alteration of rockfill, and "lubrication" of particles in shells.
- No collapse due to saturation in clay. We apply the effective stress principle, and during impounding, effective stress must decrease, hense the appearance of swelling. This phenomenon of collapse during saturation is take into account by the ultimate approach, with UDAM software.

However, it's important to specify that, with a non linear constitutive model, such as an elastoplastic model with hardening, numerical convergence criteria are difficult to reach. Some important shear strains appear in filters and core, on the boundary between these two materials, and many iteration steps are necessary to reach a acceptable result.

V.2/ PARTIALLY SATURATED APPROACH

A three-phase coupled simulation of soil is unusual. It 's adapted to unsaturated soils, with a degree of saturation lesser than 95-97%, when the water phase is not continuous , and when air and water flow simultaneously in soil. UDAM has been initially developed to evaluate safety of clayey fills, after MIRGENBACH's failure in 1982. It forecasts pore pressure increase during construction of this kind of dam, and gives an estimation of safety factor.

By an adapted simulation of unsaturated soil behaviour, we hope to find again some phenomena which appear during dam construction (Excessive water pressure increase in clayey fills) and settlements during the impounding. These settlements are due to saturation of soils and collapse of skeleton. This collapse can not be simulated by classical BISHOP's theory, but it may be obtained with a correct state surface.

Others phenomena are simulated, like the evolution of mechanical properties with suction.

This approach is recent and is still in qualification procedure actually, but recent works (Mirgenbach, La ganne,...) give some interesting results, about effects of water content during construction, speed of construction, and permeability on the safety factor.

However, two kinds of difficulties exist today, in the actual version of UDAM:

+ Choice of boundary conditions which change during construction and impounding. These conditions concern water pressures and air pressures.

+ Behaviour modelling when we reach a strong degree of saturation, near total saturation and when gas phase is non continuous.

V.2.1/ Partially saturated approach - Settlements.

The three-phase simulation was only made in core, and an uncoupled approach was used to simulate shell's behaviour. This was a first approach, since we didn't use a coupled approach in upstream shells. Displacement toward the upstream is probably not correct during the impounding, but the aim of this approach was to analyse the core behaviour during this phase, and during construction.

Vertical settlements at the end of consolidation are about 1,60 m in the core, with an horizontal displacement about 40 cm.

V.2.2/ Partially saturated approach - Stresses.

As in the two-phase approach, we observed a stress concentration around the core, at its base. At the end of construction, the maximum vertical stress was about 4,4 MPa, and the horizontal stress was about 1,7 MPa. These values are in good agreement with previous simulations. At the end of consolidation, maximal vertical stress was about 4,4 MPa in the downstream filter.

V.2.3/ Partially saturated approach - Pore pressures.

We are going to give water pore pressure values at three points in time, and we will present some phenomena which appear during the impounding.

At the end of construction, the maximum pore pressure in core was about 0,9 MPa, lesser than in previous modellings. In this case, permeability is anisotropic, with a ratio of 3.5, with a vertical value about 2.10^{-10}m/s, which varies versus saturation and void ratio. At the end of construction, this maximum value was about 1,30 MPa, in good agreement with previous results.

If we analyse air pressure evolution, and saturation variation in core during impounding, we establish the following phenomena:

+At the end of construction, the core is essentially saturated, with a saturation varying between 92,9%, in the last layer, and 100% in the lower part of core.

+ At this moment, air pressure is about 0,86 MPa.

+ During impounding, such as suction is null along the upstream core's limit, air permeability is low (about 10^{-13}m/s). With the effect of water pressure increasing, air pressure increases locally, and this air moves slowly toward the downstream face. As air pressure increases, suction also increases, and, in some parts of the core, we may establish a lessening of saturation.

All these phenomena must be subsequently analysed and further developements are necessary to understand and to confirm these constatations.

V.2.4/ Conclusion about the three-phase approach:

The study of El Infiernillo dam is an opportunity to validate and apply UDAM to a rockfill dam. The actual version of this software is provisional, and many improvements remain to do. Some difficulties have been met during this approach, due to the simulation of shells behaviour, and boundary conditions during the impounding. However, some interesting results were obtained, during construction, and impounding, and they must be subsequently analysed. We think that is a good test to compare this new three-phase approach with other modellings and software.

REFERENCES

AUBRY.D ; HUJEUX.J.C ; LASSOUDIERE.F ; MEIMON.Y ; (1982)
A double memory model with multiple mechanisms for cyclic soil behaviour.
Int. Symp. Num. Models in Geomchanics. ZURICH, Balkema 3-13.

FRY.J.J ; DELAGE.P ; NANDA.A ; GATMIRI.B ; ALONSO.E.E ; (1991)
Approche triphasique de la construction des remblais argileux.
Colloque technique n°33, Comité Français des Grands Barrages. (Avril 1991).

HAJAL.T ; (1984).
Modélisation élastoplastique des sols par une loi multimécanisme. Apllication au calcul pressiométriques.
Thèse de docteur Ingénieur. Ecole Centrale de Paris.

HUJEUX.J.C ; (1985).
Une loi de comportement pour le chargement cyclique des sols.
Genie parasismique. Ed Davidovici. Presses ENPC.

LAIGLE.F ; (1993).
Construction des barrages en remblai. Simulation du comportement du barrage de Mirgenbach durant sa construction.
Rapport interne EDF/CNEH. ED.93.069..

LAIGLE.F ; (1994).
Modélisation numérique du barrage de la Ganne.
Rapport interne EDF/CNEH. ED.94.071..

LASSOUDIERE.F ; (1984).
Modélisation du comportement des sols sous sollicitations cycliques.
Thèse de docteur Ingénieur. Ecole Centrale de Paris.

MATYAS.E.L ; RADHAKRIHNAN.A.S ; (1968).
Volume change characteristics of partially saturated soils.
Geotechnique n°18.

NANDA.A ; DELAGE.P ; NEDJAT.N ; FRY.J.J ; GATMIRI.B ; (1993).
Evaluation de la sécurité des remblais en cours de construction: Le code UDAM.
Revue française de géotechnique n°62 pp. 23 - 34.

NOTES

Third Benchmark Workshop on Numerical Analysis of Dams
Gennevilliers (France) - September 29-30, 1994

Theme B1 :

EVALUATION OF PORE PRESSURE AND SETTLEMENT OF AN EMBANKMENT DAM UNDER STATIC LOADINGS

GEFDYN ANALYSIS

O.OZANAM, B. TARDIEU

Coyne et Bellier, Bureau d'Ingénieurs Conseils
9, Allée des Barbanniers - 92632 Gennevilliers CEDEX

This contribution to the theme B1 of the Third Benchmark Workshop on Numerical Analysis of Dams by Coyne et Bellier presents a coupled solid/fluid analysis of the contruction and impounding phases of the selected El Infiernillo embankment dam using the finite element software GEFDYN [1]. It provides results in terms of effective stresses, pore pressure and settlements/displacements. Two applications have been performed in order to evaluate the influence of the initial degree of saturation (in practice the in situ water content of the material) and the influence of the numerical implementation of the Mohr Coulomb model in the code.

1. MAIN ASSUMPTIONS

The assumptions proposed in the benchmark data have been taken into account :

- the mesh used has not been modified,
- the bedrock is assumed to be rigid and impervious,
- the material properties of all materials have been set to the given data (see table 1 of B1 specifications),
- the three load cases have been modelized : construction phase followed by a 5-month consolidation period, reservoir impounding and consolidation to reach the steady state.

Additional assumptions have been adopted :

- only the behaviour of the core has been simulated with the coupled solid/fluid model; the other parts of the dam are presumed to be perfectly drained (because of the high contrast between permeability in the core and the filter);
- the initial degree of saturation in the core has been set to 1. (in saturated case) or to the given value (0.96). According to non-saturated triaxial tests performed in France, the corresponding water suction (i.e. negative pore pressure) has been chosen equal to 0 Mpa or to -0.3 Mpa;
- seepage boundary conditions have been assumed on the upstream and downstream faces of the core;

- a very small cohesion value (1 kPa) has been introduced for all materials; it is reasonable and it improves the numerical behaviour of the algorithm;
- the constitutive model for all materials is the Mohr Coulomb model with linear elasticity.

2. NUMERICAL FEATURES

Continuous medium equations

The coupled numerical model is based on Terzaghi and Biot theories and on the principle of effective stresses [1,2,3]. The main equations of this model are given here in the continuum mechanics convention (traction is positive) :

- the total equilibrium balance equation:

  $\mathbf{DIV}\ \sigma + \mathbf{F}_{ext} = 0$

  should be combined with the principle of effective stresses : $\sigma = \sigma' - S_r(p)\ p\ I$ and with the constitutive model which provides the relation between the effective stress rate and the strain rate;

- the balance equation of the fluid mass gives a relation between the inwards and outwards flows :

  $\partial_t\ (n\ S_r\ \rho_w) + \mathrm{div}\ (\rho_w\ \mathbf{V}) = 0$

  the first term corresponds to the rate of storage and it is influenced by the compressibility of water (assumed to be constant here), the rate of degree of saturation, and the rate of porosity, and the generalized Darcy law may be introduced in the last term :

  $\mathbf{V} = -\ \mathbf{K}(S_r)\ .\ \mathbf{grad}\ (p + \rho_w\ \mathbf{g.x})$

Numerical formulation for space and time discretization

For the numerical implementation in the finite element software GEFDYN [1,2]:

- the shape functions are the same for the displacement and pore pressure unknowns;
- an implicit integration scheme is used for the global equations;
- the obtained non linear system of algebraic equations must be solved at each time-step by using an iterative scheme, decomposed into a predictor stage and corrector stage; this scheme is based on a modified Newton method (elasticity auxiliary matrix);
- convergence criteria should lead to the mechanical equilibrium requirement and to the conservation of fluid mass (these criteria are : the correction of global displacement (or pore pressure) norm is smaller than 1/1000 of the initial value, and the global mechanical and hydraulic desequilibrium norm is smaller than 1%).

Seepage boundary conditions

To deal with the variations of the reservoir level and with the potential seepage on the downstream face of the core, specific hydraulic interface finite elements have been used in the present application. Their numerical implementation, based on a penalization method, is precisely described in [4,5]. With these elements, the software is able to automatically change the boundary condition type (imposed pore pressure or imposed flow conditions) in accordance with the water level outside the core and the water table inside the core.

Mohr Coulomb formulation

As mentioned above, two different numerical implementations of the Mohr Coulomb model have been used : a 2D version, in which the principal stress normal to the 2D plane is supposed to be always the intermediate principal stress, and a 3D version, in which the discontinuous geometry of the yield surface is modelized with a multi-mechanism approach. The 2D version uses the principal stress invariants with smoothing of the Coulomb hexagon. The 3D version declares the plastic strain rate as a superposition of the contribution from each plane in the principal stress space using the principal stress directions. The 3D version is more rigourous and includes less simplification than the 2D version, but it is more difficult to implement numerically. The 2D version is numerically very stable. For usual 2D analyses, the two versions provide very similar results (see section 3.1).

The 2D version has been used with the assumption of saturated soils (S_0=1. and no variation of the degree of saturation -and therefore of the permeability- during the computations), and the initial degree of saturation of 0.96 (with variation of the degree of saturation and of the permeability) has been used with the 3D version.

3. RESULTS

3.1 Simulation of triaxial tests

The requested curves for drained tests, i.e. deviatoric stress vs. axial strain and volumetric strain vs. axial strain, are drawn on Fig. 1a for the 2D version and Fig. 1b for the 3D version of the Mohr Coulomb model. For undrained tests, the corresponding curves are plotted on Fig. 2a to 2d. The main characteristics of these curves are summarized in Table 1 and compared to the theoretical values.

Table 1
Triaxial tests for core material - Mohr Coulomb model
Confining pressure 0.5 MPa and axial strain 0 to 10%

	drained (CD)			undrained (CU)		
	M.C. 2D	M.C. 3D	analytical	M.C. 2D	M.C. 3D	analytical
ε_1^e (%)	1.9	1.9	1.8 (2)	1.1	1.2	1.2 (2)
ε_v^e (%)or u_{max} (MPa)	-0.72	-0.73	-0.73 (3)	0.164	0.164	0.164 (6)
q (MPa) at $\varepsilon_1 = \varepsilon_1^e$	0.735	0.736	0.732 (1)	0.496	0.496	0.492 (5)
q_{max} (MPa) at ε_1 = 10%	0.737	0.737	0.732 (1)	0.960	0.955	0.936
ε_v (%) or u (MPa) at ε_1 = 10%	0.81	0.81	0.84 (4)	-0.154	-0.150	-0.139

(1) $q=2\ \sigma_3 \sin\varphi / (1-\sin\varphi)$
(2) $\varepsilon_1^e = q / E$
(3) $\varepsilon_v^e = -(1 - 2\nu)\ \varepsilon_1^e$
(4) $\Delta\varepsilon_v^p = 2 \sin\psi / (1 - \sin\psi)\ \Delta\varepsilon_1$
(5) $q = 6\ \sigma_3 \sin\varphi /(3 - \sin\varphi)$
(6) $u_{max} = q/3$

3.2 Effective stresses

The contour lines of horizontal, vertical and shear stresses in the dam at the end of construction, impounding and consolidation are drawn on Fig.3a to 3c for the 2D version and on Fig. 3d to 3f for the 3D version of the Mohr Coulomb model. The two versions provide some small discrepancies, mainly in the core because of the different pore pressure results (see next section).

3.3 Pore pressure

The contour lines of pore pressure in the core of the dam at the end of construction, impounding and consolidation are drawn on Fig.4a for the 2D version and on Fig. 4b for the 3D version of the Mohr Coulomb model. During the construction phase, the dissipation of pore pressure is more rapid with the 2D version. This may be due :

- partly to a better convergence of the numerical scheme with the 2D version, which is implemented explicitly, compared to the 3D one, which is implemented purely numerically(see section 2).;
- and mainly to the different initial degree of saturation : S_0=1 for 2D version and S_0=0.95 for 3D one.

The maximum excess pore pressures are 0.5 and 0.7 MPa respectively 5 months after the end of construction and reache 1.0 and 1.1 during construction, as shown on Figures 5a and 5b that represent the evolution of the pore pressure contour lines during construction and during impounding for the 2 versions.

3.4 Displacements

The required horizontal and vertical displacements along the vertical centre line AA in the core are drawn on Figures 8 and 6, and those along the horizontal lines BB and CC on Figures 9 and 7. These curves correspond to the numerical results at the last computational step, i.e. at the steady state.

In the core, the maximum settlement occurs at elevation 105 and reaches around 160 cm. The horizontal displacement reaches approximatly 120 cm at the same elevation.

3.5 General Summary

The horizontal and vertical displacements and the pore pressure at the 5 given points are given for each version of the Mohr Coulomb model (2D/3D) in Table 2.In addition to the required table, the displacements produced only by the impounding and last consolidation have been computed by subtracting the results of phase 3 (end of consolidation) from the results of phase 1b (end of first consolidation). These values exhibit the influence of the buoyancy forces in the upstream rockfill that produce a kind of swelling in the upstream embankment of the dam. This result is completely in agreement with the implemented numerical model. But it is not representative of the real behaviour of the dam during impounding due to the fact that beside the buoyancy effect, settlement occurs due to the effect of the water upon the pieces of rock, mainly for dumped large size rockfill.

Discrepancies smaller than 1 cm may occur between some load cases or between the 2 versions of the Mohr Coulomb model. But, according to the overall approximation of the input data, they could be considered as not significant. Therefore the numerical values of the displacements have been truncated in order to obtain integer values in centimeters.

4. COMPUTATION TIME

The computations were performed with an optimized GEFDYN executable file on an HP9000/715 workstation (48 Mb RAM, frequency 50 Mhz, 62 Mips, 13 Mflop). The CPU times for each load case and each version of Mohr Coulomb are given in seconds in Table 3. The long computation time used for the 3D version during the construction phase is mainly due to a slower convergence process, which is shown in Table 4. Indeed the computation time is approximately proportional to the number of iterations.

Table 2
GENERAL SUMMARY : Results of displacements and pore pressure after each phase
a / b : (a) saturated case & 2D version - (b) unsaturated case & 3D version

	Points of the Dam Section				
	CC	CM	CL	UM	DM
End of Construction (1)	0 / 0	4 / 4	8 / 8	-18 / -18	21 / 21
End of 1st Consolid. (1b)	0 / 0	4 / 4	7 / 7	-17 / -17	20 / 20
End of Impounding (2)	76 / 81	116 / 120	103 / 105	8 / 12	79 / 81
End of Consolidation (3)	76 / 81	117 / 121	106 / 108	8 / 11	80 / 82
(3) - (1b)	76 / 81	113 / 117	99 / 101	25 / 28	60 / 62

Horizontal Displacements (10^{-2} m)

	Points of the Dam Section				
	CC	CM	CL	UM	DM
End of Construction (1)	0 / 0	161 / 161	131 / 134	14 / 14	16 / 16
End of 1st Consolid. (1b)	3 / 3	165 / 165	136 / 138	14 / 14	16 / 16
End of Impounding (2)	-1 / -5	156 / 152	128 / 127	-21 / -22	12 / 12
End of Consolidation (3)	0 / -4	156 / 152	127 / 126	-21 / -22	12 / 12
(3) - (1b)	-3 / -7	-9 / -13	-9 / -12	-35 / 36	-4 / -4

Vertical Displacements (10^{-2} m)

	Points of the Dam Section				
	CC	CM	CL	UM	DM
End of Construction	0.008 / 0.008	0.084 / 0.080	0.256 / 0.270	-	-
End of 1st Consolid.	-0.028 / -0.024	0.015 / 0.016	0.092 / 0.114	-	-
End of Impounding	-0.063 / -0.052	0.260 / 0.271	0.453 / 0.466	0.481*	-
End of Consolidation	-0.073 / -0.070	0.240 / 0.246	0.435 / 0.459	0.481*	-

* this value was not computed by GEFDYN - it is equal to $\rho_w.g.h$

Pore Pressure (MPa)

Table 3
Computation time

	MC 2D	MC 3D
Construction and 1st Consolidation (10+2 steps)	4638 s = 1h17mn	11655 s = 3h14mn
Impounding and Consolidation (5+2 steps)	3309 s = 55mn	3393 s = 57mn
TOTAL CPU TIME	7947 s = 2h12mn	15048 s = 4h11mn

Table 4
Number of iterations

	MC 2D	MC 3D
Construction and 1st Consolidation (10+2 steps)	1137	2788
Impounding and Consolidation (5+2 steps)	430	573
TOTAL Number of Iterations	1567	3361

Notations

$\mathbf{F}_{ext}$: external forces (for example body forces)
$\mathbf{g}$: gravity acceleration
I : unit tensor
$\mathbf{K}(S_r)$: permeability tensor (as function of the degree of saturation)
p : pore pressure
n : porosity
$S_r(p)$: degree of saturation (as function of the pore pressure)
$\mathbf{V}$: filtration velocity
$\mathbf{x}$: current position of the material point
φ : friction angle
ψ : dilatancy angle
ρ_w : water density
σ : total stress tensor
σ' : effective stress tensor
Vectors are in **bold** characters.

References

[1] GEFDYN rev. 6.1 - Users Manual and Scientific Manual, March 1994 - Coyne et Bellier, EDF/CNEH, ECP/LMSS.
[2] D. Aubry, D. Chouvet, O.Ozanam, J.-P. Person (1986) : *Coupled mechanical-hydraulic behaviour of earth dams with partial saturation* - Eur. Conf. Num. Methods in Geomechanics, Stuttgart, Germany, Vol.2.
[3] D. Aubry, O.Ozanam, J.-P. Person (1987) : *Ecoulements non saturés en milieux poreux déformables* - 9th Eur. Conf. on Soil Mechanics and Foundation Eng., Dublin, Ireland, August 31-Sept.1st 1987, pp.537-540.

[4] D. Aubry, O.Ozanam (1988) : *Free surface tracking through non-saturated models* - 6th Int. Conf. Num. Methods in Geomechanics, April 11-15, 1988, Innsbruck, Austria, Vol.3, pp. 757-763.
[5] O.Ozanam (1988) : *Modélisation numérique des sols élastoplastiques non saturés - Application aux barrages en remblais* - Thèse de Docteur de l'Ecole Centrale Paris.

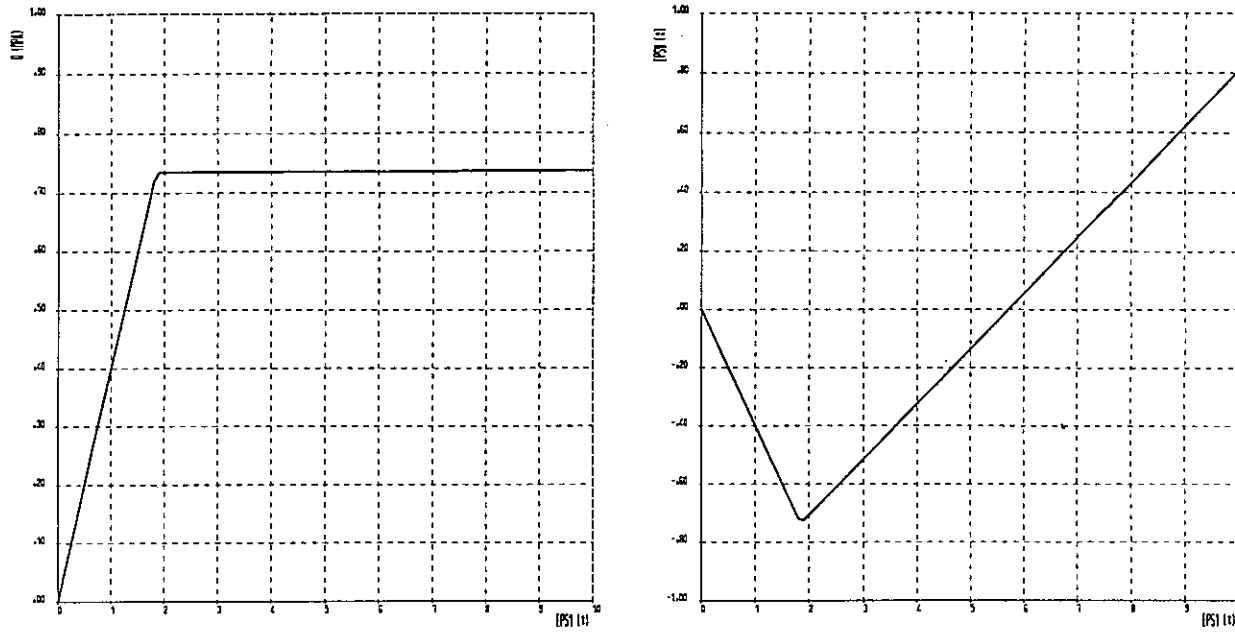

(a) 2D version

24/06/1994 | COYNE ET BELLIER | GEFDYN | EL INFIERNILLO DAM (MEXICO)
3RD BW - CIGB 94 | THEME B1 | NUMERICAL ANALYSIS OF DAMS

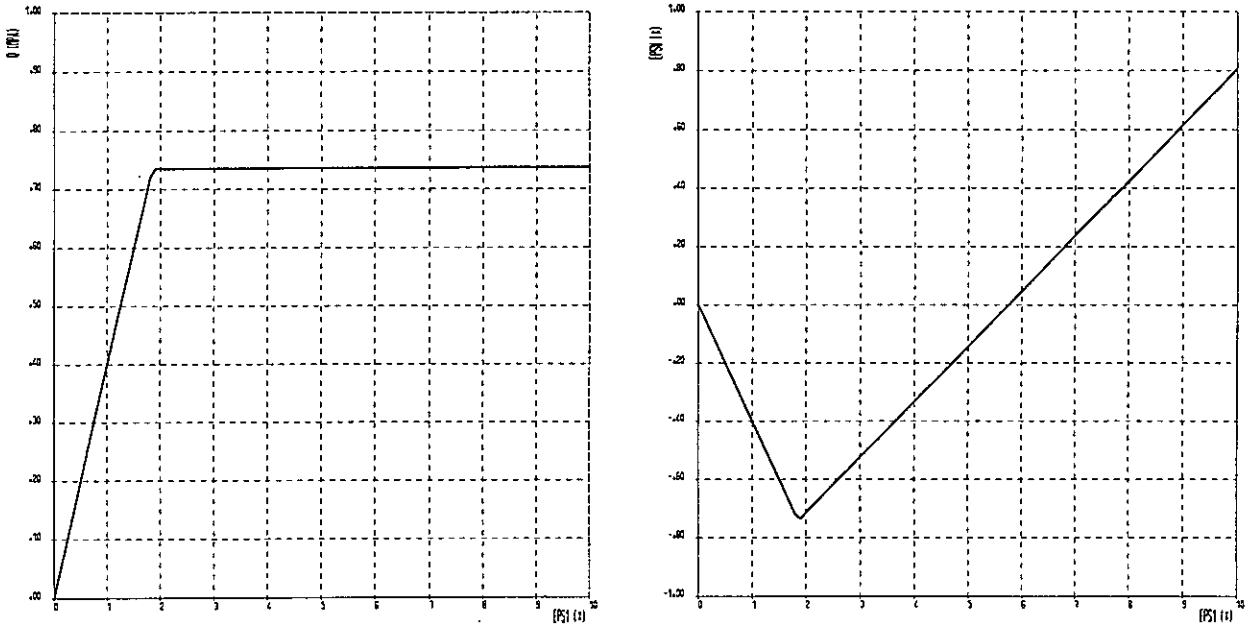

(b) 3D version

Fig. 1 : Drained triaxial test on core material - σ_3=0.5 Mpa - (q,ε_1) and ($\varepsilon_v,\varepsilon_1$) curves simulation with Mohr Coulomb's constitutive models implemented in GEFDYN

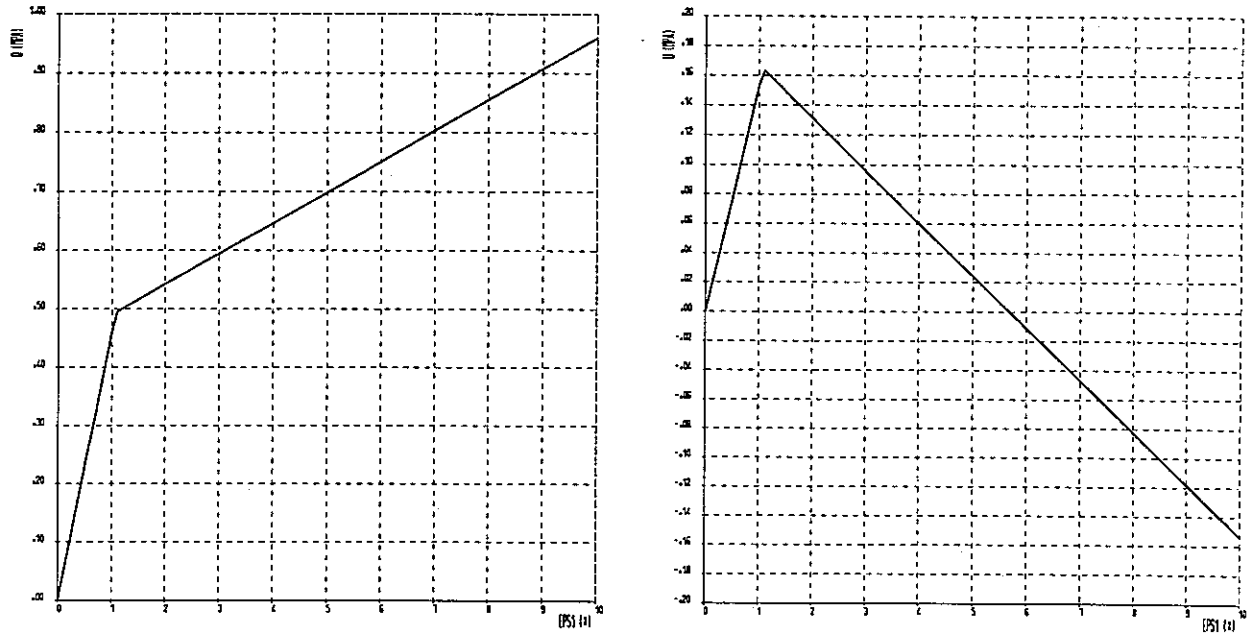

(a) 2D version

24/06/1994 | COYNE ET BELLIER | GEFDYN | EL INFIERNILLO DAM (MEXICO)
3RD BW - CIGB 94 | THEME B1 | NUMERICAL ANALYSIS OF DAMS

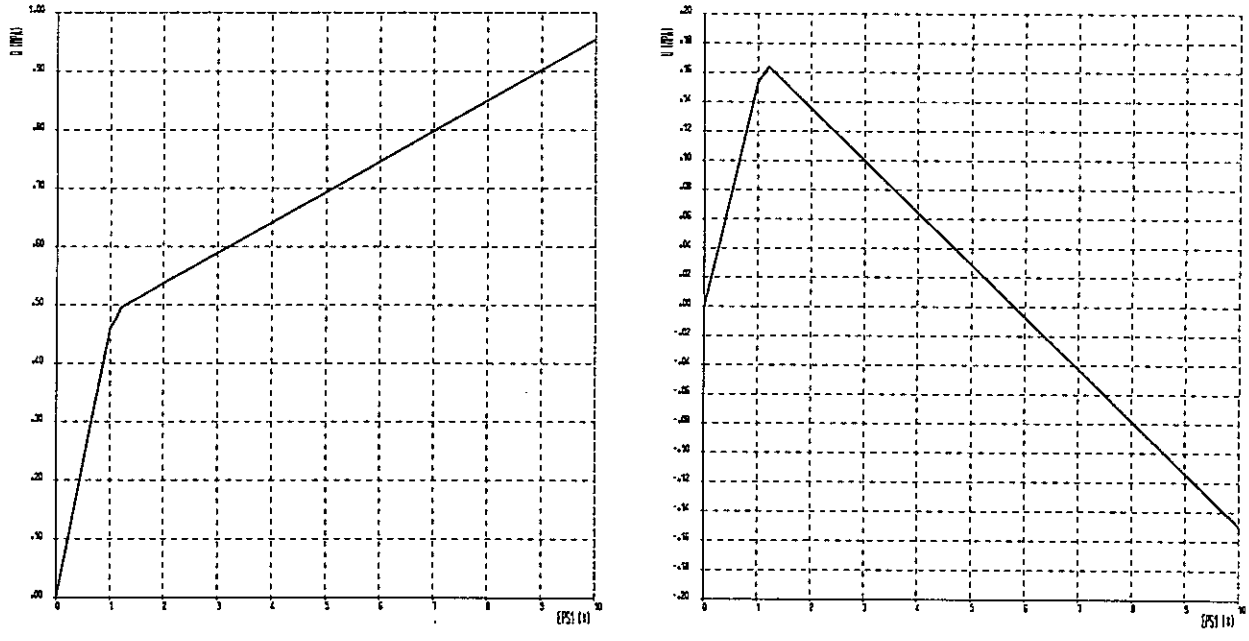

(b) 3D version

Fig. 2 : Undrained triaxial test on core material - σ_3=0.5 Mpa - (q,ε_1),(u,ε_1) curves simulation with Mohr Coulomb's constitutive models implemented in GEFDYN

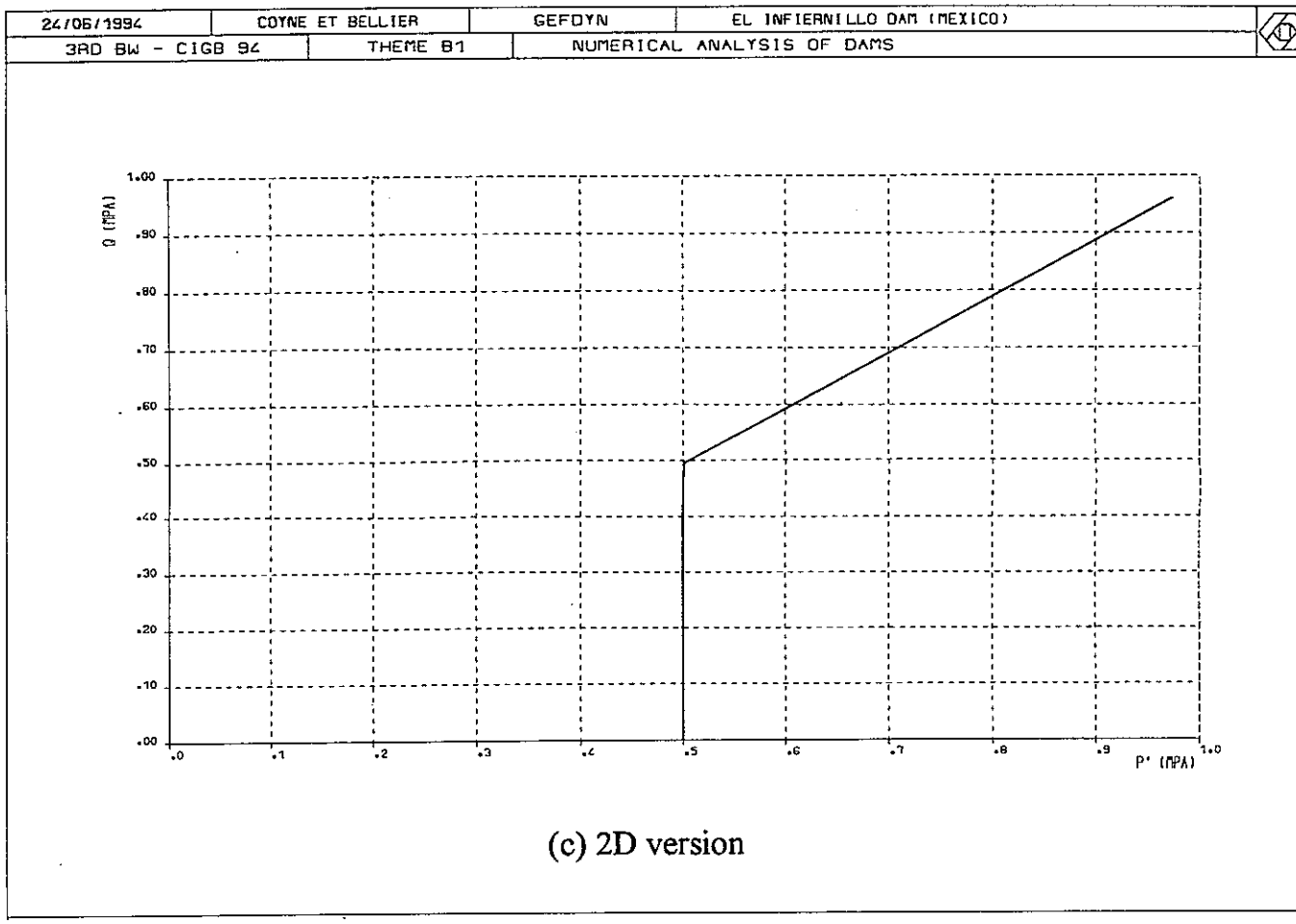

(c) 2D version

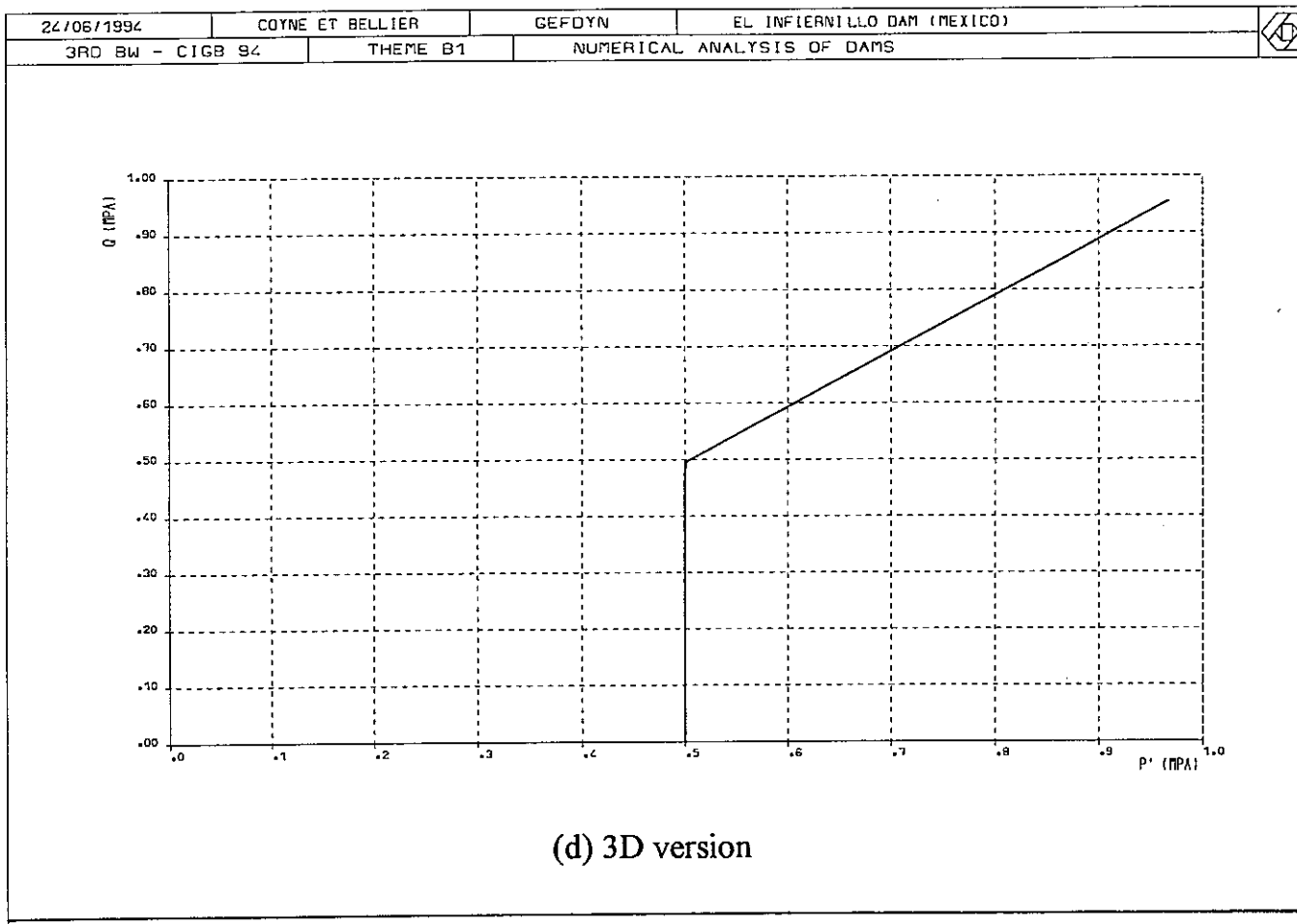

(d) 3D version

Fig. 2 : Undrained triaxial test on core material - σ_3=0.5 Mpa - (p',q) curve simulation with Mohr Coulomb's constitutive models implemented in GEFDYN

18/04/1994	COYNE ET BELLIER	GEFDYN	EL INFIE
3RD BW - CIGB 94	THEME B1	MC2D	

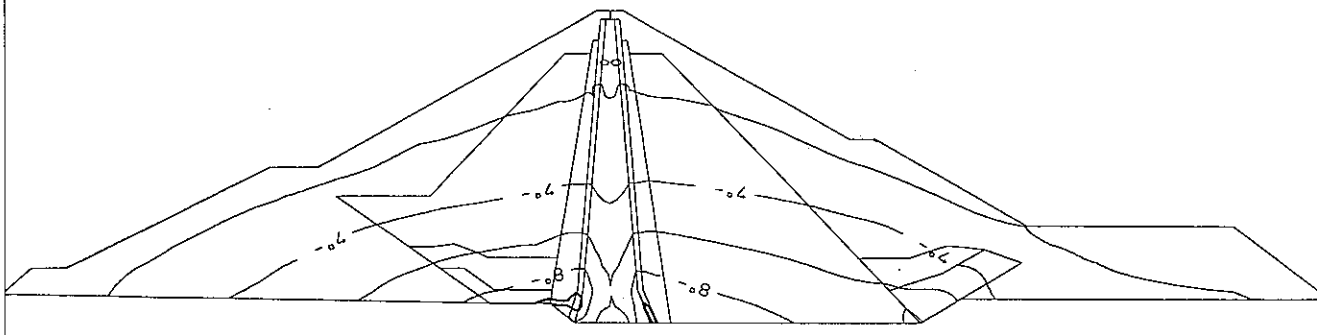

End of first consolidation period

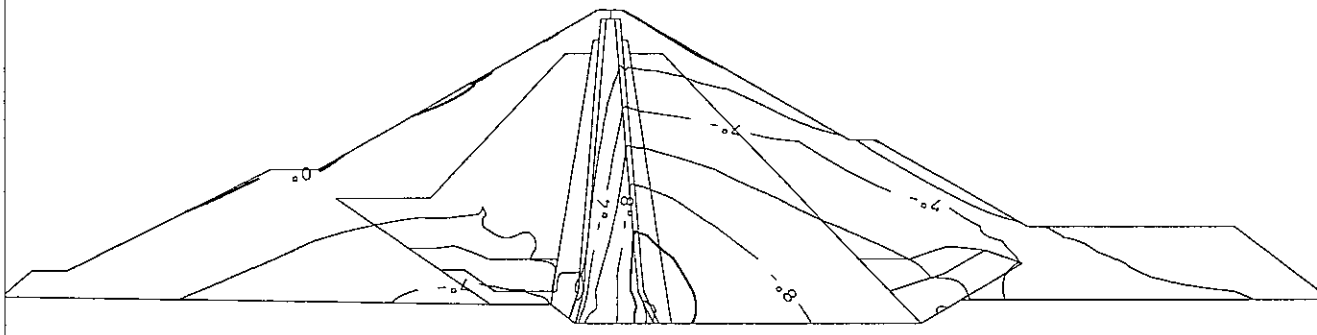

End of dam impounding

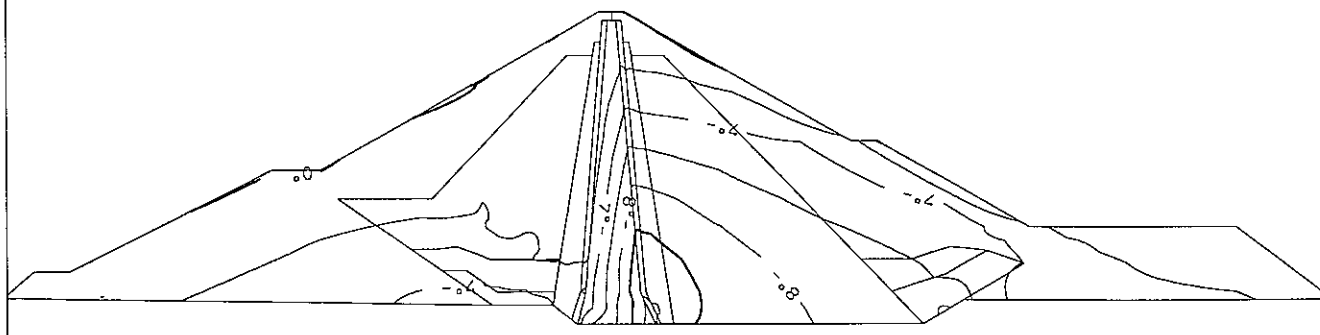

End of second consolidation period

GEOMETRICAL SCALE : .00029

Fig. 3a : Effective stress contour lines
horizontal stress - saturated case (+Mohr Coulomb 2D)

18/04/1994	COYNE ET BELLIER	GEFDYN	EL INFIE
3RD BW - CIGB 94	THEME B1	MC2D	

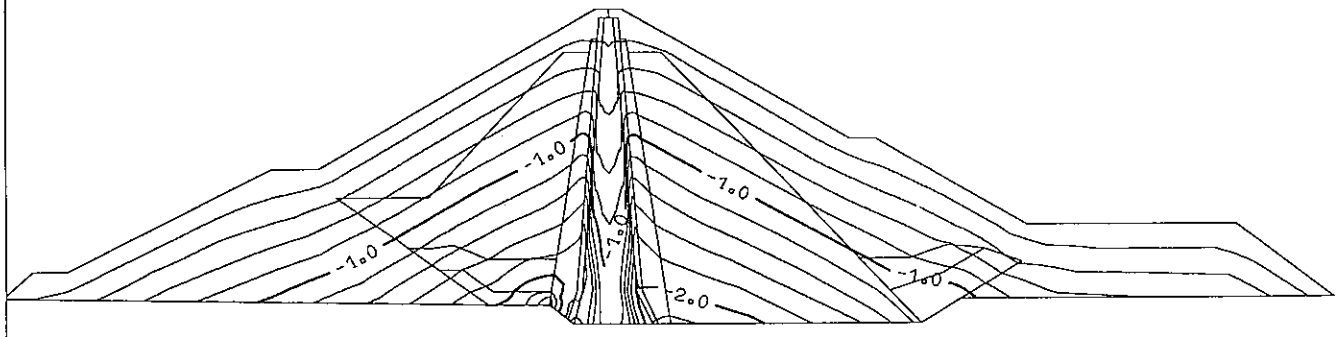

End of first consolidation period

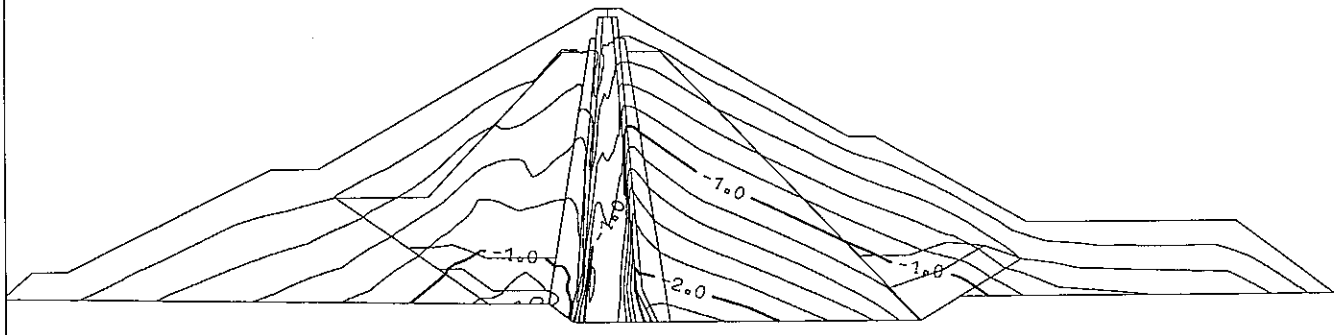

End of dam impounding

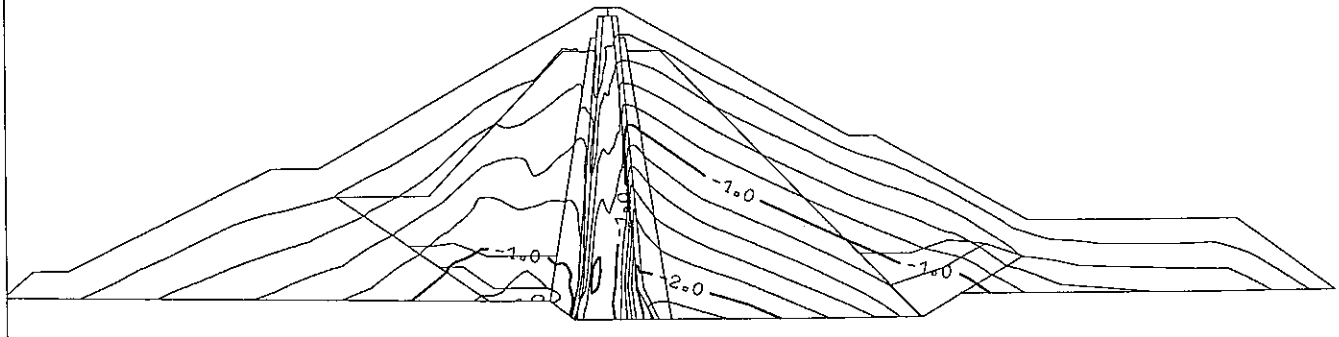

End of second consolidation period

GEOMETRICAL SCALE : .00029

Fig. 3b : Effective stress contour lines
vertical stress - saturated case (+Mohr Coulomb 2D)

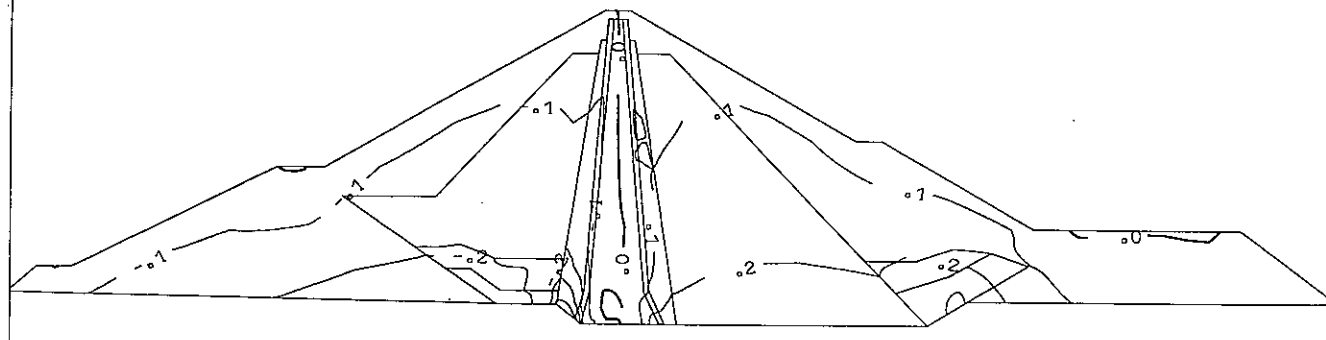

End of first consolidation period

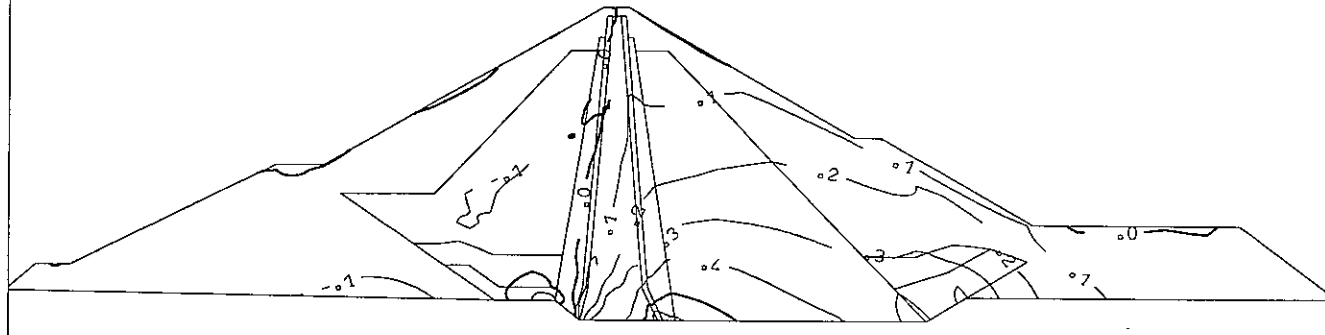

End of dam impounding

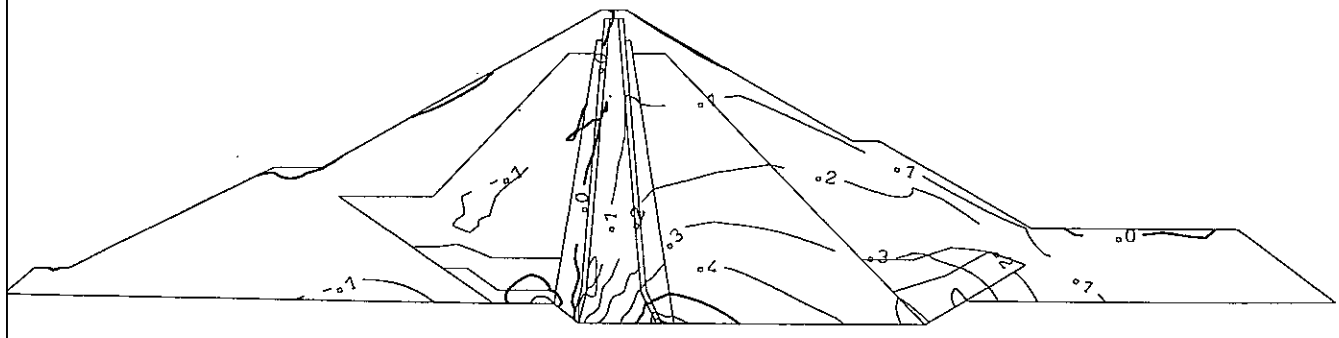

End of second consolidation period

GEOMETRICAL SCALE : .00029

Fig. 3c : Effective stress contour lines
shear stress - saturated case (+Mohr Coulomb 2D)

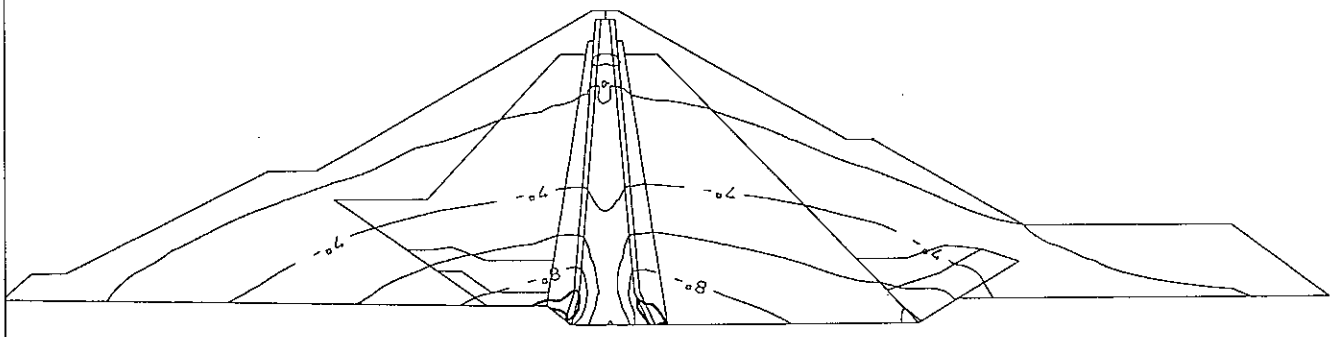

End of first consolidation period

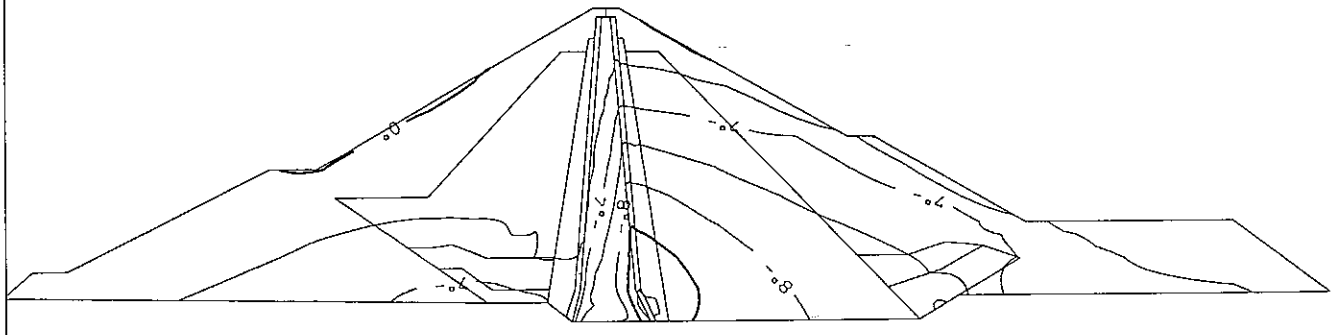

End of dam impounding

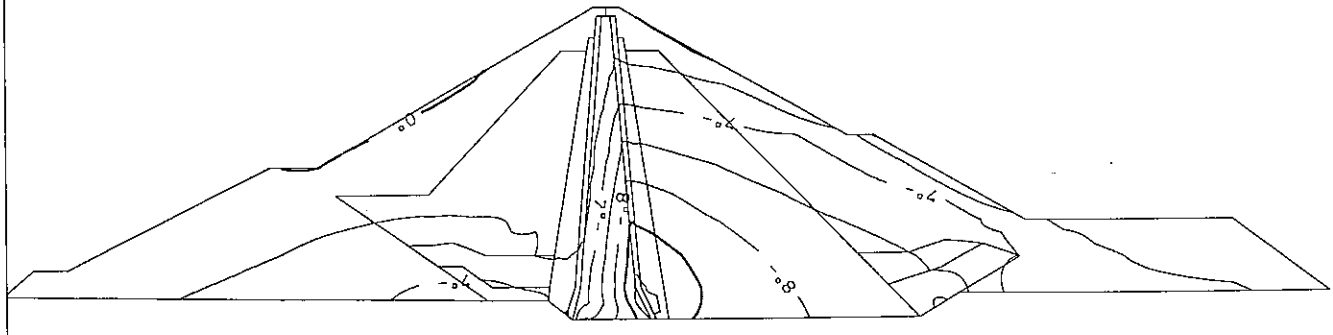

End of second consolidation period

GEOMETRICAL SCALE : .00029

Fig. 3d : Effective stress contour lines
horizontal stress - unsaturated case (+Mohr Coulomb 3D)

22/04/1994	COYNE ET BELLIER	GEFDYN	MC3D
3RD BW - CIGB 94	THEME B1	EL INFIERNILLO DAM (MEXI	

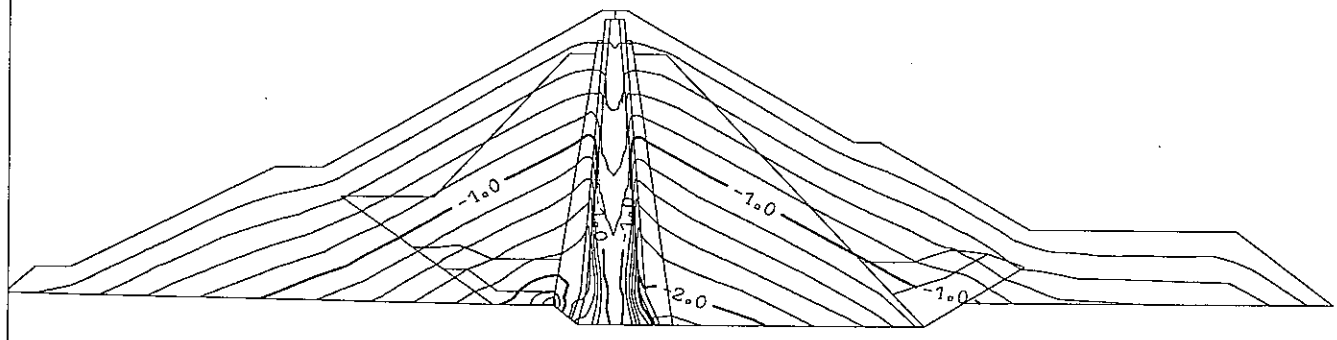

End of first consolidation period

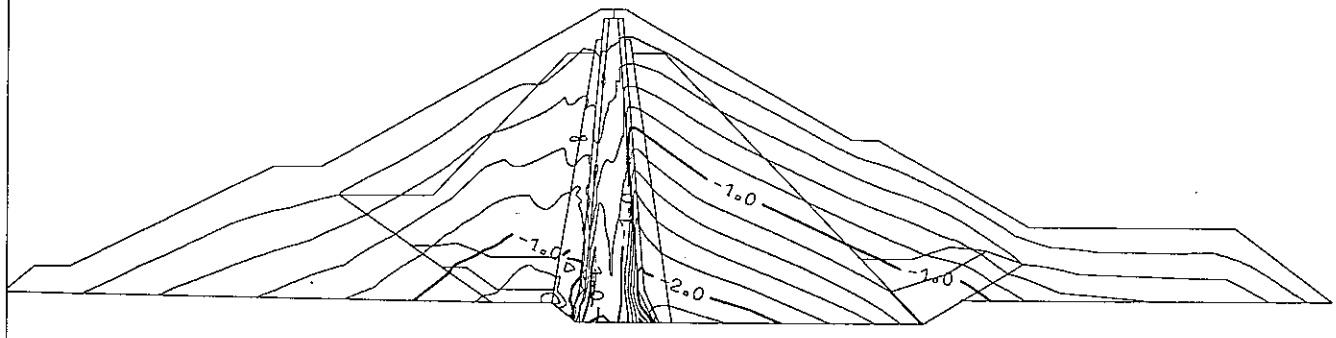

End of dam impounding

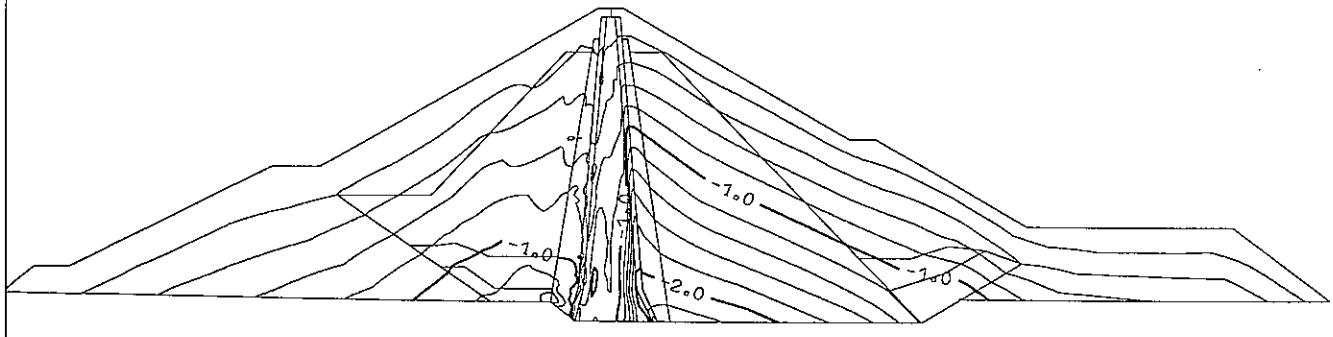

End of second consolidation period

GEOMETRICAL SCALE : .00029

Fig. 3e : Effective stress contour lines
vertical stress - unsaturated case (+Mohr Coulomb 3D)

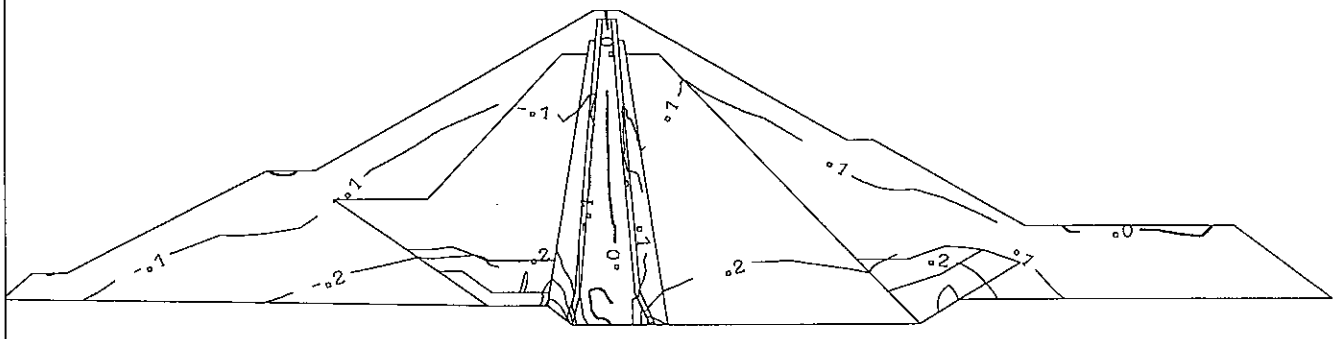

End of first consolidation period

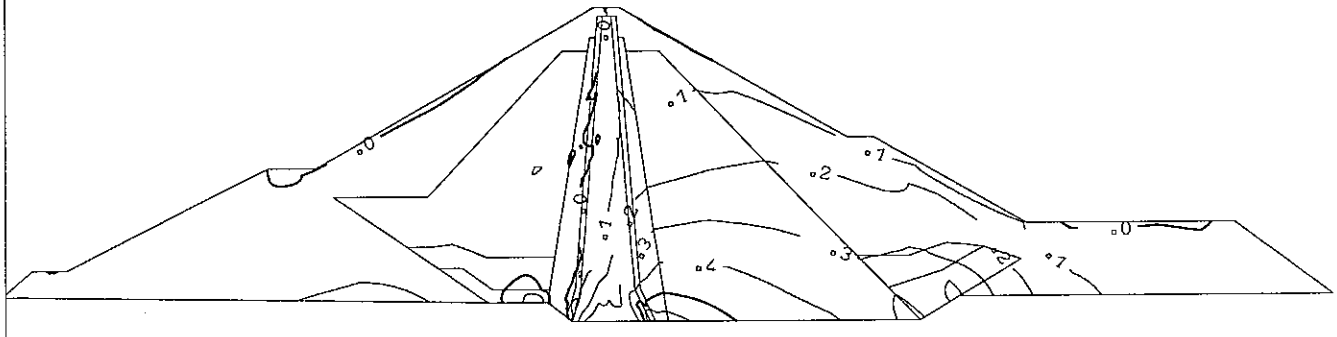

End of dam impounding

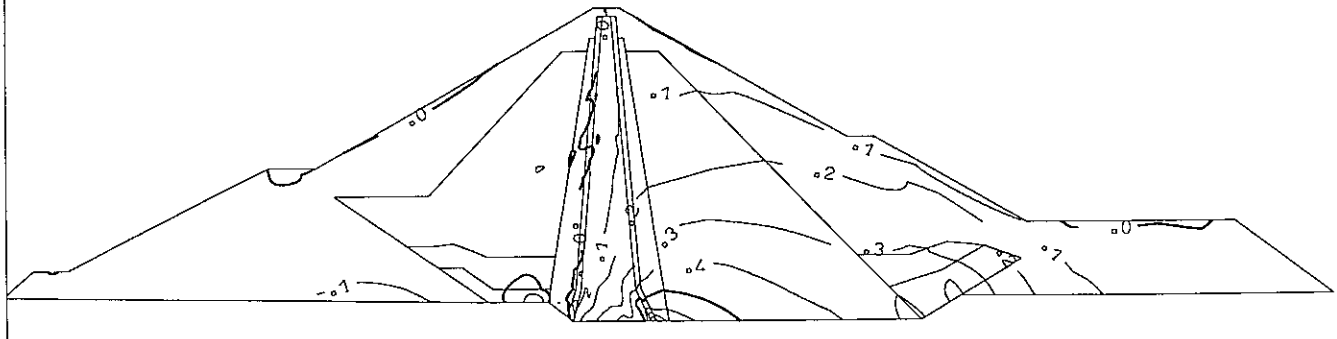

End of second consolidation period

GEOMETRICAL SCALE : .00029

Fig. 3f : Effective stress contour lines
shear stress - unsaturated case (+Mohr Coulomb 3D)

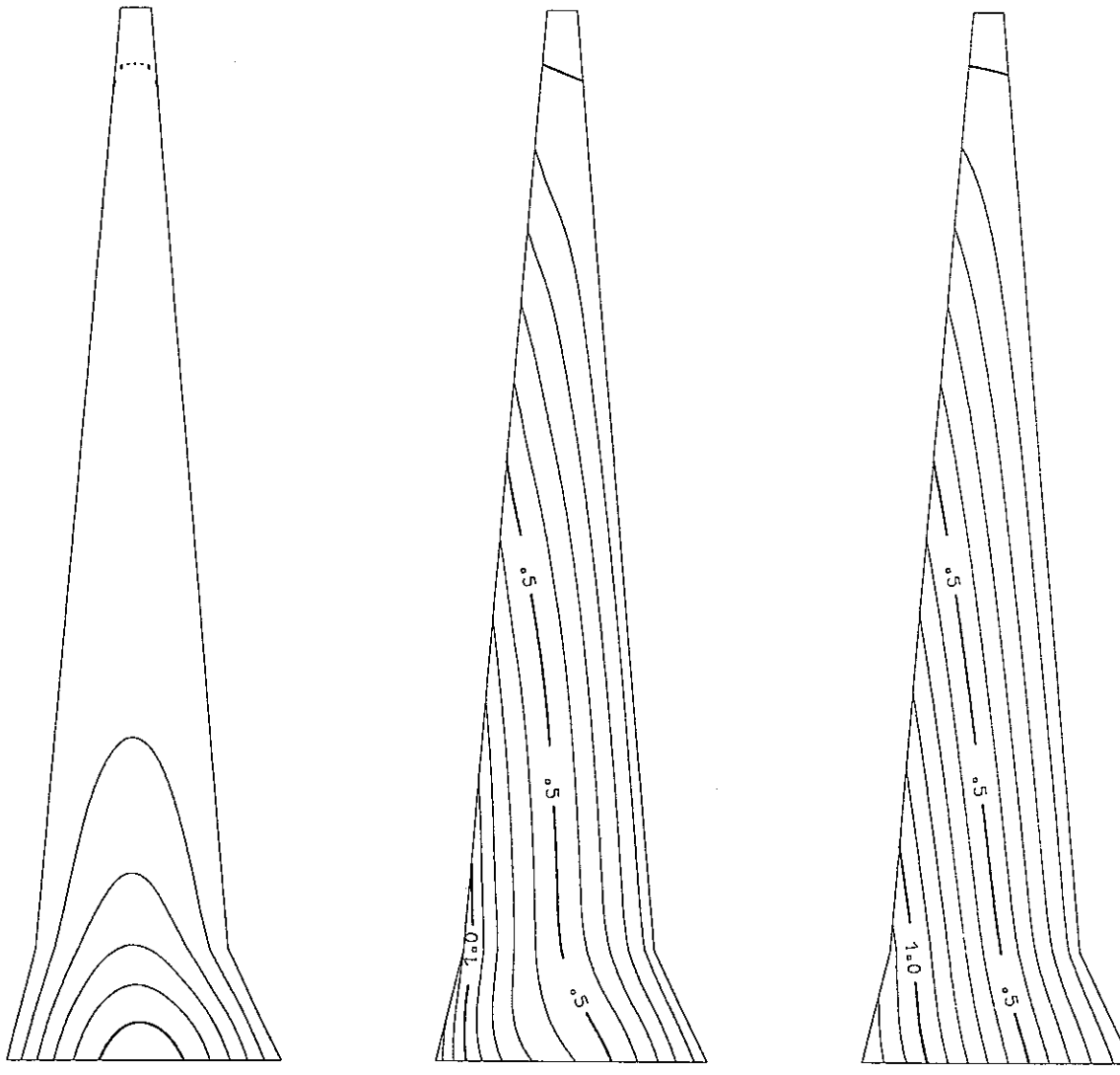

End of first consolidation period

End of dam impounding

End of second consolidation period

GEOMETRICAL SCALE : .00100

Fig. 4a : Pore pressure contour lines
saturated case (+Mohr Coulomb 2D)

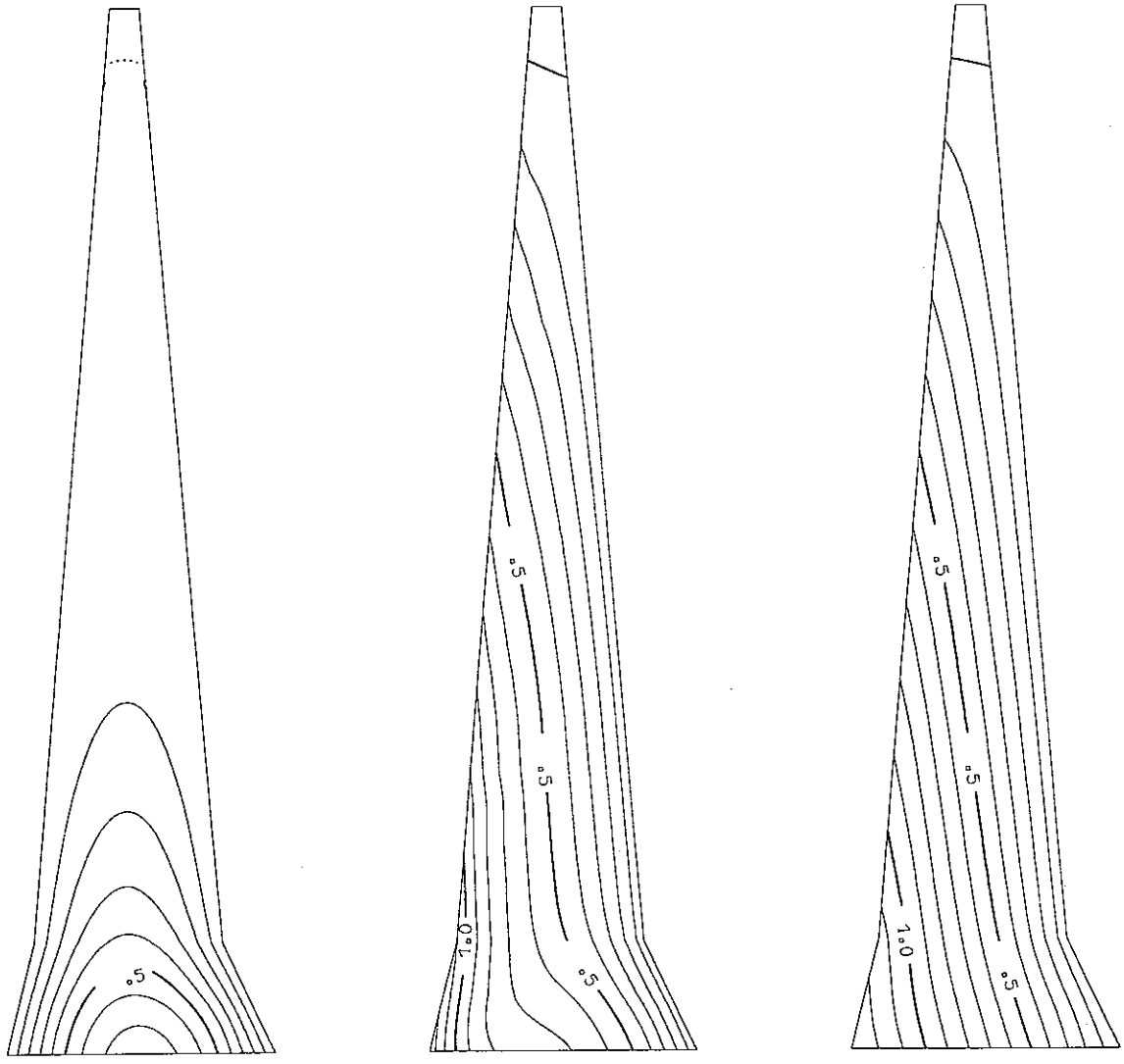

End of first consolidation period

End of dam impounding

End of second consolidation period

GEOMETRICAL SCALE : .00100

Fig. 4b : Pore pressure contour lines
unsaturated case (+Mohr Coulomb 3D)

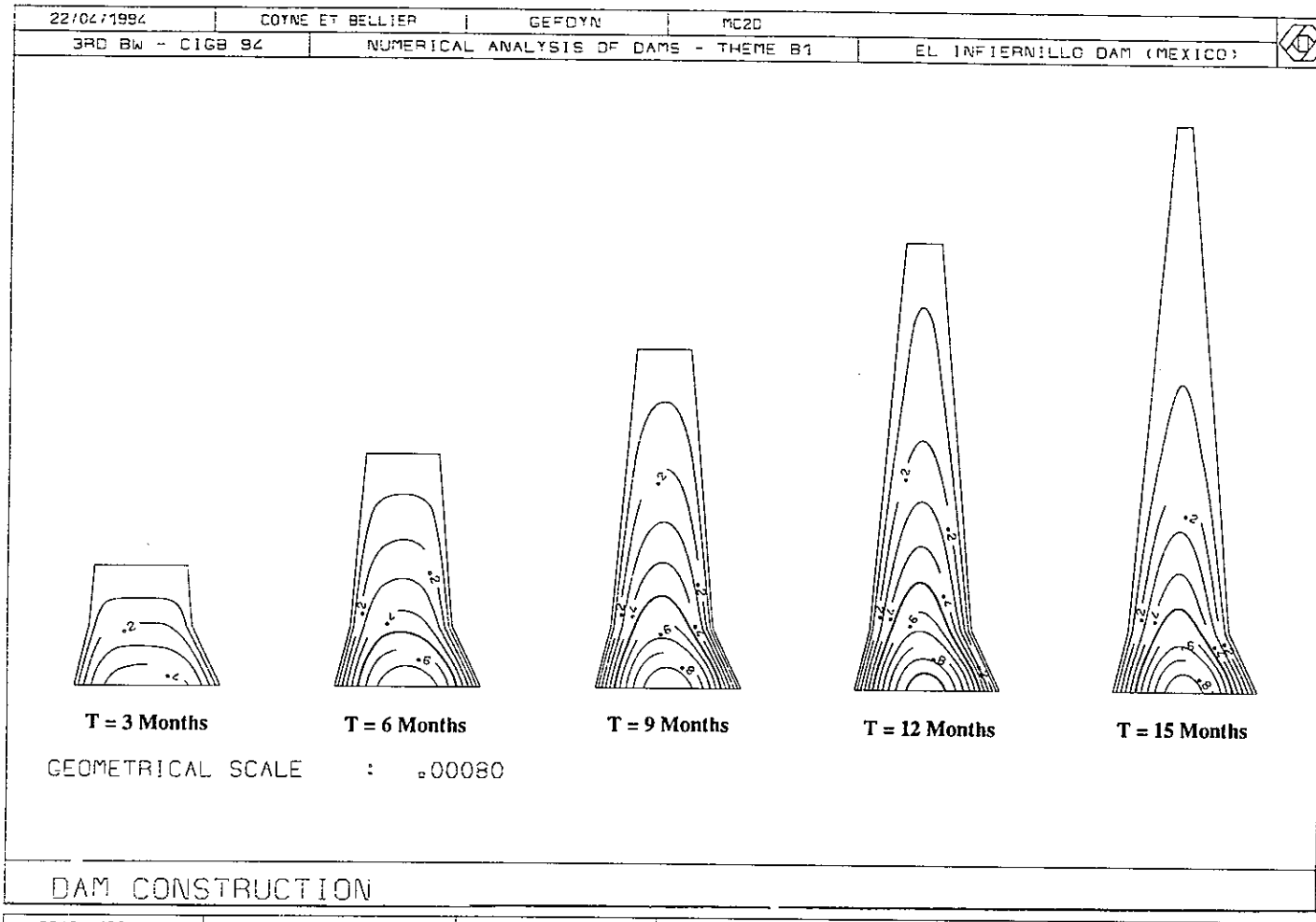

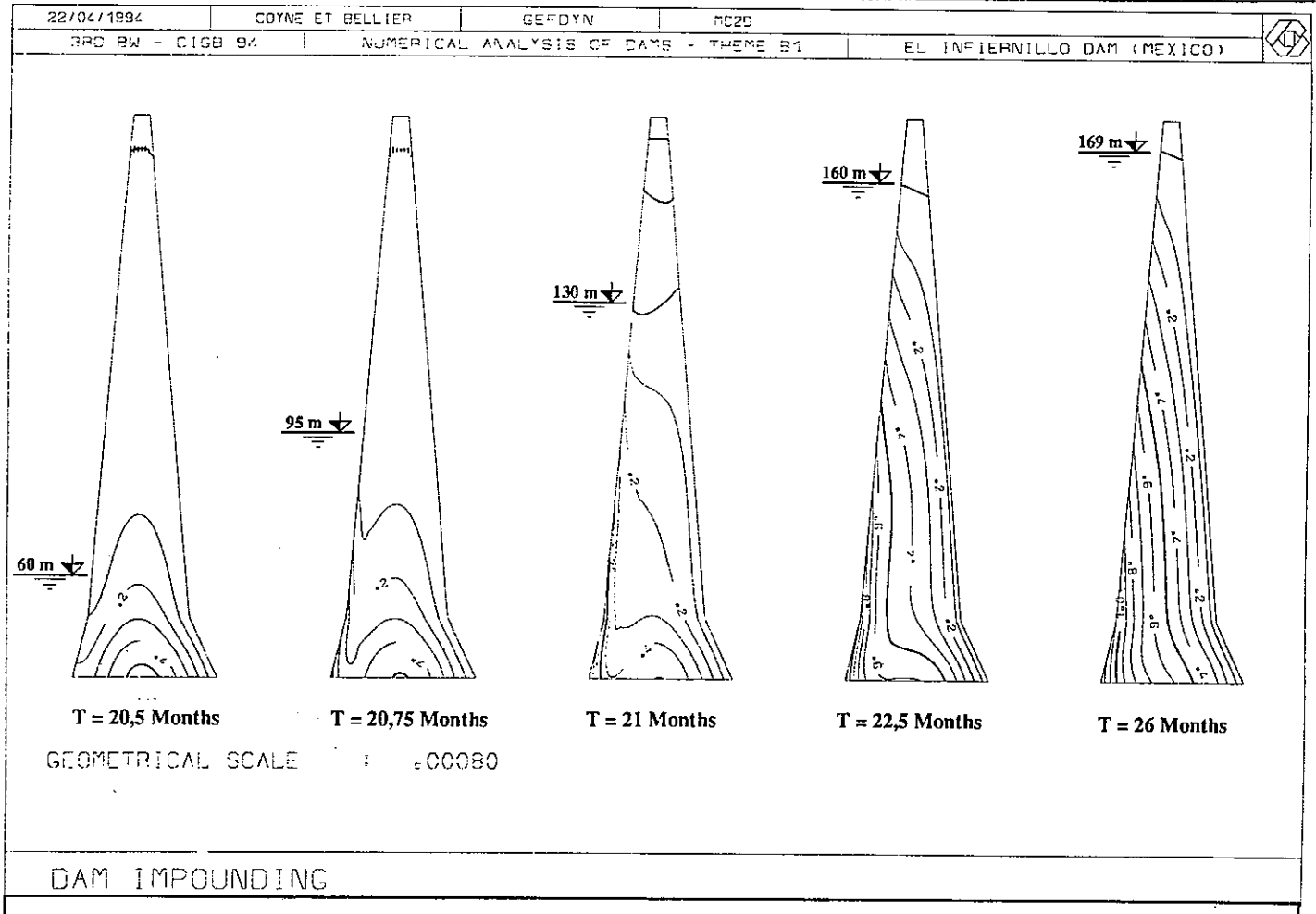

Fig. 5a : Pore pressure contour line evolution during construction and impounding saturated case (+Mohr Coulomb 2D)

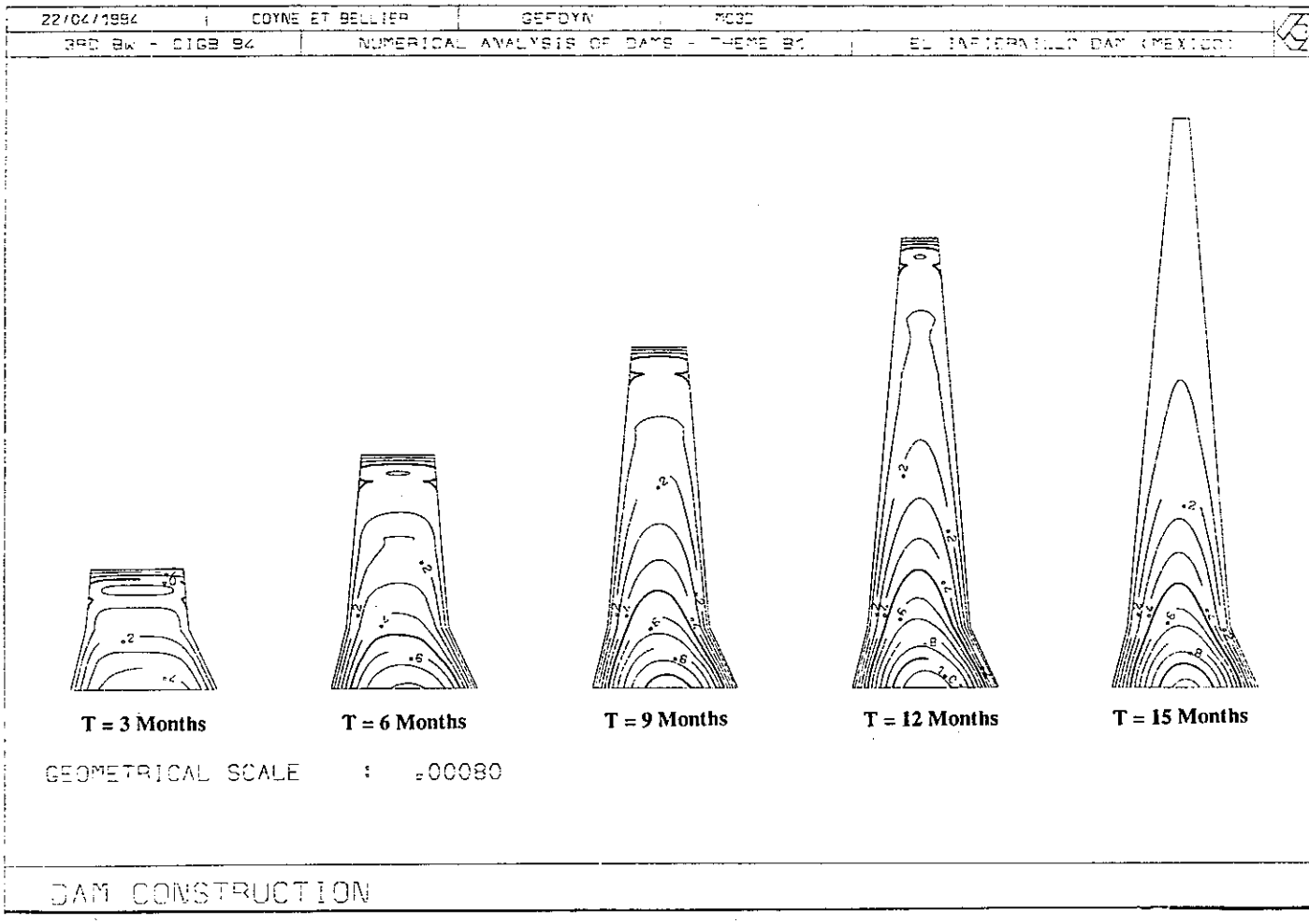

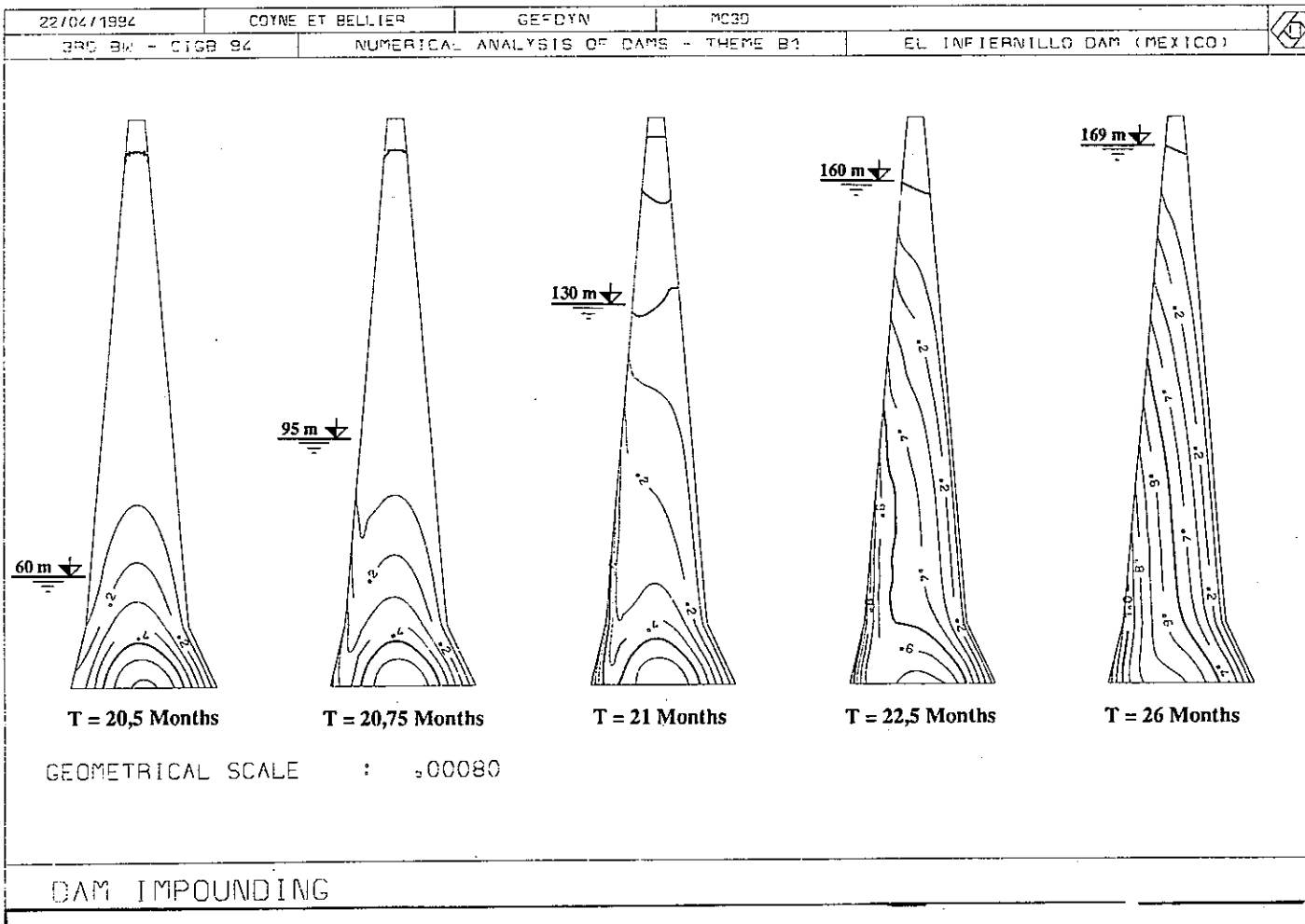

Fig. 5b : Pore pressure contour line evolution during construction and impounding unsaturated case (+Mohr Coulomb 3D)

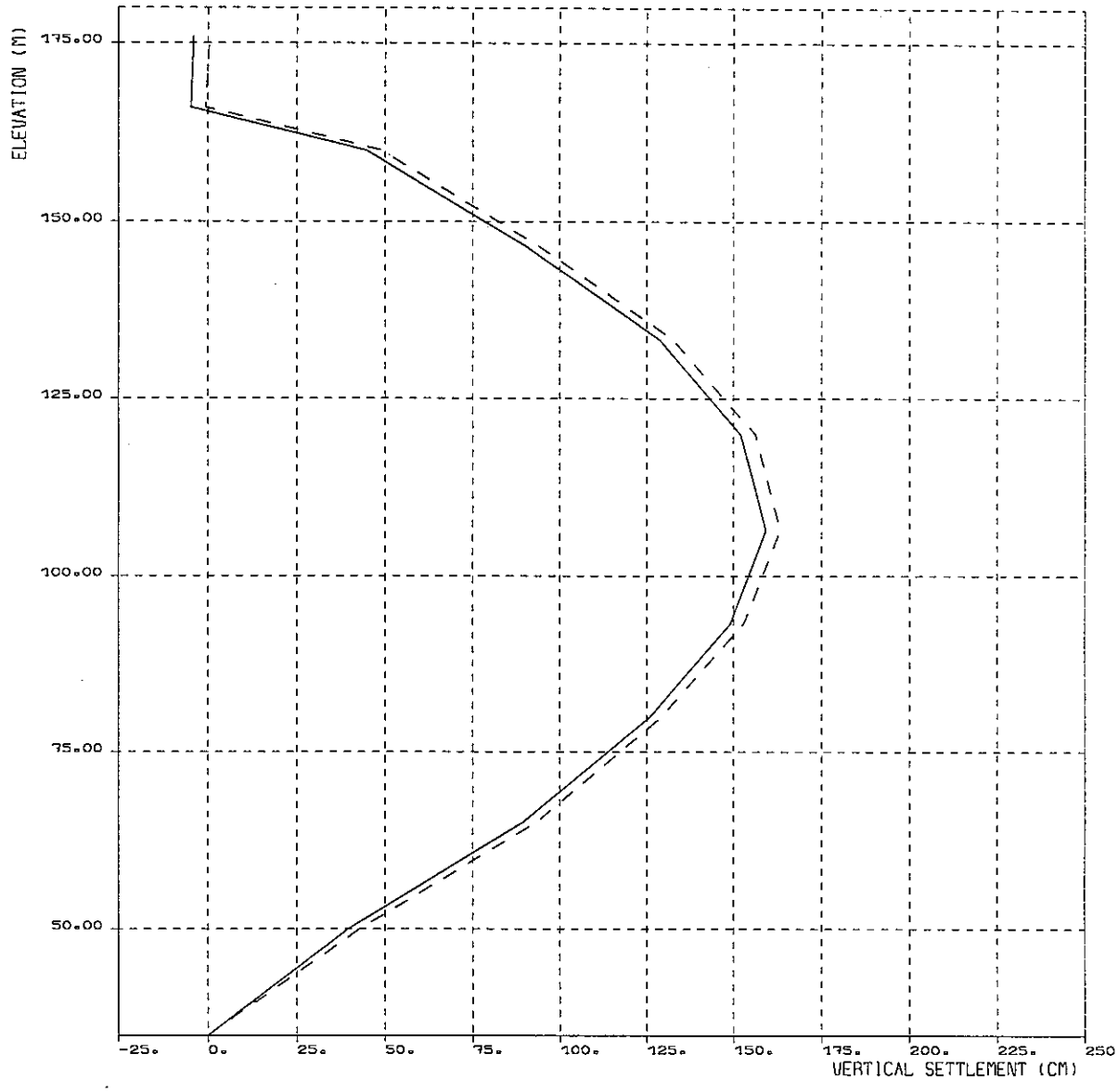

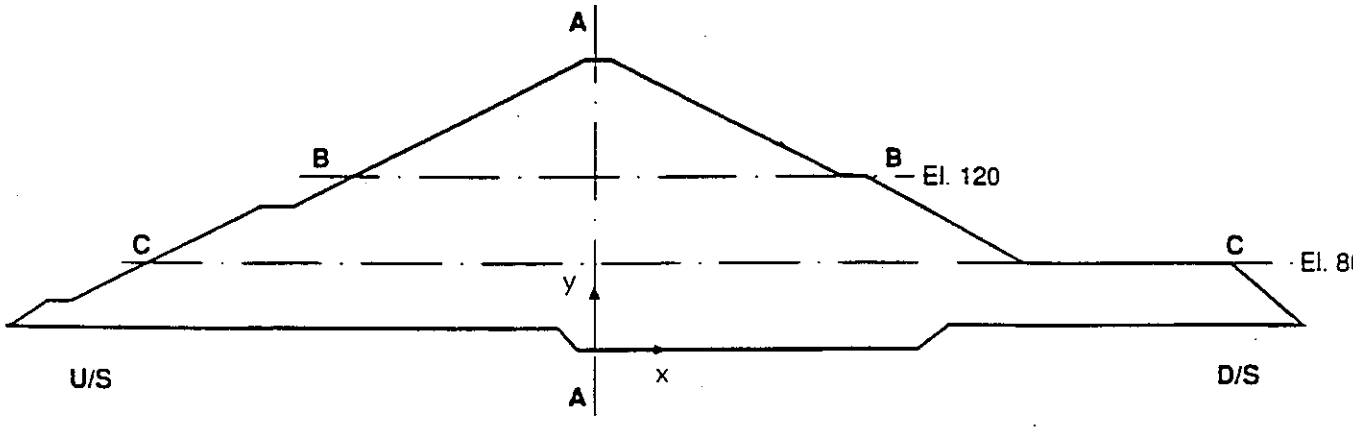

Fig. 6 : Vertical settlement at the end of consolidation along core vertical line AA

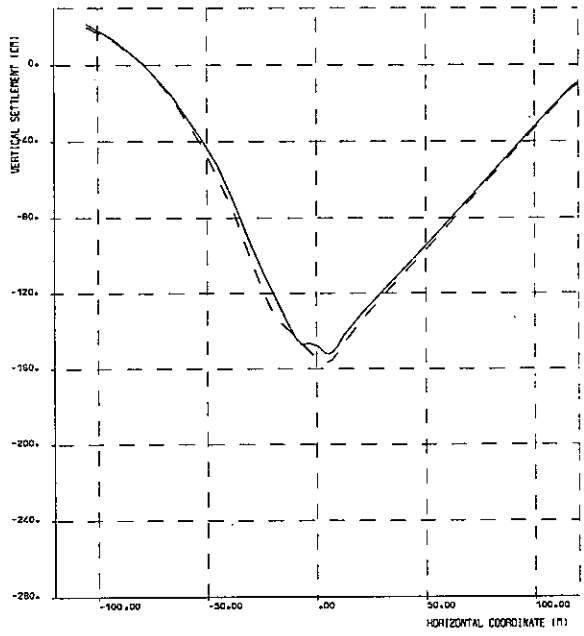

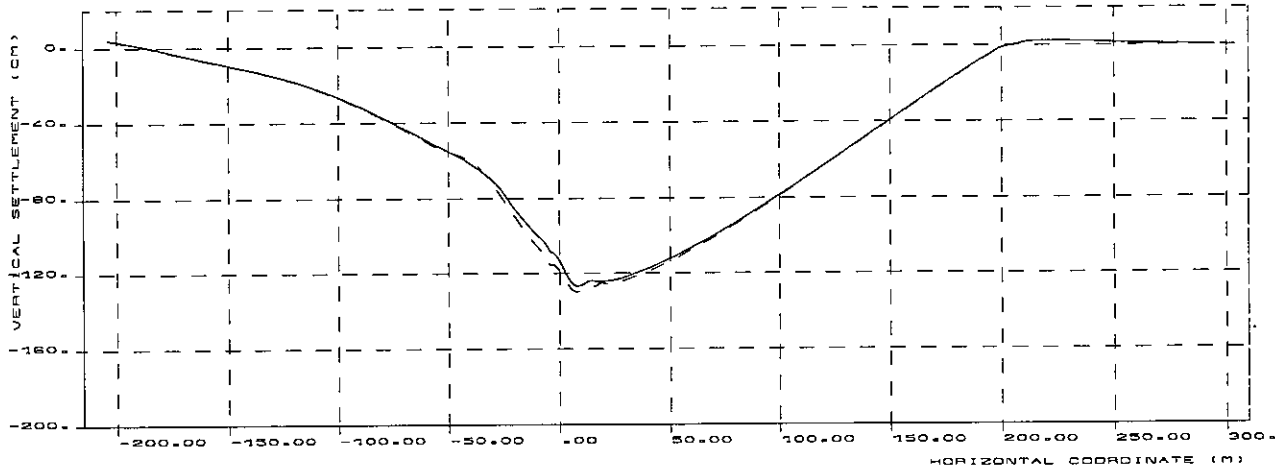

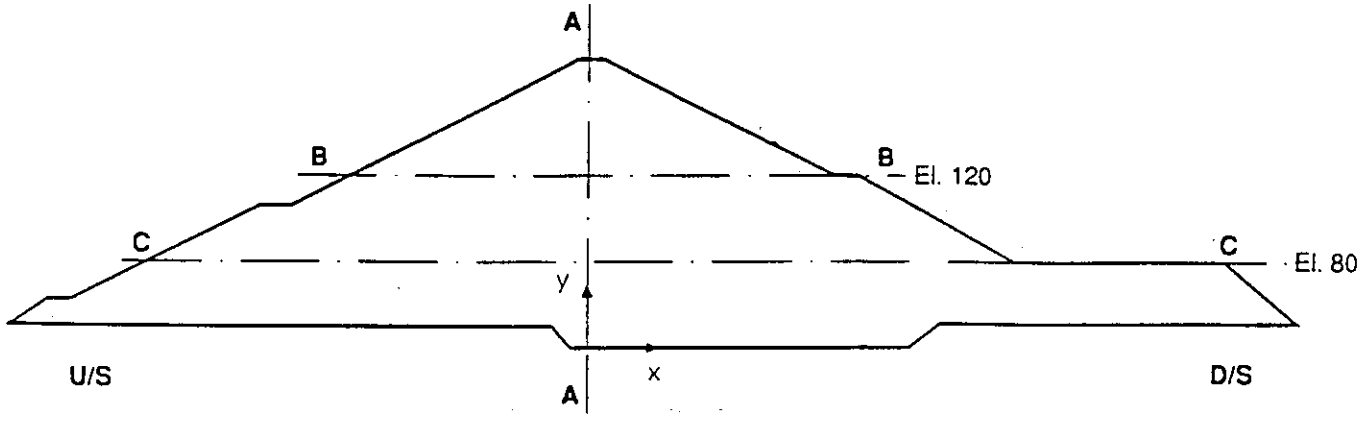

Fig. 7 : Vertical settlement at the end of consolidation along horizontal lines BB & CC

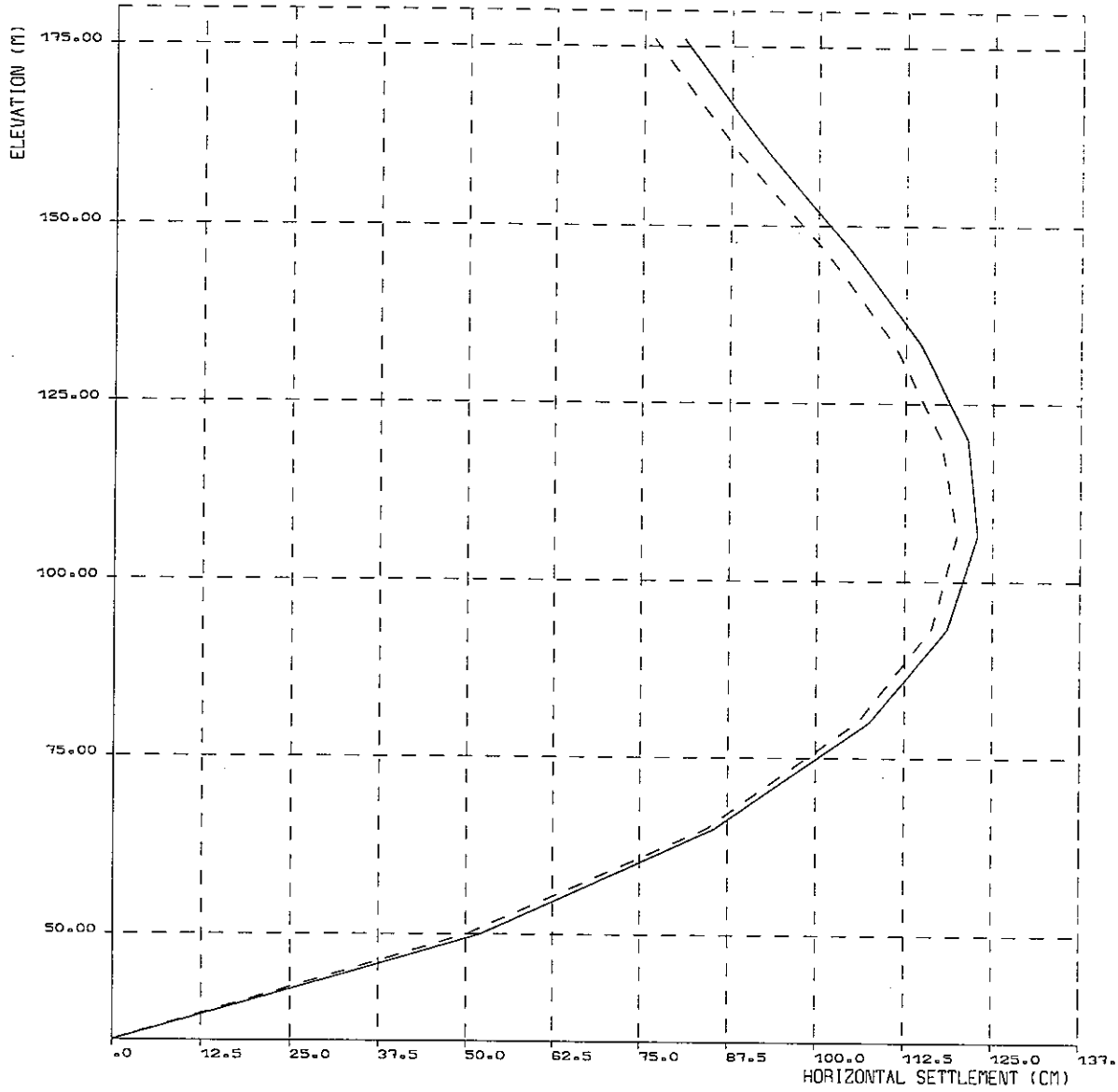

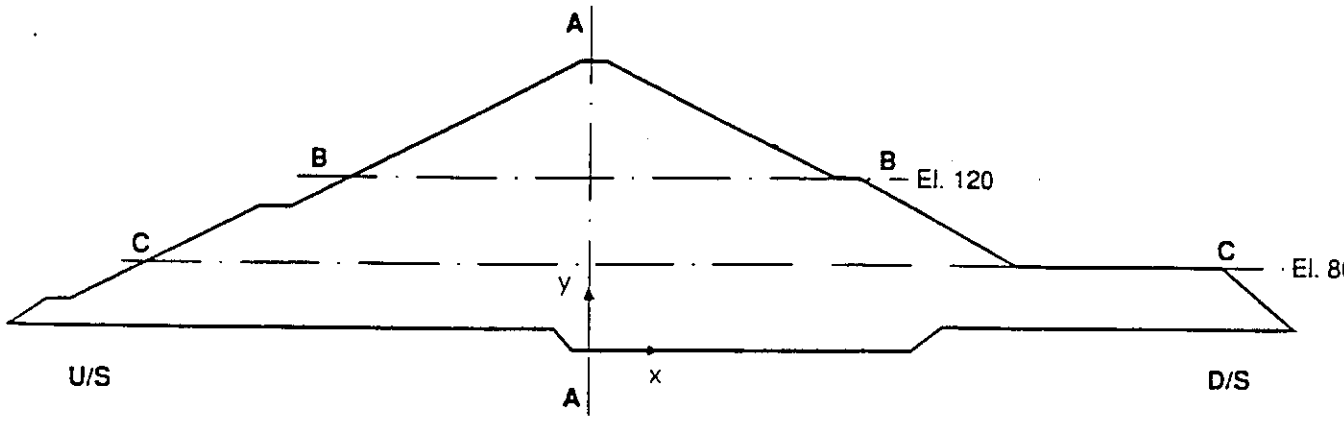

Fig. 8 : Horizontal displacement at the end of consolidation along core vertical line AA

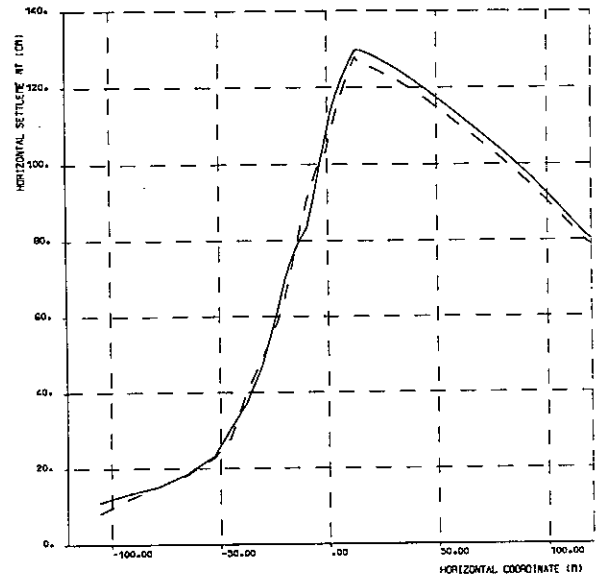

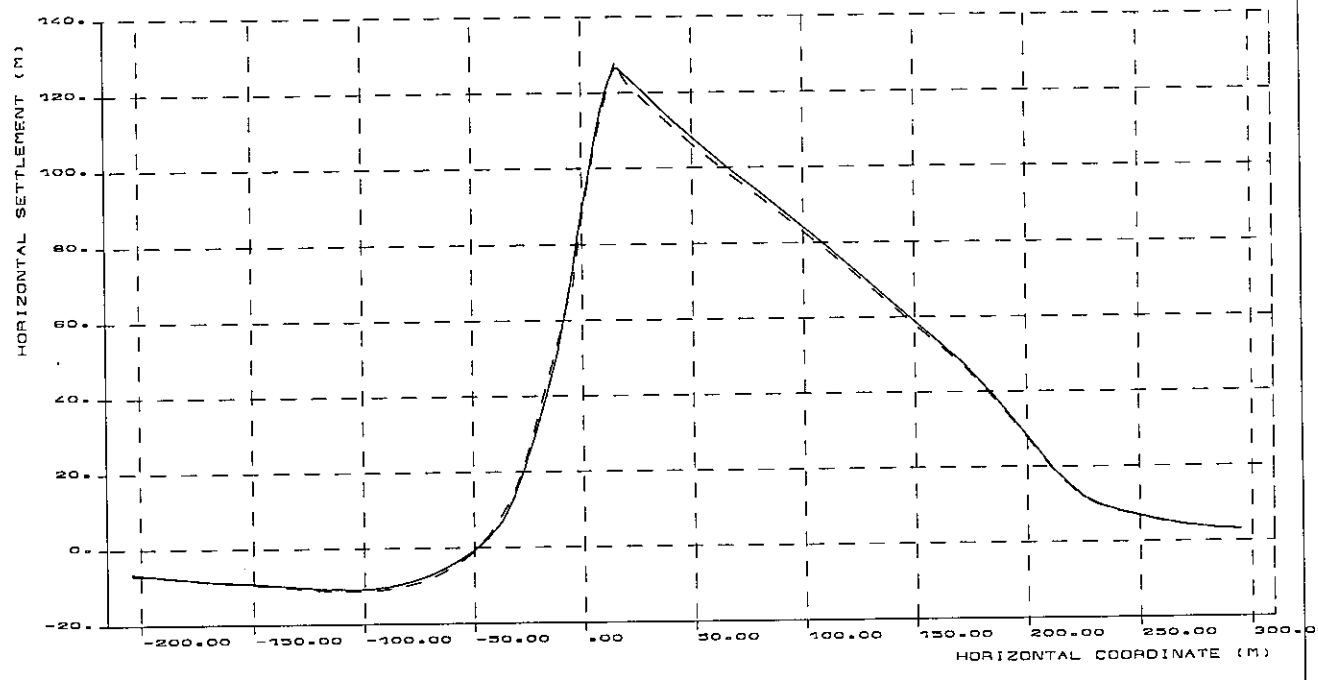

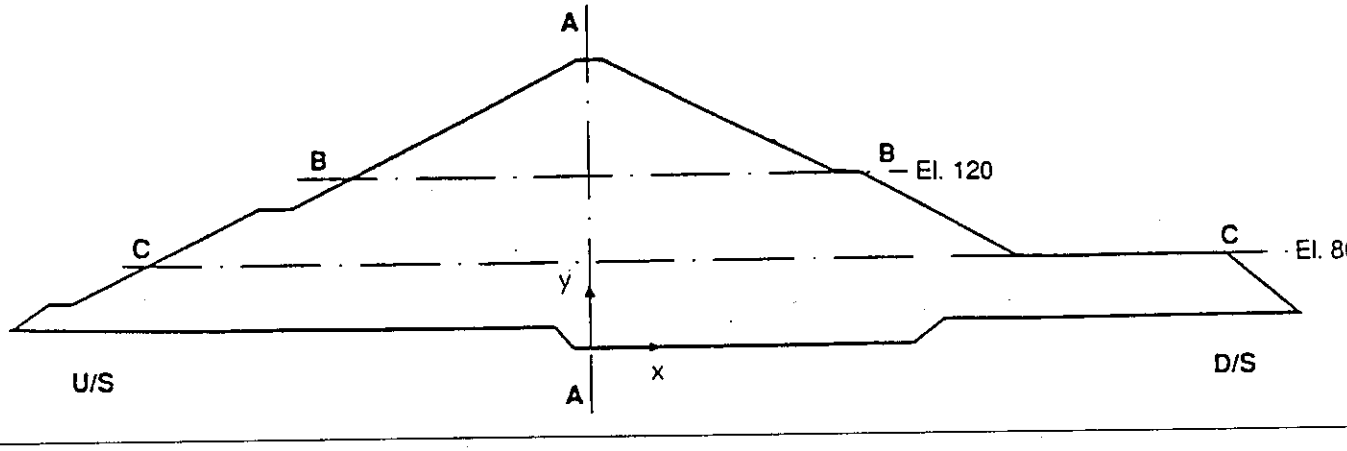

Fig. 9 : Horizontal displacement at the end of consolidation along horizontal lines BB & CC

Third ICOLD Benchmark Workshop on Numerical Analysis of Dams
PARIS (FRANCE), SEPTEMBER 29-30, 1994

THEME B1

EVALUATION OF PORE PRESSURE AND SETTLEMENTS OF AN EMBANKMENT DAM UNDER STATIC LOADINGS

G. La Barbera, A. Bani - ISMES S.p.A. Bergamo
G. Mazzà - ENEL/CRIS Milano

1. INTRODUCTION

The paper presents the results of the analysis carried out for the "El Infiernillo" dam, built in Mexico in 1962-63. It is a 145 m high rockfill dam with a central impermeable clay core (Fig. 2). The foundation is composed of sound rock consisting of silicified conglomerate with basaltic dikes and can therefore be considered rigid and impermeable.
The analysis has been performed adopting a fully coupled theory for all the different materials of the dam, even though the degree of freedom corresponding to the excess pore water pressure were considered "free" only for the core and the filter materials.
In the static analysis three load cases, corresponding to the actual history of the dam, have been considered: construction phase, reservoir impounding and consolidation phase.
The computer program used for the analysis is OMEGA, a 2-D 3-D f.e.m. code for the numerical solution of non-linear analysis of both one-phase solid and two-phases solid-fluid medium subjected to static and dynamic load conditions. The code has been jointly developed by ISMES S.p.A. (Bergamo, Italy) and CIMNE (Barcelona, Spain), on the basis of the theoretical formulation presented in [4], [5], [6], [7].
The numerical computations have been carried out on the CONVEX C3220 parallel/vectorial super computer at the ISMES computer facilities in Bergamo.

2. ADOPTED FORMULATION

A coupled solid-fluid formulation together with an incremental elasto-plastic deformations theory have been adopted. The finite element mesh (Fig. 3) is the one proposed by the Organizing Committee, optimized with an algorithm for profile and wave front reduction of sparse matrices. There are two different types of elements: the isoparametric 8-node quadrilateral and 6-node triangle. Numerical integration for the two types of elements has been performed using respectively the Gauss and the Radau rule, both with 4 integration points for each element.
The use of the Mohr-Coulomb model, proposed by the Organizing Committee, leads in many cases to numerical difficulties due to the discontinuities of the yield surface shape in the stress space. In order to avoid this problem an equivalent Drucker-Prager constitutive model has been adopted for the whole analysis of the dam. In fact in plane strain conditions, there is a theoretical equivalence for the Mohr-Coulomb and Drucker-Prager constitutive models, provided that the correct equivalent parameters φ^e, c^e are used. The equivalent φ^e value for plane strain conditions corresponds to the inscribed yield surface to the Mohr-Coulomb one.
If negative sign for compressive stresses is considered, the Drucker-Prager and Mohr-Coulomb yield surfaces may be written in terms of the stress invariants p, q as:

$$q = N - Mp$$

The M, N coefficients assume different values for the two models:

Mohr-Coulomb

$$N = \frac{3c\cos\varphi}{\sqrt{3}\cos\theta - \sin\theta\sin\varphi}$$

$$M = \frac{3\sin\varphi}{\sqrt{3}\cos\theta - \sin\theta\sin\varphi}$$

Drucker-Prager

$$N = \frac{6c\cos\varphi}{3 - \sin\varphi}$$

$$M = \frac{6\sin\varphi}{3 - \sin\varphi}$$

To obtain the Drucker-Prager yield surface inscribed in the Mohr-Coulomb one (Fig. 1), it is necessary to find the minimum value of the q invariant with respect to the θ invariant, by imposing to zero the following derivative:

$$\frac{\partial (N - Mp)}{\partial \theta} = 0$$

This condition is satisfied for the following value of the θ invariant: $\theta = -\text{atn}(\sin\varphi / \sqrt{3})$. The equivalent parameters of the Drucker-Prager model in the case of plane strain conditions are therefore:

$$\varphi^e = \arcsin\frac{3M}{6+M} \qquad (1)$$

$$c^e = \frac{N(3 - \sin\varphi)}{6 - \cos\varphi}$$

The elastic-perfectly plastic Drucker-Prager constitutive model with equivalent parameters c^e, φ^e has been adopted for the whole analysis (Fig. 1). Plastic deformations have been calculated considering an associated flow rule.

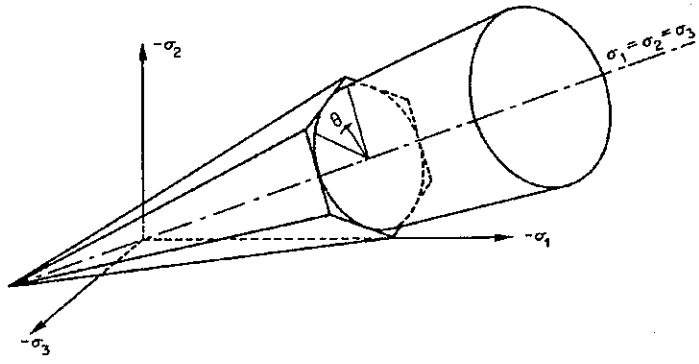

Fig. 1 A Mohr-Coulomb surface and the Drucker-Prager approximation

3. MATERIAL PARAMETERS

The materials of the various zones are described in Fig. 2. They can be divided into 4 main groups: core, filters, transition material and rockfill. The material parameters sets are indicated in Table 1. The differences between these parameters and those proposed by the Organizing Committee are the equivalent friction angles φ^e obtained from (1) and the fact that the transition zones have been considered fully drained, due to the high permeability with respect to the filters.

Densities and unit weights, used to evaluate gravity loads imposed for the construction numerical simulation, are indicated in Table 2. The unit weight (wet unit weight γ_w) for core material has been calculated as $\gamma_w = \gamma_d + S_0\, n\, \gamma_{water}$, where porosity $n = 1 - \gamma_d / \gamma_s$.

material number and description	Young modulus E (Mpa)	Poisson ratio υ	Equivalent friction angle φ^e(°)	Cohesion c (Mpa)	Horizontal permeability Kh (m/s)	Vertical permeability Kv (m/s)
1 - core	40	0.3	18.535	0.0	8.0E-10	2.0E-10
2 - filters	40	0.3	24.047	0.0	8.0E-05	8.0E-05
3 - transition zone	40	0.3	27.259	0.0	/	/
4 - compacted rockfill	40	0.3	27.259	0.0	/	/
5 - dumped rockfill	40	0.3	27.259	0.0	/	/
6 - dumped rockfill	40	0.3	27.259	0.0	/	/

Table 1

material number and description	Grain density γ_s (kN/m^3)	Dry density γ_d (kN/m^3)	Initial degree of saturation S_0	Unit weight γ (kN/m^3)
1 - core	27.5	15.9	0.96	19.9
2 - filters	27.6	18.7	/	18.7
3 - transition zone	27.5	20.2	/	20.2
4 - compacted rockfill	27.1	18.5	/	18.5
5 - dumped rockfill	27.1	17.6	/	17.6
6 - dumped rockfill	27.1	17.6	/	17.6

Table 2

4. STATIC ANALYSIS

In the static analysis three load cases, corresponding to the actual history of the dam, have been considered: construction phase, reservoir impounding and consolidation phase. The same boundary conditions for displacements have been considered at the base of the dam for the whole analysis: null horizontal and vertical displacements.

4.1 Construction simulation

The total duration of the dam construction is approximately 15 months, with a very regular rate of elevation versus time, of 10 m per month. Construction history has been simulated by applying 11 soil layers of about 15 m thickness each, as shown in Fig. 4. The own weight of each layer has been gradually applied, with a linear variation in time. Excess pore water pressure has been set equal to zero at the filters-transition zones interface, in the transition zones themselves and in the rockfill.

In order to simulate the overconsolidation due to materials compaction an initial stress state has been considered for all the materials. An isotropic initial stress state of 0.01 MPa has been applied. This is an important assumption that avoids serious numerical difficulties while dealing with effective stress cohesionless materials analysis.

The high permeability of the filters with respect to the impermeable core made their excess pore water pressure decrease to zero value during a single layer construction period. When a new layer was considered, excess pore water pressure was fixed to zero at the core-filter interface for the already built layers.
The time history of the construction and the first consolidation phases is shown in Table 3. For each interval several steps have been considered, in order to give small stress increments for an easier convergence of the numerical analysis.

layer	maximum elevation (m)	interval time (days)	starting time (days)	total time (days)
1	50.02	44	0	44
2	65.00	44	44	88
3	80.00	42	88	130
4	93.25	40	130	170
5	106.50	40	170	210
6	120.00	40	210	250
7	133.40	40	250	290
8	146.70	40	290	330
9	160.00	40	370	370
10	170.99	40	410	410
11	180.00	40	450	450

Table 3

4.2 Reservoir Impounding

At the end of construction a period of 5 months occurred before reservoir impounding, the reservoir level being at El. 60. This period has also been modeled, with the hypothesis that water pressure increased from zero to the maximum value corresponding to El. 60 in the same period. Impounding history has been modeled considering 9 water elevation increments, according to the time history shown in Table 4. For each interval several steps have been considered also in this phase.
The effect of the increasing water level have been modelled only considering the buoyancy effect induced on the submerged zone (load effect). The hydraulic effect in terms of induced not stazionary seepage phenomenon have not been considered.

impounding interval	reservoir elevation (m)	interval time (days)	starting time (days)	total time (days)
1	60.00	150	450	600
2	80.00	3	600	603
3	93.25	3	603	606
4	106.50	3	606	609
5	120.00	3	609	612
6	130.00	3	612	615
7	146.70	23	615	638
8	160.00	22	638	660
9	169.00	120	660	780

Table 4

4.3 Consolidation Phase

After the end of impounding a consolidation period has been considered, so as to obtain stabilization in pore pressures and effective stresses. An approximate evaluation of the necessary time to reach stabilization can be made with reference to one-dimensional (horizontal) consolidation according to the following expression:

$$t = \frac{T_h H^2 \gamma_w (1 + \nu) (1 - 2\nu)}{k_h E (1 - \nu)}$$

For the values of the time factor T_h = 0.848 and 1.129, respectively corresponding to a degree of consolidation of 90% and 95%, 4.2 and 5.5 years are obtained. The analysis of the stabilization phase has been carried out to 5.5 years (2000 days) after the reservoir impounding, with a complete stabilization of pore pressures, effective stresses and displacements (Fig. 16).

5. RESULTS OF THE STATIC ANALYSIS

The analysis covered all the load cases corresponding to the actual history of the dam, from construction to steady state conditions after a long period with the maximum water level.
The effective stresses, excess pore water pressures and displacements distribution at the end of the three considered load cases are shown in Figg. 5÷11. The normal effective stresses present similar characteristics, that is decreasing values in the upstream shoulder of the dam during water level growth and an almost constant distribution in the downstream shoulder. In the core, starting from low values at the end of construction, effective stresses increase particularly in the right half at the lower third due to dissipation and stabilization of pore pressures.
Tangential stresses are almost everywhere near to zero except in the lower central part of the dam, close to the foundation. After the reservoir impounding the only relevant values are near the core in the downstream shoulder, and they increase during the consolidation phase.
The distribution of excess pore water pressure inside the clay core is quite good. At the end of construction there is a symmetrical distribution with values increasing with depth; at the end of impounding phase a dissipation in the upper part is already clear, while the steady state free surface of water can be seen at the end of the consolidation phase.
In table 5 both a summary of displacements and excess pore water pressure values for 5 representative points at the end of the three phases are provided. Horizontal displacements increase during all three considered phases, with the higher rate corresponding to reservoir impounding. Vertical displacements generally decrease in time, due to the dilatancy effects of the Mohr-Coulomb (Drucker-Prager) model with the associate flow rule adopted. Some points of the dam present even upward vertical displacements. Excess pore water pressures values in the core decrease during reservoir impounding and then increase during the consolidation phase (Fig. 16).
Figures 12, 13, 14 and 15 show the horizontal and vertical displacements distribution along three main lines A-A, B-B and C-C. Dilatancy effects are more relevant in the lower and upper part of the dam.
In figure 16 plots of horizontal and vertical displacements and excess pore water pressures time histories, for the core points CL and CM are provided.

	Points of the Dam Section				
	CC	CM	CL	UM	DM
End of Construction	-0.21	10.28	11.34	-23.70	26.77
End of impounding	125.84	136.57	104.18	-1.72	102.28
End of consolidation	136.25	149.54	113.09	-7.52	126.71

Horizontal Displacements (10^{-2} m)

	Points of the Dam Section				
	CC	CM	CL	UM	DM
End of Construction	-19.29	-199.24	-148.16	-35.45	-45.38
End of impounding	23.32	-150.44	-122.24	21.74	-34.22
End of consolidation	12.61	-158.35	-119.11	22.40	-26.29

Vertical Displacements (10^{-2} m)

	Points of the Dam Section				
	CC	CM	CL	UM	DM
End of Construction	0.000	0.005	0.090	0.000	0.000
End of impounding	0.000	-0.121	-0.322	0.000	0.000
End of consolidation	0.000	-0.002	-0.040	0.000	0.000

Excess Pore Water Pressures (MPa)

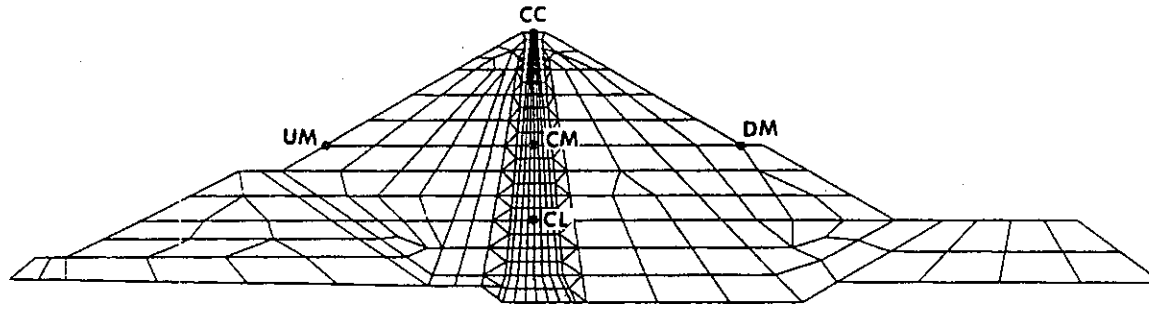

Table 5: 3rd Benchmark Workshop - Theme B1
GENERAL SUMMARY: Results of displacements and pore pressures after each phase

6. REQUIRED COMPUTATION TIMES

In Table 5 the required CPU times are summarized for each calculation phase.

Static Analysis	CPU time (hh:mm:ss)
Construction	00:08:98
Impounding	00:07:61
Consolidation	00:04:33

Table 5

7. CONCLUDING REMARKS

The whole set of results obtained from the analysis carried out for the Third Benchmark Workshop of El Infiernillo Dam are presented and discussed in this paper.
A rigorous approach based on the coupled solid fluid effective stress theory have been adopted. The results are furnished in terms of displacements, effective stresses and excess pore water pressures.
The simulation of the first impounding is not properly modellized because the hydraulic effects in terms of induced not stationary seepage have not been taken into consideration. Furthermore, the adopted model doesn't consider the "wetting collapsing behaviour" of the rockfill material while it is passing from partial to full saturation. Our opinion is that this effect may have a significant influence on the predicted behaviour of the dam (volumetric deformations in the upstrean shoulder).
The adopted Drucker-Prager elastic-perfectly plastic model seems to furnish acceptable results in terms of displacements of the dam. Some doubts remains if the volumetric strains in the core region are considered. The model, as known, is always dilatant so that it predicts negative volumetric plastic strains (swelling) and as a conseguence the induced excess pore water pressure during plastic deformations are negative. Better and more reliable experimental data are necessary to clarify the question.

8. REFERENCES

[1] Biot M.A. (1941). General theory of fhree dimensional consolidation J Appl. Phys.

[2] Biot M.A. (1956). The theory of propagation of elastic waves in a fluid saturated porous solid. J. Acou.Soc.Am., 168 191.

[3] Fusco A. (1985). Continuum mechanics and finite element numerical solutions in geomechanics. Ph. D. Thesis, University of Ottawa.

[4] Fusco A. (1993). Numerical Analysis for enginners. Monograph CIMNE, N.19

[5] Fusco A. (1993). The continuum Mechanics Theory for enginners. Monograph CIMNE, N.20

[6] Fusco A. (1993). The Finite Element Method for enginners. Monograph CIMNE, N.21.

[7] Fusco A., and Cervera M. (1993). Coupled solid-pore fluid problems solved by Finite Elements, Monograph CIMNE, N.22.

[8] Fusco A. et al. (1991). The seismic Response of the El Infernillo Embankment dam: coupled effective stress elasto-plastic analysis. First Benchmark Workshop Bergamo (Italy), May 28 29.

[9] Sandhu R.S. (1968). Fluid flow in saturated porous elastic media. PhD Thesjs, Univers. of California at Berkeley.

[10] Sandhu R.S. and Wilson E.L. (1969). Finite element analysis of seepage in elastic media Proceeding ASCE, Mechanics Division, Vol. 95, No. EM3.

[11] Seed H.B. (1979). Considerations in the earthquake resistant design of earth and rockfill dams. Geotechnique 29, No. 3.

[12] Zienkiewicz O.C., Bettess P. (1982). Soil and saturated media under transiented dynamic conditions; general formulation and the validity of various simplifying assumption In Soil Mechanics Transient & Cyclic Loads (Eds. G.N. Pande & O.C. Zienkiewicz)

[13] La Barbera G. et al. (1992). Static analysis and seismic response of the El Infrnillo Embankment dam: Coupled effective stress analysis. Second Benchmark Workshop Bergamo (Italy), July 16 17.

Third ICOLD Benchmark Workshop on Numerical Analysis of Dams
PARIS (FRANCE), SEPTEMBER 29-30, 1994

ADDENDUM
TO THEME B1
DRAINED AND UNDRAINED TRIAXIAL TEST SAMPLE

G. La Barbera, A. Bani - ISMES S.p.A. Bergamo
G. Mazzà - ENEL/CRIS Milano

In order to quantify discrepancies in the results of the analysis of the dam, which are due to different choices of the constitutive models, the results of a sample triaxial test, using the parameters of the core material listed in table 1, are provided.

material	E (Mpa)	υ	$\varphi(°)$	c (Mpa)	Kh (m/s)	Kv (m/s)
core	40	0.3	25	0.0	8.0E-10	2.0E-10

Table 1

The use of the Mohr-Coulomb model leads in many cases to numerical difficulties due to the discontinuities of the yield surface shape in the stress space. In order to avoid this problem the Drucker-Prager model has been adopted for both the triaxial test sample and for the whole analysis of the dam.
In fact in triaxial conditions, as well as in plane strain conditions, there is a theoretical equivalence for the Mohr-Coulomb and Drucker-Prager constitutive models, provided that the correct equivalent parameters φ, c are used. The equivalent φ value for triaxial conditions, in particular, is the same for both models (only for compression).
If negative sign for compressive stresses in considered, the Drucker-Prager yield surface may be written in terms of the stress invariants p', q as:

$$q = N - Mp'$$

Where $p' = (\sigma'_1 + 2\sigma'_3) / 3$ = mean effective stress, $q = \sigma_1 - \sigma_3$ = deviatoric stress, $N = 6c \cos\varphi / (3 - \sin\varphi)$, $M = 6 \sin\varphi / (3 - \sin\varphi)$.

The limit values for p' and q in triaxial conditions, considering a confining pressure σ'_3 , may be evaluated as follows:

$$p_{lim} = (N - 3\sigma'_3) / (M - 3)$$

$$q_{lim} = N - Mp_{lim}$$

The calculation has been performed considering a confining pressure $\sigma'_3 = -0.5$ MPa and by imposing an axial strain σ_1 increasing from 0 to 10%. The theoretical values of p_{lim} and q_{lim} for these boundary condition are respectively -0.74398 MPa and 0.73195 MPa.
The results of the calculations are summarized in figures 1, 2 , 3 and table 2 for drained conditions, and in figures 4, 5, 6 and table 3 for undrained conditions.

drained triaxial test

maximum deviatoric stress	q_{max} = 0.73196 Mpa
minimum volumetric strain	ε_v^e = 0.0072
axial strain when $\varepsilon_v = \varepsilon_v^e$	ε_1^e = 0.018

Table 2

undrained triaxial test

deviatoric stress q at $\varepsilon_1 = 10\%$	q = 2.1852 Mpa
excess pore pressure u at $\varepsilon_1 = 10\%$	u = -0.9927 MPa
maximum excess pore pressure	u_{max} = 0.1595 MPa
axial strain when $u = u_{max}$	ε_1^e = 0.011
deviatoric stress when $u = u_{max}$	q = 0.49514 MPa

Table 3

3rd. ICOLD 1994

DRAINED AND UNDRAINED TRIAXIAL TEST SAMPLE

Drained Triaxial Test (Drucker - Prager model)

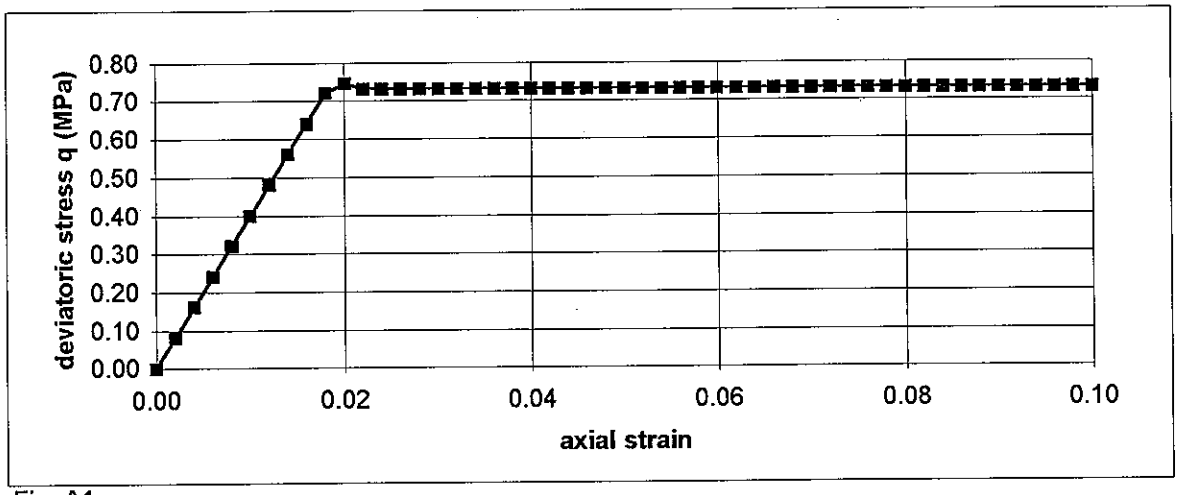

Fig. A1

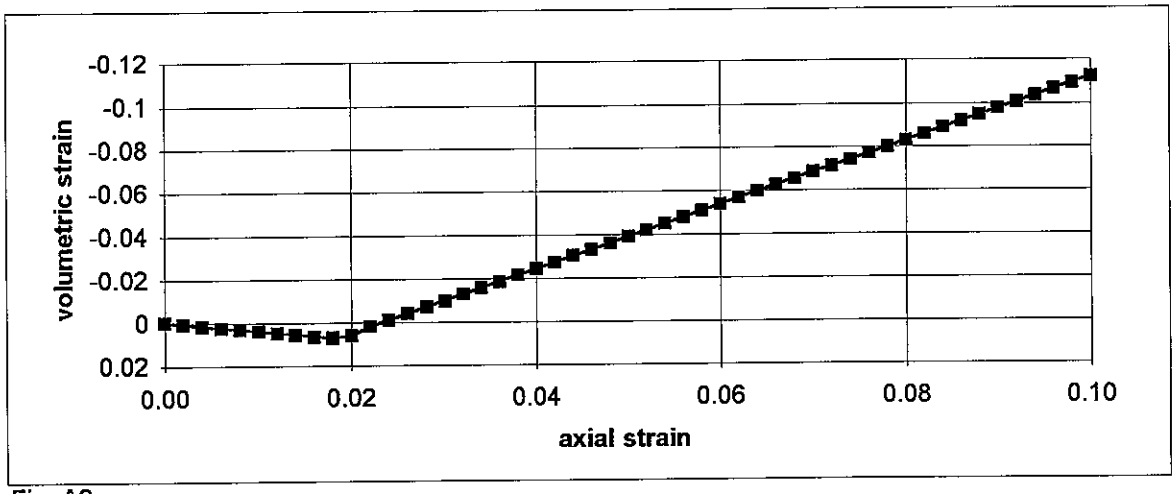

Fig. A2

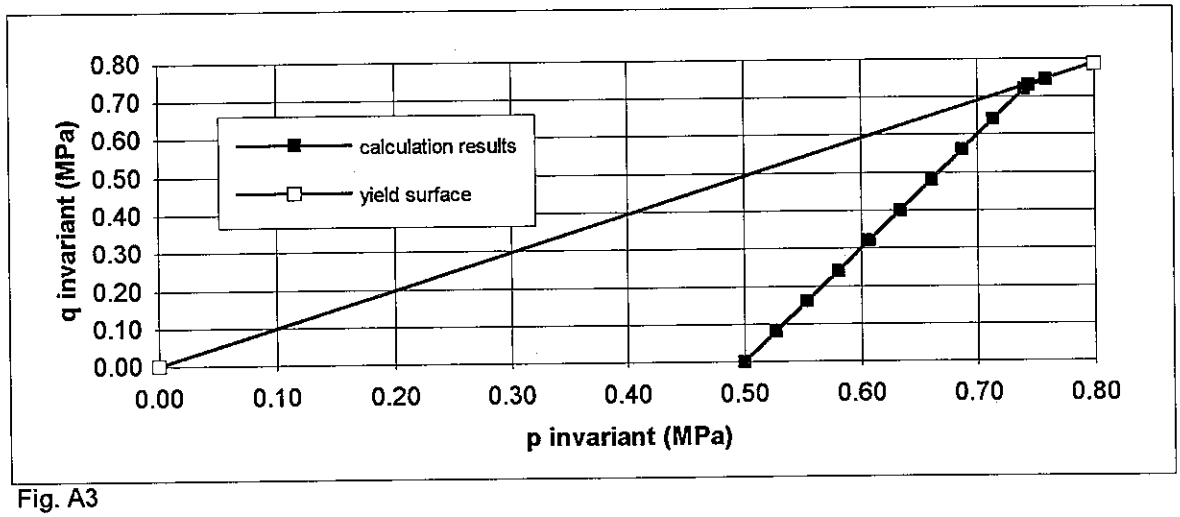

Fig. A3

3rd. ICOLD 1994

DRAINED AND UNDRAINED TRIAXIAL TEST SAMPLE

Undrained Triaxial Test (Drucker - Prager model)

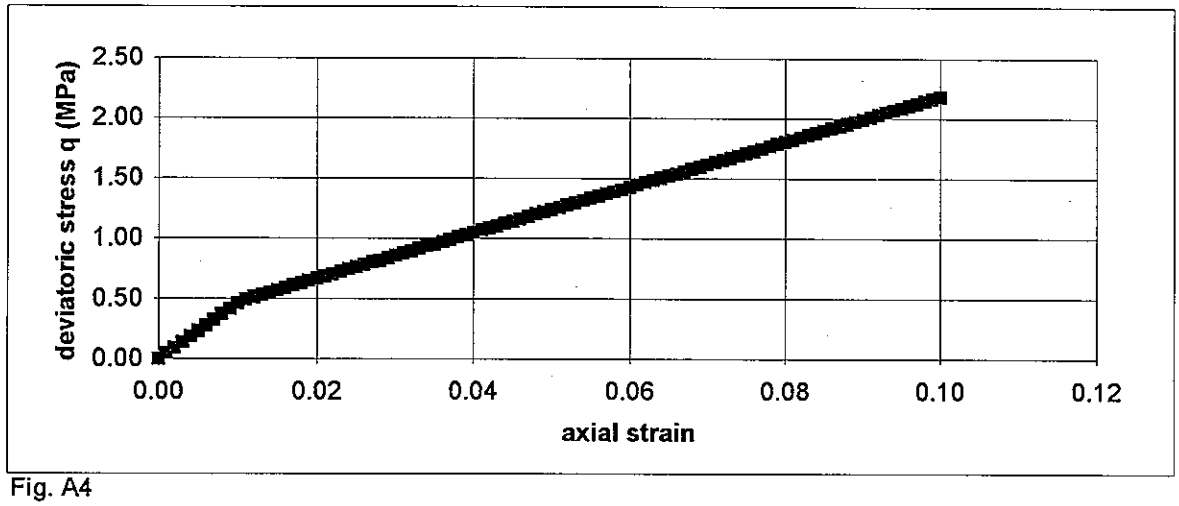

Fig. A4

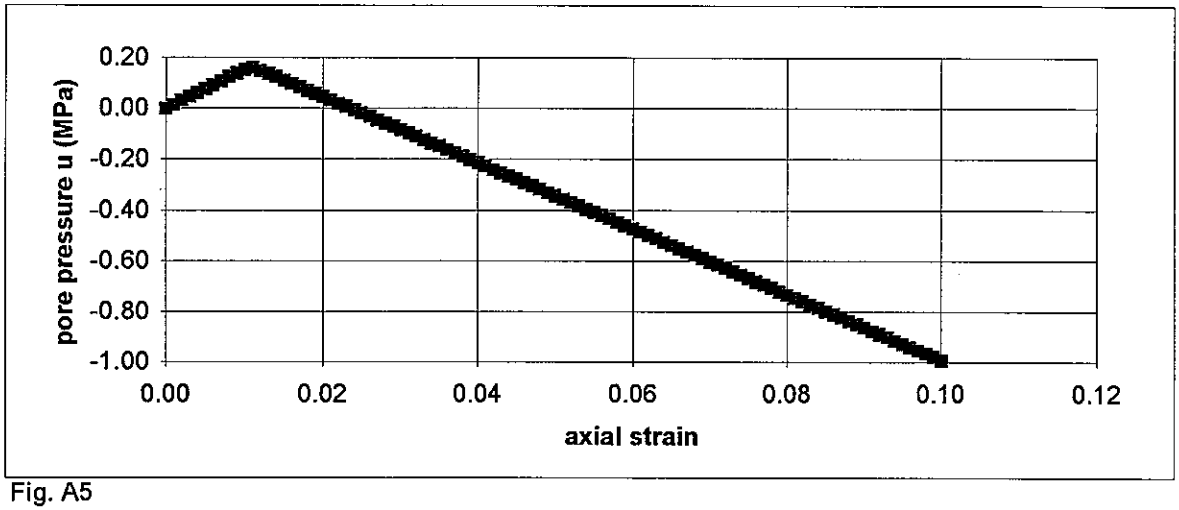

Fig. A5

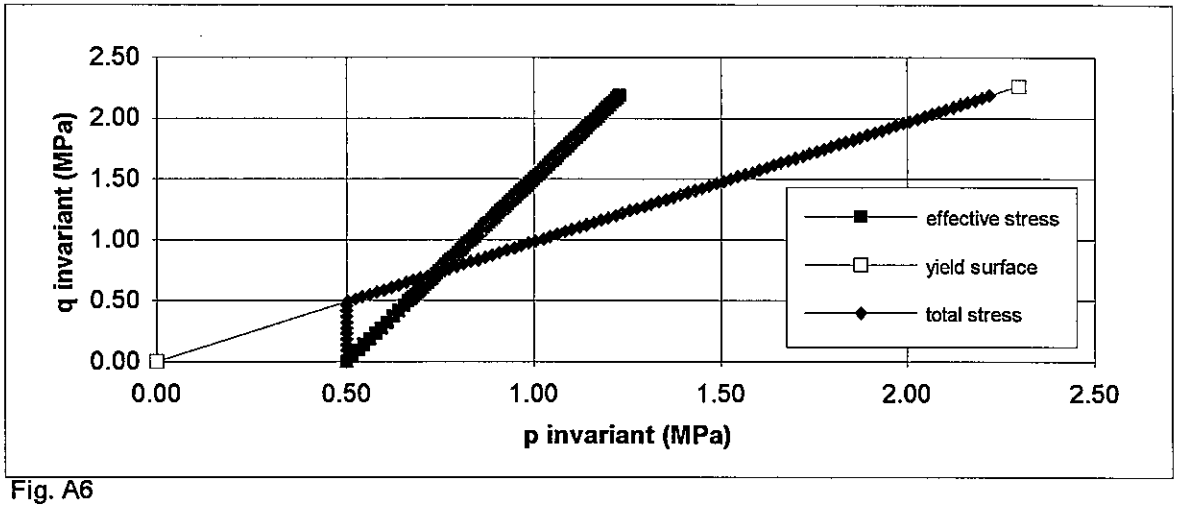

Fig. A6

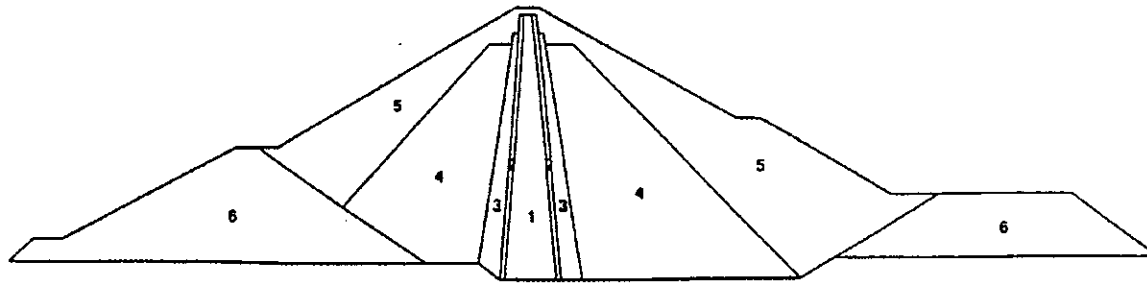

1. Impervious clay core
2. Filters (sand)
3. Transition Zone
4. Inner Shoulder compacted rockfill
5. Outer Shoulder dumped rockfill
6. Cofferdams (integrated) dumped rockfill

Fig. 2: 3rd Benchmark Workshop - Theme B1
Material property zones

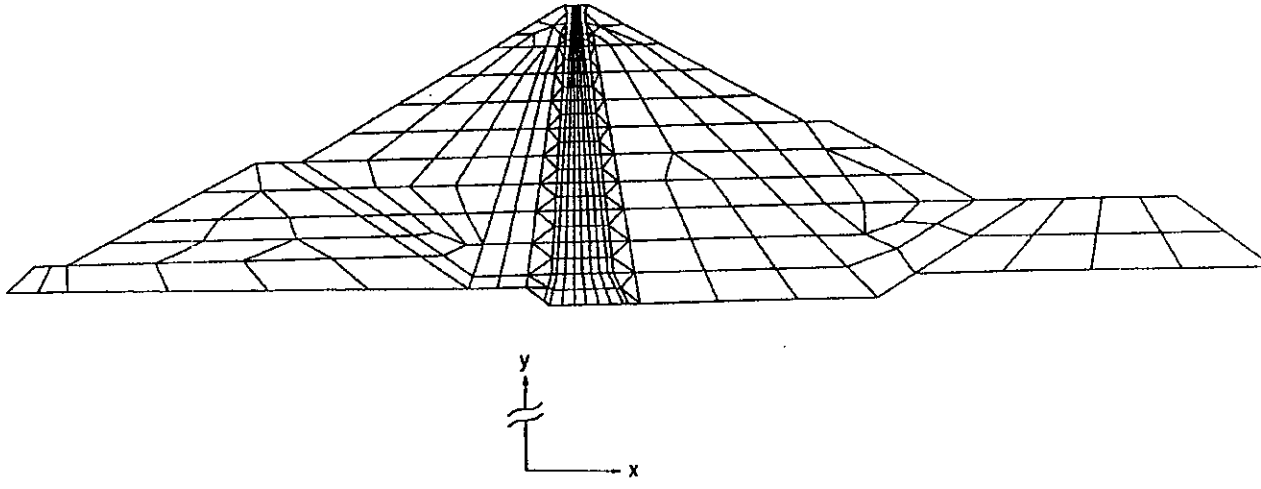

Fig. 3: 3rd Benchmark Workshop - Theme B1
Finite element mesh

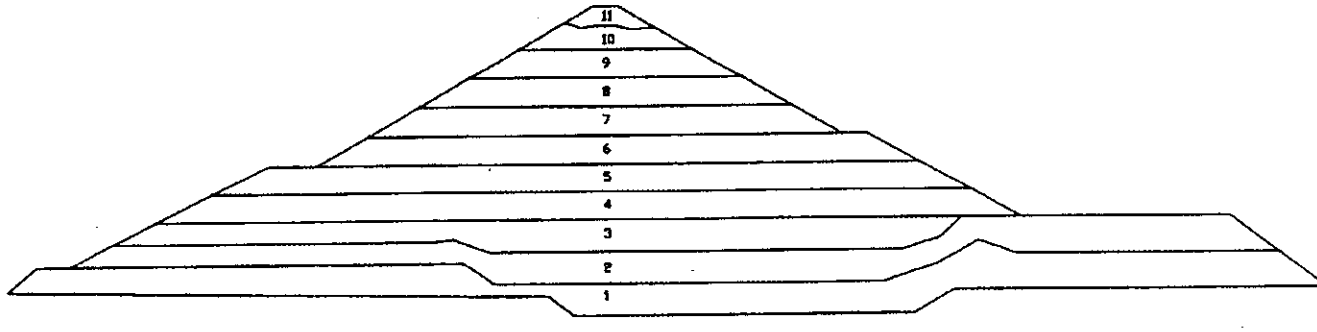

Fig. 4: 3rd Benchmark Workshop - Theme B1
Layers for costruction phases

3rd. ICOLD 1994 - STATIC ANALYSIS

HORIZONTAL STRESSES DISTRIBUTION

DRUCKER-PRAGER MODEL

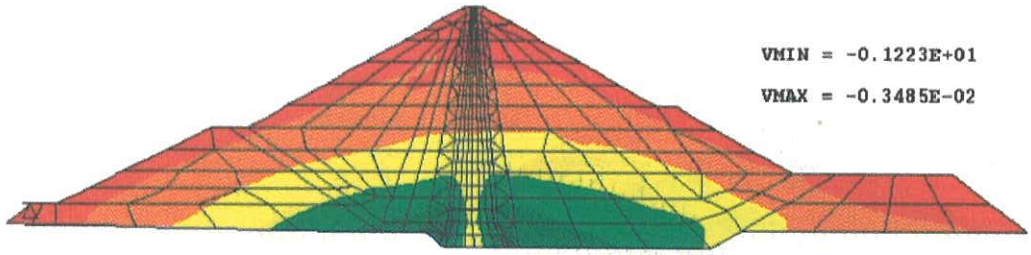

End of Construction

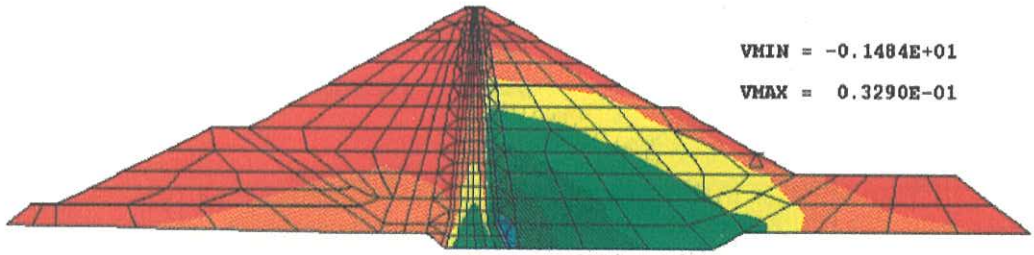

End of Impounding

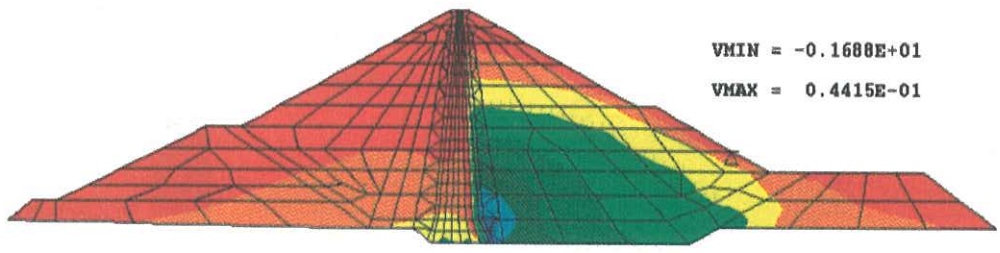

End of Consolidation

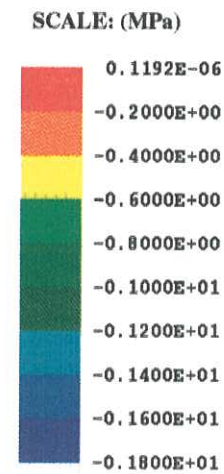

Fig. 5

3rd. ICOLD 1994 - STATIC ANALYSIS

OUT OF PLANE HORIZONTAL STRESSES DISTRIBUTION

DRUCKER-PRAGER MODEL

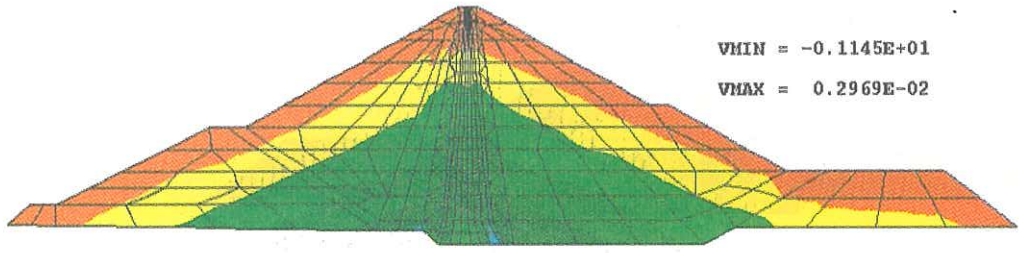

End of Construction

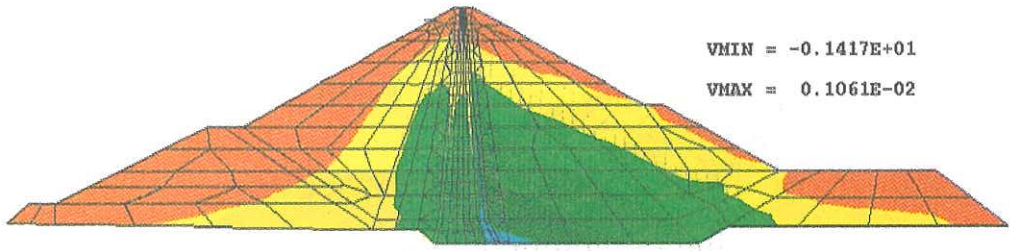

End of Impounding

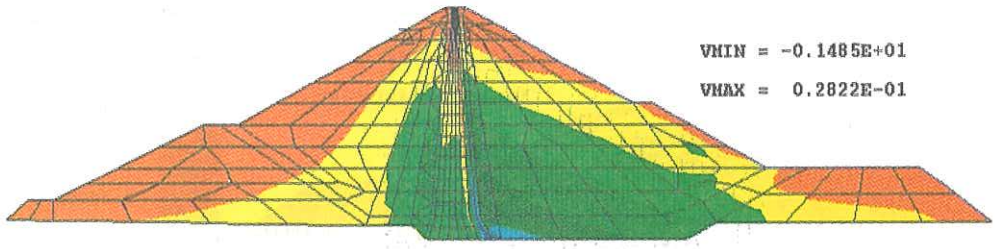

End of Consolidation

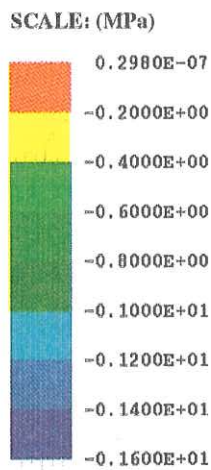

Fig. 6

3rd. ICOLD 1994 - STATIC ANALYSIS

VERTICAL STRESSES DISTRIBUTION

DRUCKER-PRAGER MODEL

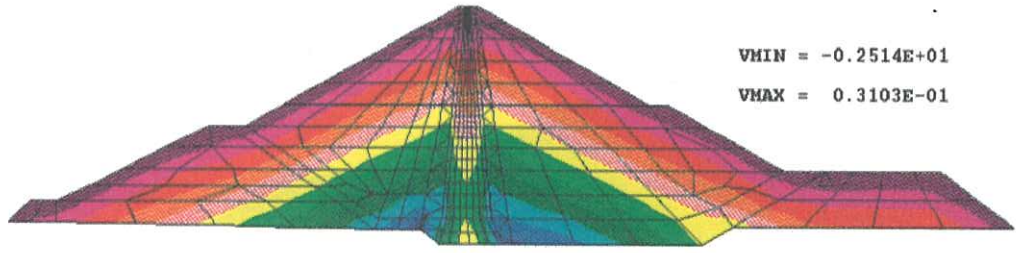

End of Construction

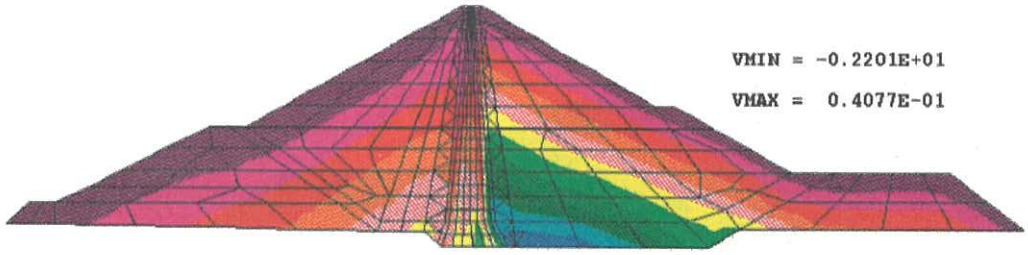

End of Impounding

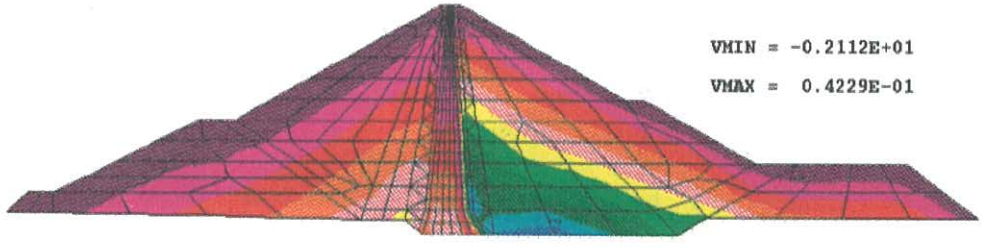

End of Consolidation

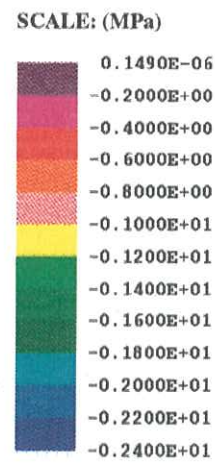

Fig. 7

3rd. ICOLD 1994 - STATIC ANALYSIS

SHEAR STRESSES DISTRIBUTION

DRUCKER-PRAGER MODEL

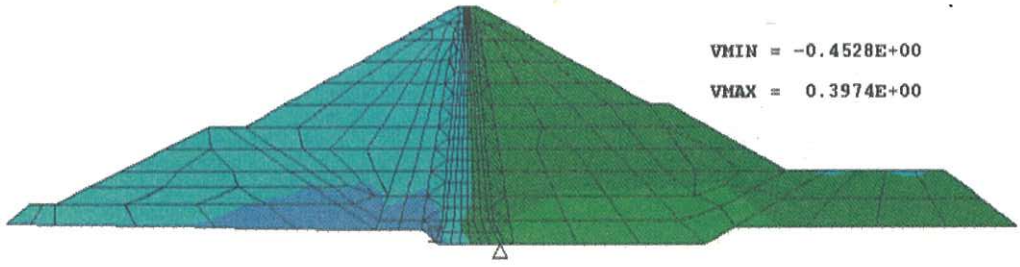

End of Construction

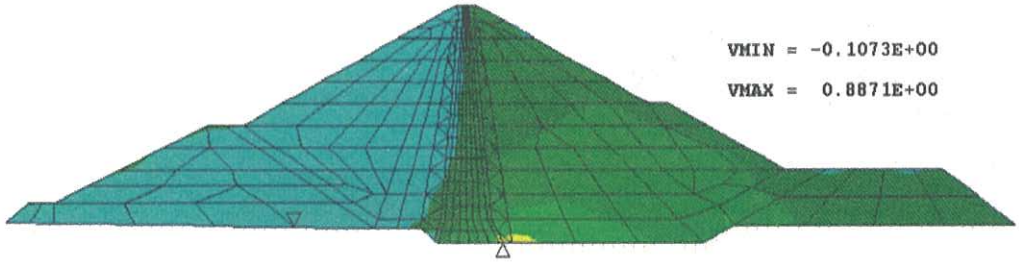

End of Impounding

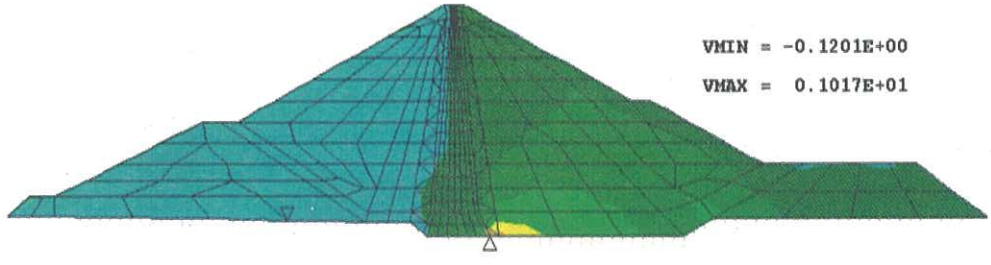

End of Consolidation

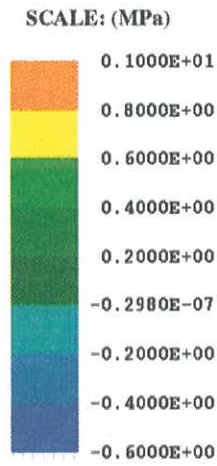

Fig. 8

3rd. ICOLD 1994 - STATIC ANALYSIS

EXCESS PORE WATER PRESSURE DISTRIBUTION

DRUCKER-PRAGER MODEL

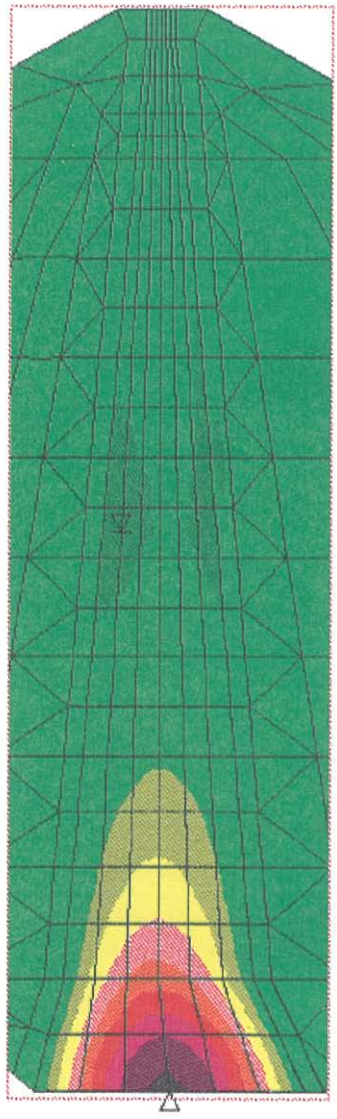

VMIN = -0.5702E-02

VMAX = 0.8283E+00

End of Construction

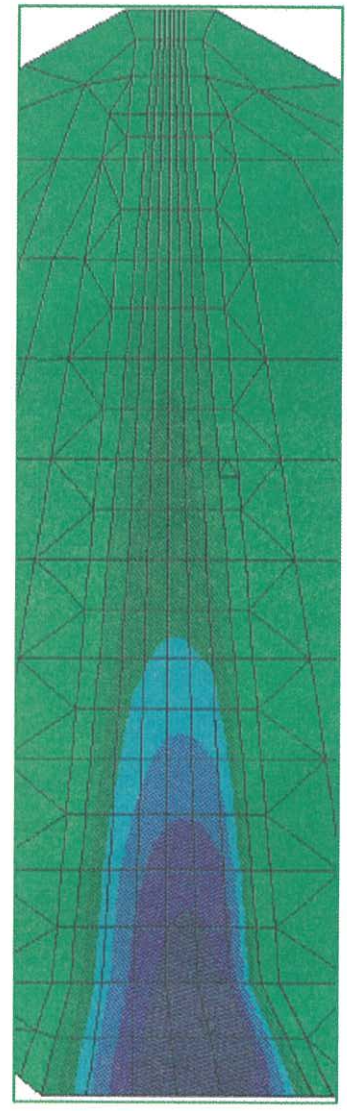

VMIN = -0.6073E+00

VMAX = 0.1246E-06

End of Impounding

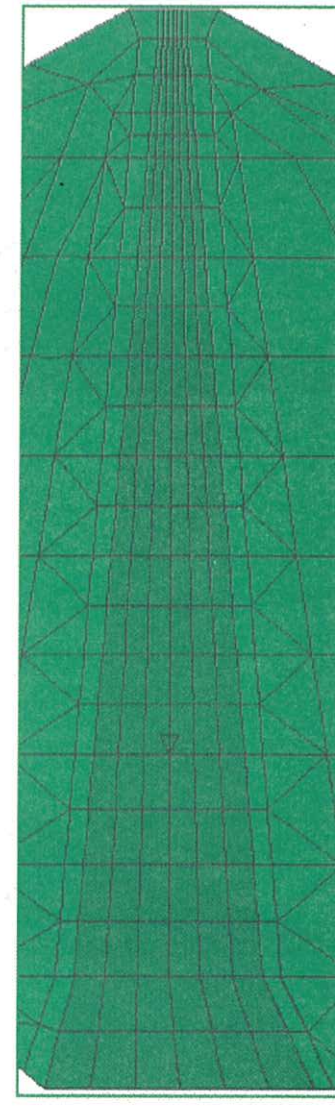

VMIN = -0.4333E-01

VMAX = 0.0000E+00

End of Consolidation

SCALE: (MPa)

0.9000E+00
0.8000E+00
0.7000E+00
0.6000E+00
0.5000E+00
0.4000E+00
0.3000E+00
0.2000E+00
0.1000E+00
-0.1490E-07
-0.1000E+00
-0.2000E+00
-0.3000E+00
-0.4000E+00
-0.5000E+00
-0.6000E+00

Fig. 9

3rd. ICOLD 1994 - STATIC ANALYSIS

HORIZONTAL DISPLACEMENTS DISTRIBUTION

DRUCKER-PRAGER MODEL

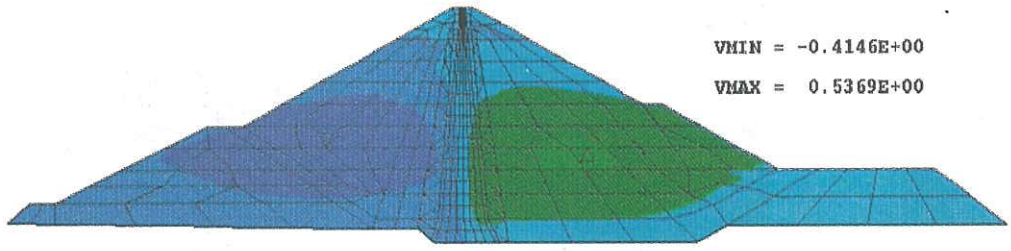

End of Construction

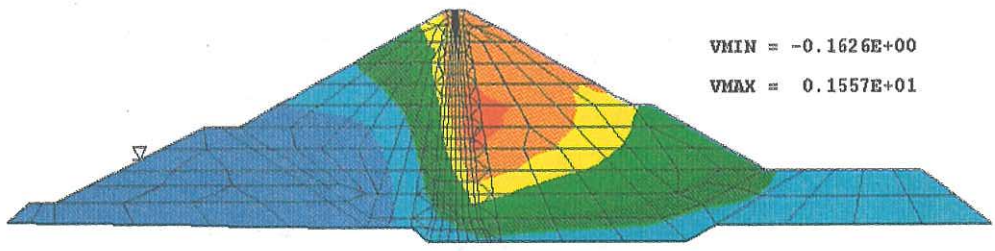

End of Impounding

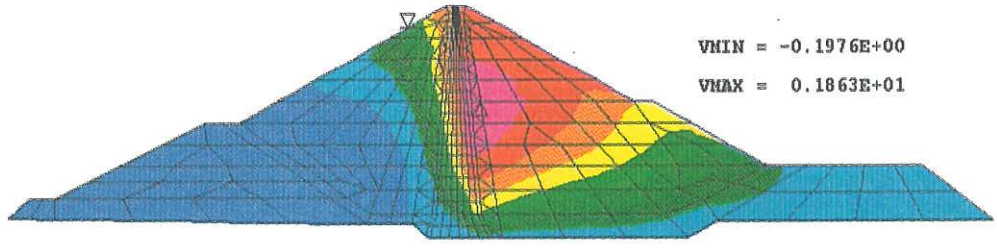

End of Consolidation

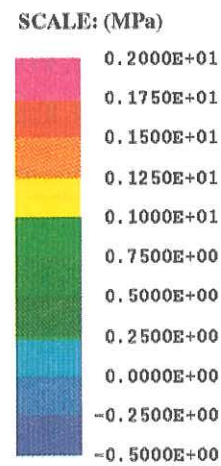

Fig. 10

3rd. ICOLD 1994 - STATIC ANALYSIS

VERTICAL DISPLACEMENTS DISTRIBUTION

DRUCKER-PRAGER MODEL

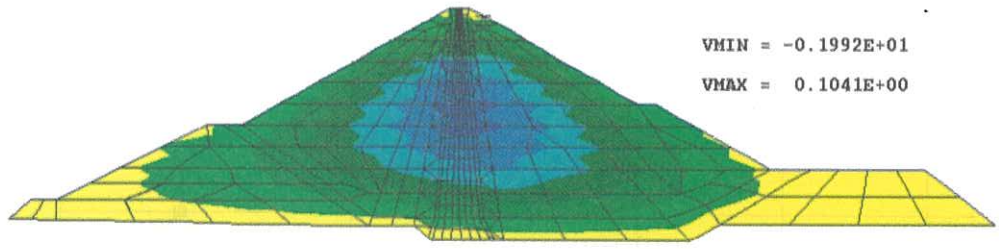

End of Construction

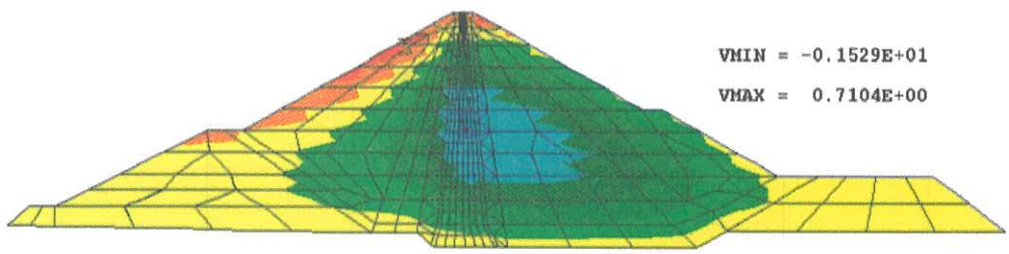

End of Impounding

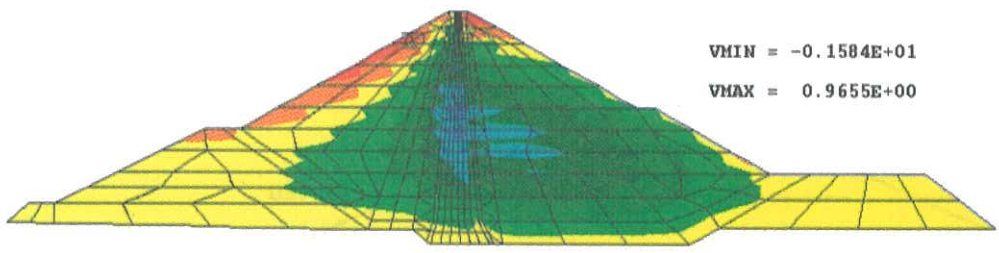

End of Consolidation

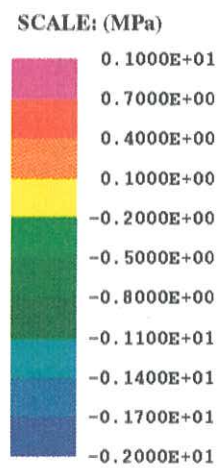

Fig. 11

3rd. ICOLD 1994 - STATIC ANALYSIS

HORIZONTAL DISPLACEMENTS AT THE END OF CONSOLIDATION PHASE
DRUCKER-PRAGER MODEL

SECTION A-A

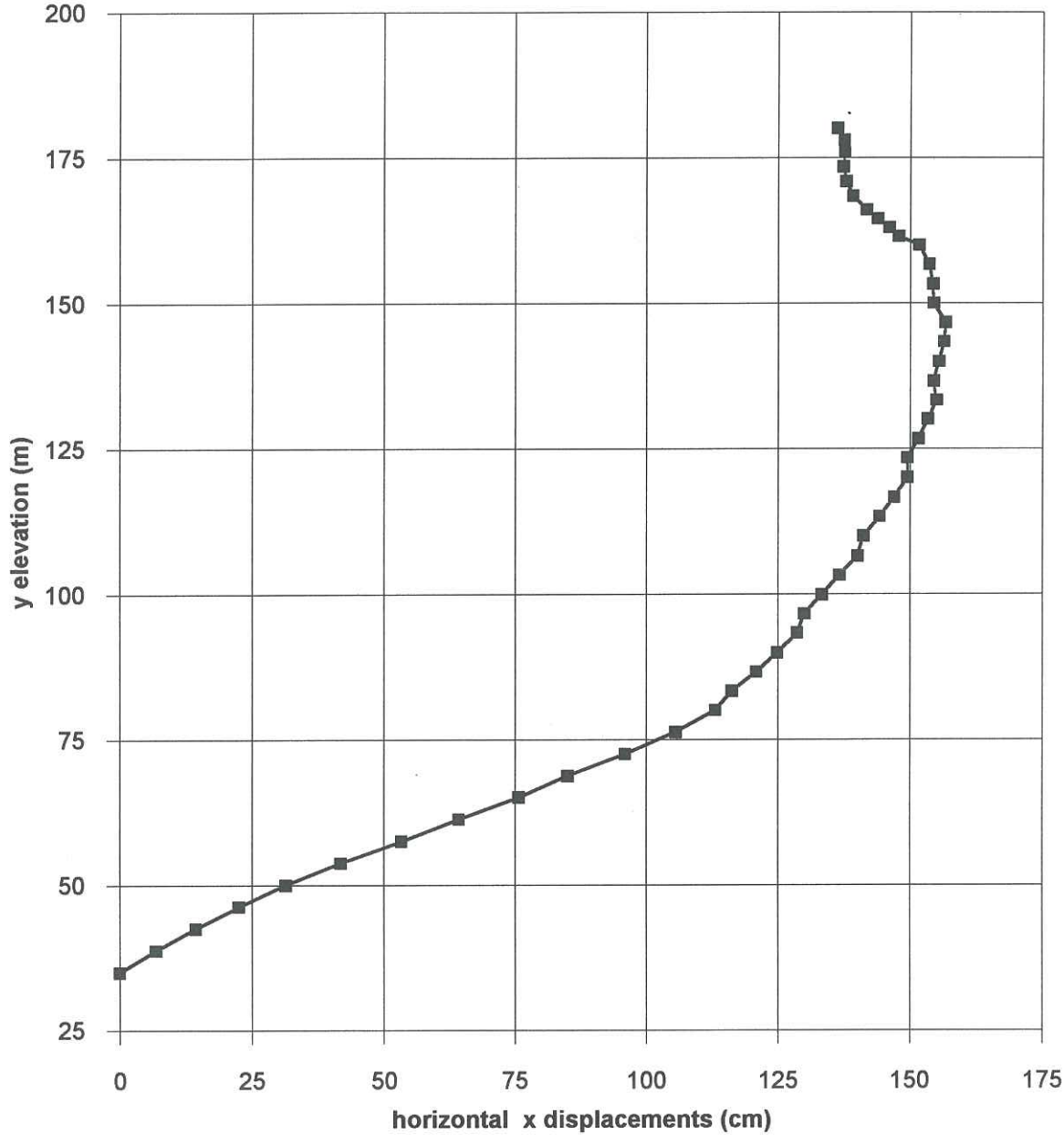

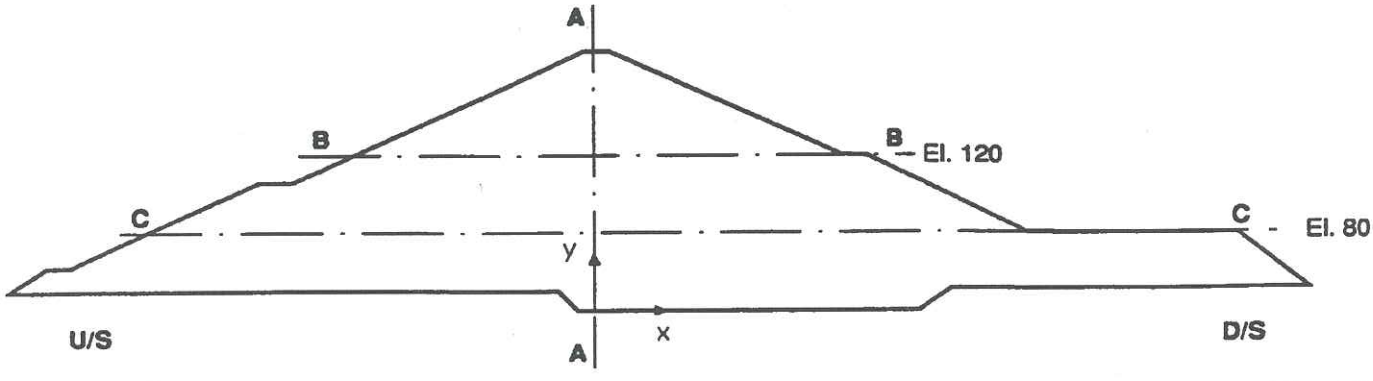

Fig. 12

3rd. ICOLD 1994 - STATIC ANALYSIS

HORIZONTAL DISPLACEMENTS AT THE END OF CONSOLIDATION PHASE
DRUCKER-PRAGER MODEL

SECTION B-B

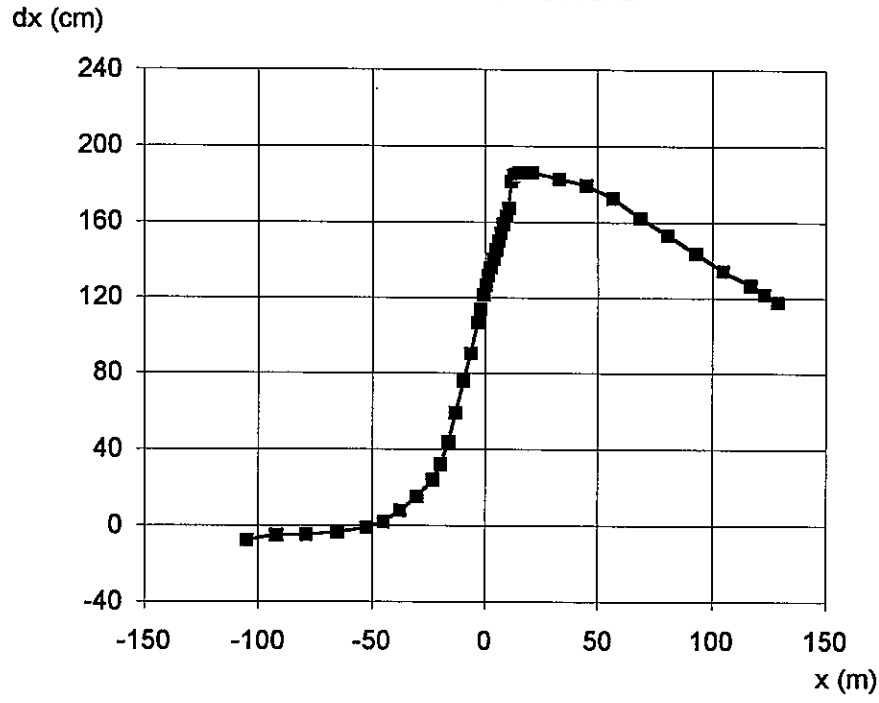

SECTION C-C

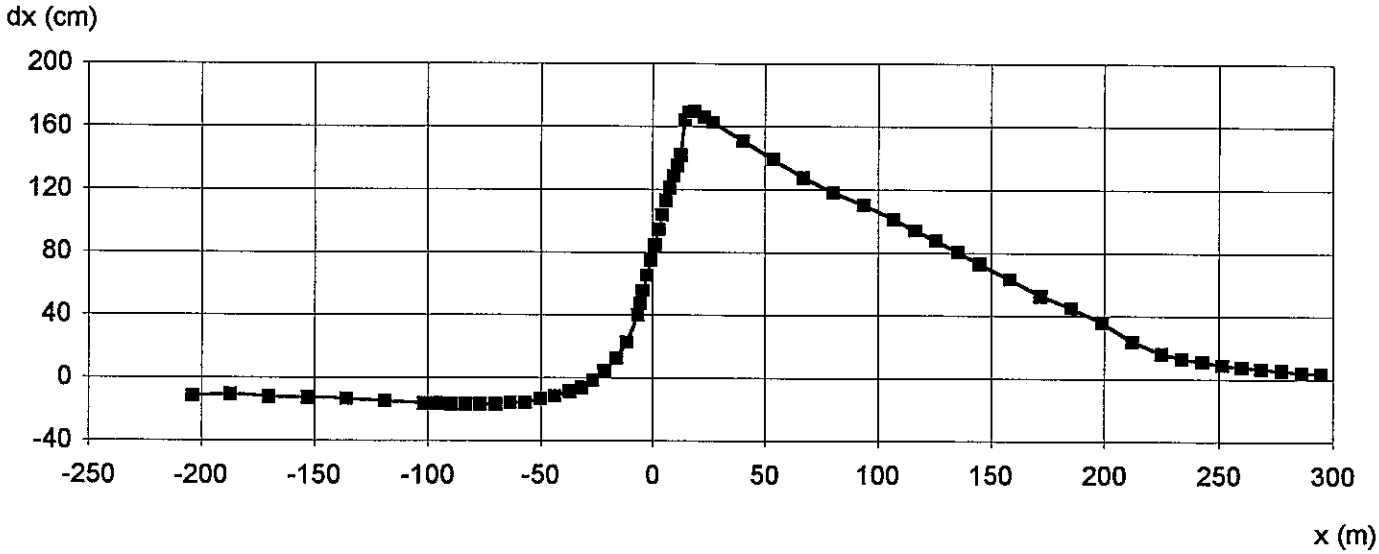

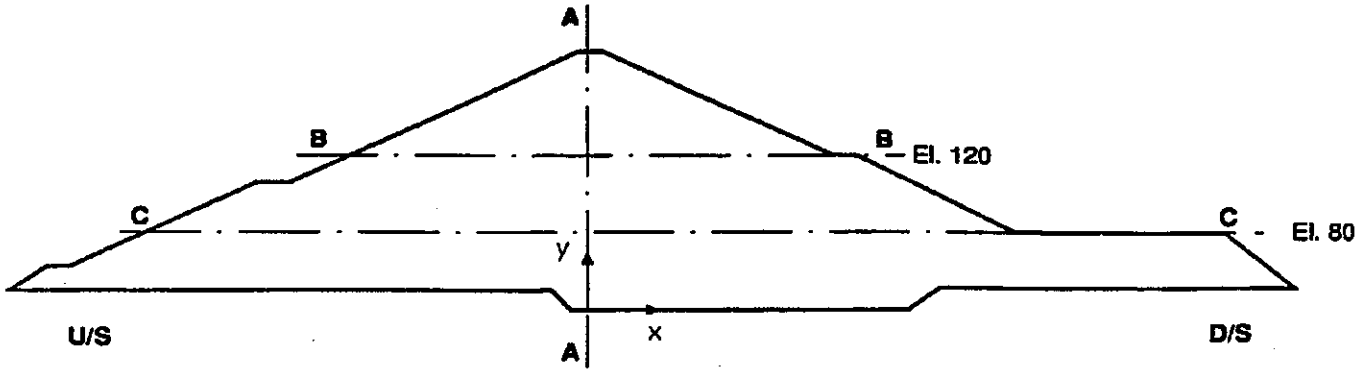

Fig. 13

3rd. ICOLD 1994 - STATIC ANALYSIS

SETTLEMENTS PROFILE AT THE END OF CONSOLIDATION PHASE
DRUCKER-PRAGER MODEL

SECTION A-A

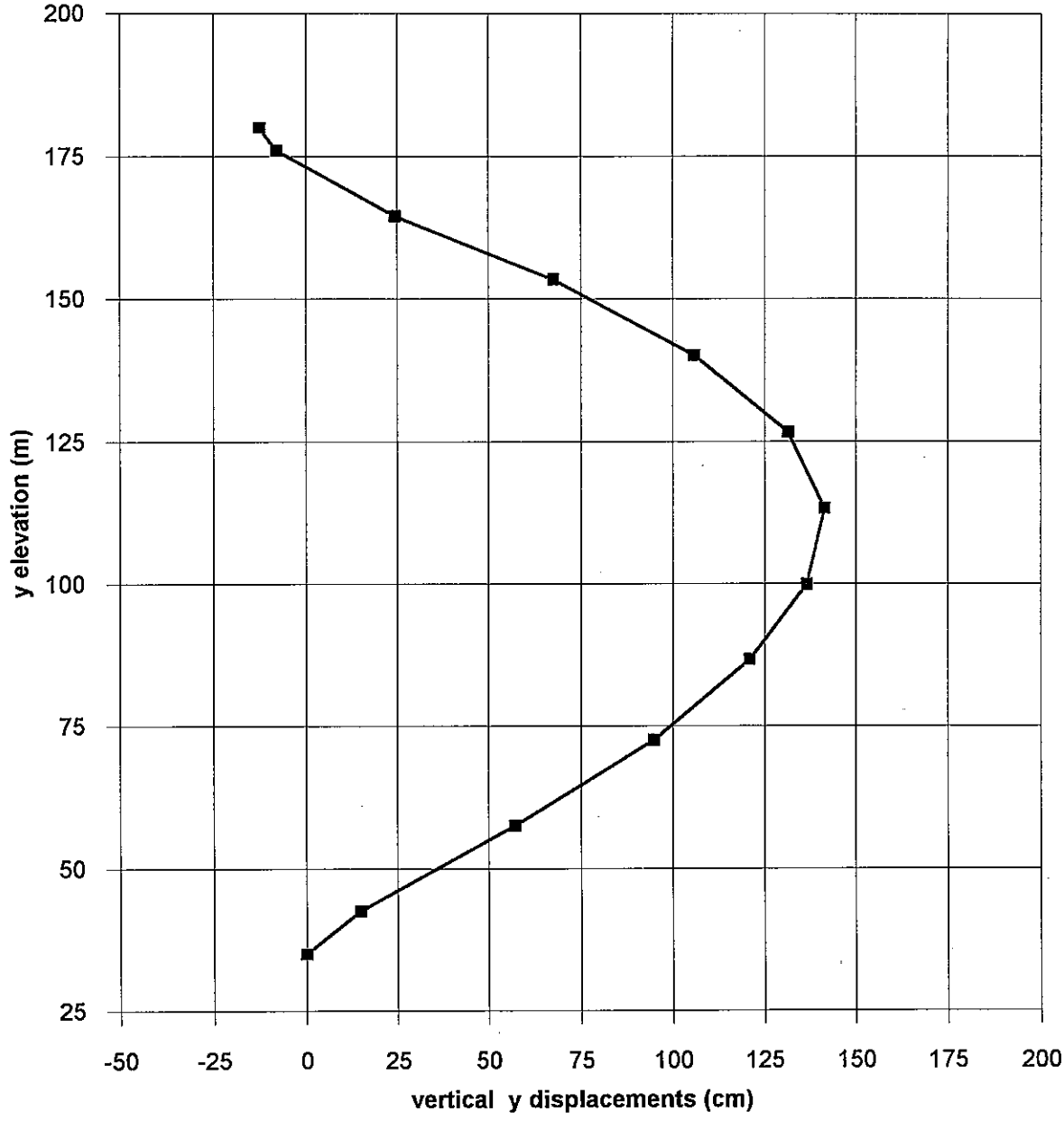

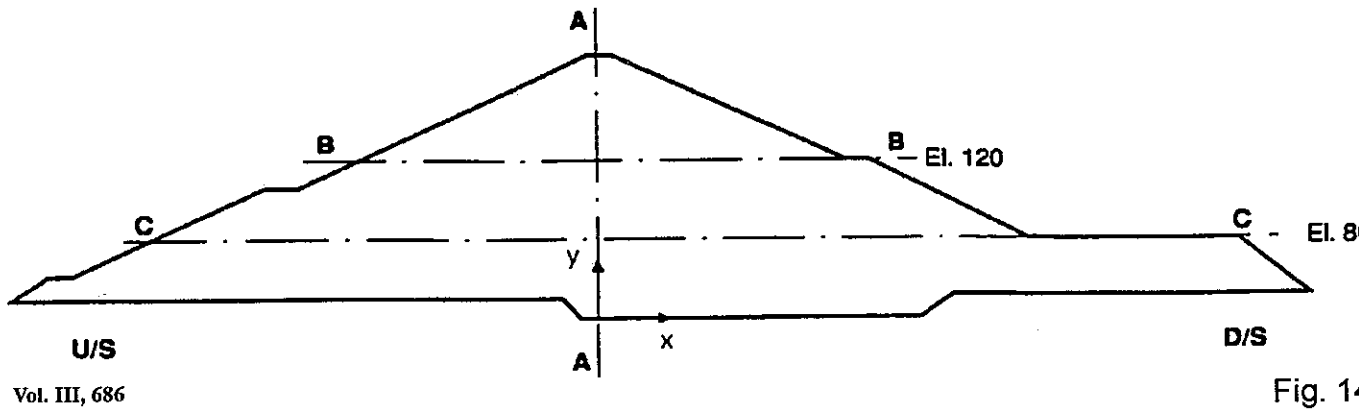

Fig. 14

3rd. ICOLD 1994 - STATIC ANALYSIS

SETTLEMENTS PROFILE AT THE END OF CONSOLIDATION PHASE
DRUCKER-PRAGER MODEL

SECTION B-B

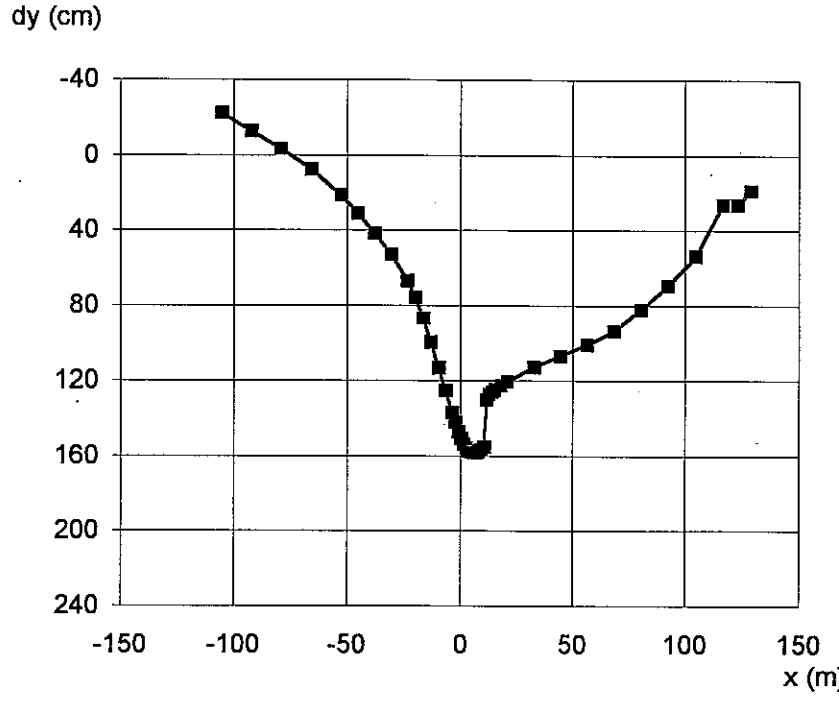

SECTION C.C

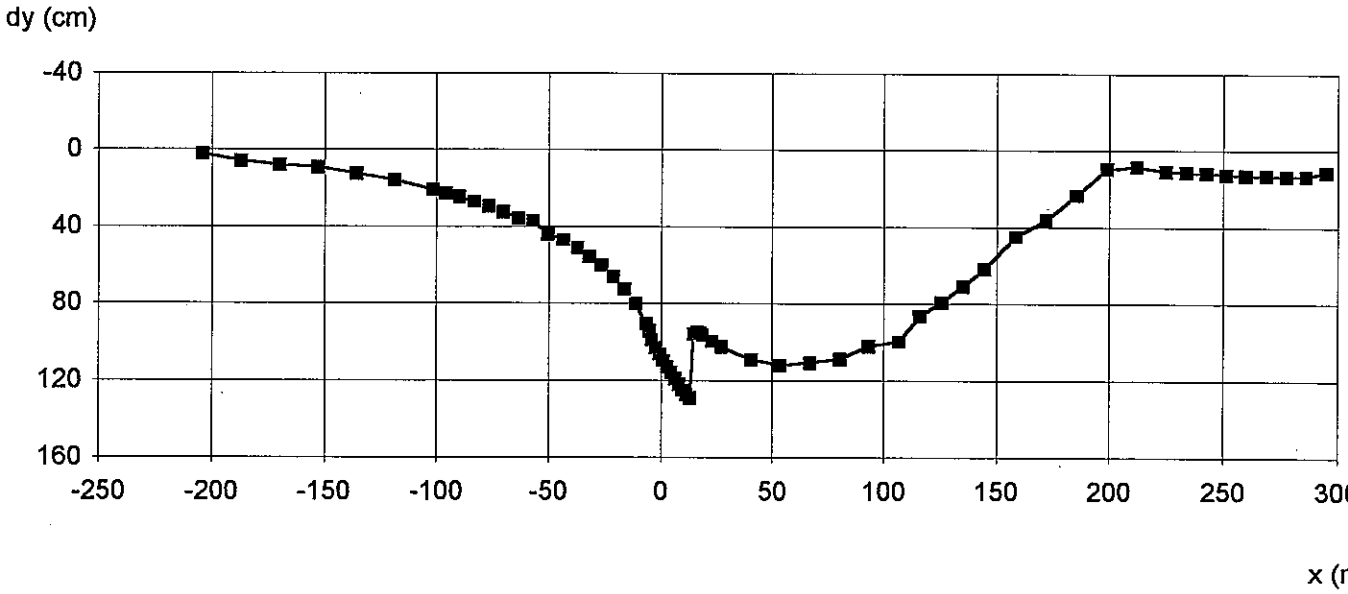

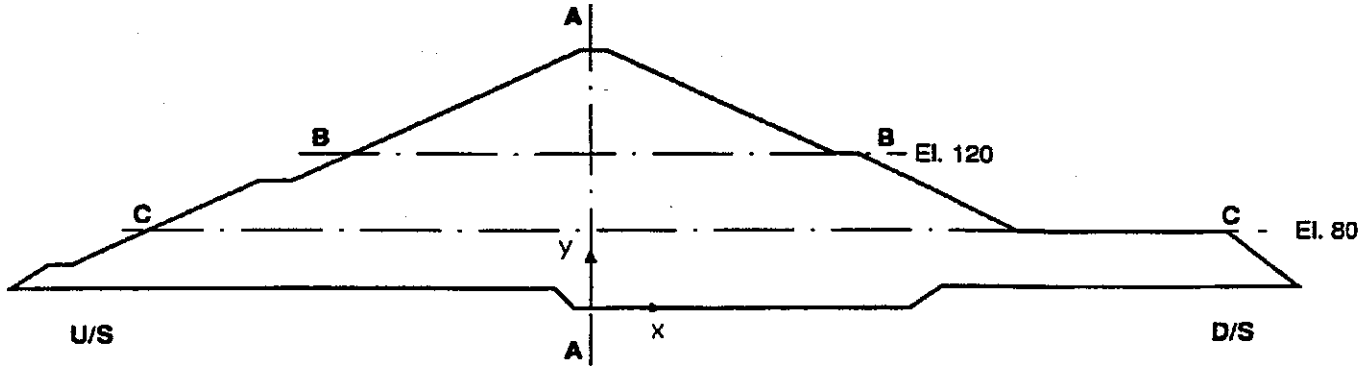

X DISPLACEMENTS - Y DISPLACEMENTS - E.P.W. PRESSURES VS TIME
DRUCKER-PRAGER MODEL

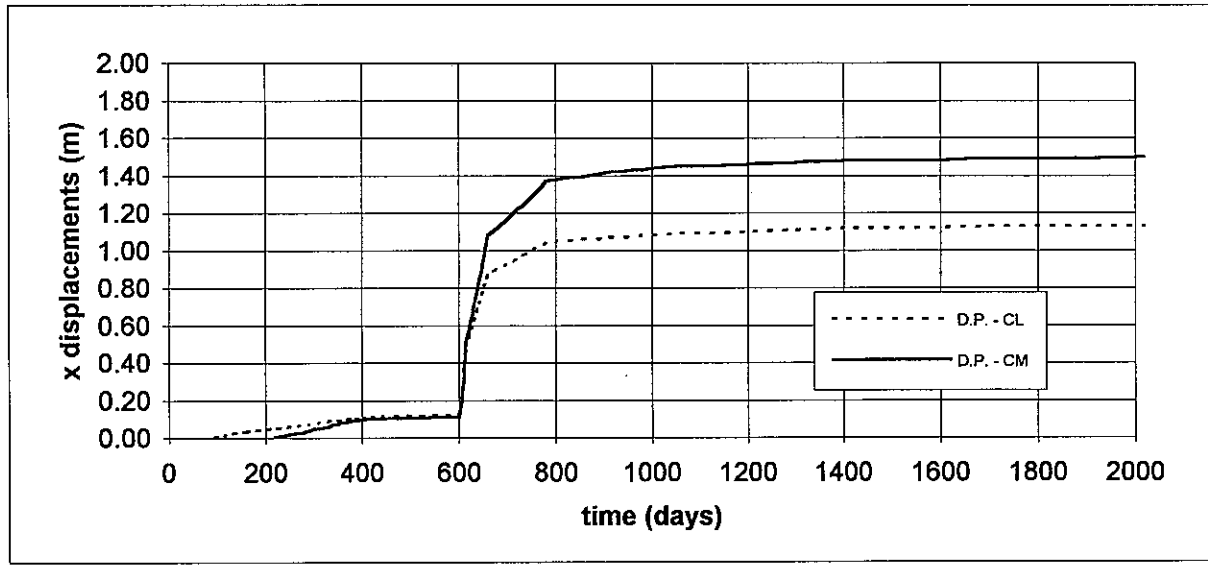

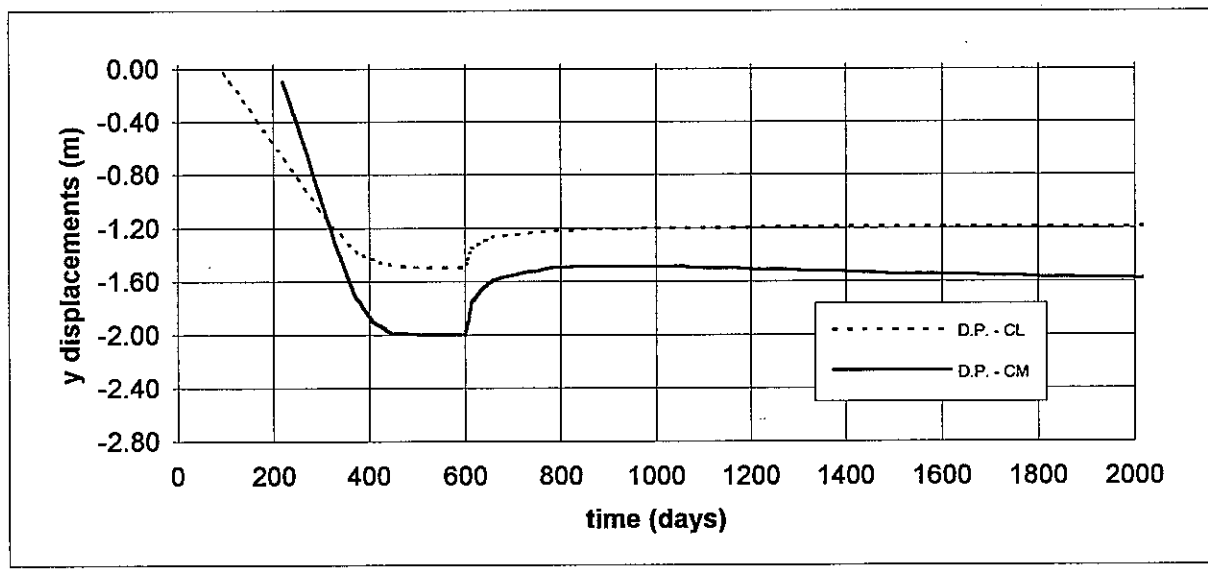

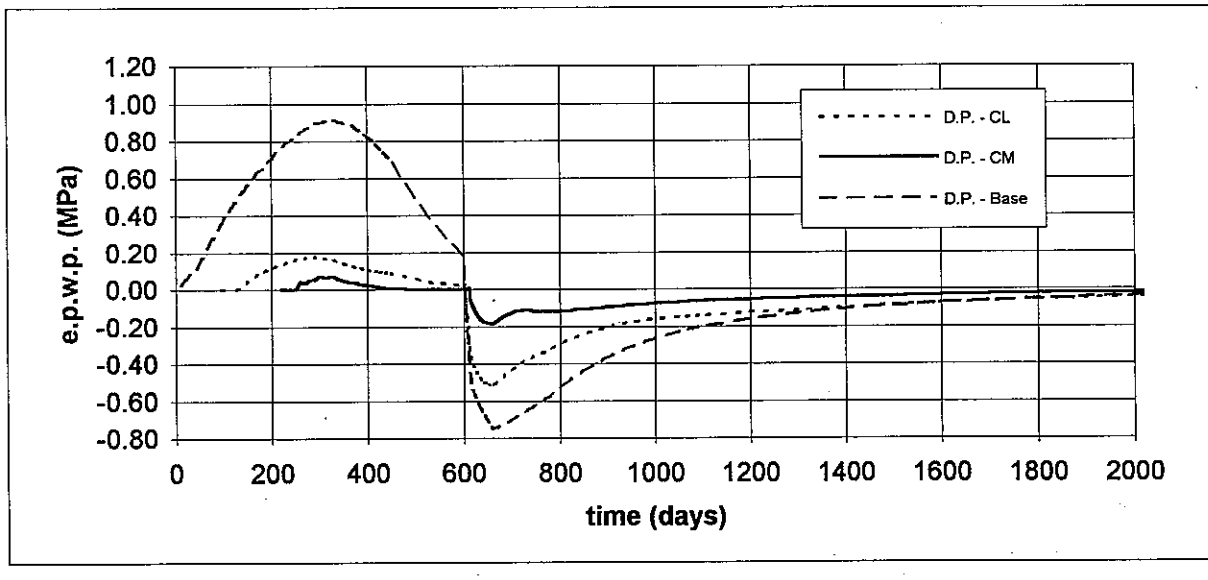

Fig. 16

ANALYSIS OF THE BEHAVIOUR OF AN EMBANKMENT DAM USING PECPLAS FINITE ELEMENT PROGRAM

I. Shahrour & H. Mroueh
Laboratoire de Mécanique de Lille
Département Sols - Structures
Ecole Centrale de Lille

INTRODUCTION

In this paper we present results of numerical simulation of an earth embankment dam. This is work is a part of the third Benchmark Workshop on Numerical Analysis of Dams organized by the International Commission on Large Dams (ICOLD) and intended to compare numerical procedures and programs used for the calculation of embankment dams.

The example proposed by the ICOLD refers to the El Infiernillo embankment Dam in Mexico. On the request of the ICOLD, calculations were carried out using a non associated elastic perfectly-plastic model with the Mohr-Coulomb criterion.

Finite element analyses were performed using the finite element program PECPLAS (Shahrour, 1992). This program offers some facilities for the resolution of geotechnical problems, mainly : (i) the description of the soil behaviour using elastic perfectly - plastic constitutive models or more advanced elastoplastic constitutive relations involving isotropic and kinematic hardening (ii) the consideration of fluid-skeleton interaction for fully saturated soil under both static and dynamic loading (iii) the consideration of interface conditions and (iv) theconsideration of the evolution of both the geometry and material properties during loading.

After a presentation of the methodology followed in this work, we will describe results obtained under static loading.

METHODOLOGY

Calculation of the dam embankment involves three phases : construction, reservoir impounding and finally the consolidation at the end impounding.

As during both construction and impounding phases, the soil material is not fully saturated, calculation should by performed using a partially saturated modelling which is not available in the finite element program PECPLAS. In order to overcome this difficulty analyses were carried out in total stresses.

- For the construction phase, no coupling was considered between pore pressure and skeleton. Two calculations were performed in order to investigate the

influence of the construction modelling. In the first one, a construction in 15 layers was considered; while in the second, only one layer was considered in the analysis.

- The impounding phase was analysed assuming a 'steady-state' condition (at the end of the consolidation phase). Calculation was performed in two steps : in the first one, a finite element analysis was performed for the determination of the pore pressure distribution. Then, the latter was considered as an external loading on the soil material.

DESCRIPTION OF THE MOHR-COULOMB CONSTITUTIVE MODEL

A non associated elastic perfectly plastic constitutive model was used in this study. The elastic part is assumed to be linear and isotropic. It involves two constitutive parameters : Young modulus and Poisson's ratio.

The Mhor - Coulomb criterion is used for the yield function :

$$f = p\sin\phi + \sqrt{J_2}\cos\theta - \sqrt{\frac{J_2}{3}}\sin\phi\sin\theta - c\cos\phi$$

c and ϕ designate the cohesion and the friction angle, respectively, while p, J2 and q stand for the mean pressure, the second invariant of the deviatoric stress tensor and the Lode angle, respectively. Their expressions are :

$$p = \frac{\sigma_{ii}}{3} \qquad J_2 = \frac{1}{2}s_{ij}s_{ij} \qquad s_{ij} = \sigma_{ij} - p\delta_{ij}$$

$$\theta = \frac{1}{3}\sin^{-1}\left[-\frac{3\sqrt{3}}{2}\frac{J_3}{J_2^{3/2}}\right] \qquad J_3 = \frac{s_{ij}s_{jk}s_{ki}}{3}$$

The plastic potential is given by :

$$g = p\sin\psi + \sqrt{J_2}\cos\theta - \sqrt{\frac{J_2}{3}}\sin\theta\sin\psi$$

where ψ is the dilatancy angle.

The set of constitutive parameters used in numerical simulation is given in table 1. It was proposed by the organisation committee of the workshop.

parameter	Core (clay)	Filters (sand & alluvial deposits)	Transition (Muck) D_{10}=2mm	Rockfill
E (MPa)	40	40	40	40
ν	0,3	0,3	0,3	0,3
ϕ	25	35	42	42
c (MPa)	0	0	0	0
ψ	5	5	5	5

Table 1 : Mechanical properties of constitutive materials

SIMULATION OF TRIAXIAL PATHS

In order to check the numerical implantation of the Mohr-Coulomb constitutive model, the organisation committee requested to provide numerical simulation of a drained and an undrained triaxial paths with the set of parameter of the core material (table 1) and a cell pressure σ_3 =5 00 kPa. Figures 1 and 2 give the results of the simulation of these paths.

RESULTS OF F.E. CALCULATIONS

The organisation committee proposed a mesh composed of 6- and 8-node isoparametric elements. As PECPLAS does not allow users to combine these elements, we used the mesh shown in figure 3. It is composed of 218 (8-node) elements.

In the following we give the distribution of both field displacement and pore pressure and their evolution along three main lines (Figure 4):

- vertical line in the core (AA)
- horizontal line at El. = 120 (BB)
- horizontal line at El. = 80 (CC).

First phase : Construction of the dam

As mentioned in the first section, this phase was simulated in total stress. No coupling was assumed between pore pressure and skeleton.

A first calculation was carried out assuming a construction procedure in 15 steps. Figure 5a shows the deformation of the dam at the end of construction. It can be observed that the latter is particularly concentrated in the core.

Figure 5b shows the evolution of the field displacement along the line A-A. The origin of the field displacement in a material point is supposed to coincide with its construction. It can be observed that vertical displacement predominates. It increases with the elevation up to El. = 110 with a maximum of about 1.78m and then it decreases.

In order to illustrate the influence of the simulation of the construction procedure, a second calculation was performed assuming a construction in one layer. Table 2 gives the result of this calculation both with those of the construction in 15 layer. In this table the field displacement is calculated relatively to the dam foundation. It can be noted that calculation assming one layer underestimates the vertical displacement. Discrepancy on the field displacement between the two hypotheses attains 15% at the dam top (CC).

Point	One layer	15 layers
CC	-3.03	-3.54
CM	-2.6	-2.82
CL	-1.34	-1.41

Table 2 : Influence of the construction procedure on the vertical displacement

Second phase : Reservoir Impounding

Calculation of this phase was carried out in tow steps. In the first one, the pore pressure field was calculated at the ''steady-state' condition. Then, this field was considered as an external loading on the soil material.

Distribution of the of pore pressure

The distribution of the pore pressure was determined by the resolution of a seepage problem with free surface condition. At the upstream face a hydraulic load of 125 m was considered, while the foundation dam was assumed to be impermeable. Figure 6 shows the contour lines of the pore pressure. It can be observed that the latter decreases sharply in the core of the dam.

Field displacement :

Figure7 shows the deformation of the dam induced by both construction and impounding of the reservoir. We can observe that the latter induces an important horizontal displacement in the dam. Figures 8 and 9 show the evolution of the field displacement along lines AA, BB and CC. It can be observed that : in a horizontal line, settlement increases sharply in the vicinity of the core. In the latter, settlement increases with the elevation up to El = 110m and then it decreases. The maximum of settlement is equal to 1.25m. We can observe also that the horizontal displacement increases with elevation up to El. = 110 m and then it stabilizes. The maximum of the horizontal displacement is equal to 1.2m.

CONCLUSION

In this paper we presented a simplified calculation of an embankment dam using the non associated Mohr-Coulomb constitutive model. Since during construction and reservoir impounding, the soil medium in not fully saturated, numerical simulations were carried out in total stresses. The influence of pore pressure was not considered during construction. For the impounding phase, pore pressure was calculated at the ''steady-state' condition by the resolution of a seepage problem with free surface conditions. The pressure distribution was then applied as external loading.

A confrontation of our results to those performed by other predictors will permit us to check the validity of hypotheses assumed in this work.

REFERENCES

I. SHAHROUR "PECPLAS: A finite element software for the resolution of earthwork problems" - Actes du Colloque International Géotechnique, Informatique, Edition Presse ENPC, Paris, pp. 327-334, Sept 1992.

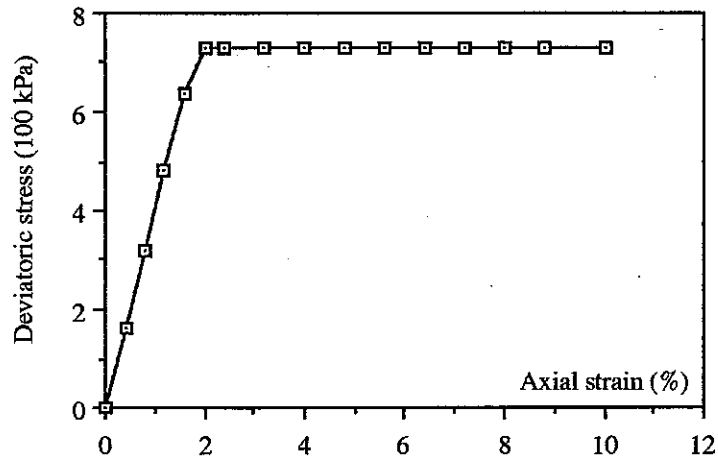

(a)

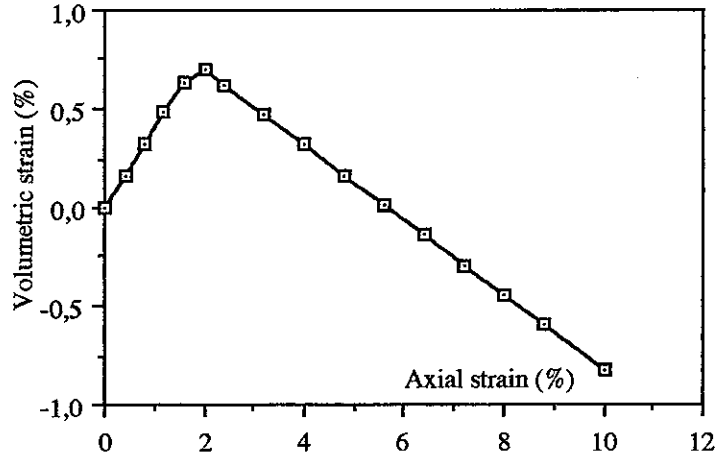

(b)

deviatoric stress	Axial strain	Volumetric strain
732 kPa	0.02	0,007

(c)

Figure 1 : Simulation of the drained triaxial path
(confining pressure = 500 kPa, set of parameters of the core material in table 1)

(a) Evolution of deviatoric stress
(b) Evolution of volumetric strain
(c) Values at the maximum deviatoric stress

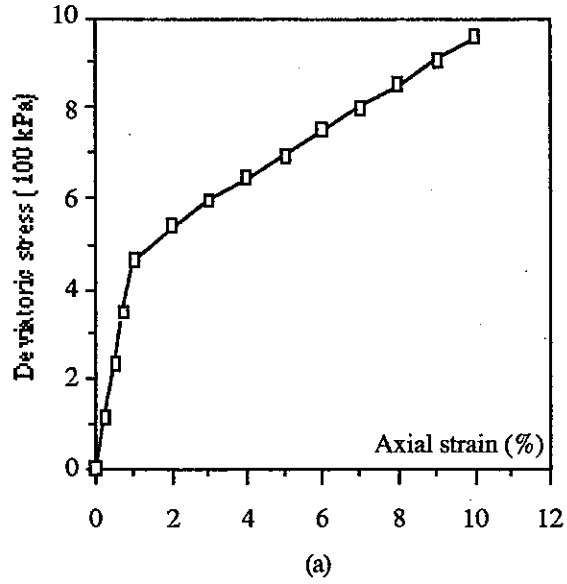

(a)

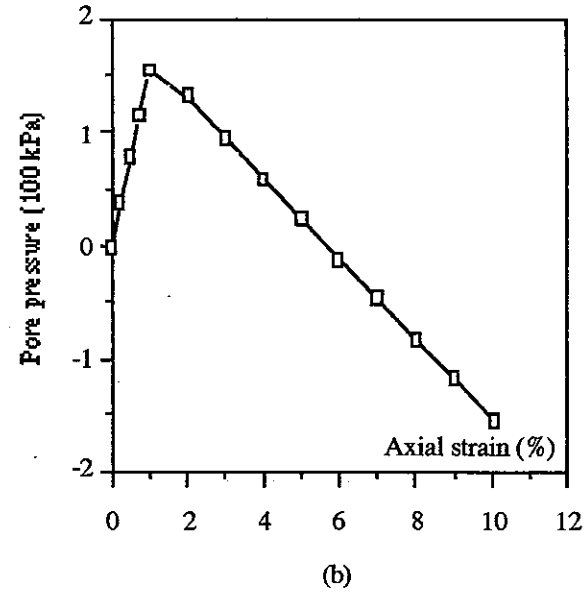

(b)

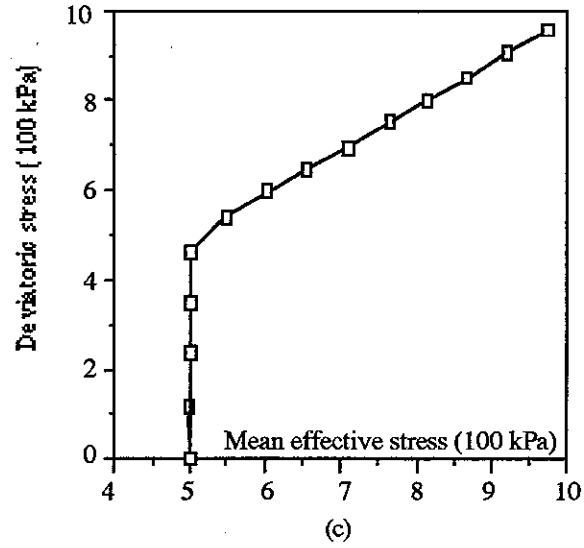

(c)

Deviatoric stress	Excess pore pressure
96 kPa	-155 kPa

(d)

Excess pore pressure	Axial strain	Deviatoric stress
154 kPa	0.01	46,2 kPa

(e)

Figure 2 : Simulation of undrained triaxial path
(confining pressure = 500 kPa, set of parameters of the core material in table 1)
(a) Evolution of deviatoric stress (b) Evolution of pore pressure
(c) Stress path in the (p', q') plane (d) Values at axial strain = 0.01
(e) Values at the maximum of pore pressure.

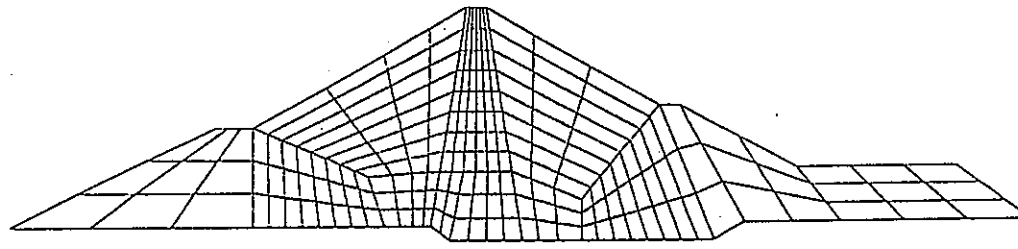

Figure 3 : Finite element mesh used in F.E. calculation
721 nodes 218 (8-node) elements

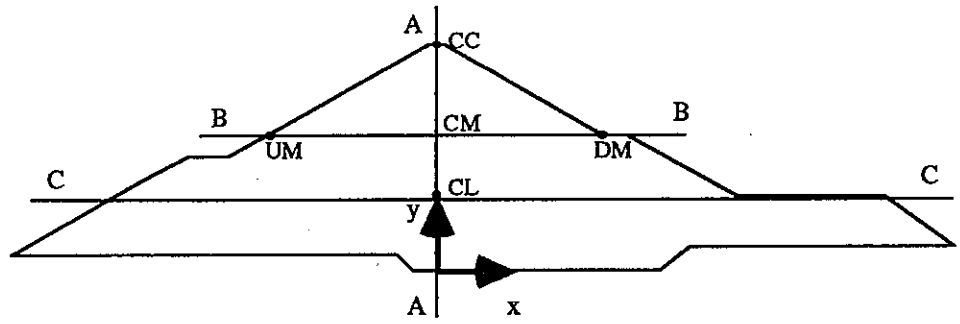

Figure 4 : Position of lines and points used for results displaying

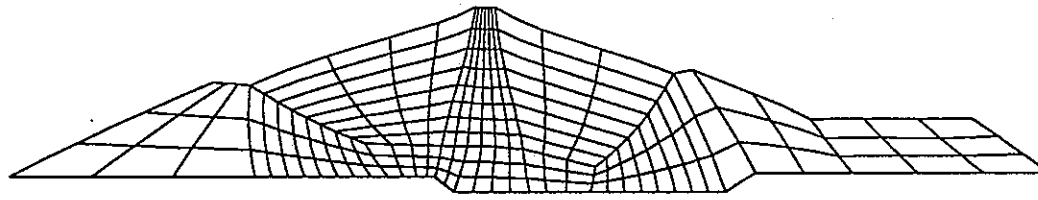

(a)

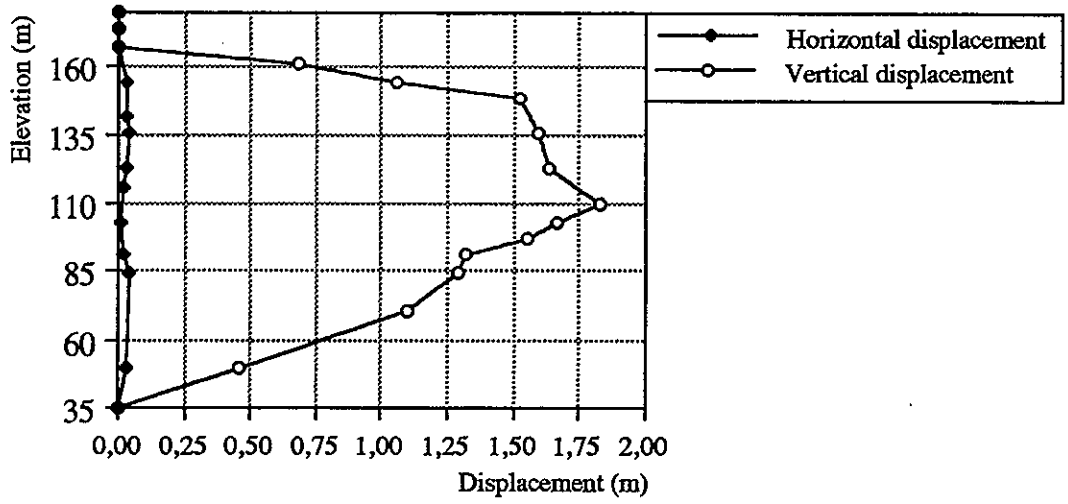

(b)

Point	One layer	15 layers
CC	-3.03	-3.54
CM	-2.6	-2.82
CL	-1.34	-1.41

(c)

Figure 5 : Field displacement at the end of the dam construction

(a) Deformation pattern
(b) Displacement field along the line AA
(c) Influence of the modelling of the construction procedure

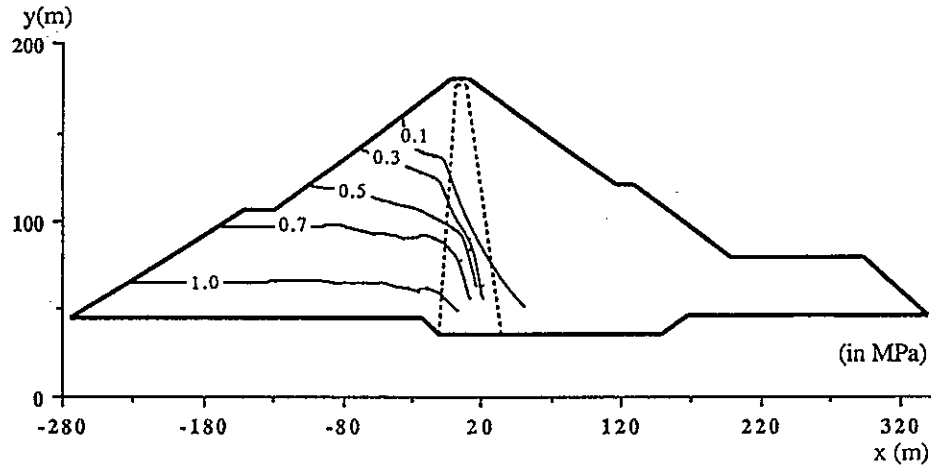

(a)

Point	CC	CM	CL	UM	DM
Pore pressure (100 kPa)	0	3.14	6.96	5	0

(b)

Figure 6 : Pore pressure distribution at the 'steady-state' condition
(a) Contour lines
(b) Values at different points

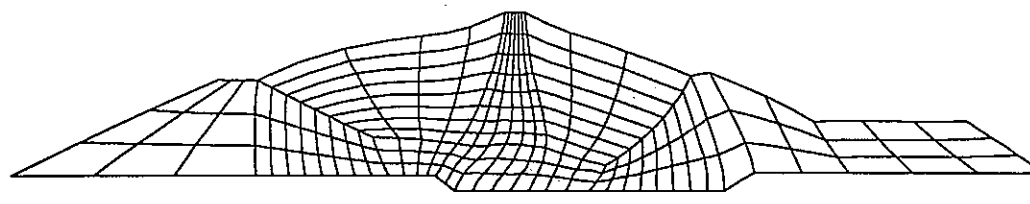

Figure 7 : deformation pattern at the end of consolidation

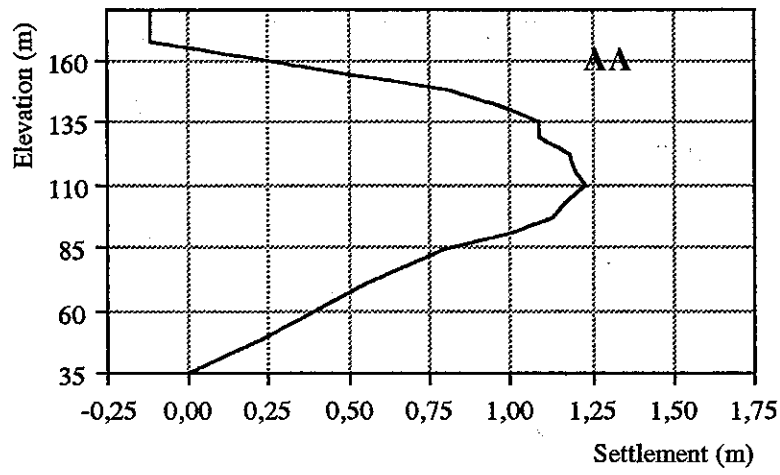

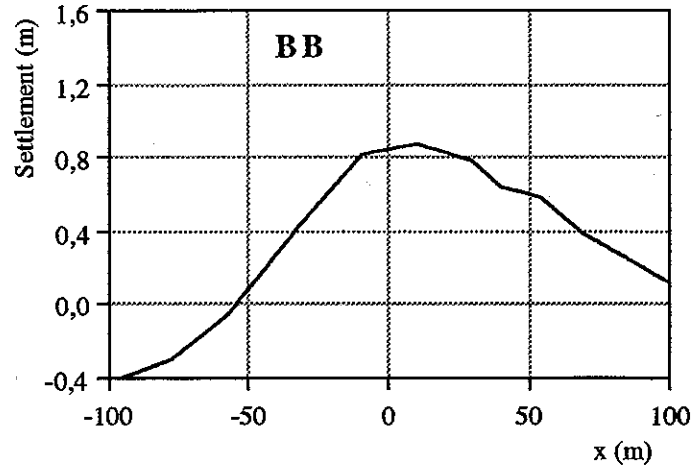

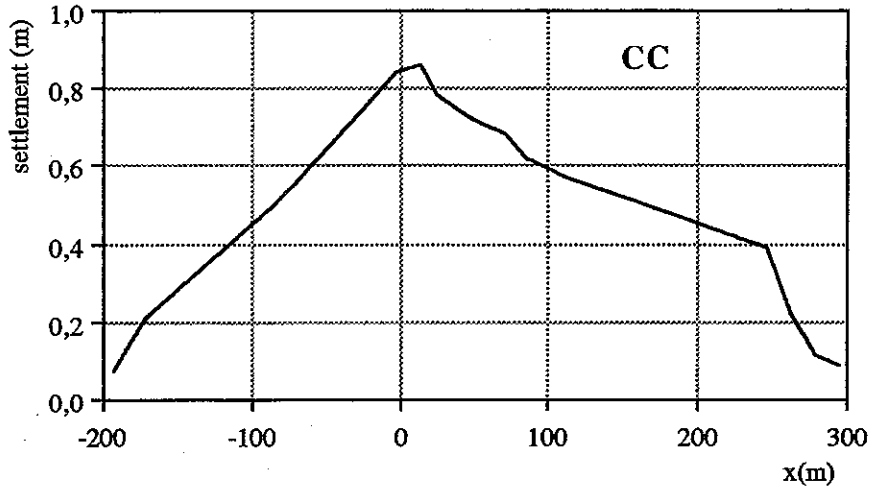

Figure 8 : Settlement at the end of consolidation

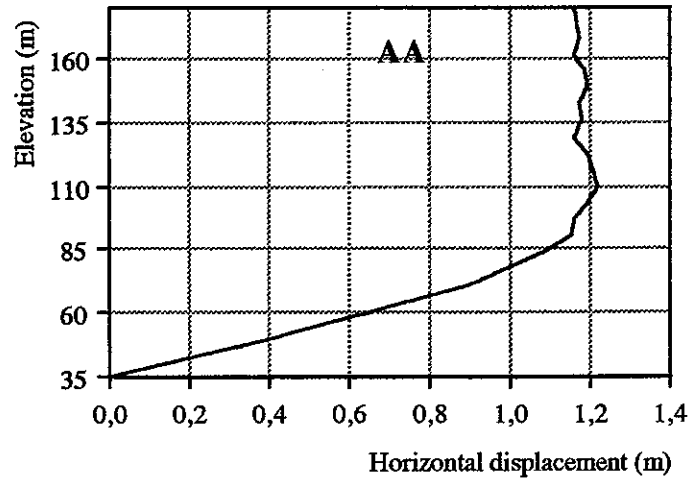

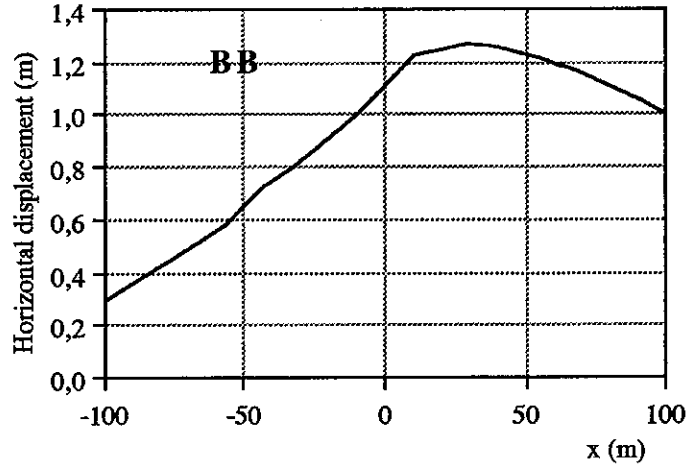

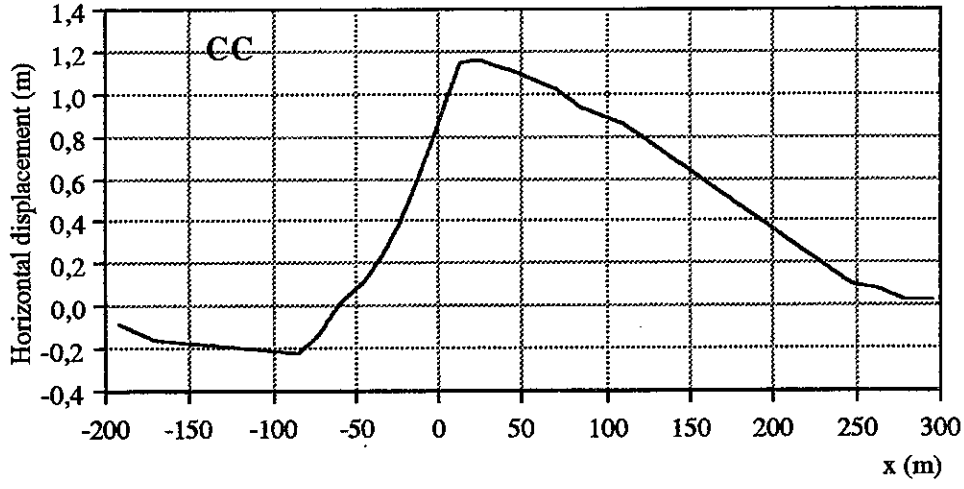

Figure 9 : Horizontal displacement at the end of consolidation

EVALUATION OF PORE PRESSURE AND SETTLEMENTS OF AN EMBANKMENT DAM UNDER STATIC LOADINGS

L.Guellouz[1,2] - S.Bonelli[1] - O.Débordes[2] - P.Royet[1]

(1) French Institute of Agricultural and Environmental Engineering Research CEMAGREF - Le Tholonet BP31, 13612 Aix-en-Provence cedex 1, France.

(2) Mediterranean Institute of Technology - Laboratory of Mechanic and Acoustic IMT / LMA - Technopôle de Château Gombert, 13451 Marseille cedex 20, France.

This paper deals with the construction, impounding and consolidation of El Infiernillo embankment dam. The difficulties are of several kinds : complex loading, hydromechanical coupling, non-linear behaviour and important heterogeneity of material properties. A fully coupled model is presented. Some assumptions corresponding to this special case lead to numerical simplifications.

1. HYDROMECHANICAL MODEL

The small displacements and small strains assumption yields to the usual definition of the infinitesimal strain :

$$\vec{\vec{\varepsilon}}=\frac{1}{2}\left(\vec{\nabla}_x\vec{u}+\vec{\nabla}_x\vec{u}^T\right)$$

The total strains and stresses are decomposed into deviatoric and spheric parts :

$$\vec{\vec{\varepsilon}}=\vec{\vec{\varepsilon}}^d+\frac{\varepsilon^v}{3}\vec{\vec{\delta}} \qquad \vec{\vec{\sigma}}=\vec{\vec{\sigma}}^d+\sigma_m\vec{\vec{\delta}}$$

The mass conservation of the incompressible solid phase leads to the relation of the porosity function of the volumetric strain :

$$n=1-(1-n^0)\exp(-\varepsilon^v)$$

The influence of the air phase is omited in the mass-conservation and equilibrium equations :

$$n\rho_w\dot{S}_r+nS_r\dot{\rho}_w+S_r\rho_w\dot{\varepsilon}^v+\vec{\nabla}_x\cdot\vec{m}=0$$

$$\vec{\nabla}_x\cdot\vec{\vec{\sigma}}-((1-n)\rho_s+nS_r\rho_w)g\vec{e}_z=\vec{0}$$

The anisotropic Darcy law is assumed :

$$\vec{m}=-\frac{\lambda_r}{g}\vec{\vec{K}}\cdot\left(\vec{\nabla}_x u_w-\rho_w g\vec{e}_z\right)$$

where the permeability tensor is constant :

$$\vec{\vec{K}}=\begin{bmatrix} k_x & 0 \\ 0 & k_z \end{bmatrix}$$

The compressibility of water is described by its bulk modulus in saturated zones :

$$\rho_w=\begin{cases}\rho_w^0 & \text{if } u_w<0\\ \rho_w^0\exp\left(\dfrac{u_w}{\chi_w}\right) & \text{if } u_w\geq 0\end{cases}$$

The retention and relative permeability curves are of Van-Genuchten/Mualem type in unsaturated zones ([1]) :

$$S_r=\begin{cases}\left(1+\left(\dfrac{-\alpha u_w}{p_{atm}}\right)^{\beta}\right)^{1/\beta-1} & \text{if } u_w<0\\ 1 & \text{if } u_w\geq 0\end{cases}$$

$$\lambda_r=S_r^{1/2}\left(1-\left(1-S_r^{\beta/(\beta-1)}\right)^{1-1/\beta}\right)^2$$

The partition of total stresses in effective stresses and pore pressure is defined by the Bishop principle ([1], [2]) :

$$\sigma_m=\sigma'_m-S_r u_w$$

The skeleton behaviour is described by a non associated perfect elastoplastic model in effective stresses.

The total strains are assumed to be the sum of an elastic and a plastic contribution. The elasticity is isotropic linear :

$$\sigma'_m=\chi(\varepsilon^v-\varepsilon^{pv}) \qquad \vec{\sigma}^d=2G(\vec{\varepsilon}^d-\vec{\varepsilon}^{pd})$$

$$\chi=\frac{E}{3(1-2\nu)} \qquad 2G=\frac{E}{1+\nu}$$

The non-cohesive Mohr-Coulomb failure surface is approximated by the deviatoric yield criterion of the C.J.S. model ([1]), with fitting parameters giving the same results in triaxial compression and in pure shear loading :

$$f(\sigma'_m,\vec{\sigma}^d)=\|\vec{\sigma}^d\|h(\vec{\sigma}^d)+\sin\varphi'\sigma'_m\leq 0$$

where

$$\|\vec{\sigma}^d\|=\sqrt{\frac{1}{2}\vec{\sigma}^d:\vec{\sigma}^d} \qquad \gamma=1-\left(\frac{3-\sin\varphi'}{2\sqrt{3}}\right)^5$$

$$h(\vec{\sigma}^d)=\left(1+\gamma\frac{3\sqrt{3}\det(\vec{\sigma}^d)}{2\|\vec{\sigma}^d\|^3}\right)^{1/5}$$

The deviatoric plastic strain rate is associated, the volumetric plastic strain rate is non-associated :

$$\dot{\varepsilon}^{pv}=\dot{\lambda}\sin\psi \qquad \dot{\vec{\varepsilon}}^{pd}=\dot{\lambda}\vec{Q}^d$$

The plastic multiplier is defined by the plastic consistency condition in plastic loading :

$$\dot{\lambda}=\frac{2G\vec{Q}^d:\dot{\vec{\varepsilon}}^d+\chi\dot{\varepsilon}^v}{4G\|\vec{Q}^d\|^2+\chi\sin\varphi'\sin\psi} \qquad \vec{Q}^d=\left(\vec{\nabla}_\sigma f\right)^d$$

In an undrained analysis, the volumetric moisture content is constant, leading to :

$$\rho_w S_r e=\rho_w^0 S_r^0 e^0 \qquad e=\frac{n}{1-n}$$

In this case, the pore pressure depends on volumetric strain via the retention curve in unsaturated zone or via the water bulk modulus in saturated zone ([2], [3], [4]) :

$$u_w=\begin{cases}-\frac{p_{atm}}{\alpha}\left(\left(\frac{S_r^0 e^0}{e}\right)^{\beta/(1-\beta)}-1\right)^{1/\beta} & \text{if } e>S_r^0 e^0\\ \frac{\chi_w}{n}\ln\left(\frac{1+S_r^0 e^0}{1+e}\right) & \text{if } e\leq S_r^0 e^0\end{cases}$$

The materials properties ρ_s, E, ν, φ', ψ, k_x and k_z are defined by the benchmark for each material; g=9,81 m/s^2 and p_{atm}=100 kPa. The drained permeabilities are $k_x=k_z=10^{-1}$ m/s. For the water, $\chi_w=2.10^5$ kPa and $\rho_w^0=10$ kN/m^3. The S_r and λ_r curves are defined by $\alpha=10^{-3}$ and $\beta=2$ for the core and by $\alpha=10^{-2}$ and $\beta=2,5$ for the drained materials.

2. NUMERICAL METHOD

The boundary problem defined by the mass-conservation and the equilibrium equations is discretized with quadratic finite elements and reduce integration, and with a fully implicit Euler scheme ([1]). The proposed mesh is used for both hydraulical and mechanical problems.

During the construction phase, the core is almost saturated. The low value of permeability allowed to negate the water flow and to perfom an undrained analysis. Only the equilibrium equation is solved (figure 1).

During the impounding phase, the problem is fully coupled. A sequentially decoupled scheme ([2]) is choosen for the sake of simplicity (figure 2) :

1. the displacements field is estimated with an undrained analysis;

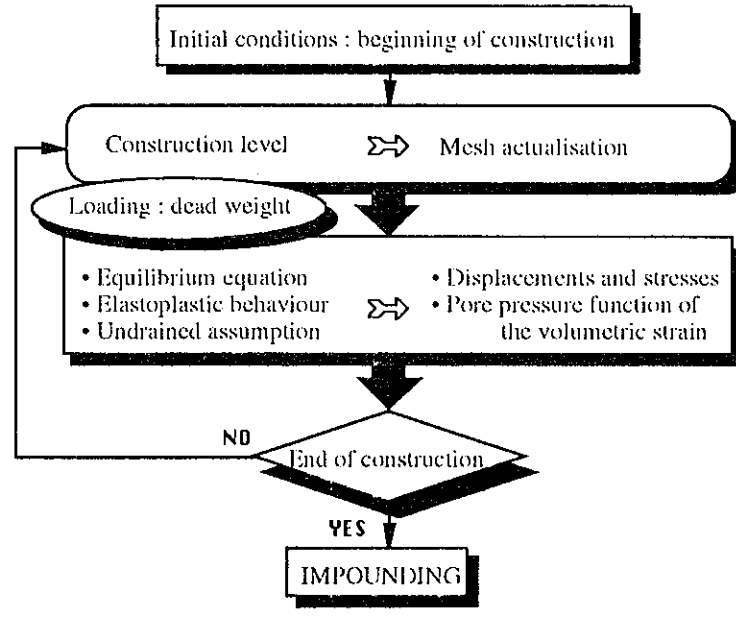

Fig. 1 • Construction phase analysis

2. the unsteady mass-conservation equation is integrated to compute the pore pressure field;

3. the equilibrium equation is then solved to compute the displacements.

The consolidation phase ends when the pore pressure and the displacement velocity are negligible at constant reservoir level (169 m). The pore pressure field is calculated by solving the steady mass-conservation equation, allowing to compute the displacement field by solving the equilibrium equation (figure 3). As the elastoplastic model is of dissipative type, this choice is limited by small variations of pore pressure between the end of impounding and the end of consolidation.

The Newton-Raphson method is used to solve non linear equations. The convergence norms are of maximum undimensional type :

- $\frac{\|\text{residual forces}\|_\infty}{\|\text{internal forces}\|_\infty} \leq \text{tol}$

  (tol=10^{-8} for the mass-conservation equation and tol=10^{-3} for the equilibrium equation);

- $\frac{\|\text{iteration incremental solution}\|_\infty}{\|\text{step incremental solution}\|_\infty} \leq \text{tol}$

  (tol=10^{-4}).

Time steps are manually choosen, big enough to avoid spurious oscillations, and small enough to insure the validity of sequential coupling and the convergence of non linear resolutions.

At each spatial integration point, the elastoplastic model is written as an ordinary differential equation. The five order explicit scheme of Dormand&Prince with adaptative time sub-steps is used (tol=10^{-6}) ([1], [5]).

The undrained and drained triaxial simulations of the core are performed with a single axisymmetric finite element and are given in appendix.

The initial state is defined by zero displacements, zero stresses. The initial porosity, degree of saturation and hydraulic head are given in table 1. The initial degree of saturation in the core is 0.96, corresponding to a succion of 0.3 MPa [7]. The initial hydraulic head is not a data and is assumed.

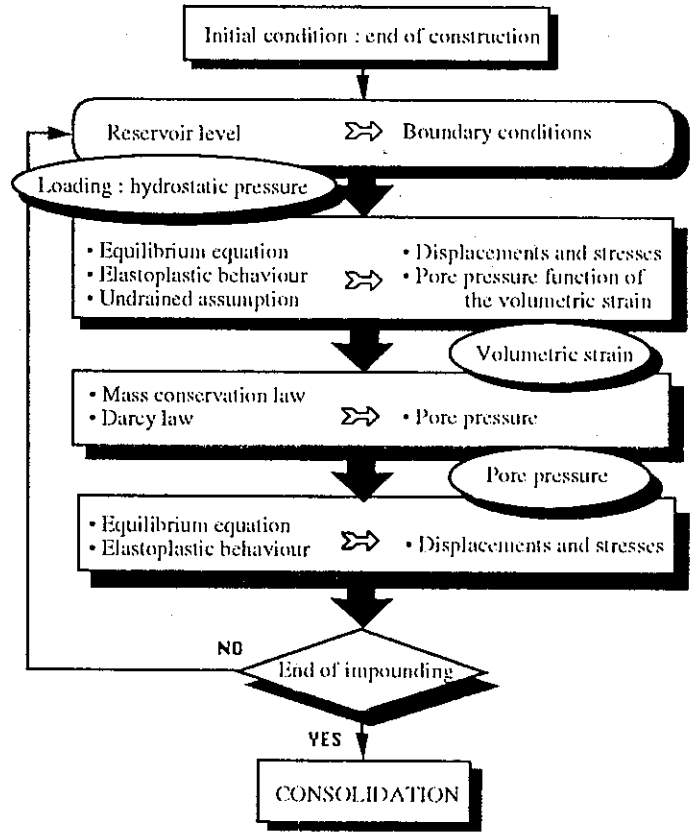

Fig. 2 • Impounding phase analysis

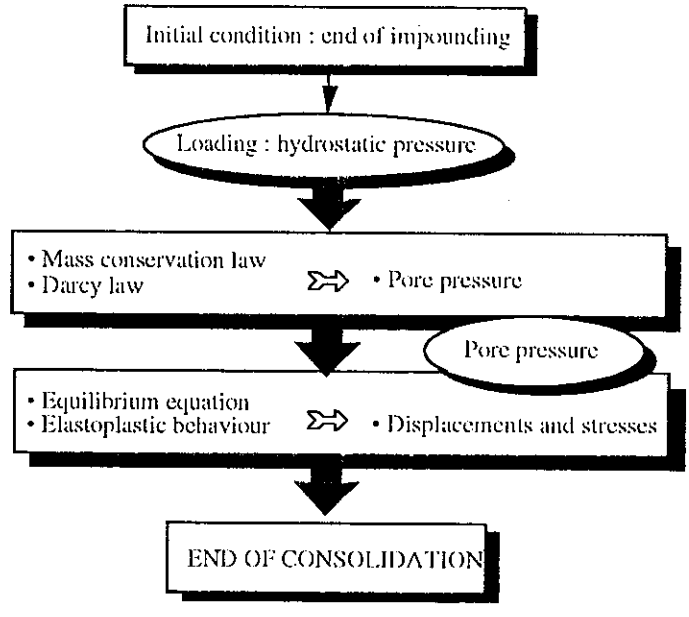

Fig. 3 • Steady state analysis

	Core	Filters	Trans.	Rockfill Dum.	Rockfill Comp.
n^0	0.421	0.322	0.265	0.350	0.317
S_r^0	0.96	-	-	-	-
$H^0=\frac{u_w^0}{\rho_w^0 g}-z$	-	35 m	35 m	35 m	35 m

Table 1 • Initial conditions of construction

The main assumptions depending on the construction and the impounding level are summarized on figure 4.

The hydraulical and mechanical boundary conditions are described on figures 5.a and 5.b. As all the mesh is considered, no seepage problem has to be solved at the downstream face of the core.

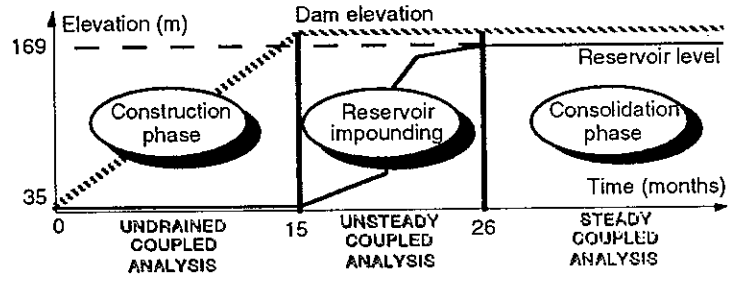

Fig. 4 • Assumptions

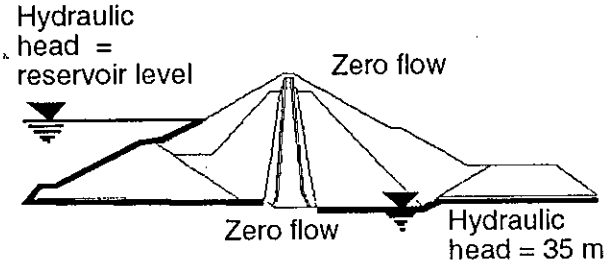

Fig. 5.a • Hydraulical boundary conditions

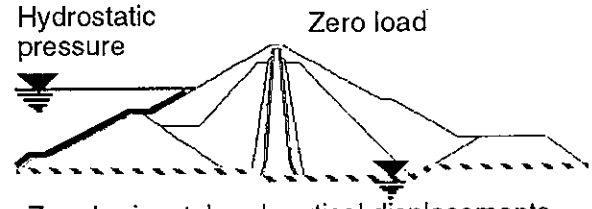

Fig. 5.b • Mechanical boundary conditions

3. SOFTWARE

The software is S.I.C.3 (Interactive Computing System - University of Technology of Compiègne [6]), on a Station DEC Alpha 3000. The geomechanical software has been developped by the CEMAGREF since 1990.

The mass-conservation equation is solved in ≈100 iterations : the tangent matrix is ill-conditionned because all materials are considered. The equilibrium equation is solved with ≈3 iterations.

The hydraulical problem involves 1156 equations with a symmetric tangent matrix. The mechanical problem involves 2206 equations with an unsymmetric tangent matrix.

The contour lines are performed with MOSAIC 2.7 (Framasoft+CSI).

The elapsed time are 15mn for the construction (45 steps), 2h for the impounding (39 steps) et 2mn for the end of consolidation.

4. RESULTS

The contour lines of effectives stresses are given figures 7a, 7b et 7c. The contour lines of pore pressure are given figures 7d and 8. The pore pressure at the end of construction at the core base are important (≈1.2 MPa). The displacements are given in table 2, 3 and 4 and figures 9, 10, 11 and 12.

The construction phase is performed with an undrained analysis : the rate of elevation is thus non considered. This assumption leads to under-estimated displacements and over-estimated pore pressure.

The impounding phase is performed with a fully coupled analysis, but the resolution scheme is explicit (no iteration between the hydraulical and the mechanical problems).

	Points of the Dam Section				
	CC	CM	CL	UM	DM
End of construction	0	3	6	-16	20
End of Impounding	77	130	111	2	74
End of consolidation	77	132	112	2	75

Table 2 • Horizontal displacements (10^{-2}m)

	Points of the Dam Section				
	CC	CM	CL	UM	DM
End of construction	-4	-132	-109	-13	-7
End of Impounding	-19	-141	-117	28	-6
End of consolidation	-17	-137	-113	28	-5

Table 3 • Vertical displacements (10^{-2}m)

The end of consolidation is reached with a steady state analysis. Because the elastoplastic model is dissipative, this assumption can lead to under-estimated displacements and over-estimated pore pressure.

According to the low permeability of the core, it would be better to take a layer of foundation in the mesh, to get easier boundary conditions and a better description of the groundwater flow. This point is important too for the numerical treatement when the mesh involves all materials : the addition of a saturated layer of foundation usually leads to better convergence of the hydraulical problem.

Between the end of construction (fig 6.a) and the end of impounding (fig 6.b), the buoyancy forces cause an important uplift of the upstream rockfill (40 cm). As this fact is not physically realistic, more research are needed to describe the real mechanical behaviour of rockfills from dry to wet conditions.

These results can be considered as a first approach, allowing to handle more complex numerical treatement and sophisticated models.

	Points of the Dam Section				
	CC	CM	CL	UM	DM
End of construction	-	-0.15	0.20	-0.85	-0.85
End of Impounding	-0.12	0.37	0.52	0.49	-0.72
End of consolidation	-0.12	0.40	0.59	0.49	-0.72

Table 4 • Pore pressure (MPa)

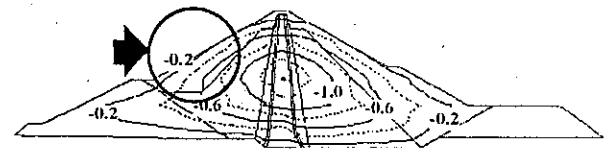

Fig 6.a • Vert. disp. (m) - end of construction

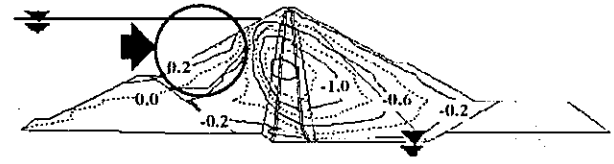

Fig 6.b • Vert. disp. (m) - end of impounding

5. CONCLUSION

The hydromechanical model has been choosen as complete and as simple as possible. The results have to be considered like approximations of the physical phenomenon, according to the simple behaviour considered here. The mesh definition, the order of the spatial integration and the size of the time steps play an important role for the accuracy of the results, but this importance is still difficult to assess today for coupled problems. The choice of the initial conditions and the boundary conditions are essential too, mostly when the foundation is not modelized. This over-simplified model can however give a good description of the interaction between the volumetric strain and the pore pressure and improves understanding for how the soil actually responds to the applied loads.

REFERENCES

[1] S.BONELLI (1993), 'Contribution à la résolution de problèmes élastoplastiques de mécanique des sols et d'écoulement non saturés par la méthode des éléments finis', Thèse de doctorat, Université Aix-Marseille II, 253 p.

[2] A.MODARESSI (1990), 'Stratégies de résolution des problèmes couplés', GRECO Géomatériaux, Rapport Scientifique 1990, pp 503-506.

[3] A.GENS, E.E.ALONSO, A.LLORET & F.BATTLE (1988), 'Analysis of construction and consolidation of earthdams', CIGB, Seizième Congrès des Grands Barrages, San Francisco, pp 1371-1386.

[4] R.CHARLIER (1987), 'Approche unifiée de quelques problèmes non linéaires de mécanique des milieux continus par la méthode des éléments finis', Thèse de doctorat, Université de Liège, 287 p.

[5] E.HAIRER & WANNER (1991), 'Solving Ordinary Differential Equations - Vol II - Stiff and Differential-Algebraic Problems', Springer-Verlag, 595 pages.

[6] P.BREITKOPF & G.TOUZOT (1992), 'Architecture des Logiciels et Langages de Modélisation', Revue européenne des éléments finis, vol. 1, N°3, pp 33-368.

[7] O.OZANAM, F.LACROIX & E.DE BONNECHOSE (1992), 'Static and dynamic coupled analyses of El Infiernillo dam', Sd Bench.Workshop on Num. Analysis of Dam, Bergamo, Italy, July 16-17.

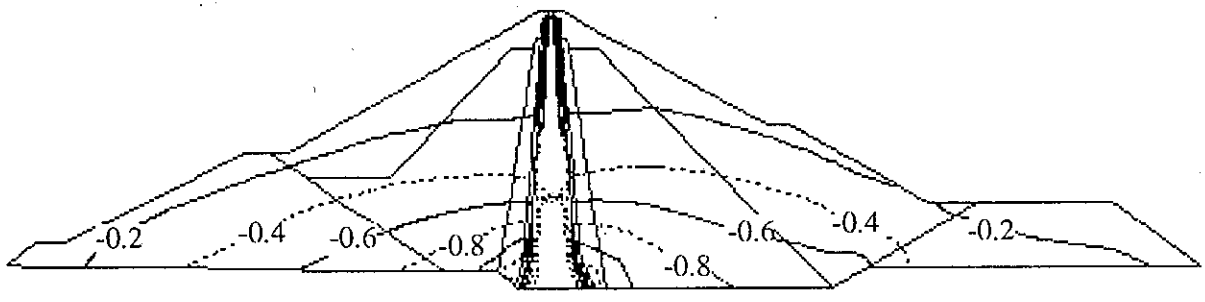

End of construction

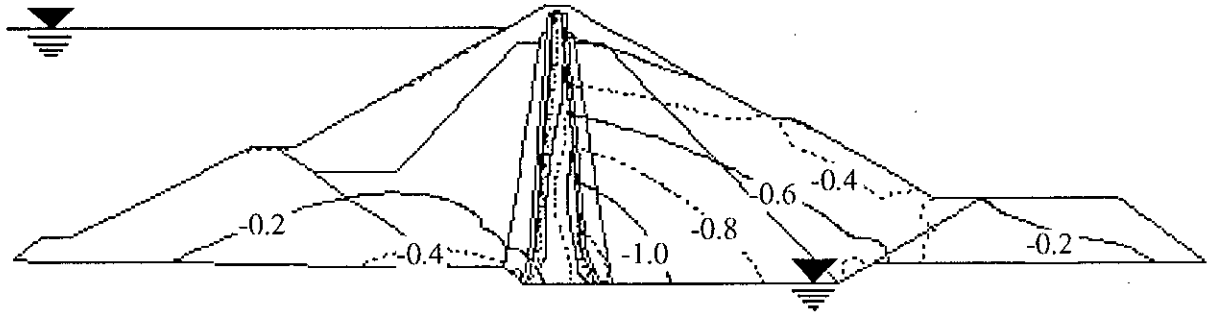

End of impounding

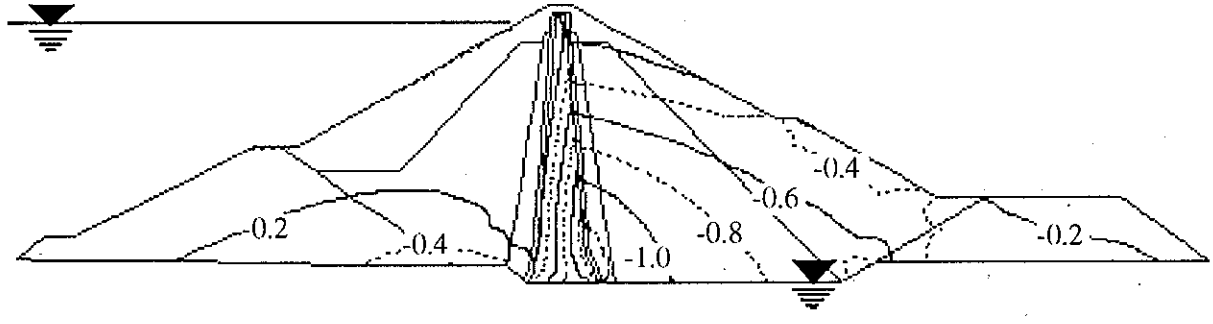

End of consolidation

Fig. 7a • Horizontal effective stresses σ'_x (MPa) (compression are negative) Quasi-static analysis

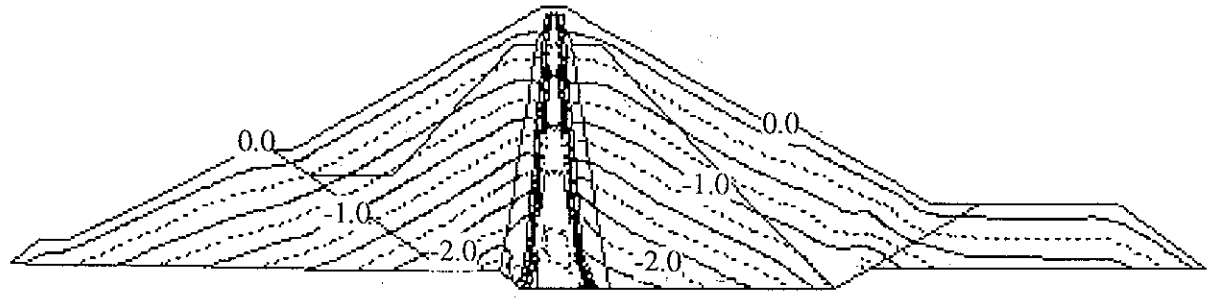

End of construction

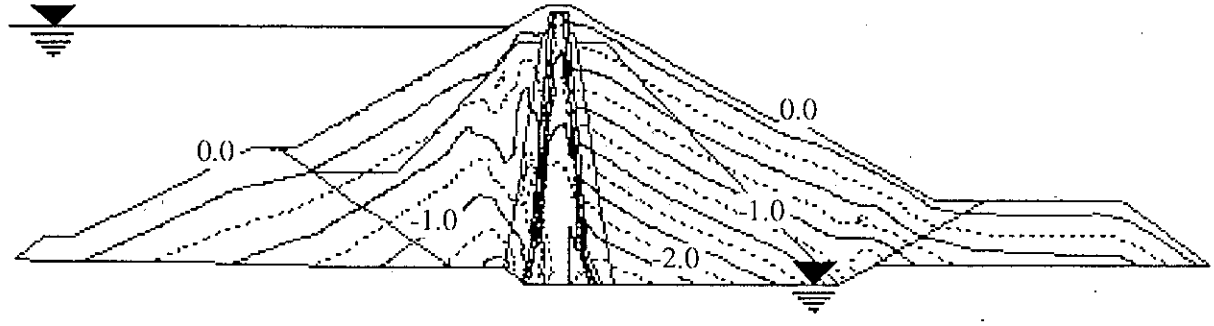

End of impounding

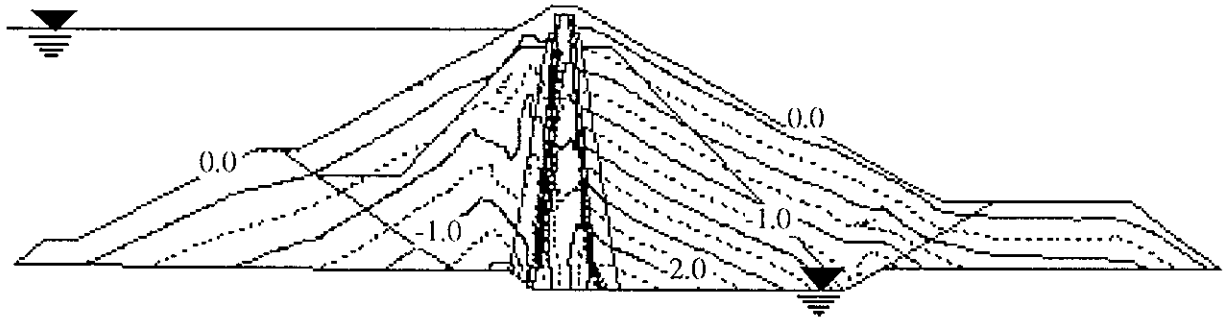

End of consolidation

Fig. 7b • Vertical effective stresses σ'_y (MPa) (compression are negative) Quasi-static analysis

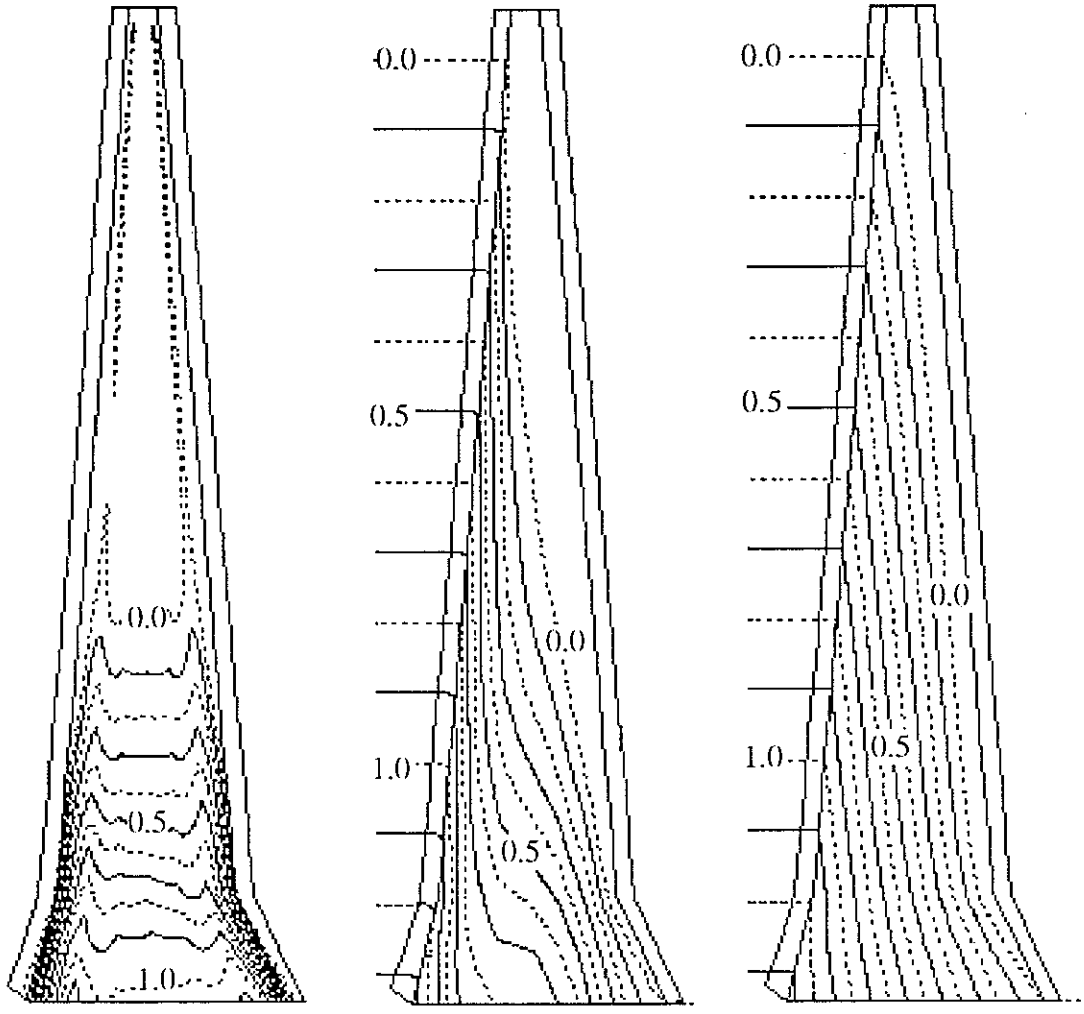

Fig. 8 • Pore pressure u_w in the core (MPa) (compression positive) Quasi-static analysis

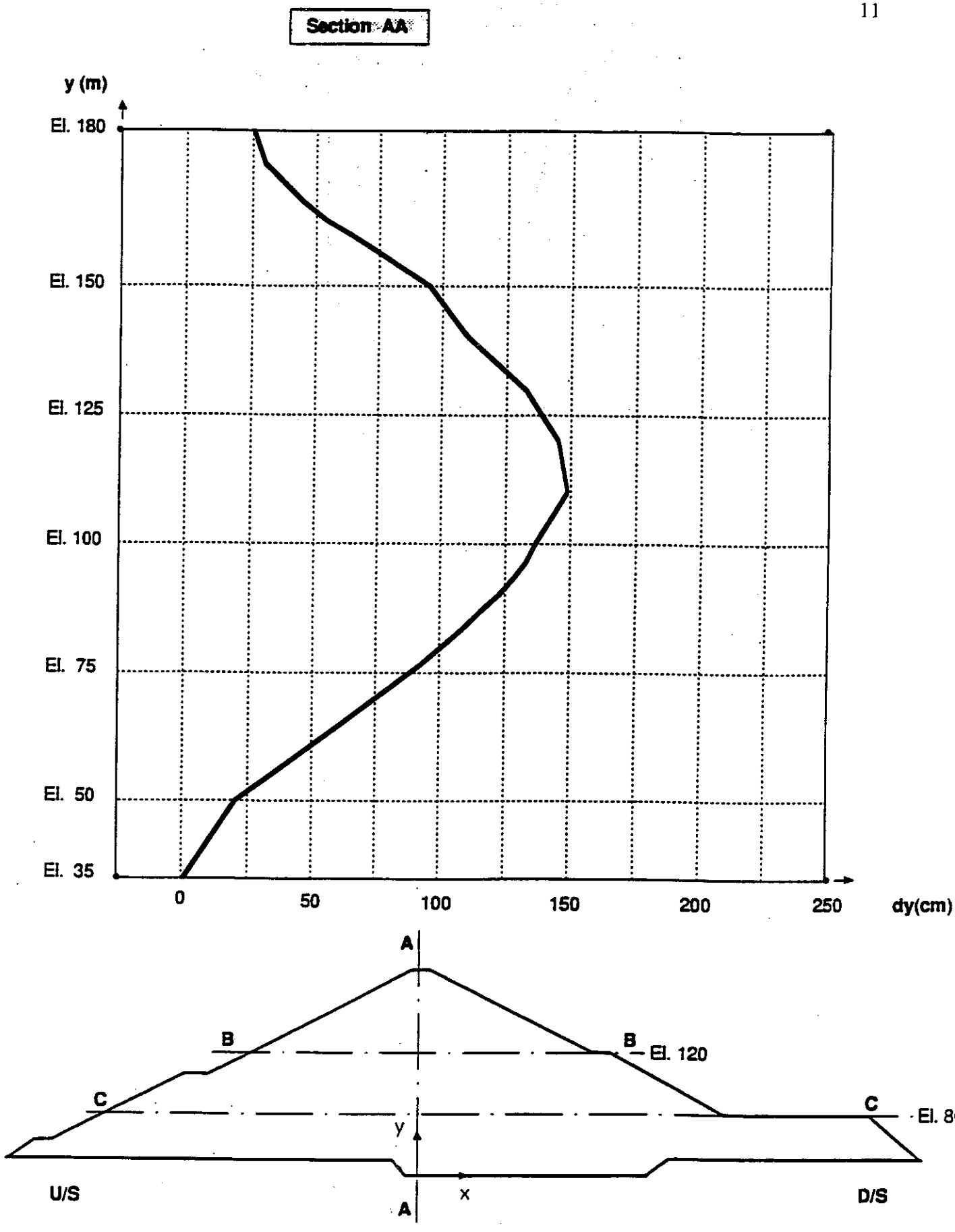

Fig. 9 • Settlements - section AA
Quasi-static analysis

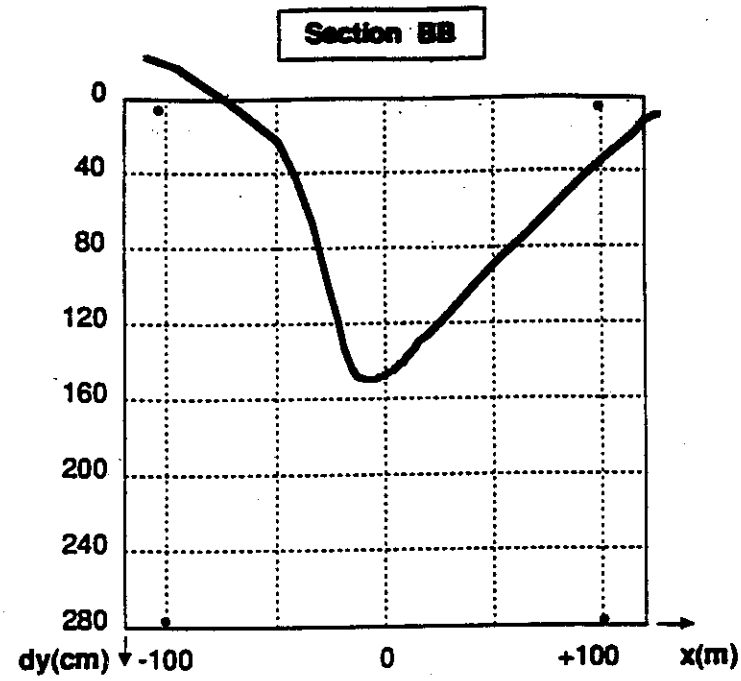

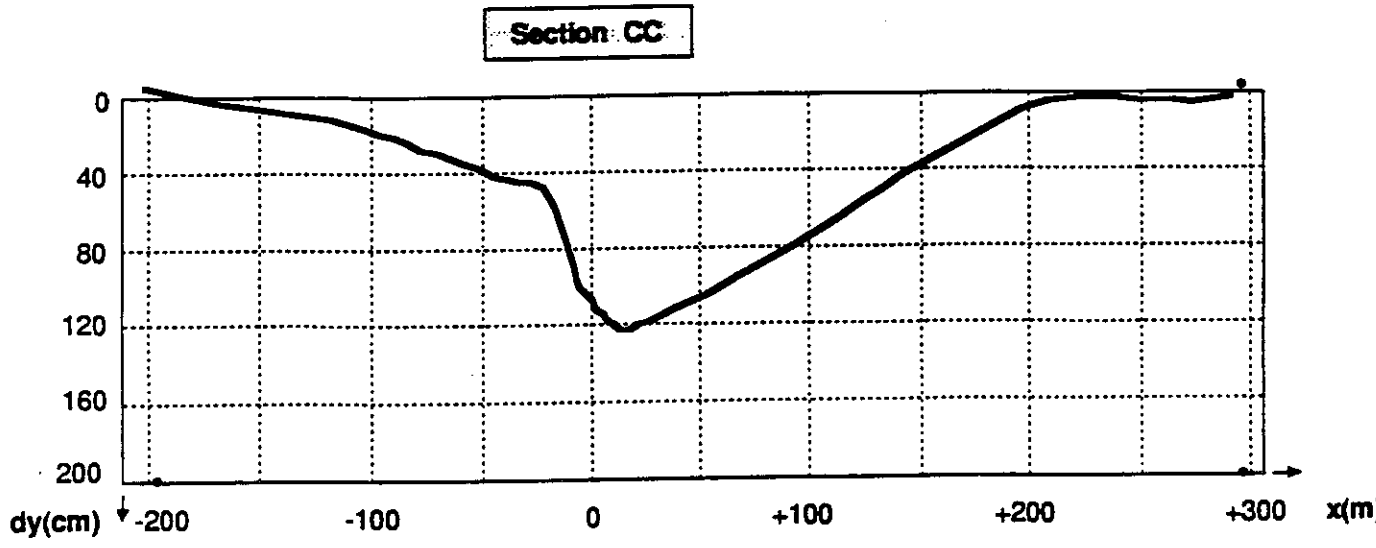

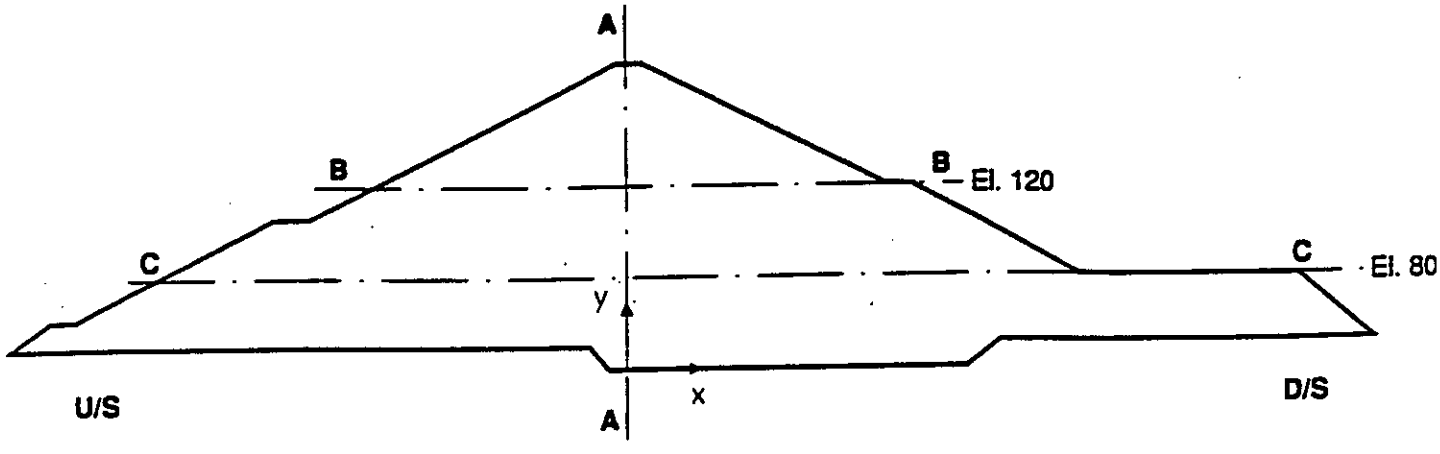

Fig. 10 • Settlements - sections BB and CC
Quasi-static analysis

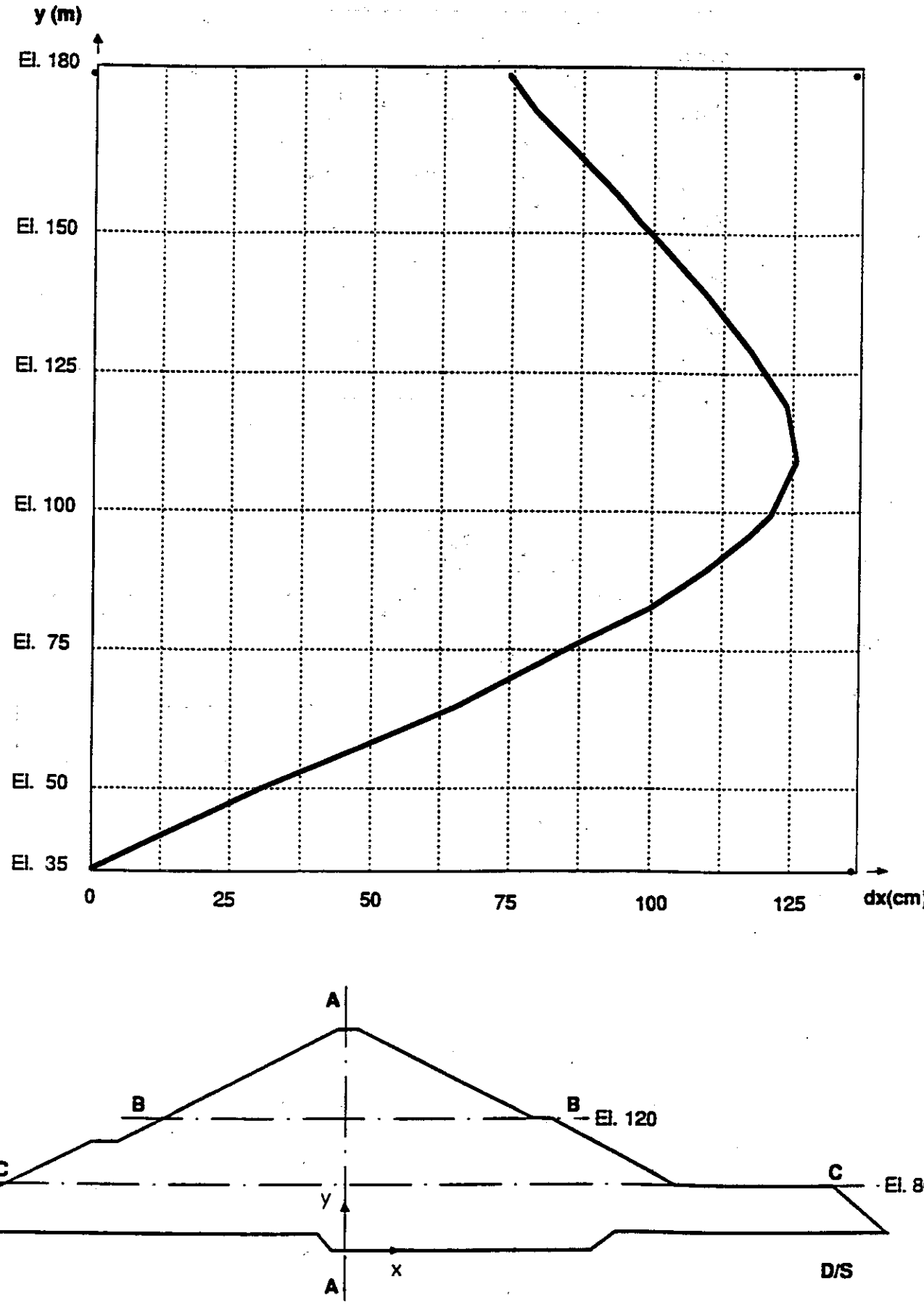

Fig. 11 • Horizontal displacements - section AA
Quasi-static analysis

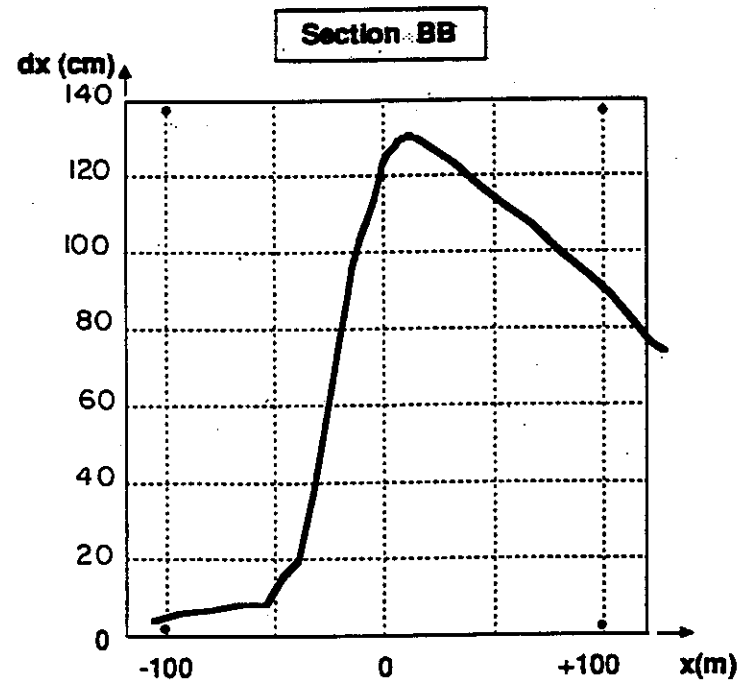

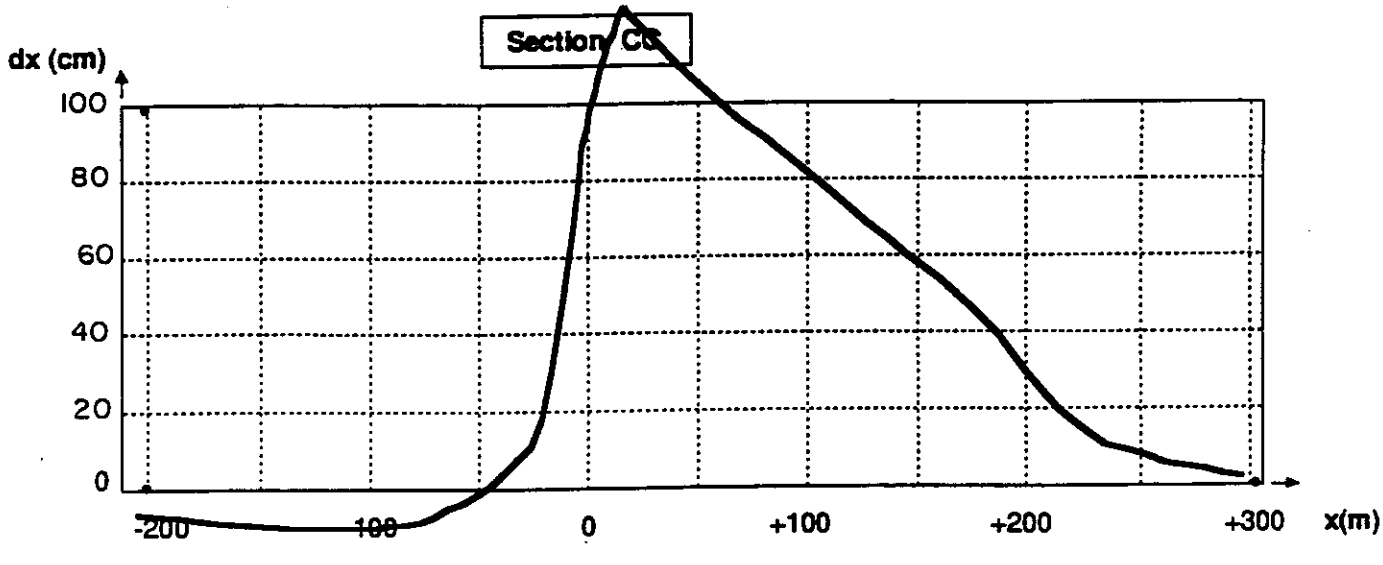

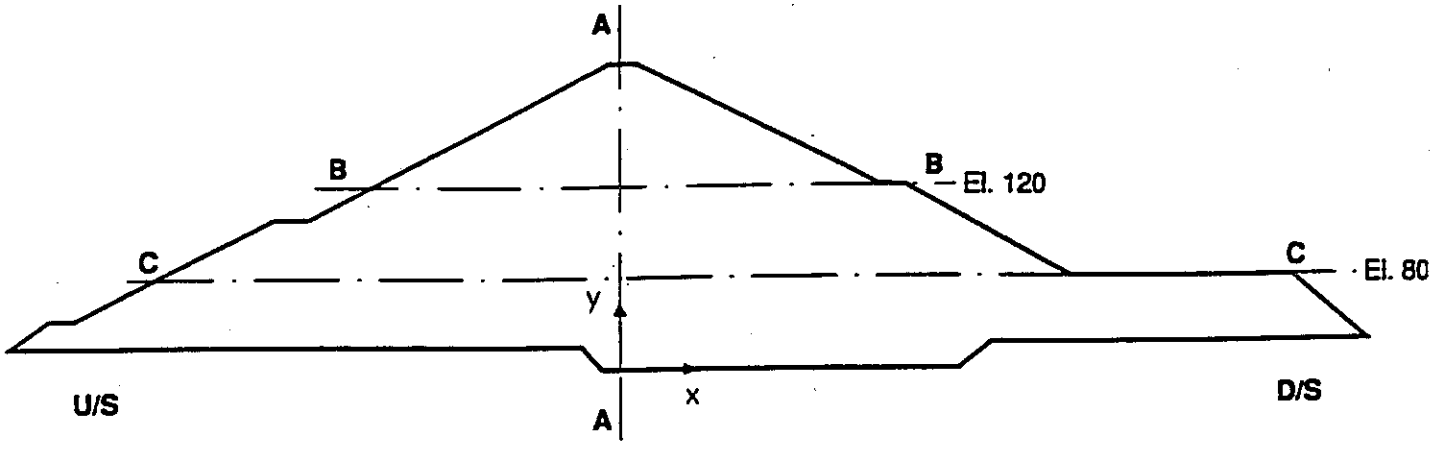

Fig. 12 • Horizontal displacements - sections BB and CC
Quasi-static analysis

APPENDIX : TRIAXIAL SIMULATIONS

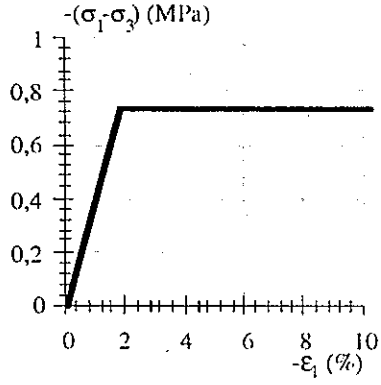

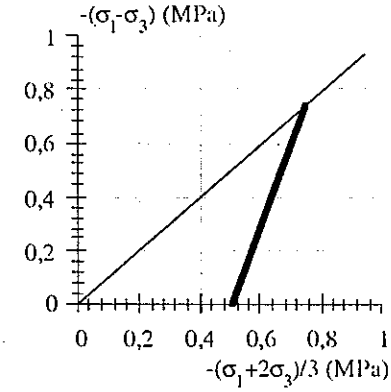

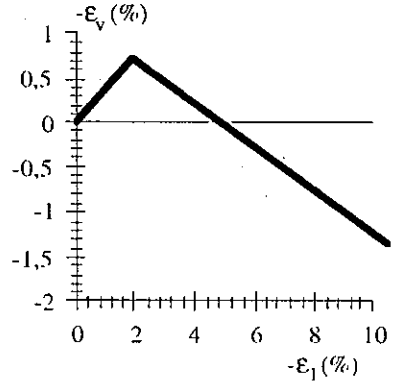

Maximum dev. stress	$-(\sigma_1-\sigma_3)_{max}$=0.735 MPa
Minimum vol. strain	$-\varepsilon^{ve}$=0.73%
Axial strain when $\varepsilon^v=\varepsilon^{ve}$	$-\varepsilon_1^e$=1.84%

Simulation of drained triaxial test on the core material • -σ3=0.5 MPa.

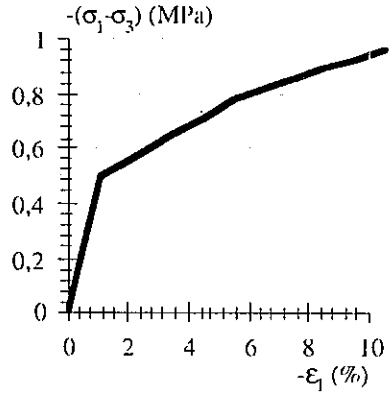

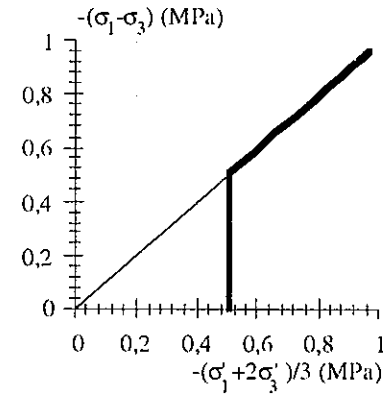

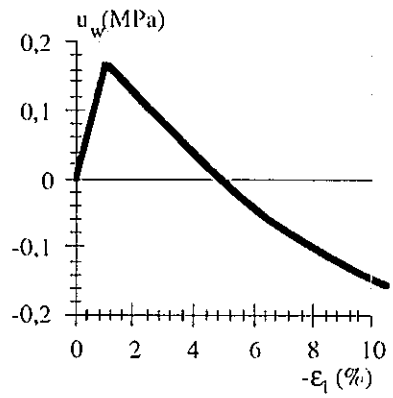

Dev stress at 10%	$-(\sigma_1-\sigma_3)$=0.932 MPa
Pore pressure at 10%	u_w=-0.136MPa
Max pore pressure	$u_{w\,max}$=0.163 MPa
Axial strain when $u_w=u_{w\,max}$	$-\varepsilon_1^e$=1,08%
Dev. stress when $u_w=u_{w\,max}$	$-(\sigma_1-\sigma_3)$=0.496 MPa

Simulation of undrained triaxial test on the core material • -σ3=0.5 MPa.

APPENDIX : NOMENCLATURE

$\vec{e}_z$	vertical axis oriented upward	n	porosity
$\vec{\nabla}_x$	spatial gradient operator	e	void ratio
$\vec{\nabla}_x\bullet$	spatial divergence operator	S_r	degree of saturation
$(\dot{})$	partial time derivative	λ_r	relative permeability
$\vec{\vec{\delta}}$	kronecker delta tensor	$\vec{\vec{K}}$	saturated permeability tensor
$\vec{u}$	displacement vector	k_x	horizontal saturated permeability
$\vec{m}$	mass of water flux vector	k_z	vertical saturated permeability
u_w	pore pressure	α, β, γ	Van-Genuchten curves parameters
$\vec{\vec{\varepsilon}}$	infinitesimal strain tensor	g	acceleration of gravity
$\vec{\vec{\varepsilon}}^d$	deviatoric strain tensor	p_{atm}	atmospheric pressure
ε^v	volumetric strain	χ_w	water bulk modulus
$\vec{\vec{\varepsilon}}^{pd}$	plastic deviatoric strain tensor	χ	skeleton bulk modulus
ε^{pv}	plastic volumetric strain	G	skeleton shear modulus
$\vec{\vec{\sigma}}$	total stress tensor	E	skeleton Young's modulus
$\vec{\vec{\sigma}}^d$	deviatoric stress tensor	ν	Poisson's ratio
σ_m	total mean stress	φ'	angle of internal friction
σ'_m	effective mean stress	ψ	angle of dilatancy
$\dot{\lambda}$	plastic multiplier	ρ_s	solid phase specific mass
$\vec{\vec{\nabla}}_\sigma f$	gradient of the yield function	ρ_w	water specific mass

Numerical Analysis of Bath County Upper Reservoir Dam

by

Philippe P. Martin and Aniruddha Sengupta
Harza Engineering Company, Chicago, U.S.A

1. INTRODUCTION

This paper presents the results of a study specifically undertaken to assess the ability of GEFDYN [1], a finite element computer program acquired under license by Harza Engineering Company of Chicago, to predict the mechanical and hydraulic behavior of an earthfill/rockfill dam during construction, reservoir filling and operational phases and to gain sufficient confidence in this numerical tool for possible use in future projects. No attempt was made during the course of this study to recalibrate the material model parameters to match the records of dam response. In other words, the predictions of the numerical model presented in this report are the true predictions of the mathematical model.

The Upper Reservoir Dam at the Bath County Pumped Storage Project [5, 6, 7, 8, 9] was selected for this study because the dam is well instrumented and a comprehensive monitoring program has been in place since early contruction. Observational and instrument data are collected and plotted regularly and provide an up-to-date check on the performance of the dam. Of particular interest are the readings from some piezometers in the core that have indicated porewater pressures during the later construction stage and early years of operation as high as 70% of overburden pressure.

The approach assumed in this study required three steps:

1) data gathering on materials, dam performance, and reservoir operation,
2) material tests simulation to define the parameters entering the numerical model of the constitutive soils, and,
3) finite element analysis simulating the construction, impoundment and operation of the upper reservoir at the Bath County Project.

The Bath County Pumped Storage Station, owned jointly by Virginia Power and Allegheny Power System, is located 70 miles (113 Km) north of Roanoke, Virginia. The six unit 2100 MW pump generating station has been operating continuously since late 1985, when the construction of the dams was completed. The project consists of the upper and lower reservoirs impounded by the Upper Dam and Lower Dam, three power tunnels, six penstocks, the power house and a recreational area. All the project features were designed by Harza and built under the supervision of Harza.

The Upper Reservoir Dam at the Bath County project is 2200 feet (670 meters) long and 460 feet (140 metres) high. The 105-foot (32 metres) daily drawdown of the Upper Reservoir required special design features such as a free-draining rockfill zone on the upstream side between El. 3205 and El. 3331. The main features of the Upper Reservoir Dam consist of an impervious central core, rolled rockfill and free-draining rockfill shell materials, and filter and transition fill zones between rockfill shells and impervious core. The upstream slope of the dam is 2.5H:1V from the original ground surface to El. 3205, and 2.25H:1V from El. 3205 to the crest. The downstream slope is 2.75H:1V from the original ground surface to El. 3200, and 2H:1V above El. 3200. The impervious central core is 25 feet (7.6 metres) wide at the crest, with upstream and downstream slopes of 1H:4V. A transition zone of weathered rock is provided adjacent to the upstream side of the core below El. 3205. A two stage filter/drain system is provided on the upstream side of the core, above El. 3205, and on the entire downstream side. The outer shells are mostly constructed of weathered and unweathered rockfill materials obtained from required excavation and borrow in the upper reservoir area. The upstream shell above El. 3205 consists of a free-draining sandstone.

The upper dam is founded on the Chemung Formation which is comprised of sandstones, siltstones, and shales. The permeability and seepage characteristics of the rock mass beneath the upper dam were investigated by water-pressure testing along the dam axis. The results of the tests show the Chemung Formation to be relatively impervious. A single line grout curtain was placed under the core along the centerline of the dam. The depth of the grout curtain generally extends to 200 feet (61 metres) below the core trench.

There is one main instrumented section at Station 14+00 in the upper dam. The cross section of the Upper Reservoir Dam at Station 14+00 is shown in Figure 1. Piezometers have been installed in the foundation, upstream shell, core and downstream shell. One pair of open standpipes is also installed 260 feet (79 metres) downstream of the centerline. One piezometer in each pair is installed in the foundation, the other at the top of rock. Two inclinometers are installed through the upstream and downstream shells. Most of the piezometers are still responding reasonably well to the daily drawdown and filling cycles of the upper reservoir. Besides piezometers and inclinometers, six settlement monuments are also installed on the upper dam crest 15 feet (4.6 metres) downstream of the centerline and 400 feet (122 metres) apart. Weirs, flumes, accelerometers are also installed in the section to monitor seepage quantity and the dam response to earthquake motions. Continuous data are available to date for the piezometers and settlement monuments. Inclinometer readings are only available for the period of dam contruction. The large amount of data gathered over a period of 10 years makes it possible to study the performance of the dam and use it to verify a computer model.

2. MATERIAL MODELS AND MODEL CALIBRATION

The choice of a proper material model hinges upon the requirements of the analysis and upon the availability of representative test data. The selection criteria required that the material model be able to respond to various effective stress paths, thus requiring compliance between hydraulic and mechanical behavior of the soil. In this study, Hujeux's material model [1, 2, 3] was chosen to simulate the constitutive behavior of the impervious core and rockfill shells of the Upper Dam. This particular model is capable of modeling shear as well as consolidation behavior of a material along various stress paths. The Hujeux model is a parametric model describing the coupled hydraulic and elastoplastic behavior of soils, based on the theory of plasticity with strain softening/hardening and the concept of critical state. It provides improvements over the Cam-clay model [4] by better predicting soil behavior beyond the critical line and by providing a more accurate estimate of shear deformations beyond the elastic limit (Hajal, 1984 [3]).

For the foundation rock no triaxial data is available. The foundation rock was modeled by a simpler constitutive model known as Drucker-Prager model.

As a part of the exploration and testing program (1976) for embankment construction materials and later under the quality assurance program during the construction of the dam, a limited number of laboratory tests was performed on the impervious core, transition fill and rockfill materials placed within the Upper Dam. Laboratory testing consisted of determining triaxial shear strength, permeability, moisture content, density, Atterberg limits, specific gravity and grain size distribution. These data have been used for the determination of material properties, such as, permeabilities, densities, elastic constants, etc., and for the calibration of the nonlinear material models used in the finite element program to represent the stress strain behavior of the soils.

The pre-processor PARASOLS available in GEFDYN was used to test the Hujeux material models and compare their behavior in simulated CIU triaxial tests to that of the actual materials. The results of the simulation are shown in terms of shear stress vs. strain and pore pressure vs. strain in Figures 2 and 3. It may be seen that there is an overall excellent agreement between the prototype test data and the model behavior for the selected set of parameters. The set of model parameters that have been selected for impervious core, upstream and downstream rockfill shell and foundation materials are shown in Table 1. These parameters were used in the elastoplastic analysis of dam response during construction, impounding and reservoir operation phases.

3. FINITE ELEMENT MODEL

The maximum valley section at Sta. 14+00 of the Upper Reservoir Dam is modeled in this study.

Sufficient laboratory test results are not available for the upstream transition zone, downstream filter and downstream drain materials. Those zones, however, do not contribute to the overall mechanical behavior of the dam, and therefore were not considered as distinct zones in the finite element mesh. In the two-dimensional finite element discretization, the impervious core, upstream and downstream rockfill shells and the foundation rock are idealized as an assemblage of quadrilateral and triangular elements. The finite element mesh for the simplified section of the Upper Dam is shown in Figure 1. The mesh consists of 1077 nodes and of 1024 elements.

The location of the nodes and elements was chosen in such a way as to match actual locations of piezometers in the Upper Dam. This makes it possible to directly compare pore pressures predicted by the model with the dam performance record. The number of layers of elements and their elevations were selected to match the dam construction sequence delineated in Figure 4. No attempt was made to simulate the actual lift thickness implemented to construct the dam. However every attempt was made to follow the actual rate of construction. All the reported pauses of construction activity were incorporated in the timeline modeling the fill construction.

Three different types of elements have been used to model the Upper Dam.

The central impervious core of the dam whose constitutive behavior is simulated by the nonlinear Hujeux model, has been discretized by triangular and quadrilateral isoparametric elements with a pore pressure degree of freedom at each node. This particular combination of element type and material model allows one to model pore pressure development and dissipation with time and the consolidation behavior of the soil. The soil under this condition exhibits essentially undrained behavior.

The downstream shell of the dam was discretized by triangular and quadrilateral isoparametric elements with the pore pressure degree of freedom removed at each node. In other words, the downstream shell is modeled as a drained material.

The piezometer readings for the instruments located on the upstream rockfill and transition fill zones show them essentially free draining (that is no excess pore water pressure) during impoundment of the reservoir and daily drawdowns. No pore pressure buildup was recorded during construction. In fact all the piezometer readings showed the upstream shell to be dry during construction. For this reason, the upstream shell, like the downstream shell, was modeled

with triangular and quadrilateral isoparametric elements with the pore pressures degree of freedom removed at each node. This makes the upstream shell behave like a free draining zone. The prediction of deformations requires the calculation of the correct state of effective stresses and strains. In turn, the effective stresses depend on pore pressures. Thus it is essential that the pore pressures within the upstream shell be consistent with the hydraulic head imposed by the upper reservoir pool. The Hujeux material model under drained condition lets one define independently the desired pore pressures by linking one of its parameters to the pool elevation. Thus the upstream shell is modeled as a drained zone where the pore water pressures used to calculate the effective stresses at each element accurately reflect the effect of the pool elevation.

The foundation rock, which is modeled by the Drucker-Prager material model, is discretized with isoparametric quadrilateral elements with a pore pressure degree of freedom at each node. The bottom of the foundation rock is assumed to be fixed and impervious. The pore pressures at the upstream and downstream ends of the mesh are assumed to be caused by the upstream pool and the tailwater.

The interface seepage elements have been used at the interface between the upstream and downstream shells and the core. They have also been used at the interface between shell and foundation. Those elements serve two purposes. They make the interface between the drained and undrained elements compatible and also they let the seepage analysis be performed in the core and the foundation zones modeled as undrained.

Simulation of Construction

Dam construction was simulated by adding successive layers to their specified elevation, bringing the dam crest to the design El. 3334 at the end of construction. The analysis of the response of the dam to the loads applied during its construction is made necessary by the nonlinear and irreversible nature of the relationship between stresses and strains. The 434 feet (132 metres) of dam fill was constructed in 20 steps with an average height of lift of about 22 feet (6.7 metres). The six months of pause in construction activities when the fill had reached El. 3053 and later El. 3220 were simulated. During these periods significant dissipation of pore water pressures were predicted by the model.

Simulation of Reservoir Impoundment

Ten months of waiting period between the end of construction and reservoir impoundment to El. 3320 were simulated. The Upper reservoir level rose from El. 2850 to maximum pool El. 3320 in two months. The raising of the Upper Reservoir was simulated by 11 load steps in the finite element analysis.

Simulation of Reservoir Operation

The final simulation covered the long term consolidation (over six years) of the dam and daily cycles of reservoir operation. A total of 59 load steps were used in the finite element model to account for the six years of operation after the impoundment of the reservoir. The first six months of reservoir drawdown and filling was modeled. For the purpose of the analysis, the reservoir was kept at maximum pool elevation of 3320 for the next 5 1/2 years to evaluate the long term consolidation behavior of the dam fill. Drawdown tests are performed at the Upper Reservoir dam periodically. For the present study, one such drawdown test performed during 05/31/91 and 06/01/91 (refer Fig. 10) was selected to evaluate the capability of the finite element algorithm to model the effect of daily cyclic operation of the reservoir. A total ten steps of loading and unloading was assumed during which the reservoir was drawn down from El. 3320 to El. 3253 and then filled back to El. 3296.

4. RESULTS OF THE ANALYSIS

Porewater Pressure Data

Figure 4 shows graphically the measured response of piezometers located in the upstream shell, impervious core and foundation of Upper Reservoir Dam during its operation. Piezometers at the downstream shell and chimney drain have recorded zero pressures indicating that these zones are essentially dry during construction and daily operations. Figure 4 indicates that the Zone 4 materials are correctly fulfilling their purpose as a fully drained zone in the upstream shell. The pore pressure response of this zone was almost immediately and 100% to changing reservoir levels. This fact is illustrated by piezometer 14PP102P located 100 ft (30 metres) from the reservoir. The pore pressures recorded by the foundation piezometers upstream of the grout curtain indicate some head loss in the foundation. The piezometric levels measured at locations downstream of the grout curtain are about at the ground surface or lower.

Figures 5 and 6 show the hydraulic regime predicted within the dam and its core at the end of construction, end of reservoir filling and at the end of six years of operations. Pore pressure reading during impoundment is available for only one piezometer, 14PP110P, located in the core of the dam. Figure 7 shows that the pore pressure predicted by GEFDYN at that location is very close to the measured pore pressure. A good agreement is achieved between the predicted and recorded pore pressures in the dam core and shells. The pore pressures in the foundation rock are less accurately predicted.

Settlement and Horizontal Movement

In order to monitor the horizontal movements and internal settlement in the upper dam embankment during construction, two inclinometers 16I101 and 16I103 were installed. Inclinometers 16I101 and 16I103 are located in the shells 147.25 ft. (45 metres) upstream from the axis and 253.3 ft. (77 metres) downstream, respectively.

Inclinometer 16I101 recorded 15 in. (38.1 cm) of upstream deflection by the time the dam had reached El. 3180. The maximum deflection occurred at about one-half of the dam height. About 4 inches (10.2 cm) of deflection towards the left abutment was recorded in the direction parallel to the dam axis. Inclinometer 16I103 recorded about 9 inches (22.9 cm) of deflection in the downstream direction at about the mid-height of the dam when the dam under construction had reached El. 3180. About 7 inches (17.8 cm) of deflection toward the left abutment was recorded.

The vertical settlement along the centerline of the dam at the end of construction, at the end of filling and after six years of dam operation is shown in Figure 8. The vertical settlement predicted under the crest at the end of reservoir filling is about 15 inches (38.1 cm) as opposed to 7 inches (17.8 cm) recorded by the settlement monuments. The crest settlement at the end of six years of operation is predicted to be about 18 inches (45.7 cm) as opposed to about 22 inches (55.9 cm) recorded by settlement monument. The difference between record and analysis is not significant. The simulation shows the dam to respond immediately to reservoir impoundment while record shows it to be progressive. The horizontal deformations of the upstream and downstream shells during construction phase are shown in Figure 9. The magnitude of horizontal deformations were found to match very well with the records of inclinometers 16I101 and 16I103. However the locations where maximum deformations took place in the section of the dam are different from that recorded by inclinometers 16I101 and 16I103.

The deformation of the dam section at the end of construction, reservoir filling and six years of operation are shown in Figure 10.

Pool Fluctuation Data

The piezometer response to the rate of reservoir drawdown and filling has been monitored over the last six years of reservoir operations with the help of a large number of piezometers embedded in the dam. The piezometric response (14PP110P) to the drawdown test performed between 5/31/91 and 6/1/91 was used to check the ability of the mathematical model to predict pore pressure response to reservoir drawdown and filling. The numerical prediction and the actual response of piezometer 14PP110P, located in the core of the dam, to the drawdown test performed is shown in Figure 11. As

can be seen from the figure, the pore pressure response within the core is comparable to that of the actual record. The numerical model is found to model the long term consolidation behavior of the impervious core very well.

5. CONCLUSIONS

In the present study, the general purpose finite element program, GEFDYN, has been found to be an extremely good predictor of the mechanical and hydraulic behaviors of an earthfill/rockfill dam. The pore pressures and deformations predicted by the program at different locations of the Upper Dam at Bath County are found to be very close to the records obtained during the construction, reservoir filling and six years of operation of the dam. No attempt was made during the study to recalibrate these properties to match the records of dam response. In other words, the predictions of the numerical model presented in this report are the true predictions of the mathematical model. The mismatch in pore pressures and deformations in the foundation are due to a lack of adequate tests for the foundation rock and simplification of the foundation geometry.

6. REFERENCES

1. GEFDYN © Copyright Coyne et Bellier - École Centrale Paris/LMSS - EDF/REAL "A Computer Program for **GE**omechanics **F**inite Element **DYN**amics - Two/Three-Dimensional Quasi-Static/Dynamic Coupled Mechanical - Hydraulics Software for Non Linear Geomaterials Analysis," Version V.3, Paris, France, February 1991.

2. Aubry, D., Hujeux, J. C., Lassoudière, F., Meimon, Y., "A Double Memory Model with Multiple Mechanisms for Cyclic Soil Behavior," *International Symposium on Numerical Methods in Geomechanics,* Zurich, Balkema, pp. 3-13 (1982).

3. Hajal, T., "Modélisation élastoplastique des sols par une loi multimécanisme - application au calcul pressiomètrique," Doctoral Dissertation, Ecole Centrale des Arts et Manufactures, Paris, France (1984).

4. Roscoe, K. H., Schofield, A. N. & Wroth, C. P. (1958). On the yielding of soils. *Géotechnique 8,* No. 1, 22-53.

5. Harza Engineering Company, "Construction Materials Exploration and Testing for Construction of Dams and Other Miscellaneous Work, Bath County Pumped Storage Project," July, 1976.

6. Harza Engineering Company, Geotechnical Properties of

Undisturbed Samples of Core Materials from Upper and Lower Dams, Bath County Pumped Storage Project, March, 1984 Report, March, 1983 Report and 1982 Report.

7. Harza Engineering Company, Instrumentation Data, Bath County Pumped Storage Project, 15th Report (July 1984) and 14th Report (Dec. 1983).

8. Bath County Pumped Storage Project Monitoring Group, Annual Evaluation Report of Geotechnical Monitoring Program, 1 Dec. 1980 - 13 Oct. 1991.

9. Wong, K. L., Kleiner, D. E., Wood, A. M., Geary, M. C., Oechsel, R. G., "Design and Performance of Bath County Upper Dam and Reservoir Slopes," Conf. on Stability and Performance of Slopes and Embankments, Berkeley, CA, 1992.

TABLE 1

SUMMARY OF MATERIAL PARAMETERS

Material	Impervious Core	Rockfill Shell	Foundation Rock
Elastic Parameters			
E (tsf)	350	400	200000
ν	0.31	0.30	0.20
n	0.58	0.04	—
Frictional Parameters			
ϕ' (deg)	36	43	45
c' (tsf)	0	0	1.0E+20
Critical State Parameters			
β	65.82	42.0	—
e_{cr} at 1.0 tsf P_{cr}	0.30	0.15	—
d	5.8	8.0	--
Dilatancy Parameters			
ψ (deg.)	39	43	45
α	0.6795	0.3559	—
Deviatoric Parameters			
a	0.0003	0.7224	—
a_{cyc}	0.001	0.0016	—
b	0.29	0.224	—
r_{el}	0.0001	0.0005	--
r_{hys}	0.05	0.0403	--
r_{mbl}	1.0	0.9851	--
Isotropic Parameters			
c	0.05	0.05	--
ccyc	0.004	0.001	--
x_m	2.4	4.543	--
DLTELA	0.001	0.001	--
Permeability			
k_x (cm/s)	1.0×10^{-6}	1.0	1.0×10^{-3}
k_y (cm/s)	1.0×10^{-6}	1.0	1.0×10^{-3}

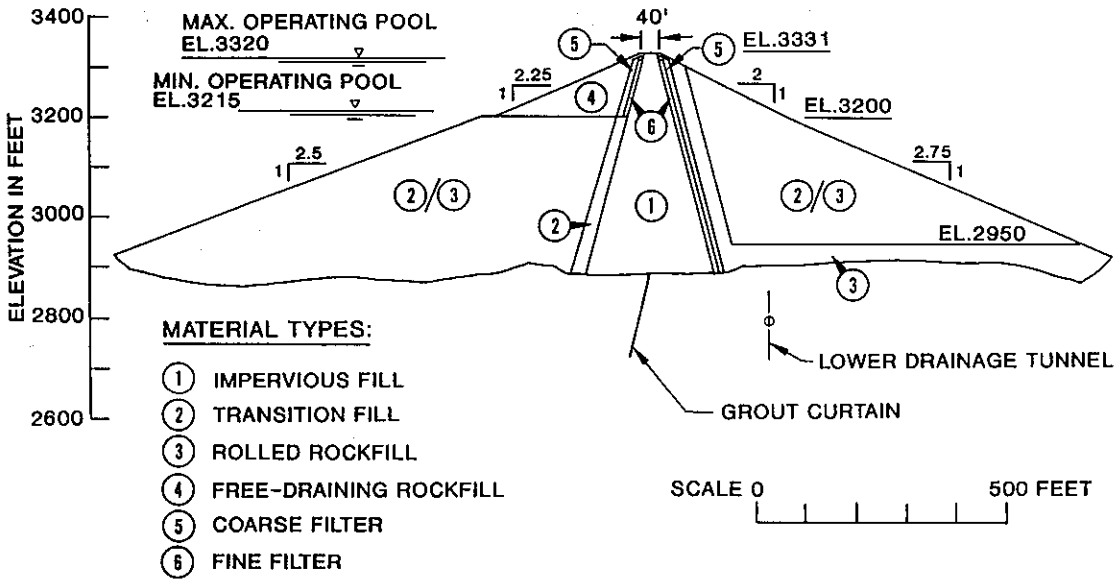

(a) DAM CROSS SECTION

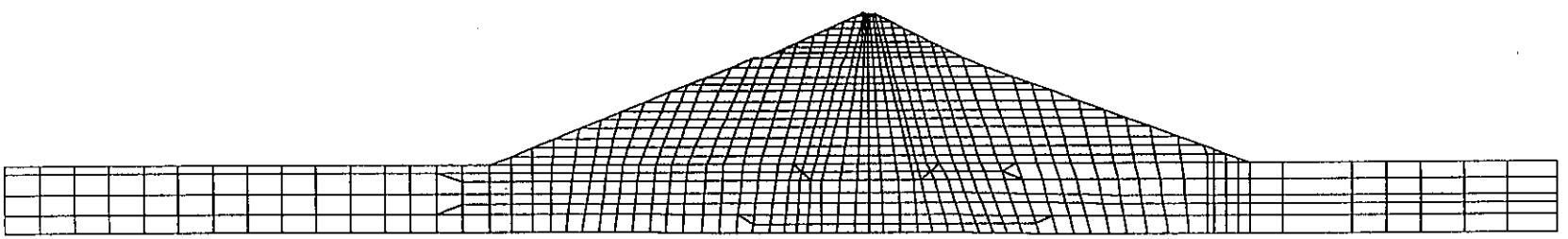

(b) FINITE ELEMENT MESH

FIGURE 1

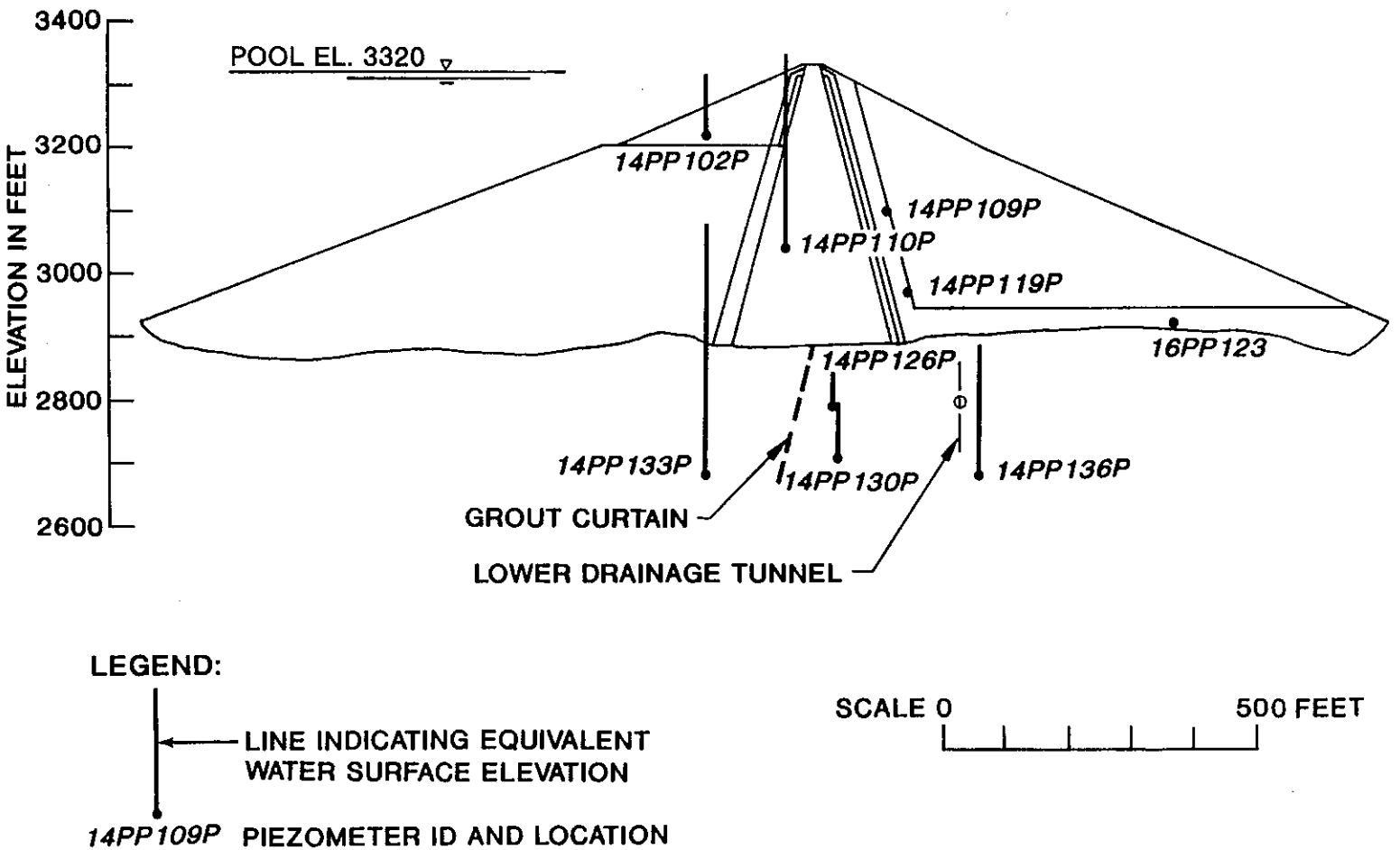

PIEZOMETER LOCATIONS AND MEASURED HEADS DURING DAM OPERATION

FIGURE 2

FIGURE 3

CONFINING PRESSURES: 3.6, 7.2, & 14.4 TSF

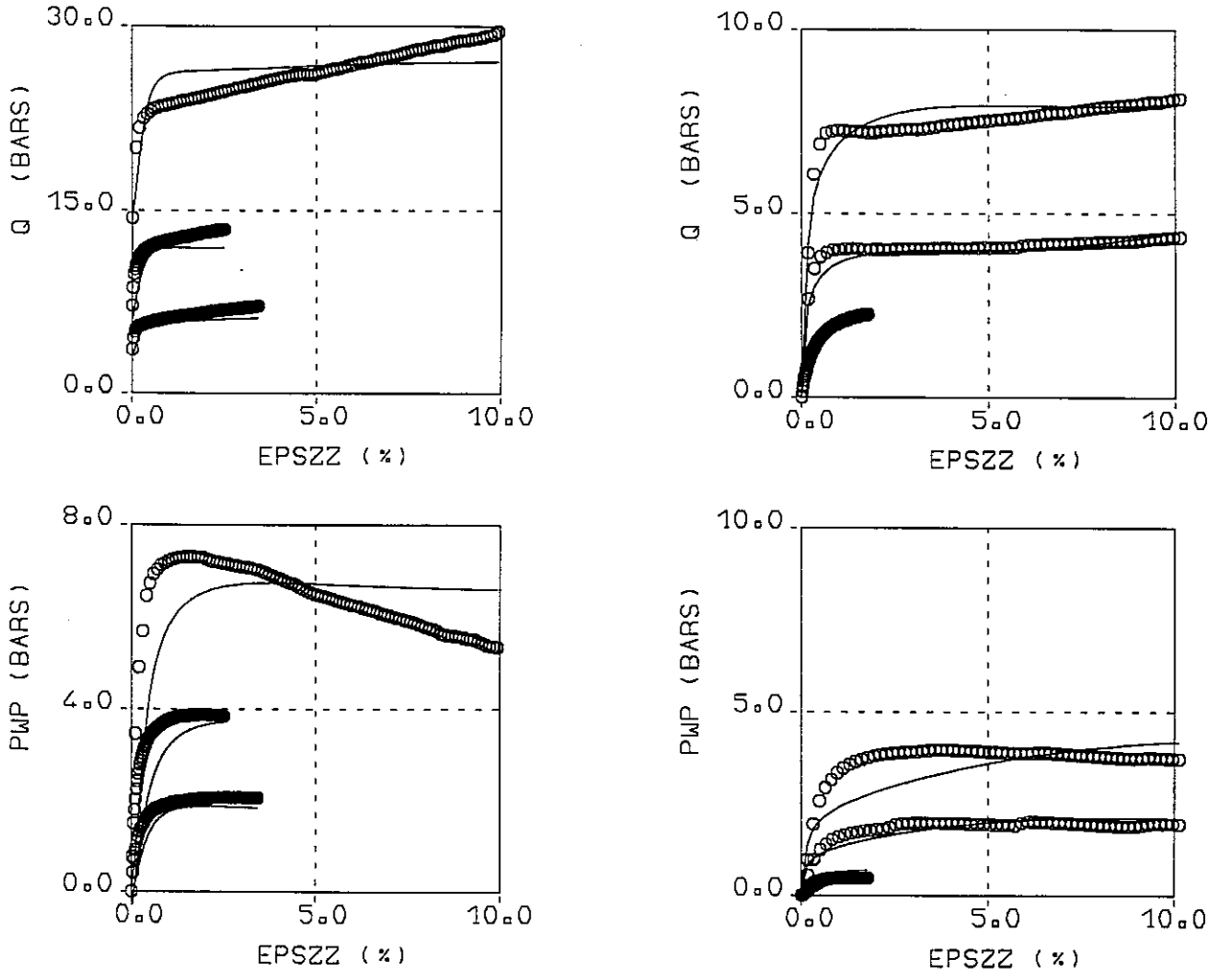

CORE MATERIAL

ROCKFILL MATERIAL

— — — INITIAL SIMULATION

——— FINAL SIMULATION

O EXPERIMENTAL PATH

SIMULATION OF TRIAXIAL TEST DATA

FIGURE 4

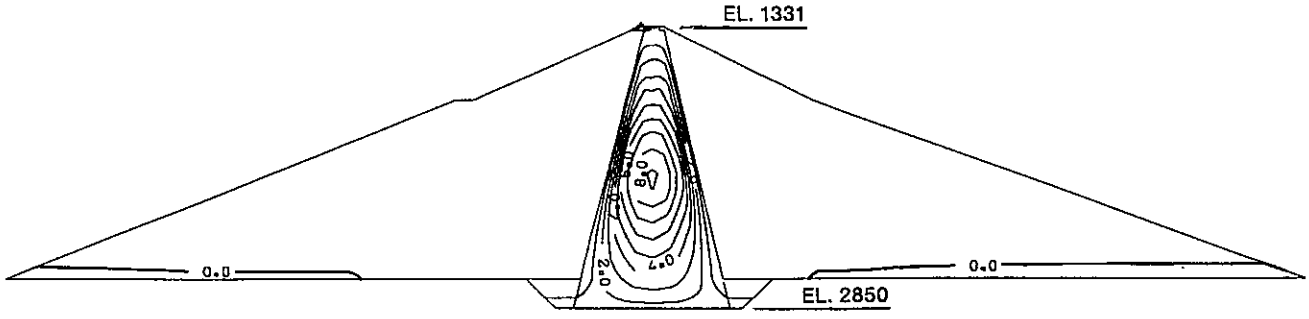

(a) AT THE END OF CONSTRUCTION

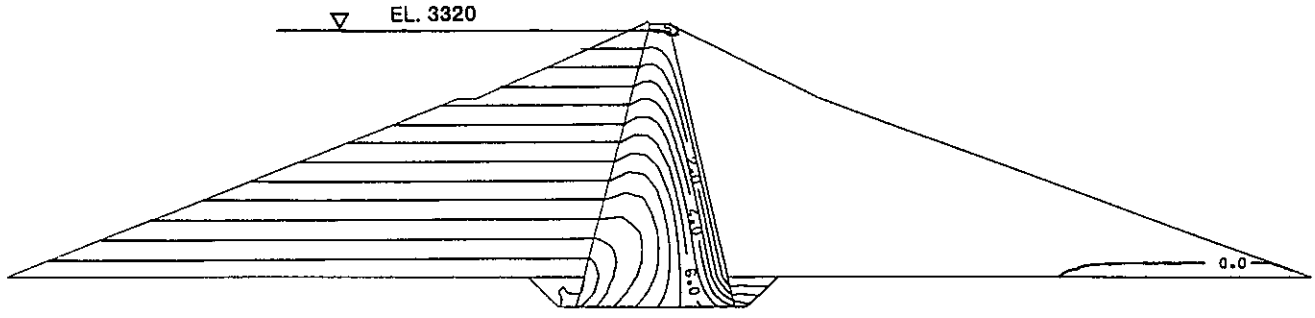

(b) AT THE END OF IMPOUNDMENT

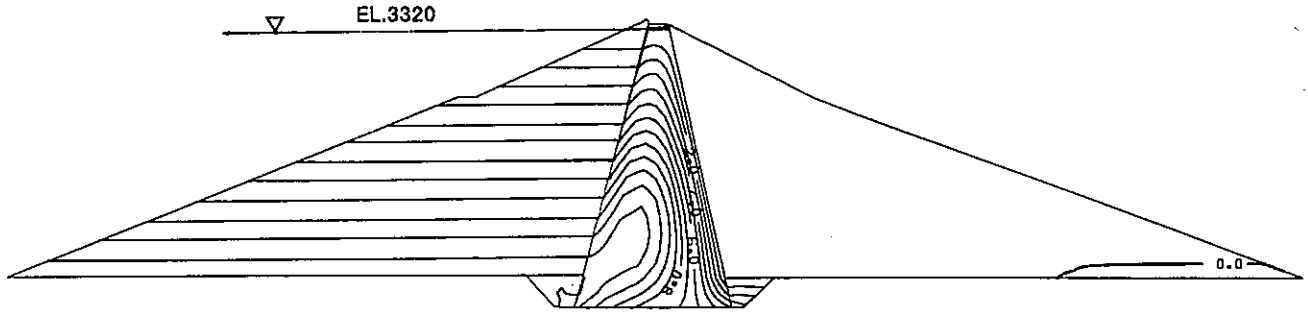

(c) AT THE END OF 6 YEARS OF OPERATION

BATH COUNTY DAM – PORE PRESSURE DISTRIBUTION

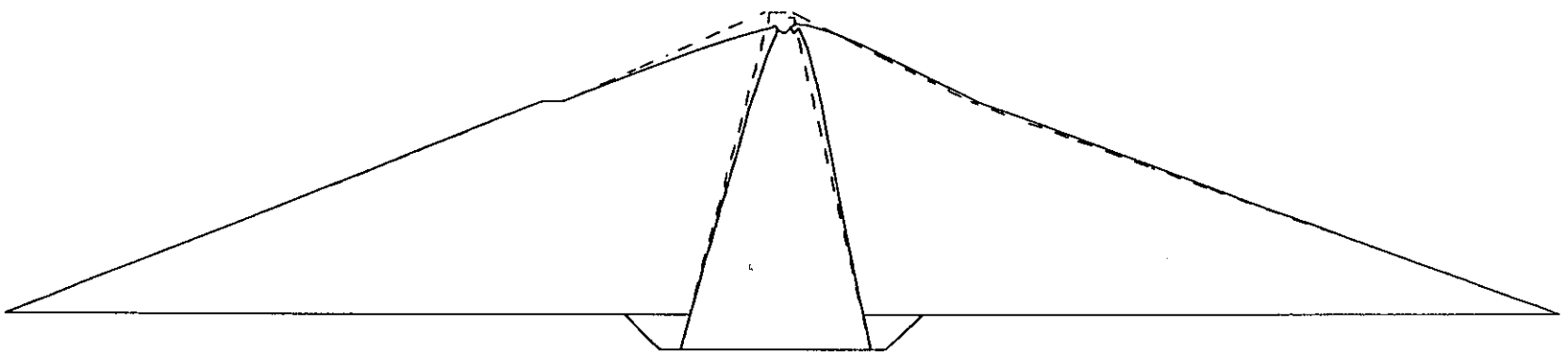

GEOMETRIC SCALE: 1" = 253'
DEFORMATION SCALE: 1" = 14'

BATH COUNTY DAM – DEFORMED MESH AT THE END OF 6 YEARS OF DAM OPERATION

FIGURE 5

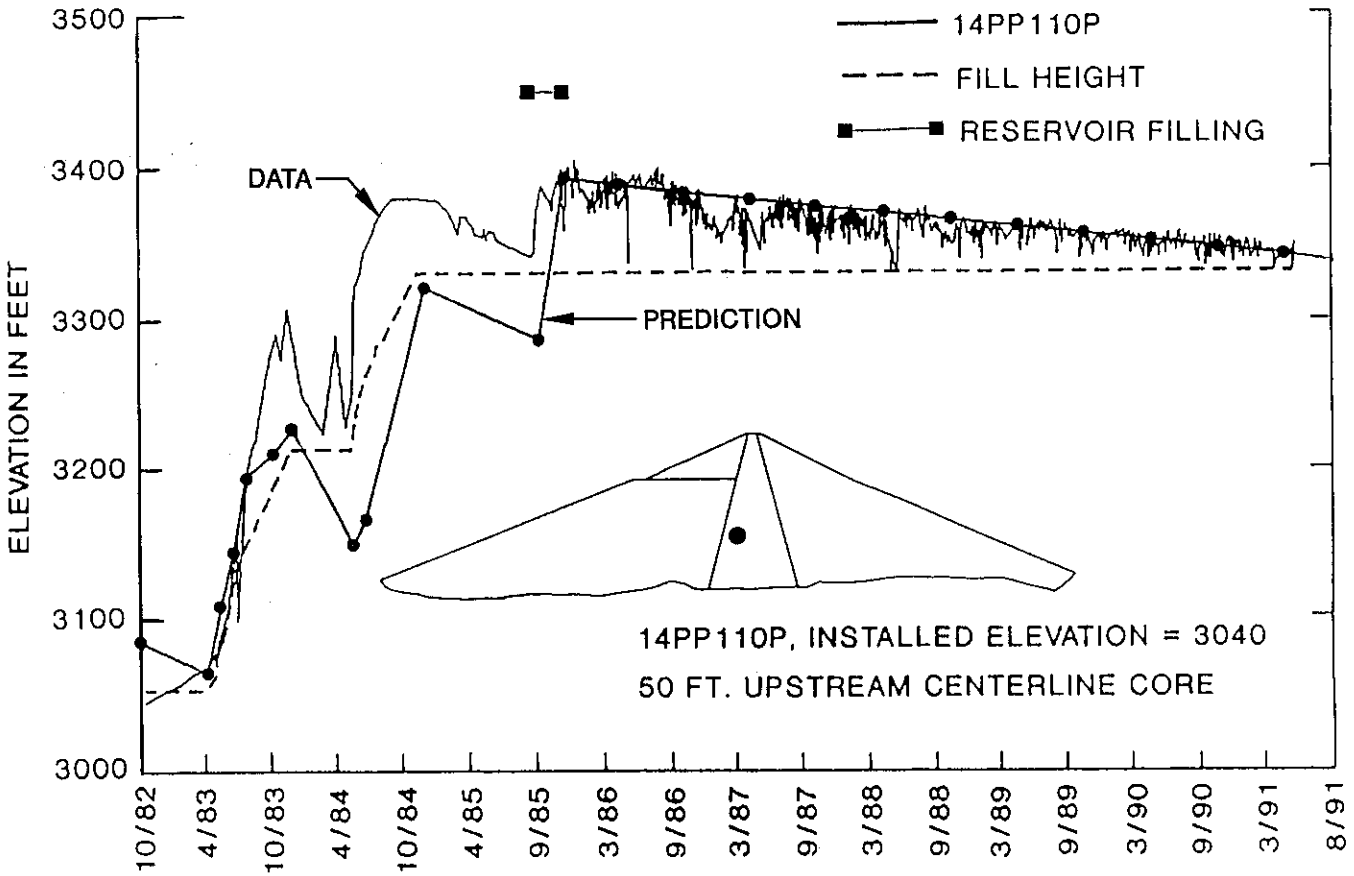

CORE PIEZOMETER 14PP110P TIME CURVE

FIGURE 6

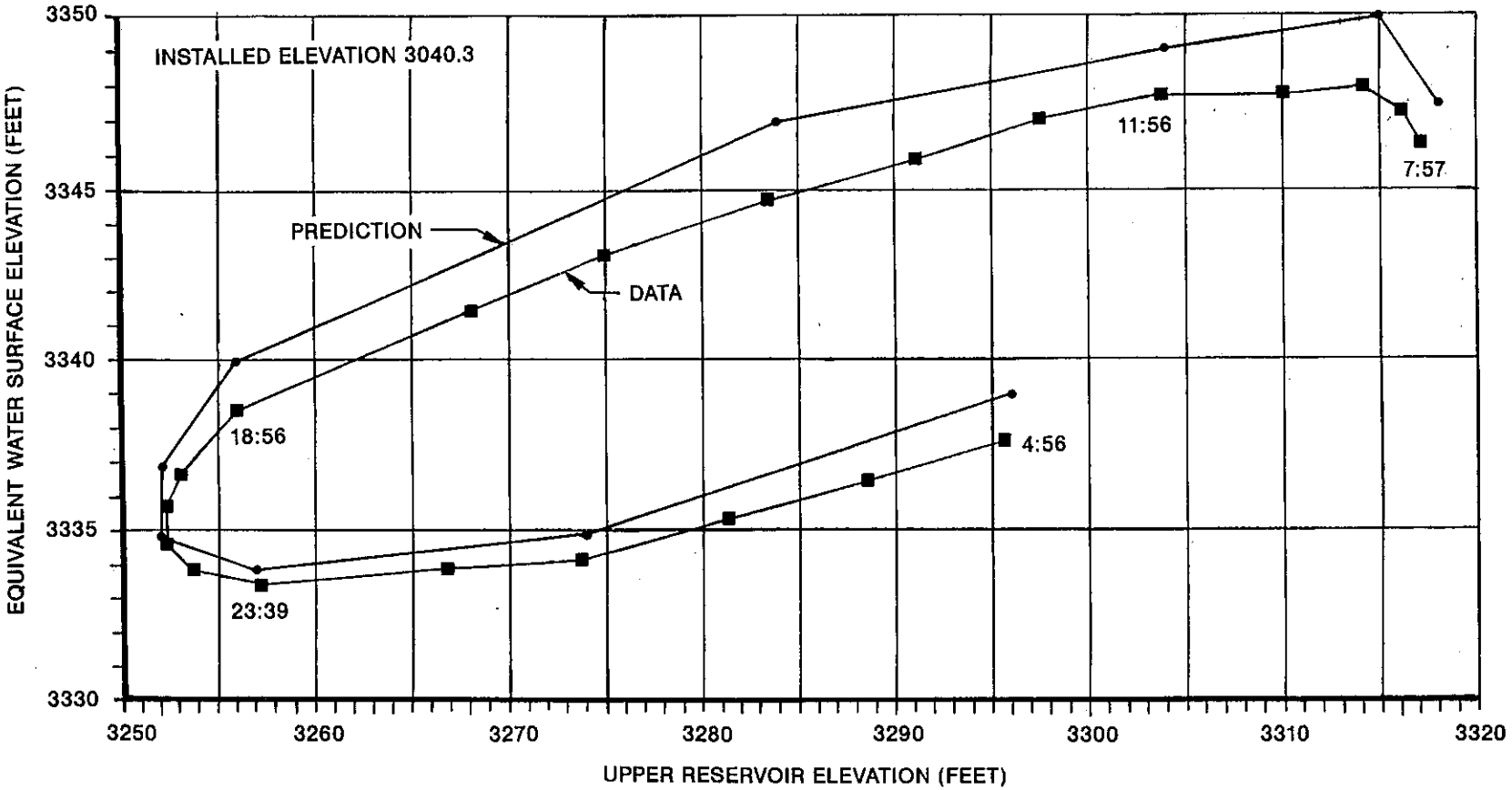

14PP110P, 50' U/S CORE, RESPONSE TO DRAWDOWN, 5/31/91 TO 6/1/91

FIGURE 7

FIGURE 8

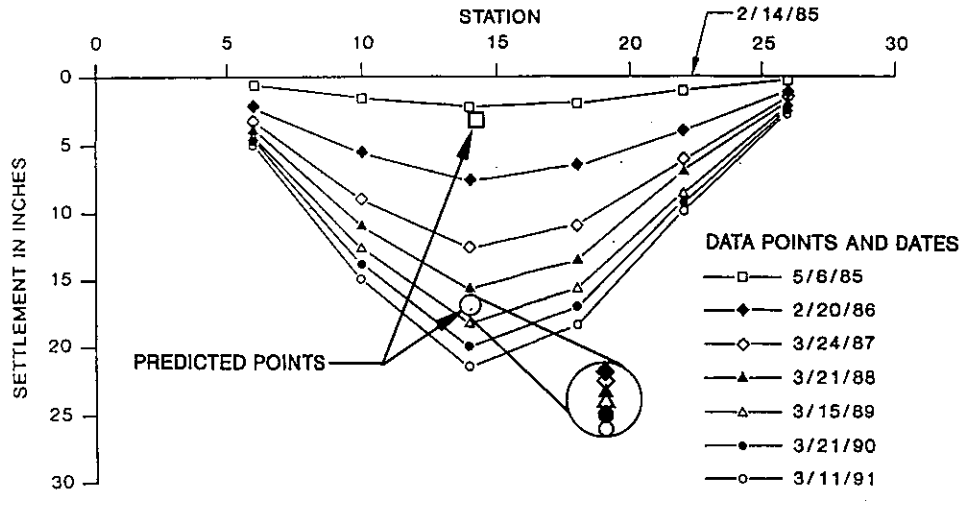

(a) CREST SETTLEMENT

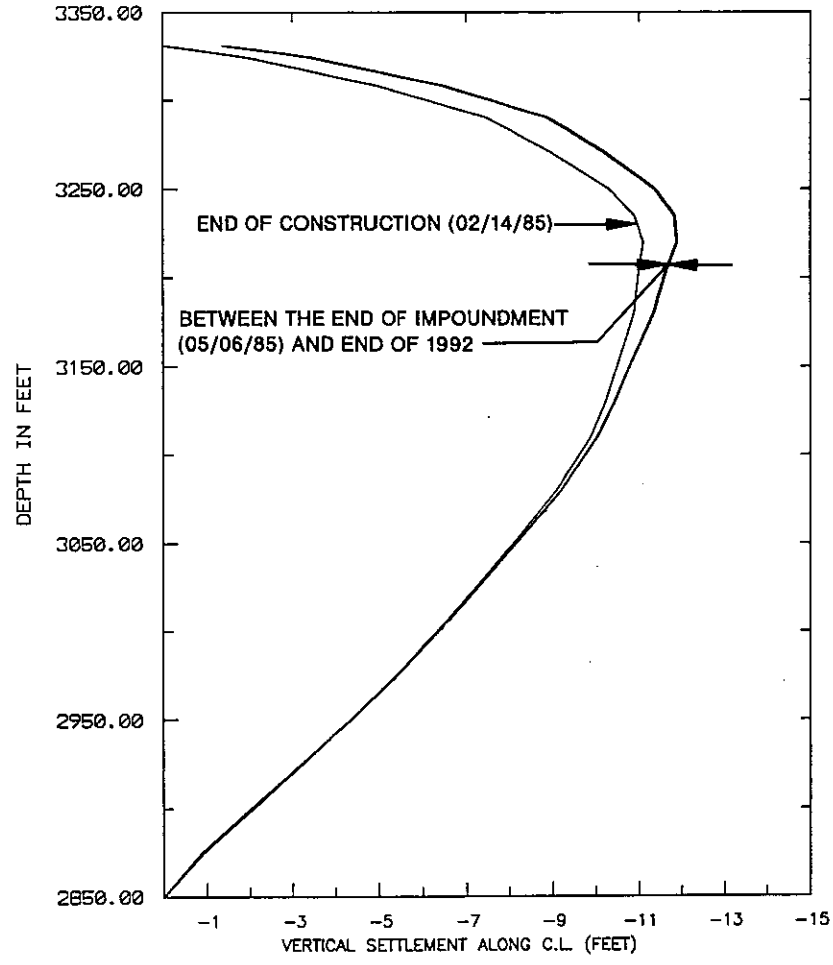

(b) VERTICAL SETTLEMENT ALONG CENTERLINE AT STA. 14+00

FIGURE 9

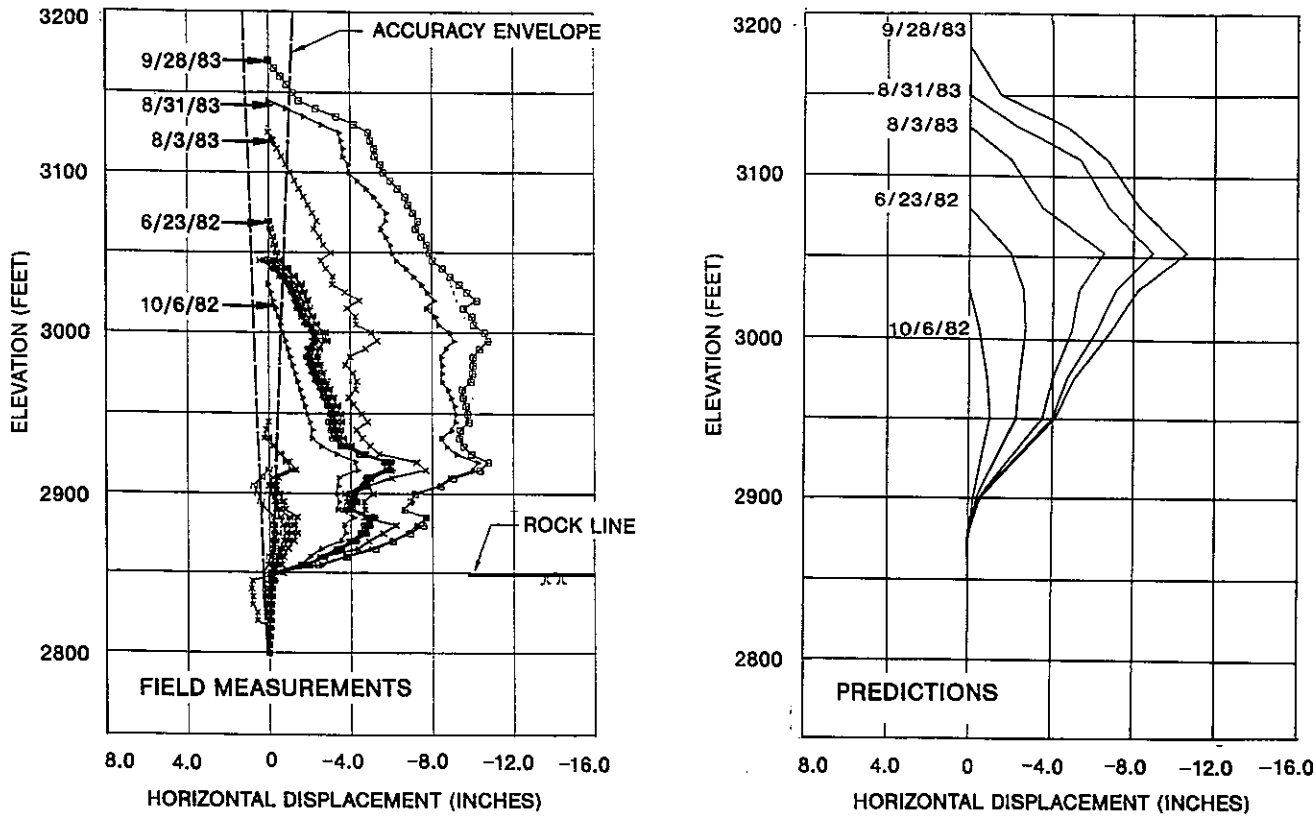

(a) INCLINOMETER 16I01 (167' U/S)

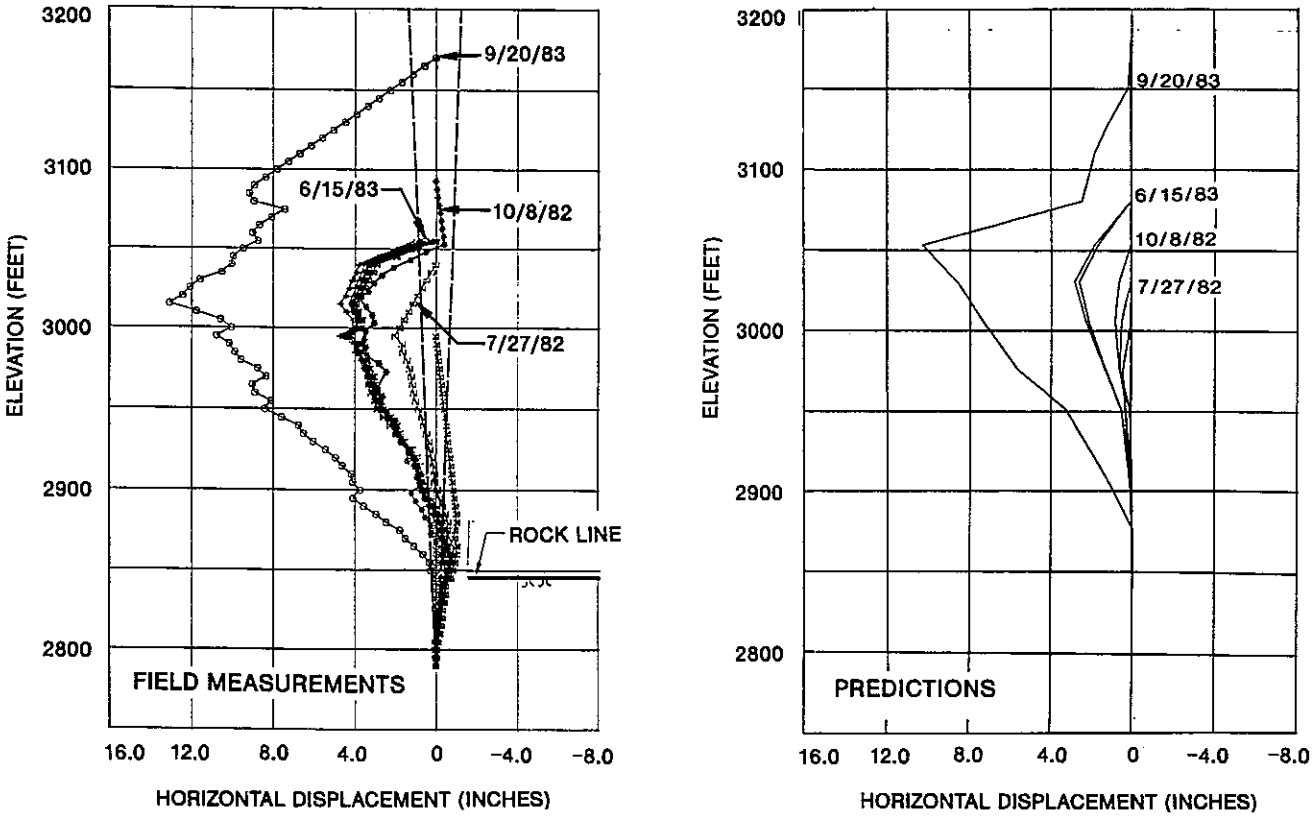

(b) INCLINOMETER 16I103 (253' D/S)

BATH COUNTY DAM – HORIZONTAL DEFLECTION (+U/S,–D/S)

NOTES

NOTES

NOTES